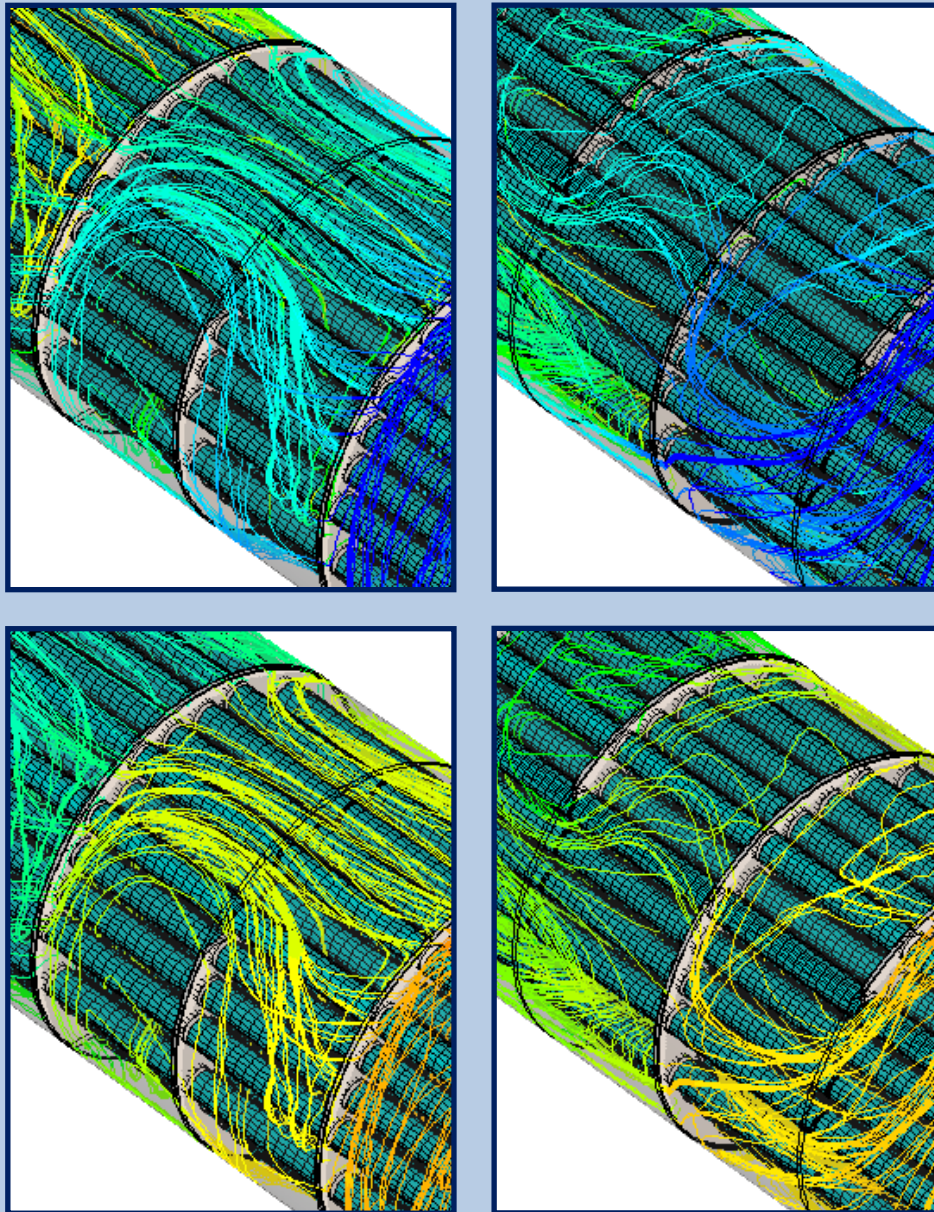# Investigation of the Effects of Baffle Orientation, Baffle Cut and Fluid Viscosity on Shell Side Pressure Drop and Heat Transfer Coefficient in an E-Type Shell and Tube Heat Exchanger

Koorosh Mohammadi

Investigation of the Effects of Baffle Orientation, Baffle Cut and Fluid Viscosity on Shell Side Pressure Drop and Heat Transfer Coefficient in an E-Type Shell and Tube Heat Exchanger

A Dissertation accepted by the Faculty of
Energy Technology, Process Engineering and Biological Engineering of the
University of Stuttgart
in Partial Fulfillment of the Requirements
for the Degree of Doctor of Engineering Sciences (Dr.-Ing.)

by
Koorosh Mohammadi, B. Sc., M. Sc.
born in Abadan, Iran

Institute for Thermodynamics and Thermal Engineering
University of Stuttgart, Germany
February 2011

Supervisor : Prof. Dr. Dr.-Ing. habil. H. Müller-Steinhagen
Co-Referee : Prof. Dr.-Ing. habil. Holger Martin

Date of Oral Examination: 28. February, 2011

Dedication

This work is dedicated to my wife, Parvaneh Jafari, without whose caring supports it would not have been possible, and to the memory of my father, Fathollah Mohammadi, who passed on a love of reading and respect for education.

Contents

Acknowledgments

Render thanks each moment from thy heart, for gratitude is not the work of the tongue alone.
Saadi (1184 – 1283/1291)

The essence of all beautiful art, all great art, is gratitude.
Friedrich Wilhelm Nietzsche (1844 – 1900)

Each of us has cause to think with deep gratitude of those who have lighted the flame within us.
Albert Schweitzer (1875 – 1965)

As we express our gratitude, we must never forget that the highest appreciation is not to utter words, but to live by them.
John F. Kennedy (1917 – 1963)

Nomenclature

All dimensional parameters and variables are in SI units.

- Latin symbols

Symbol	Definition
$4r_h$	Hydraulic diameter ($=4A_{min} n_{rc} d_o X_l / A_H$)
A	Area / Magnitude of $\vec{A}$
A_H	Heat transfer area
A_{min}	The minimum free flow area in the tube bank
B_C	Segmental baffle cut percentage
C	Heat capacity rate ($=\dot{M}c_p$)
C_0, C_1, C_2, C_3	Constant coefficients in the semi-analytical model for the performance factor of water at baffle cut 24% / Constant coefficients in polynomial functions of physical properties of shell-side fluid
c_p	Fluid constant-pressure specific heat
cs	Control surface
cv	Control Volume
$C_{\varepsilon1}, C_{\varepsilon2}$	Coefficients in approximated turbulent transport equations in RNG k-ε model
C_μ	Coefficient in k-ε eddy viscosity formulation (for RNG k-ε model this coefficient is equal to 0.0845)
d_{Hsh}	Hydraulic shell diameter for heat transfer calculation
d_{Hsp}	Hydraulic shell diameter for pressure drop calculation
D_n	Inside diameter of inlet/outlet nozzle
d_o	Tube outside diameter
D_{otl}	Diameter of the circle circumscribed to the outermost tubes of the tube bank
D_s	Shell inside diameter
E	Empirical constant in the law of the wall ($=9.81$ for RNG k-ε model)
e_s	Sensible enthalpy
F	Function describing the influence of main cross-flow stream on other streams
f	Friction factor
G	Geometrical function of shell and tube heat exchanger
h	Convective heat transfer coefficient
i	Direction i of coordinate x_i / Direction i of axis x in Cartesian coordinate
j	Direction j of coordinate x_j / Direction j of axis y in Cartesian coordinate
J_b	Correction factor for bypass flow in Delaware method for calculation the shell-side heat transfer coefficient
J_c	Correction factor for baffle cut and spacing in the Delaware method for calculating the shell-side heat transfer coefficient

J_l	Correction factor for baffle leakage effect including both shell to baffle and tube to baffle leakages in the Delaware method for calculating the shell-side heat transfer coefficient
J_r	Correction factor for adverse temperature gradient build-up in the Delaware method for calculating the shell-side heat transfer coefficient
J_s	Correction factor for variable baffle spacing in the Delaware method
k	Kinetic energy of turbulence fluctuations per unit mass
k_f	Fluid thermal conductivity
L	Tube or heat exchanger length / Length / Effective flow length
L_{bc}	Central baffle spacing
L_{bch}	Baffle cut height
L_{bi}	Inlet baffle spacing
L_{bo}	Outlet baffle spacing
L_n	Nozzle minimum length or nozzle neck length
L_{sb}	Inside shell-to-baffle clearance (diametral)
L_{tb}	Diametral clearance between tube outside diameter and baffle hole
l_{tp}	Tube pitch
m	Power factor in polynomial functions of shell-side physical properties
Max	Maximum of a function
MSD	Minimum shortcut distance
n	Refers to measurable variables in a system / Refers to the particular number of an geometrical entity like tubes, tube rows, tube columns, segments, baffle windows or baffles and etc. / Iteration
NMSD	Normalized minimum shortcut distance
NMSDR	Normalized minimum shortcut distance ratio
n_t	Tube number
O	Orientation function explaining the effect of baffle orientation and baffle cut on stream s
p	Static pressure
P_n	Tube pitch normal to flow direction
P_p	Tube pitch parallel to flow direction
P_t	Tube pitch
Q	Heat flow rate
Q_{AR}	Aspect ratio quality
Q_{EAS}	EquiAngle skewness
R	Flow resistance of stream
r_s	Shell inside radius
T	Static temperature
t	Time/ Time average in Reynolds-averaged Navier-Stokes equations
Tr	Function explaining the transfer rate of heat and momentum
$tubes_l$	Number of tubes in the longitudinal direction, i.e. in the direction of X_l
$tubes_t$	Number of tubes in the transverse direction, i.e. in the direction of X_t
U	Conductance or total heat transfer coefficient of heat exchanger
u_τ	Friction velocity

u	Characteristic velocity fluctuation of turbulence $(= \sqrt{u_i'^2 + u_j'^2 + u_k'^2}$) / Characteristic velocity of fluid motion
u′	Velocity fluctuation
u_{max}	Maximum fluid velocity between the tubes at the central row
V	Instantaneous velocity magnitude of fluid
w	Velocity of the fluid in the empty cross section of the channel
x	x axis, coordinate or component in Cartesian coordinates / Axis of a desired coordinate system / Distance / Displacement in two-point velocity correlation tensor
X_l	Longitudinal pitch ratio $(=P_p/d_o)$
X_t	Transverse pitch ratio $(=2P_n/d_o)$
y	y axis, coordinate or component in Cartesian coordinates / Distance to the wall
y^*	Dimensionless, sublayer-scaled, distance
y^+	Dimensionless, sublayer-scaled, distance
z	z axis, coordinate or component in Cartesian coordinates

- Greek symbols

Symbol	*Definition*
α	Thermal diffusivity
Γ	Gain factor $\equiv h/\Delta p$
Δ	Difference
ε	Dissipation rate of kinetic energy of turbulence fluctuations per unit mass
ε_{Nu}	Relative error in Nusselt number calculation or evaluation
ε_T	Relative error in static temperature calculation or evaluation
$\varepsilon_{\Delta p}$	Relative error in pressure drop calculation or evaluation
ζ	Kolmogorov microscale of length / Face of the computational cell
η_{ph}	Physical property of the shell-side fluid
Θ	Angle between MSD and the axis which passes through the shell center and is parallel to the inlet nozzle neck
Θ_{ca}	Centri-angle of the baffle cut intersection with the inside shell wall
θ	Ratio of tube wall temperature to inlet temperature $\equiv T_{wall}/T_{in}$
θ_o	Ratio of outlet temperature to inlet temperature $\equiv T_{out}/T_{in}$
ϑ_{max}	Maximum angle in radian between the edges of elements
ϑ_{min}	Minimum angle in radian between the edges of elements
l_i	Average length of the edges in a coordinate direction (**i**) local to the element
μ	Fluid dynamic (absolute) viscosity
ν	Fluid kinematic (molecular) viscosity
ξ	Displacement between two points in turbulent flow
ρ	Fluid density
σ_ε	Effective turbulent Prandtl number for ε
τ	Kolmogorov microscale of time
τ_W	Surface (wall) shear stress

υ	Kolmogorov microscale of velocity
φ	Void fraction of tube bank
ϕ	Hypothetical function
ω	Specific dissipation rate ω in k-ω model for turbulence modeling

- Special and mathematical symbols

Symbol	*Definition*
‾	Average value / intermediate value
$\|$	Mathematical symbol which means "restriction of one value or function to a parameter" or "as"
•	Dot product in vector algebra
:	Mathematical symbols which means "such that"
$\|\ \|$	Absolute value
$\|\|\ \|\|$	Absolute deviation / Absolute error / Norm
{ }	Shows a set of property, variables, parameters or entities
(,)	Open interval
⟨ ⟩	Average value
→	In limit of a function or parameter means "approaches to"
∝	Proportionality: is proportional to, varies as
≈	Mathematical symbol which means "approximately equal to"
≡	Mathematical symbol which means "it is equivalent or congruent to"
≫	Strict inequality: is much greater than
∧	Logical conjunction: and
∀	Universal quantification: for all, for any, for each
∃	Existential quantification: there exists, there is, there are
∃!	Uniqueness quantification: there exists exactly one
∈	Set membership: is an element of
$\vec{A}$	Area of control surface in vector notation
$\vec{bf}$	Baffle-vector
f	Hypothetical function
f_A	Nondimensional geometrical correction factor presented in correlation of heat transfer coefficient of tube bank
f_B	Bypass-stream factor in VDI method
f_G	Geometrical factor in VDI method
f_L	Leakage-stream factor in VDI method
f_W	Correction factor in calculation of shell-side heat transfer coefficient by use of VDI method ($=f_G f_L f_B$)
$\vec{i}$	Unit vector of x axis in Cartesian coordinates
$\vec{i}_i$ or $\vec{i}_j$	Cartesian unit vector in the direction of the coordinate x_i or x_j
$\vec{j}$	Unit vector of y axis in Cartesian coordinates
$\vec{k}$	Unit vector of z axis in Cartesian coordinates
ℓ	Turbulence length scale / Integral length scale
ℓ_H	Hydraulic length of heat transfer for heat exchanger
$\dot{M}$	Mass flow rate

max{ }	The largest value of a set of parameters
min{ }	The smallest value of a set of parameters
$\overline{n\vec{z}}$	Face-vector of inlet-plane imagined in nozzle
$\bar{\bar{O}}$	Order of magnitude / Magnitude of a parameter or value
$\bar{\bar{O}}\{f, X\}$	Order of magnitude of function f with respect to parameter X
$\overline{U}$	Mean velocity component in x, y, z direction
$\vec{u}$	Instantaneous velocity of fluid in vector notation
$\vec{V}$	Instantaneous velocity of fluid in vector notation relative to control volume of fluid
$\forall$	Volume of fluid / Volume of system
$\vec{x}$	Displacement vector in two-point velocity correlation tensor
$\{X\}$	Set of geometrical parameters (={tube layout, tube outside diameter, tube length})
$\vec{\xi}$	Displacement vector between two points in the flow
$\vec{\nabla}$	Divergence $(= \partial/\partial x \bullet \vec{i} + \partial/\partial y \bullet \vec{j} + \partial/\partial z \bullet \vec{k})$
$\left|\vec{\nabla}\eta\right|_{n,\zeta}$	Magnitude of $\vec{\nabla}\eta$ normal to face ζ
$\angle(\vec{a},\vec{b})$	Counter-clockwise angle of rotation of vector $\vec{a}$ towards vector $\vec{b}$

- Subscripts

Symbol	Definition
0	Related to the value at x=0
24%|Water,ISO	Refers to a value at baffle cut 24% for water as the shell-side fluid with constant physical properties at 20 °C and 1 atm.
95%Φ∞	Related to 95% of ultimate value of Φ
$\angle(\overrightarrow{bf},\overrightarrow{nz})$	Shell and tube heat exchanger with baffle orientation equal to $\angle(\overrightarrow{bf},\overrightarrow{nz})$
A	Related to tube-baffle leakage stream (flow stream A)
Air	Refers to the air at desired operating conditions
B	Related to main effective cross-flow stream (flow stream B)
baffle	Related to the baffle
BC	Refers to baffle cut BC
bp	Related to bypass streams
C	Related to tube bundle bypass stream (flow stream C)
CFD	Refers to the CFD calculation
cl	Related to the central line which presents the middle of the inlet
cold	Related to the cold fluid or cold fluid side
E	Related to baffle-shell leakage stream (flow stream E)
F	Related to bypass stream in tube pass partition (flow stream F)
fluid 1 or 2	Related to the shell-side fluid 1 or 2
H	Refers to the heat transfer
h	Values, variables, parameters or dimensionless numbers base on hydraulic diameter $4r_h$
hor./horizontal	Shell and tube heat exchanger with horizontal baffle orientation

hot	Related to the hot fluid or hot fluid side
i	Refers to direction i of coordinate x_i in a defined coordinate
in/inlet	Inlet nozzle / Property calculated at inlet temperature
ISO	Related to the reference temperature and pressure according to the International Organization for Standardization (p=1 atm, T=20 °C)
j	Refers to direction j of coordinate x_j in a defined coordinate
max	Refers to the maximum value
min	Refers to the minimum value
o	Refers to the outside diameter of tube
out/outlet	Outlet nozzle / Property calculated at outlet temperature
rc	Refers to the total number of tube rows crossed the flow
s	Refers to stream flow
Semi-Analytical	Refers to the calculation based on the semi-analytical model
shell	Related to shell-side / Property calculated at average shell-side temperature $(T_{in}+T_{out})/2$
turb	Refers to turbulent flow
ver./vertical	Shell and tube heat exchanger with vertical baffle orientation
wall	Related to tube wall / Property calculated at tube wall temperature
Water	Refers to the water at desired operating conditions
WF	Refers to working fluid
window	Related to baffle window / Refers both upper and lower baffle
x, y, z	Refers to the x, y and z axis direction in Cartesian coordinates
φ	Refers to modified values base on void fraction of tube bank

- Superscripts

Symbol	Definition
*	Sublayer-scaled value
+	Sublayer-scaled value
csf	Cross sectional flow area
ms	Main stream / Related to the stream in heat exchanger exclusive
n	Refers to iteration n
SATP	Standard Ambient Pressure and Temperature (p=100 kPa, T=25 °C)

- Dimensionless numbers

Symbol	Definition
f	Modified Fanning friction factor $\equiv 2r_h\Delta p/(\rho u^2 L)$
Nk	Shell-side Kârmân number $\equiv \rho d_{Hsp}^3(\Delta p_{shell}/L_{bc})/\mu^2$
Nu	Nusselt number $\equiv (h\times \text{characteristic length})/k_f$
Nu_0	Nusselt number at zero Reynolds number
$Nu_{0, bank}$	Nusselt number of ideal tube bank defined by Gnielinski
Nu_{shell}	Shell-side Nusselt number $\equiv h_{shell}d_{Hsd}/k_f$
Pe	Peclet number $\equiv \rho VL/\Omega$
Pr	Prandtl number $\equiv (\mu C_p/k_f)$

xvi

Re	Reynolds number $\equiv \rho u(\text{characteristics length})/\mu$
Re_{inlet}	Reynolds number based on the inlet nozzle diameter, the fluid velocity in the inlet nozzle and the physical properties at inlet conditions $\equiv u_{inlet}D_n/\nu$
Re_o	Reynolds number based on the maximum fluid velocity between the tubes at the central row and the tube diameter as the characteristic length $\equiv \rho_{inlet}u_{max}d_o/\mu_{inlet}$
$Re_{trans,ll}$	Lower limit transitional Reynolds number
$Re_{trans,ul}$	Upper limit transitional Reynolds number
Re_φ	Modified Reynolds number based on the stream length $\pi d_o/2$, the velocity of the fluid in the empty cross section of the channel and the void fraction of the tube bank $\equiv w\pi d_o/(2\varphi\nu)$
St	Stanton number $\equiv Nu/(Re.Pr)$
γ	Dimensionless number used in the equation of sensibility analysis $\equiv \left(\mu_{in}/\overline{\mu}\right)(\ell_H/D_n)(A_{in}/A_H)$
Γ	Gain factor $\equiv Nu/Nk$
Θ_{BC}	Baffle cut preference $\equiv \Phi_{BC}/\Phi_{24\%}$
Θ_{WF}	Working fluid preference $\equiv (\Phi_{WF}/\Phi_{Water})|_{BC}$
Φ	Performance factor $\equiv (\Gamma_{shell})_{hor.}/(\Gamma_{shell})_{ver.}$

Zusammenfassung

Zur Bestimmung des Einflusses der Umlenkblechanordnung und des Umlenkblechausschnitts sowie der Viskosität des Arbeitsfluids auf den mantelseitigen Wärmeübergang und Druckverlust eines Rohrbündelwärmeübertragers im laminaren und turbulenten Bereich wird das kommerzielle CFD-Programm FLUENT eingesetzt. Luft, Wasser und Motoröl werden als mantelseitige Arbeitsmedien betrachtet. Die betrachteten Rohrbündelwärmeübertrager erfüllen die TEMA-Standards. Die Untersuchung wurde in drei Schritten durchgeführt:

1. Der Rohrbündelwärmeübertrager besteht aus 660 glatten Rohren mit festem Außendurchmesser, die in Dreieckteilung versetzt angeordnet sind. Es wird eine horizontale und vertikale Anordnung der Umlenkbleche sowie drei Öffnungsweiten, 20%, 24% und 30% des Mantelinnendurchmessers betrachtet. Die Leckageströme in den Bohrungsspielräumen und im Spalt zwischen Umlenkblech und Mantel werden nicht berücksichtigt. Die Untersuchung wurde auf die Einlasszone angewendet, um den Effekt der Umlenkblechanordnung, des Umlenkblechausschnitts und der Viskosität des mantelseitigen Fluids auf die mantelseitige Leistung in der Einlasszone zu bestimmen.

   Für die jeweiligen Umlenkblechanordnungen, Umlenkblechausschnitte und Arbeitsfluide werden verschiedene Strömungsgeschwindigkeiten am Einlass untersucht. Diese Geschwindigkeiten werden durch die Reynoldszahl am Einlass Re_{inlet} charakterisiert, welche sich auf die Geschwindigkeit in dem Einlassstutzen, den Innendurchmesser des Einlassstutzens und die physikalischen Eigenschaften des mantelseitigen Fluids bei Einlassdruck und –temperatur bezieht. Wärmeübergang und Druckverlust werden als allgemeine Nusselt-Zahl (Nu oder Nu_{shell}) beziehungsweise Kârmân-Zahl (Nk) angegeben. Die Definition von Nu_{shell} erfolgt entsprechend dem VDI Wärmeatlas [VDI-2006]. Ergebnisse für alle geometrischen Variationen zeigen, dass sich Nk proportional zu Re^2 und Nu zu Re^m verhält, wobei $0{,}6 \leq m \leq 0{,}8$.

   Ein für die Bewertung von Rohrbündelwärmeübertragern geeigneter mantelseitiger Gewinnfaktor wird als Verhältnis von mantelseitigem Wärmeübergangskoeffizienten zu mantelseitigem Druckverlust eingeführt. Um die Unterscheidung zwischen horizontaler und vertikaler Orientierung der Umlenkbleche zu vereinfachen, wird ein Leistungsfaktor Φ, als das Verhältnis des Gewinnfaktors von horizontal angeordneten Umlenkblechen zum Gewinnfaktor bei vertikaler Umlenkblechanordnung, verwendet. Die Simulationsergebnisse zeigen den Vorteil der horizontalen Umlenkblech-orientierung im Vergleich zur vertikalen Orientierung, insbesondere für Luft (d.h. Gas) als mantelseitigem Fluid. Bei einem Umlenkblechausschnitt von 30% erreicht der Leistungsfaktor seinen Maximalwert für alle mantelseitigen Fluide, während der minimale Wert des Leistungsfaktors bei einer Umlenkblechöffnung von 24% beobachtet wird.

   Simulationsergebnisse für den Einlassbereich zeigen, dass die horizontale Umlenkblechorientierung im Vergleich zur vertikalen Orientierung einen bis zu 20% höheren Druckverlust zur Folge hat. Weiterhin zeigen die Ergebnisse, dass die Nusselt-Zahl für die horizontale Umlenkblechanordnung etwa 15% bis 52% höher ist, als die Nusselt-Zahl für die vertikale Anordnung.

   Für Wasser und Motoröl ist der Gewinnfaktor Γ für die horizontale Umlenkblechorientierung bis zu 20% größer als der Gewinnfaktor für die vertikale Orientierung. Für Luft als mantelseitigem Fluid ist der Wert für Γ für die horizontale Orientierung bis zu 40% größer als bei der vertikalen Orientierung.

2. Um einen vollständigen Rohrbündelwärmeübertrager zu simulieren, wird ein Rohrbündelwärmeübertrager mit denselben geometrischen Abmessungen wie im

vorhergehenden Schritt betrachtet. Wieder werden keine Leckageströme berücksichtigt. Für die numerischen Berechnungen wird der Wärmeübertrager in acht verschiedene Strömungsbereiche, wie Ein- und Auslasszone und sechs mittlere Strömungsabschnitte, die sich zwischen benachbarten Umlenkblechen befinden, geteilt. Um den Einfluss der Viskosität auf den Wärmeübergang und den Druckverlust zu bestimmen, werden Simulationen für die beiden Arbeitsfluide Luft und Wasser durchgeführt.

Für alle Umlenkblechorientierungen und –ausschnitte, sowie für alle Arbeitsfluide werden Simulationen für fünf Einlassreynolds-Zahlen, $3{,}9 \times 10^4 \leq Re_{inlet} \leq 1{,}16 \times 10^6$, durchgeführt.

Die Simulationsergebnisse zeigen den Vorteil der horizontalen gegenüber der vertikalen Umlenkblechanordnung, insbesondere in der Ein- und Auslasszone, für alle untersuchten mantelseitigen Arbeitsfluide.

Der Leistungsfaktor für die horizontale Anordnung der Umlenkbleche ist in den mittleren Umlenkblechbereichen etwa gleich dem Leistungsfaktor für die vertikale Anordnung, wenn flüssiges Wasser als mantelseitiges Fluid verwendet wird. Für Luft ist ein Vorteil der vertikalen gegenüber der horizontalen Umlenkblechanordnung erkennbar.

3. Um einen realen vollständigen Rohrbündelwärmeübertrager zu simulieren, wird ein Rohrbündelwärmeübertrager bestehend aus 76 Rohren mit festem Außendurchmesser betrachtet. Die Rohre sind in Dreieckteilung versetzt angeordnet. Die Leckageströme in den Bohrungsspielräumen und den Spalten zwischen Umlenkblechen und Mantel werden mit einbezogen. Wie bei den vorhergehenden Schritten wird die horizontale und vertikale Umlenkblechanordnung berücksichtigt, der Umlenkblechausschnitt jedoch auf 20% des Mantelinnendurchmessers festgelegt. Dadurch wird das Verhältnis der Wärmeübergangsfläche der Rohre im Umlenkblechfenster zur Wärmeübergangsfläche der Rohre in einem Umlenkblechzwischenraum annähernd so groß wie der zugehörige Wert des Rohrbündelwärmeübertragers mit 660 Rohren. Um den Einfluss der Viskosität auf den Wärmeübergang und den Druckverlust zu bestimmen, werden Simulationen für die drei Arbeitsfluide Luft, Wasser und Motoröl bei Prandtl-Zahlen zwischen 0,7 und 1798,8 bezogen auf SATP-Bedingungen durchgeführt.

Für alle Umlenkblechorientierungen und -ausschnitte, sowie für alle Arbeitsfluide werden Simulationen für fünf Einlassreynolds-Zahlen im Bereich von $2{,}0 \times 10^4 < Re_{inlet} < 10^5$ durchgeführt.

Die Simulationsergebnisse zeigen den Vorteil der horizontalen gegenüber der vertikalen Umlenkblechanordnung, insbesondere in der Ein- und Auslasszone, für alle untersuchten mantelseitigen Arbeitsfluide.

Die Simulationsergebnisse zeigen einen signifikanten Einfluss der Umlenkblechorientierung auf den mantelseitigen Druckverlust und Wärmeübergang von Rohrbündelwärmeübertragern. Im Gegensatz zu den Ergebnissen der vorausgegangenen Simulationen zeigen die Ergebnisse, dass die vertikale Umlenkblechorientierung in Rohrbündelwärmeübertragern mit Verlustströmen vorteilhafter als die horizontale Orientierung ist. Dieser Vorteil (einer vertikalen gegenüber einer horizontalen Anordnung der Umlenkbleche) ist bei Gasen deutlicher.

Als Fazit ergibt sich, dass ein Vergleich der Rechenergebnisse mit und ohne Berücksichtigung der Leckageströme unterschiedliche Verhalten aufzeigt. Dies macht deutlich, dass die Berücksichtigung von Leckageströmen in den Bohrungsspielräumen und im Spalt zwischen Umlenkblech und Mantel sowie von Bypassströmen von Bedeutung ist.

Abstract

The commercial CFD code FLUENT is used to determine the effect of baffle orientation and baffle cut as well as viscosity of the working fluid on the shell-side heat transfer and pressure drop of a shell and tube heat exchanger in the domain of laminar and turbulent flow. Air, water and engine oil are considered as shell-side fluids. The shell and tube heat exchangers considered follow the TEMA standards. The investigation has been completed in three stages:

1. The shell and tube heat exchanger consists of 660 plain tubes with fixed outside diameter which are arranged in a triangular layout. Horizontal and vertical baffle orientations as well as three baffle cuts, 20%, 24% and 30% of shell inside diameter, are considered. No leakage flow in tube-to-baffle gaps and baffle-to-shell gaps is considered. The investigation has been applied for the inlet zone, in order to find the effect of baffle orientation, baffle cut and viscosity of shell-side fluid on the shell-side performance of the inlet zone.

    For each baffle orientation, baffle cut and working fluid, different flow velocities at inlet are investigated. These velocities are introduced as inlet Reynolds number Re_{inlet} which is defined based on the velocity at the inlet nozzle, inside diameter of the inlet nozzle and the physical properties of the shell-side fluid at inlet pressure and temperature. Heat transfer and pressure drop are reported as overall Nusselt number (Nu or Nu_{shell}) and Kârmân number (Nk), respectively. Nu_{shell} is defined according to VDI Wärmeatlas [VDI-2006]. Results for all geometrical variations show that Nk is proportional to Re^2 and Nu is proportional to Re^m, where $0.6 \leq m \leq 0.8$.

    A shell-side gain factor suitable for the assessment of shell and tube heat exchangers is introduced as ratio of the shell-side heat transfer coefficient to the shell-side pressure drop. To facilitate the decision between horizontal and vertical baffle orientation, a performance factor Φ is used as ratio of the gain factor for horizontally orientated baffles to the gain factor for vertical baffle orientation.

    The simulation results show the advantage of the horizontal baffle orientation over the vertical orientation, especially for air (i.e. gas) as shell-side fluid. At baffle cut 30%, the performance factor reaches its maximum value for all shell-side fluids, while the minimum value of performance factor is observed at baffle cut 24%.

    Simulation results for the inlet region show that the horizontal baffle orientation produces up to 20% higher pressure drop than the pressure drop in vertical baffle orientation. The results also show that the Nusselt number for horizontal baffle orientation is approximately 15% to 52% higher than the Nusselt number for vertical orientation.

    For water and engine oil, the gain factor Γ for horizontal baffle orientation is up to 20% more than the gain factor for vertical baffle orientation. For air as shell-side fluid, the value of Γ for horizontal baffle orientation is up to 40% more than the value of Γ for vertical baffle orientation.

2. In order to simulate the complete shell and tube heat exchanger, a shell and tube heat exchanger with the same geometrical aspects used in the previous stage is considered. Again, no leakage flows are taken into account. For the numerical investigations the heat exchanger is subdivided into eight different flow sections such as the inlet zone, six intermediate flow sections located between adjacent baffles and the outlet zone. In order to determine the effect of viscosity on heat transfer and pressure drop, simulations are performed for the two working fluids; air and water.

    For each baffle orientation, baffle cut and working fluid, simulations are performed for five inlet Reynolds numbers; $3.9 \times 10^4 \leq Re_{inlet} \leq 1.16 \times 10^6$.

The simulation results show the advantage of the horizontal baffle orientation over the vertical orientation, particularly in the inlet and outlet zone for all investigated shell-side fluids.

The performance factor for horizontal baffle orientation is approximately equal to the performance factor for vertical baffle orientation at intermediate baffle spacing zones when liquid water is used as shell-side fluid. For air, the benefit of vertical baffle orientation on horizontal baffle orientation is noticeable.

3. In order to simulate a real complete heat exchanger, a shell and tube heat exchanger consisting of 76 tubes with fixed outside diameter is considered. The tubes are arranged in a triangular layout. The tube-to-baffle and baffle-to-shell leakages are also taken into account. Similar to the previous stages, horizontal and vertical baffle orientations are considered, but the baffle cut is fixed to 20% of shell inside diameter. This will make the ratio of the heat transfer area of the tubes in the baffle window to the heat transfer area of the tubes in one baffle spacing zone similar to the corresponding ratio for the heat exchanger with 660 tubes. In order to determine the effect of viscosity on heat transfer and pressure drop, simulations are performed for three working fluids air, water and engine oil with Prandtl numbers in the range of 0.7 to 1798.8 based on the standard ambient pressure and temperature.

   For each baffle orientation, baffle cut and working fluid, simulations are performed for five inlet Reynolds numbers in the range $2.0 \times 10^4 < \text{Re}_{\text{inlet}} < 10^5$.

   The simulation results show the advantage of the horizontal baffle orientation over the vertical orientation, particularly in the inlet and outlet zone for all investigated shell-side fluids.

   The simulation results show a significant influence of the baffle orientation on the shell-side pressure drop and heat transfer of shell and tube heat exchangers. Contrary to the outcomes of the previous simulations, the results show that in shell and tube heat exchanger with leakage flows the vertical baffle orientation seems to be more advantageous than the horizontal orientation. The benefit of vertical baffle orientation over horizontal baffle orientation is more noticeable for gases.

As a final conclusion, the comparison of calculation results with and without leakage flows identifies different behaviour and underlines the importance of a consideration of tube-to-baffle and baffle-to-shell leakage and bypass streams for the prediction of the performance factor of technical heat exchangers.

1. Introduction

1.1 Industrial Heat Exchangers

Most operations that are carried out by engineers involve the production or absorption of thermal energy. The laws governing the transfer of heat and the types of apparatus that have for their main object the control of heat flow are therefore of great importance [McCabe, 2005]. A heat exchanger is a piece of equipment in which heat is transferred from a hot fluid to a colder fluid. In most applications the fluids do not mix but transfer heat through a separating wall which takes on a wide variety of geometries. In industries, heat exchangers are widely used in refrigeration, air conditioning, space heating, electricity generation, and chemical processing.

Heat exchanger design aims in most cases at minimum cost, balancing the cost of pumping the fluids and initial cost of the exchanger against the savings resulting from heat transfer. In some cases, such as missile, aircraft or shipboard applications, design may be governed by necessity of minimizing either volume or weight [Palen, 1986].

Shell and tube heat exchangers are probably the most widespread and commonly used basic heat exchanger configuration in oil refineries and other large chemical processes and are suited for higher-pressure applications. Reasons for this general acceptance are several: The shell and tube heat exchanger provides a comparatively large ratio of heat transfer area to volume and weight (up to 1000 m²/m³) [Hesselgreaves, 2001]. It provides this surface in a form which is relatively easy to construct in a wide range of sizes (Figure 1.1 and 1.2) and which is mechanically rugged enough to withstand shop fabrication stress, shipping and field erection stress, and normal operating conditions [Palen, 1986; Driedger, 1996; Wolverine, 2001]. There are many modifications of the basic configuration which can be used to solve special problems. [Saundres, 1988; Wolverine, 2001]. It is essential to mention that a heat exchanger is not only an apparatus for transferring heat from one medium to another, but is at the same time a pressure and/or containment vessel. In addition to heating up or cooling down fluids in just a single phase, shell and tube heat exchangers can be used either to heat a liquid to evaporate (or boil) it or used as condensers to condense a vapor back to a liquid.

Figure 1.1: Left: shell and tube heat exchanger made by Addison Fabricators Inc., Addison, Alabama, USA (8000 tubes/90 tonnes). Right: titanium shell and tube heat exchanger made by TITAN Metal Fabricators, Camarillo, California, USA (1.07 m shell outside diameter, 7.3 m maximum length, 25 tonnes, 1282 tubes).

1.2 Shell and Tube Heat Exchangers: Applications and Main Components

In shell-and-tube exchangers, many tubes are mounted inside a shell; one fluid flows through the tubes (the tube side) and the other flows outside the tubes but inside the shell (the shell-side). Heat is transferred from one fluid to the other through the tube walls, either from tube side to shell-side or vice versa. The fluids can be either liquids or gases on either the shell or the tube side. In order to transfer heat efficiently, a large heat transfer area should be provided.

Shell and tube heat exchangers with only one phase (liquid or gas) on each side are called single-phase heat exchangers.

Two-phase heat exchangers are usually condensers or boilers.

From the design point of view, while there is an enormous variety of specific design features that can be used in shell and tube heat exchangers, the number of basic components are relatively small. The construction of a shell and tube heat exchanger is illustrated by Figure 1.3, in which the main components, discussed below, are numbered [Saundres, 1988].

Figure 1.2: Shell and tube heat exchanger for temperature control systems made by Exergy LLC (inside shell diameter = 22.5 mm, maximum length = 248 mm and tube number = 24)

1.2.1 Tubes

The tubes are the basic component of the shell and tube exchanger, providing the heat transfer between one fluid flowing inside the tubes and the other fluid flowing across the outside of tubes. From the point of view of thermal design features, the most substantial characteristics of tubes are tube diameter, tube wall thickness, tube length and tube pitch.

•Tube diameter

Compact, economical units are obtained by using small diameter, closely spaced tubes but the surface may foul up quickly and may be difficult to clean by mechanical means. The problems of fouling and cleaning may be overcome by using large-diameter, widely spaced tubes, but then the unit will be less compact and more costly. The selection of the tube diameter is therefore a compromise taking into account the fouling nature of the fluids, the space available and the cost. Tube of 19.05 and 25.4 mm (¾ -1 in) outside diameter are most widely used, but small units with clean fluids may use tubes as small as 6.35 mm (¼ in) outside diameter, and units handling heavy tars may use tubes up to 50.8 mm (2 in) outside diameter.

•Tube wall thickness

The tube wall thickness must be checked against the internal and external pressure separately. However, in many cases the pressure is not the governing factor determining the wall thickness. For example, a steel tube with 19.05 mm (¾ in) outside diameter, 2.11 mm thick (0.083 in), at 350 °C, is suitable for design pressure up to 200 bar, which is adequate for many applications. Except when pressure governs, tube thickness is selected to provide an adequate margin against corrosion, resistance to flow-induced vibration, axial strength, standardization for the stocking of spare parts and cost.

2

•Tube length

For a given surface area the cheapest exchanger is one which has a small shell diameter and a long tube length, consistent with the space and handling facilities at site and fabricator's shop. Therefore, the incentive is to make exchangers as long as possible, limited only by the tube length available from tube suppliers. Tube lengths of 2438, 3658, 4877, 6096 and 7315 mm (8, 12, 16, 20 and 24 ft) are often regarded as standard tube length.

•Tube pitch

It is customary practice to arrange the tube pitch (center-center distance) such that it is not less than 1.25 times the outside diameter of the tubes. In certain applications involving clean fluids and small tubes, e.g. 12.7 mm (½ in) outside diameter and less, the pitch/diameter ratio is sometimes reduced to 1.20. Different tube pitch arrangements are shown in Figure 1.4. In Table 1.1 typical pitch angles for various flow regimes and nature of shell-side fluids are listed.

For a given pitch/diameter ratio and shell inside diameter, about 15% more tubes can be accommodated for 30° and 60° pitch angle compared with 45° and 90°. To achieve compactness the incentive is to use 30° and 60° pitch angles, which is satisfactory for clean services. However, these patterns are not suitable if external mechanical cleaning is required.

1.2.2 Tube Sheets

Tube sheet is usually a single round plate of metal that has been suitably drilled and grooved to take the tubes in the desired tube layout, the gaskets, and the bolt circle where it is fastened to the shell.

Figure 1.3: Diagram of typical shell and tube heat exchanger. A: Tubes, B: Tube Sheets, C: Shell, D: Tube-Side Inlet (Outlet) Nozzle, E: Tube-Side Outlet (Inlet) Nozzle, F: Pass Divider, G: Baffles, H: Shell-Side Inlet (Outlet) Nozzle, I: Shell-Side Outlet (Inlet) Nozzle.

1.2.3 Shell and Shell-Side Nozzles

The shell is simply the container for the shell-side fluid, and the nozzles are the inlet and exit ports.

1.2.4 Tube-Side Nozzles

The tube-side nozzles (and channels) control the flow of the tube-side fluid into and out of the tubes of the exchanger.
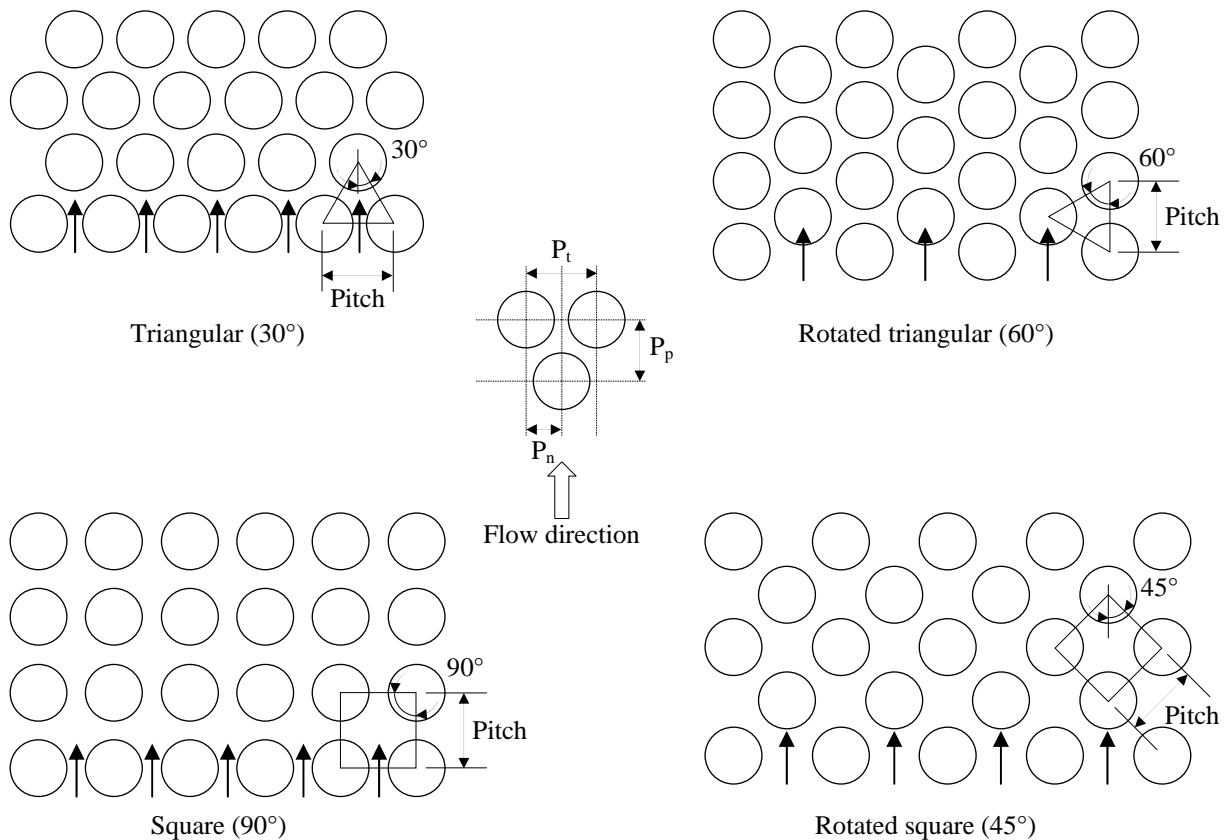
Figure 1.4: Tube layout and arrangement. The definition of tube pitch and tube pitches parallel and normal to flow (P_t, P_p and P_n) is typically shown for equilateral triangular arrangement.

Pitch pattern	Pitch angle	Nature of shell-side fluid	Flow regime
triangular	30°	clean	turbulent and laminar
rotated triangular	60°	clean	rarely used (30° is better to use)
square	90°	fouling	turbulent
rotated square	45°	fouling	laminar

Table 1.1: Selection of pitch angle based on the nature of shell-side fluid and the flow regime.

1.2.5 Pass Divider

A pass divider is required in one channel or bonnet for an exchanger having two tube-side passes, as the one illustrated in Figure 1.3. They are needed in both channels and bonnets for an exchanger having more than two passes.

1.2.6 Baffles

One of the most important parts in shell and tube heat exchangers are the baffles. Baffles serve mainly two functions:
- Fixing of the tubes in the proper position during assembly and prevention of tube vibration caused by flow-induced eddies.
- Guidance of the shell-side flow across the tube field, increasing the velocity and the heat transfer coefficient.

The most common baffle shape is single segmental as shown in Figure 1.5.

The segmental baffle cut must be less than half of the shell inside diameter in order to ensure that adjacent baffles overlap at least one full baffle tube row. For liquid flows on the shell-

4

side, a baffle cut of 20 to 25 percent of the shell inside diameter is common. For low pressure gas flows, 40 to 45 percent is more common, in order to minimize the pressure drop. The baffle spacing should be correspondingly chosen to make the free flow areas through the baffle window and across the tube bank roughly equal [Ball, 2000]. For many high velocity gas flows, the single segmental baffle configuration results in an undesirably high shell-side pressure drop [Palen and Taborek, 1969; Perry and Chilton, 1999]. One way to retain the structural advantages of the segmental baffle and reduce the pressure drop is to use double segmental baffles as shown in Figure 1.6 [Poddar and Polley, 2000]. For sufficiently large units, it is possible to go to triple segmental arrangement.

Other baffle patterns and configurations such as disc-and-donut and orifice baffles have been used in the past but are seldom seen now.

A small gap (clearance) between tube outside diameter and baffle-hole diameter, which is called tube-baffle clearance, is required in order to allow assembly of the tube bundle and tube replacement if required.

Excessive clearance provides too little tube support and possible vibration, as well as excessive leakage of fluid across the baffle. Too little clearance makes assembly and tube replacement difficult. According to the standards of the Tubular Exchanger Manufacturers Association (TEMA), the tube-baffle clearance is.

Figure 1.5: Schematic configuration of single segmental baffles.
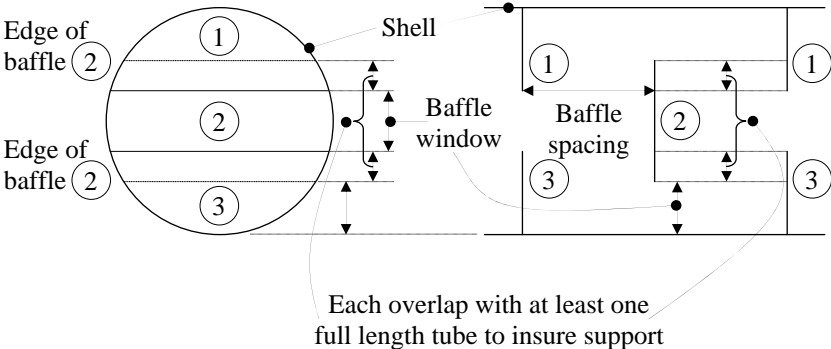
Figure 1.6: Schematic configuration of double segmental baffles.

$1/32$ inches (0.8 mm) for tubes larger in outside diameter than 1¼ inches (31.8 mm). If the maximum unsupported tube length exceeds 36 inches (914 mm) or if the tube outside diameter is less than 1¼ inches (31.8 mm), the baffle-tube clearance is $1/64$ inches (0.4 mm) [TEMA, 1999]. In some air-conditioning applications, the tubes are expanded after assembly in order to eliminate the clearance altogether. This significantly complicates tube replacement, but might solve some potential tube vibration problems.

The outer diameter of the baffle must be less than the shell inside diameter to allow assembly. But the clearance which is called shell-baffle clearance, should be as little as possible to minimize the shell-to-baffle leakage flow rate. The shell-to-baffle leakage typically is the greatest penalty against the shell-side heat transfer coefficient. If the shell-to-baffle leakage reaches a substantial magnitude, e.g. more than 15% of the total shell-side flow, the design effectiveness is poor and double segmental baffles or other modifications should be considered [Taborek, 1979; Kuppan, 2000].

A shell and tube heat exchanger may be divided into different zones or spacing due to the presence of baffles. The first zone is the sector between the inlet nozzle and the first baffle and therefore may be called inlet zone. Moreover, the inlet baffle spacing may also refer to the longitudinal distance of the inlet zone and will be represented by L_{bi}. Similar to the inlet zone, the sector between the last baffle and the outlet nozzle is the outlet zone and will also be named as outlet baffle spacing. The outlet baffle spacing may also refer to the length of the outlet zone and will have the symbol L_{bo}. The second baffle zone or the second baffle spacing is the region between the first baffle and the second baffle. Using this definition, a shell and tube heat exchanger could have different baffle zones or baffle spacing zones. In most heat exchanger designs, the longitudinal distances between first, second, third and etc. baffle are equal. Therefore, these equal lengths are termed as central baffle spacing or L_{bc}. In most handbooks, the region consisting of inlet baffle spacing and the first baffle zone is called the inlet region. Similar to the inlet region, the outlet region is defined as a region of shell and tube heat exchanger which includes the outlet zone and its neighbouring baffle spacing. This definition is again used because of the effect of outlet zone on the pressure drop and heat transfer of shell and tube heat exchanger.

In order to minimize the pressure drop in inlet and outlet zones, the inlet baffle spacing and the outlet baffle spacing are longer than the central baffle spacing. The region consisting of all the other baffle zones is termed the intermediate region. Figure 1.7 represents schematically the different baffle zones and regions in a shell and tube heat exchanger.
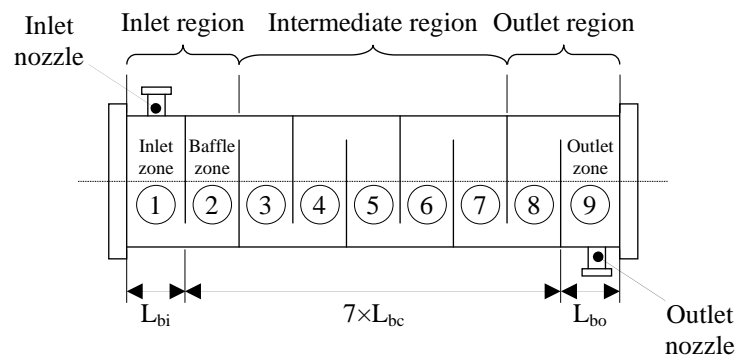
Figure 1.7: Schematic representation of different zones and regions in a shell and tube heat exchanger.

1.3 Tubular Exchangers Manufacturers Association (TEMA) Design Code

A wide variety of configurations are available in shell and tube heat exchanger designs. The pressure parts of a shell and tube heat exchanger are designed in accordance with pressure vessel design codes such as ASME (American Society of Mechanical Engineers), BSS (British Standards Specifications), AD Merkblätter, and so on, but a pressure vessel code alone cannot be expected to deal with all the special features of shell and tube heat exchangers. To give guidance and protection to designers, fabricators, and purchasers alike, a supplementary code is desirable that provides minimum standards for design, materials, thicknesses, corrosion allowances, fabrication, tolerances, testing, inspection, installation, operation, maintenance, and guarantees for shell and tube heat exchangers [Hewitt, 1992].

A widely accepted standard is published by the Tubular Exchanger Manufacturers Association TEMA, which is intended to supplement the ASME Boiler and Pressure Vessel Code, Section VIII, Division 1, although most of the information may be used to complement other pressure vessel codes if required [Saundres, 1988; ASME, 2004]. TEMA was founded in 1939 and is a group of leading manufacturers who have pioneered the research and development of heat exchangers for more than seventy years. The TEMA standard was prepared by a committee comprising representatives of 27 USA manufacturing companies and their combined expertise and experiences provide exchangers of high integrity at reasonable costs.

TEMA also provided and developed a standard type designation and notation system for the major types of shell and tube heat exchangers. This standard system simplifies the specifications and identifies by three letters the basic configuration of shell and tube heat exchangers. The first letter identifies the front head, the second letter describes the shell and the third letter explains the rear head. Figure A.1 in "Appendix A" shows the TEMA designation system for shell and tube heat exchangers [TEMA, 1999].

Of the various shell geometries available, the simplest is the so called E-Shell. With a single tube pass unit and good baffling, the flow can be considered as pure counter current flow. This flow arrangement makes the best use of available temperature driving force and results in the smallest exchanger size [Poddar and Polley, 2000], see Figure 1.8. Even though the E-Shell is the most common configuration, variety of other designs, namely shell types F, G, H, J, K, and X, are used (Appendix A) [Palen, 1986].

1.4 Shell and Tube Heat Exchangers with E-Shell

The most common design of the shell-side of shell and tube heat exchangers is the E-shell due to its simplicity and its acceptable temperature driving force.

For instance, most shell and tube heat exchangers in nuclear power plants are one; two, or four pass designs on the tube side and have an E-shell design on the shell-side. Another example of E-shell design are steam turbine condensers.

Figure 1.8: Schematic configuration of E-Shell based on TEMA notation system.

Some typical TEMA shell and tube heat exchangers with E-shell design are shown in Figure 1.9.

(a) BEM shell and tube heat exchanger with one tube side pass

(b) BEM shell and tube heat exchanger with two tube side passes

(c) AEM shell and tube heat exchanger with two tube side passes

(d) AES shell and tube heat exchanger with split ring (floating head with backing device) and two tube side passes

Figure 1.9: Schematic representation of typical TEMA shell and tube heat exchangers with E-shell.

BEM shell and tube heat exchangers with fixed tube sheet are a standard choice with one or two tube side passes, as it is shown in Figures 1.9 (a) and (b). In order to clean the inside of the tubes, the front head piping must be unbolted and the heads must be removed. However, it is not possible to clean the outside surface of the tubes as these are inside the fixed part.

AEM design is very similar to BEM, but the removable cover allows the inside of the tubes to be inspected and cleaned. An AEM shell and tube heat exchanger is schematically illustrated in Figure 1.9 (c).

The AES design is excellent for applications where the difference in temperature between the hot and cold fluid causes unacceptable stresses in the axial direction of the shell and tubes. The floating head can move, i.e. provides the possibility to expand in the axial direction. For maintenance both the front and rear end head including the backing device, must be disassembled. An example of an AES shell and tube heat exchanger is shown in Figure 1.9 (d). Due to the importance of shell and tube heat exchangers with E-shell design, the present work will focus on the thermo-hydraulic behavior of this type, even though some results may be valid for other shell and tube heat exchanger as well.

2. Shell and Tube Heat Exchanger Design Methods

2.1 Performance of Heat Exchanger

The design of a heat exchanger involves a consideration of both, heat transfer rates between the fluids and mechanical pumping power expended to overcome fluid friction and move the fluids through the heat exchanger. For a heat exchanger operating with high density fluid, the friction power expenditure is generally small relative to the heat transfer rate. However, for low density fluids, such as gases, it is very easy to expend as much mechanical energy in overcoming friction power as is transferred as heat.

It can be readily shown that for most flow passages the heat transfer rate per unit of surface area can be increased by increasing fluid flow velocity. This rate varies as something less than the first power of the velocity. The friction power expenditure increases also with increasing flow velocity, but in this case the power varies by as much as the third power of the velocity and never less than the square [Kays and London, 1984].

If the friction power expenditure in a particular application tends to be high, the designer may reduce the velocities by increasing the number of flow passages in the heat exchanger. This will also decrease the heat transfer rate per unit of surface area, but according to the above relations the reduction in heat transfer rate will be considerably less than the friction power reduction. The lost heat transfer rate is then compensated by increasing the surface area like lengthening the tubes, which in turn also increases the friction power expenditure, but only in the same proportion as the heat transfer surface area is increased.

In gas flow heat exchangers the friction power limitations generally force the engineers to arrange the design for moderately low mass velocities. Low mass velocities, together with the low thermal conductivity of gases (compared to most liquids), results in a low heat transfer rate per unit of surface area. Thus a large amount of surface area becomes a typical characteristic of gas flow heat exchangers. Gas-to-gas heat exchangers may require up to 10 times of the surface area of liquid-to-liquid heat exchangers.

Summarizing the archetypical problem in heat exchanger design is to evaluate the thermal and pressure drop behaviour.

2.2 Basic Design Equations and Methods

The steady state overall adiabatic heat exchanger behavior can be presented in terms of dependent fluid outlet temperatures or as functions of four operating variables and three design controlled parameters:

$$
\underbrace{T_{hot,\,outlet},\ T_{cold,\,outlet},\ Q}_{\text{dependent variables}} = \phi\ (\ \underbrace{T_{hot,\,inlet},\ T_{cold,\,inlet},\ C_{hot},\ C_{cold}}_{\text{operating variables}},\ \underbrace{U,\ A,\ \text{flow arrangement}}_{\substack{\text{parameters under}\\\text{control of designer}}})
$$

$$\underbrace{\qquad\qquad\qquad\qquad\qquad}_{\text{independent variables and parameters}}$$

$$(2.1)$$

with C and U as heat capacity rate and overall heat transfer coefficient, respectively. Equation (2.1) contains six independent and one or more dependent variables for a given heat exchanger flow arrangement. Any independent variable and/or parameter in Equation (2.1) can be made dependent if unknown. In that case, one of the three dependent variables in Equation (2.1) becomes an independent variable and/or parameter. Thus the most general heat

exchanger design problem is to determine any two unknown variables from this set when the rest of them are known.

For heat exchanger analysis, it is difficult to understand and work with such a large number of variables and parameters as outlined in Equation (2.1). From dimensional analysis, three dimensionless groups are formulated from six independent and one or more dependent variables of Equation (2.1). The reduced number of nondimensional variables and parameters simplifies much of the analysis, provides a clear understanding of the performance behavior, and the results can be presented in more compact graphical and tabular forms. The specific form of these groups is to some extent optional.

Four such options have been used, depending on which method of heat transfer analysis has been selected: the effectiveness–number of heat transfer units method, the mean temperature difference (MTD) method, the nondimensional mean temperature difference–temperature effectiveness method and the generalised mean temperature difference method (GMTD) [Gardner, 1945; Kakaç, 1981; Bačlič, 1990; Hewitt, 1992; Bott, 1995; Oosthuizen, 1999; Sekulić, 1999; Hesselgreaves, 2001; Kraus and Aziz, 2001; Lienhard, 2002; Naterer, 2003; Nellis, 2003; Shah, 2003; VDI, 2006; Luben Cabezas-Gómez, 2007; Utamura, 2008].

2.3 Calculation of Shell-Side Heat Transfer Coefficient and Pressure Drop

The capital investment in heat exchangers throughout the world is exceedingly large and their maintenance and renewal are often costly hence proper initial design is an important economical consideration. Good design requires an accurate prediction of the pressure drop and heat transfer both inside and outside the tubes, in order that safety factors need not be made excessively large and that economic balances can be made between pumping and exchanger costs. Although satisfactory correlations are available for flow inside tubes, the status of information for flow across tube banks leaves much to be desired and therefore offers an attractive field for research.

Research on pressure drop and heat transfer coefficient for flow outside of tubes is restricted either to results for flow across single banks of tubes, or to selected results on the industrial type of baffled, cylindrical shell and tube heat exchanger.

In subsection 2.3.1, the correlations which evaluate the heat transfer coefficient and pressure drop of an ideal tube bank will be explained. An ideal tube bank can be defined as an unbaffled tube bank in which the tubes are arranged in-lined or staggered (in-lined arrangement refers to the tube layout Square 90°, while the staggered arrangements refer to the tube layouts Triangular 30°, Rotated triangular 60° and Square 45°, as it is illustrated in Figure 1.4) and the fluid flows across the tubes and normal to the tube lengths. Most of the correlations and methods which evaluate the heat transfer coefficient and pressure drop of a shell and tube heat exchanger are based on data and correlations valid for the ideal tube bank.

In subsection 2.3.2, the correlations and methods for prediction of shell-side heat transfer coefficient and pressure drop of shell and tube heat exchangers will be discussed.

Analytical and semi-analytical approaches have shown that these correlations can be presented in a general form as shown in Equation (2.2) [Achenbach, 1971; Eckert, 1972; Görtler, 1975; Shames, 1982; Hesselgreaves, 2001; Zlokarnik, 2002; Zwillinger, 2003]:

$$\Delta p = \frac{\rho u_{max}^2}{2} f(\text{Re}, f, \{X\}) \quad \text{and} \quad \text{Nu} = f\left(\text{Re}, \text{Pr}, f, \{X\}, \frac{\mu}{\mu_{wall}}\right) \qquad (2.2)$$

In Equation (2.2), {X} denotes a set of dimensionless geometrical parameters and f is the friction factor.

10

2.3.1 Heat Transfer and Pressure Drop for Unbaffled Tube Bank

Early studies of heat transfer and pressure drop done by U.S. and German sources go back to the 1910's and are usually based on ideal tube banks [Palen, 1986]. The heat transfer equations assumed the basic tube side form.

The pressure drop was correlated as a function of the maximum mass flux based on the minimum cross-sectional area in flow direction, total number of tube rows crossed by the flow and friction factor.

For studying the pressure drop in tube banks, substantial experimental contributions have been made by Huge [1937], Pierson [1937] and Ter Linden [1939]. Based on the data then available, general correlations for pressure drop and heat transfer coefficient of tube banks were presented [Chilton and Genereaux, 1933; Grimison, 1937; Jakob, 1938; Colburn, 1942; McAdams, 1942; Gunter and Shaw, 1945; Boucher and Lapple, 1948].

As part of a comprehensive research program on pressure drop and heat transfer on the shell-side of tubular heat exchangers, Bergelin et al. conducted experiments in the region of viscous flow on seven different ideal tube banks. The results were presented graphically and the correlations for pressure drop and heat transfer coefficient of ideal tube banks were recommended [Bergelin, 1950].

Kays, London and Lo studied heat transfer and flow friction for flow normal to ideal tube bank for six staggered tube layouts and one in-lined tube arrangement in laminar and turbulent domain. Data were also provided so that the influence of the longitudinal and transverse pitch and the number of tube rows on the mean coefficient may be estimated accurately. They presented graphically correlations for the heat transfer coefficient and the pressure drop as a function of Reynolds number [Kays, 1954].

Žukauskas analysed the pressure drop in a tube bank using the pressure drop around a single tube by comparing the separation angle of a single tube and the frontal tube in a bank with in-line arrangement [Žukauskas, 1972]. He recommended seven correlations for in-line arrangement and nine correlations for staggered tube layouts. Each correlation was defined for different Reynolds numbers based on the free stream velocity and the tube outside diameter as well as different longitudinal pitches.

Gnielinski presented a method for calculating the average heat transfer coefficient for a bank of tubes [Gnielinski, 1978]. The Reynolds number used in this method was modified to include the velocity of the fluid in the empty cross-section of the channel, the void fraction and the stream length. The method introduced by Gnielinski covers a wide range of experimental data obtained by different authors like Colburn, Grimison, Huge, Pierson, Bergelin, Kays et al., Bressler [1958] and Žukauskas. This method plays a significant role in the calculation of the shell-side heat transfer coefficient of shell and tube heat exchangers [VDI, 2006].

Martin introduced a new method based on the generalized Lévêque equation and discovered a new type of analogy between pressure drop and heat transfer that may be used in the corrugated channels of plate heat exchangers, in packed beds, in tube bundles and in many other space-wise periodic arrangements [Martin, 2002]. The author believes that this method can be proposed as the best available method to calculate the heat transfer coefficient of an ideal tube bank due to its simplicity and superb validity.

The abovementioned correlations and methods are the basic concepts to calculate the shell-side heat transfer and pressure drop of a shell and tube heat exchanger, since the core of the tube bundle in a shell and tube heat exchanger may be considered as an ideal tube bank. However, due to some other geometrical factors like the cylindrical shape of the shell, the gap between the tube bundle and the shell wall, the configuration of baffles and the effect of baffle windows, the presence of tube-baffle and baffle-shell leakages, various modifications have to be considered. In the following subsection, the correlations, methods and approaches which

may predict the shell-side heat transfer coefficient and pressure drop of practical shell and tube heat exchangers will be assessed.

2.3.2 Shell-Side Heat Transfer and Pressure Drop
The available methods for the prediction of shell-side heat transfer coefficient and pressure drop of shell and tube heat exchangers can be divided into five groups:
- The early developments based on flow over ideal tube banks or even single tubes.
- The analytical approach based on Tinker's multi stream model and his simplified method [Tinker, 1947].
- The stream analysis method, which utilizes a rigorous reiterative approach based on Tinker's model [Tinker, 1947; Serth, 2007].
- The Delaware method which uses the principles of the Tinker model but applies them on an overall basis without iterations [Bergelin, 1958].
- The integral approach, which recognizes baffled cross-flow modified by the presence of windows. Initially, treatment of the problem was on an overall basis without consideration of the modifying effects of leakages and bypass flows.

In the following, firstly the early model developments will be discussed in a few words. Secondly, the stream analysis of Tinker will be explained succinctly. This analysis will be explained in more detail in the subsequent chapters of the present work, where the effect of baffle cut and baffle orientation will be discussed. Then the Delaware method [Bergelin, 1958] will be outlined. Finally, the integral approach [VDI, 2006] will be explained.

•Early developments:
It was recognized in the early 1930's that baffled shell-side flow will behave similarly to flow across ideal tube banks. The first heat transfer correlation suggested is due to Colburn [1933]. The validity of this correlation was restricted to turbulent flow and staggered tube layout.
In 1937; based on the equation for ideal tube banks and Colburn's correlation, Grimison suggested a correlation which was modified to include the nonisothermal effects [Grimison, 1937]. For very quick estimations, Grimison's correlation may still be used due to its simplicity.

• Stream analysis method:
In the late 1940's it became obvious that baffled shell-side flow is so complex that it cannot be adequately expressed on a general basis by simple correlations and approaches [Emerson, 1963]. Only parts of the fluids take the desirable path through the tube nest, whereas a potentially substantial portion flows through the leakage and the bypass areas between tube bundle and the shell wall. However, these clearances are inherent to the manufacturing and assembly process of shell and tube exchangers, and the flow distribution within the exchanger must be taken into account.
The early analysis of the shell-side flow is based on the schematic flow pattern depicted in Figure 2.1. Tinker applied an analytical approach for the shell-side method and suggested a schematic flow pattern, where the shell-side flow is divided into a number of individual streams. The individual streams of the shell-side flow may be defined as follows:
- Stream A is the leakage stream in the orifice formed by the clearance between the baffle hole and tube wall.
- Stream B is the main effective cross-flow stream, which can be related to flow across ideal tube banks.
- Stream C is the tube bundle bypass stream in the gap between the bundle and the shell wall.
- Stream E is the leakage stream between the baffle edge and the shell wall.

12

- Stream F is the bypass stream in flow channel due to omission of tubes in tube pass partition. This stream has been appended to the original Tinker model [Palen and Taborek, 1969]. This stream behaves similarly to stream C, but will be present only in some tube layouts.
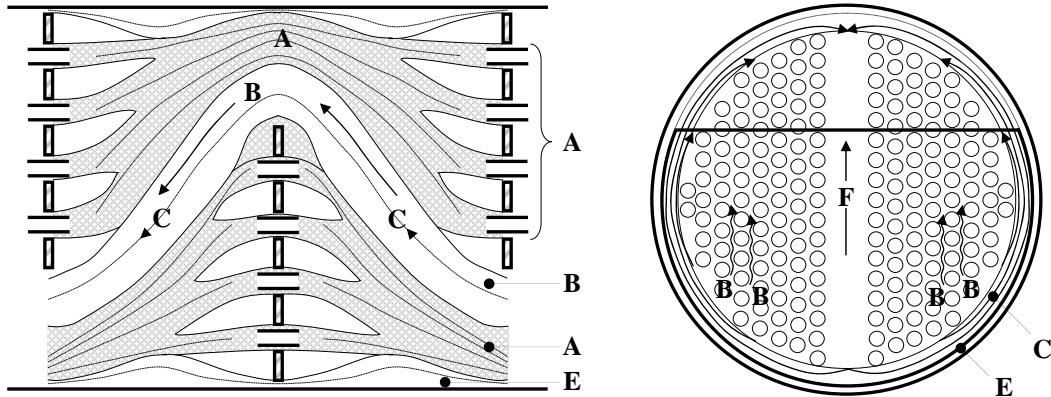
Figure 2.1: Flow paths of various streams through the shell of a cross-baffled shell and tube heat exchanger.

In principle the stream analysis states that the pressure drop of the cross-flow stream B will act as a driving force for the other streams, forcing part of the flow through the leakage and bypass clearances [Tinker, 1951 and 1958].

• Delaware method:
From 1947 to 1963 the Department of Chemical Engineering at the University of Delaware carried out a comprehensive research program on shell-side fluid flow and heat transfer in shell and tube heat exchangers, beginning with measurements of heat transfer and pressure drop during flow across ideal tube banks. These efforts were successively extended to introduce the various design features characteristic of shell and tube heat exchangers in commercial use. Sequentially, various baffle cuts and spacing configurations were investigated inside a cylindrical shell with no baffle leakage and minimal bypass clearance. Baffle leakages between baffles and shell, and between the tubes and baffles were added in later studies. Finally, bypass flow around the bundle between the outer tube limit and the shell inside diameter was studied together with the effect of sealing devices. The first and second report were published in 1950 [Bergelin, 1950] and 1958 [Bergelin, 1958], respectively, and in 1960 a preliminary design method for E shell exchangers was published [Bell, 1960]. The final report was published in 1963 [Bell, 1963]. The shell-side heat transfer coefficient is given by the following equation:

$$\begin{pmatrix} \text{shell-side heat} \\ \text{transfer coefficient} \end{pmatrix} = (J_c J_l J_b J_s J_r) \begin{pmatrix} \text{heat transfer coefficient} \\ \text{of an ideal tube bank} \end{pmatrix} \quad (2.3)$$

In Equation (2.3) the effect of baffle cut and spacing is shown by J_c. J_l represents the correction factor for baffle leakage, including both shell to baffle and tube to baffle leakages. J_b is the correction factor for the bypass flow and J_s is the correction for variable baffle spacing. J_r is the laminar heat transfer correction factor for adverse temperature gradient. This gradient lowers the local and the average heat transfer coefficient with increasing distance. The correction factor J_r has been worked out mathematically for flow in well defined geometries like inside the round tubes, but it is also found experimentally to exist during flow

13

across tube banks. For large heat exchangers in deep laminar flow, it can result in a decrease in the average heat transfer coefficient by a factor of two or more compare to what would have been predicted based on flow across a 10-row tube bank. This correction factor; J_r, applies only if the shell-side Reynolds number is less than 100 and is fully effective only in deep laminar flow characterized by shell-side Reynolds numbers less than 20.

The shell-side pressure drop is correlated as a linear function of the pressure drop in one cross flow section and the pressure drop in one baffle window section without leakage or bypass flow. However, in this correlation, three correction factors are considered for the effect of bypass flow, leakages, and also inlet and outlet zone on the pressure drop.

•Integral approach:

Donohue [1949] and Kern [1965] published shell-side methods based on overall data from baffled exchangers which assumed that the baffles are used to direct the shell fluid perpendicularly to the tubes. Due to the limited number of available data only an insufficient variation of basic geometrical parameters like baffle spacing, baffle cut and tube layout were presented. To overcome this deficiency, safety factors were introduced which lead to poor accuracies for the prediction of the shell-side heat transfer coefficient and pressure drop.

The Donohue method became quite popular for its simplicity while presenting a more systematic treatment than anything known before. The heat transfer correlation was based on a flow area that is the geometric mean between the minimum cross-flow area at the inside of the shell and the baffle window longitudinal flow area. The Nusselt equation has a form similar to Grimison's correlation, except for the above mentioned interpretation of the mass velocity. For pressure drop, a set of friction factor curves based on Grimison's work with a large safety factor was used. Even though Donohue's method represented a step in the right direction, being based on a non-systematic set of data, it provided up to several hundred percent over-prediction on pressure drop and heat transfer coefficient.

Kern's book was used as a virtual industrial standard for many years. The merits of Kern's method are not so much that better correlations are used, but rather in the way the overall design problem is approached as an entity, including numerous practical hints and calculated examples. Both heat transfer and pressure drop are presented for 25% baffle cut only, which is reasonably close to the best design. The length term in the Nusselt and Reynolds numbers is an equivalent diameter based on longitudinal flow projection, in order to account for the tube layout variations. No account is taken for variations in bypass or leakage areas. Pressure drop prediction are almost invariably on the safe side and usually more than 100%, whereas heat transfer may vary from slightly unsafe to very safe, because of the poor treatment of the bypass and leakage effects. The prediction accuracy decreases further in laminar flow, because very few data were available at that time and the simple method is not equipped to handle the complex problem. Although Kern's method cannot be recommended any more, many of the practical comments on design remain qualitatively valid.

Gnielinski and Gaddis [1977, 1978 and 1983] developed a method based on the integral approaches which is used for ideal tube banks, to evaluate the shell-side heat transfer coefficient and pressure drop. This method predicted a large number of experimental data with a good validity. Due to its systematic treatment and the acceptable validity, the VDI Wärmeatlas recommends this method [VDI, 2006]. Therefore, in the present work, this method will be termed as VDI method.

In the VDI method, the average shell-side Nusselt number $\overline{Nu}_{shell}$ is calculated as follows:

$$\overline{Nu}_{shell} = f_W Nu_{0, bank} \qquad (2.4)$$

14

The Nusselt number $Nu_{0, bank}$ and the average shell-side Nusselt number $\overline{Nu}_{shell}$ are based on the stream length $\pi d_o/2$ as characteristic length. All physical properties are calculated for average bulk temperature.

The correction factor f_W is a geometrical factor and has to be calculated as follows:

$$f_W = f_G f_L f_B \qquad (2.5)$$

In Equation (2.5) the correction factor f_W describes the effect of geometry on the heat transfer. The influence of baffle window or baffle cut is considered by the geometrical factor f_G. The effect of leakages is taken into account by considering the leakage-stream factor f_L and the bypass effect by considering the bypass-stream factor f_B.
f_G depends on the total number of tubes located in both upper and lower baffle windows, and the total number of tubes in the shell. f_L is a function of the total area of tube-baffle leakages and baffle-shell leakages, and the minimum free flow area in tube bundle. f_B depends on the number of pairs of sealing strips, the number of the tube rows located between the baffles, and the minimum free flow area in tube bundle.
Figure 2.2 presents the minimum free flow area in tube bundle for three tube layouts.
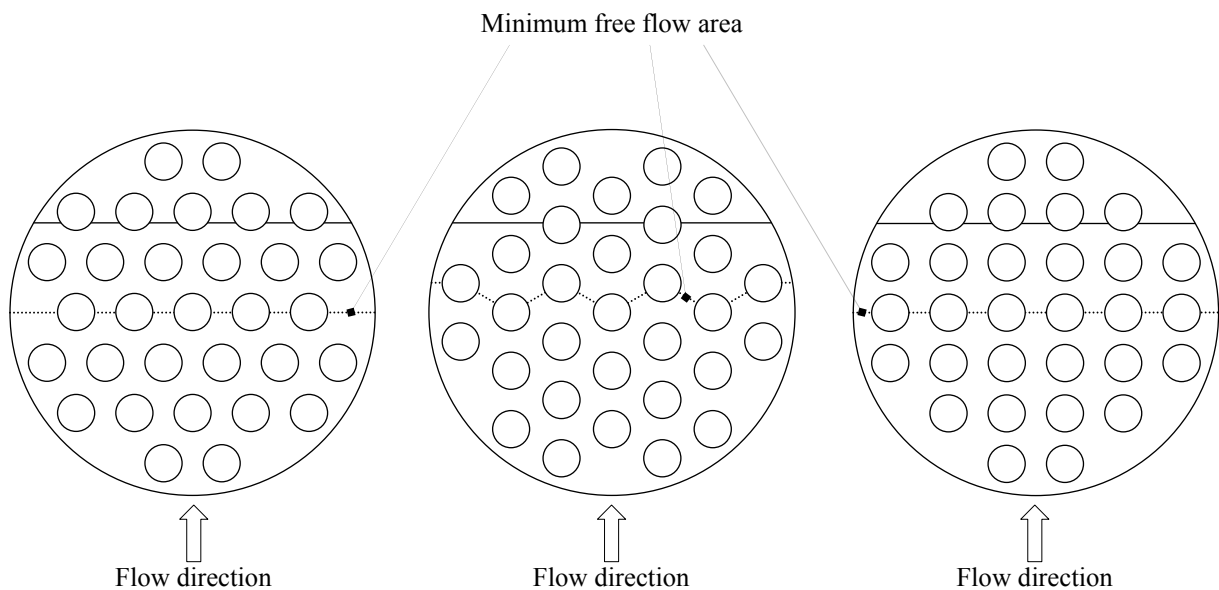
Figure 2.2: Definition of minimum free flow area for different tube layout in a shell and tube heat exchanger. The dotted lines represent this area.

The method recommended by VDI Wärmeatlas to calculate the pressure drop is based on the integration of different pressure drops in different domains consisting of inlet and outlet zones, inlet and outlet nozzles, baffle windows and the tube banks which are located between the baffle.

3. Limitation of Common Calculation Methods with Respect to the Effect of Baffle Orientation

3.1 Geometrical Difference in Baffle Orientation

It is well known that the inlet and outlet zones have a significant influence on the performance of a shell and tube heat exchanger due to the presence of nozzles. Therefore, it is valuable to study the effects of the end-zones on the shell-side heat transfer and pressure drop. In this study, only the inlet zone where the shell-side fluid enters the shell will be considered.

The horizontal and vertical baffle orientation is presented by case (a) and (b) in Figure 3.1. Even though the effect of the baffle orientation is not taken into account in the VDI and Delaware methods, due to the definition of flow direction and minimum cross-flow area, it is possible to calculate the shell-side heat transfer coefficient and pressure drop for both cases shown in Figures 3.1 and 3.2. In this case it is assumed that there is no leakage; which means that the leakage-stream factor f_L (see Equation (2.5) in subsection 2.3.2) in the VDI method is equal to 1. Depending on the orientation of baffles, the hypothetical flow direction defined for the VDI and Delaware methods is different. Because of this flow direction, the minimum cross-flow area will be different in case (a) and case (b) as it is shown by the dotted lines in Figure 3.2.

(a)   (b)
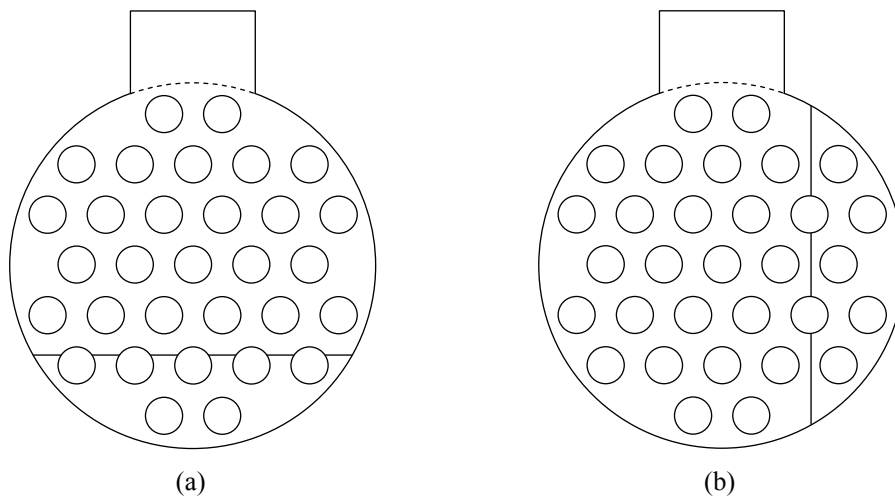
Figure 3.1: Inlet zone for two shell and tube heat exchangers. Case (a) and (b) represents the horizontal and vertical baffle orientation, respectively.

(a)   (b)
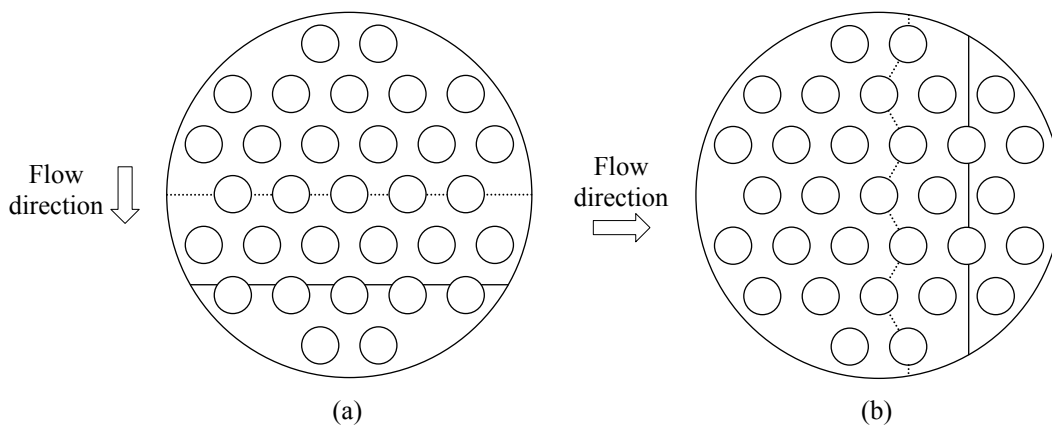
Figure 3.2: Hypothetical flow direction due to the presence of baffles according to the definition of VDI and Delaware methods for case (a) and case (b). The minimum cross-flow areas are shown by dotted lines.

The shell-side pressure drop and average Nusselt number are calculated at different Reynolds numbers for a typical shell and tube heat exchanger. The shell and tube heat exchanger considered is an ideal heat exchanger without leakages and consists of 660 tubes. The shell inside diameter is 23.3" and the tube outside diameter is ⅝". The tube layout is triangular 30° and the tube pitch is $^{13}/_{16}$". The baffle cut is 24% of the shell inside diameter. The shell-side fluid is water and the heat transfer process is heating.

Shell-side pressure drop and average Nusselt number versus modified Reynolds number calculated according to the VDI method are presented in Figures 3.3 and 3.4, respectively.

$$Re_\varphi = \frac{w\pi d_o}{2\varphi\nu}$$
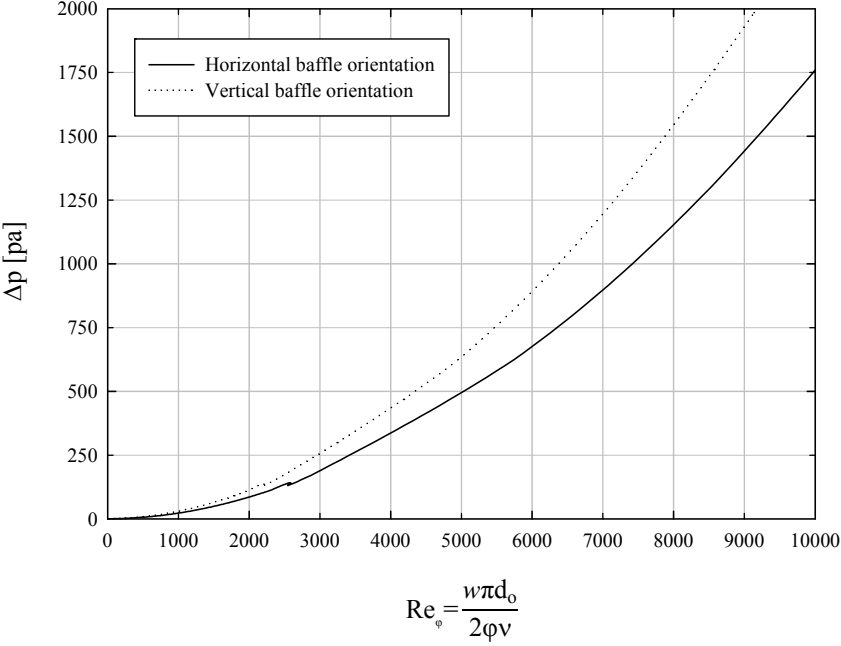
Figure 3.3: Shell-side pressure drop versus modified Reynolds number for horizontal and vertical baffle orientation and 24% baffle cut according to the VDI method. The shell-side fluid is water and the heat transfer process is heating.

$$Re_\varphi = \frac{w\pi d_o}{2\varphi\nu}$$
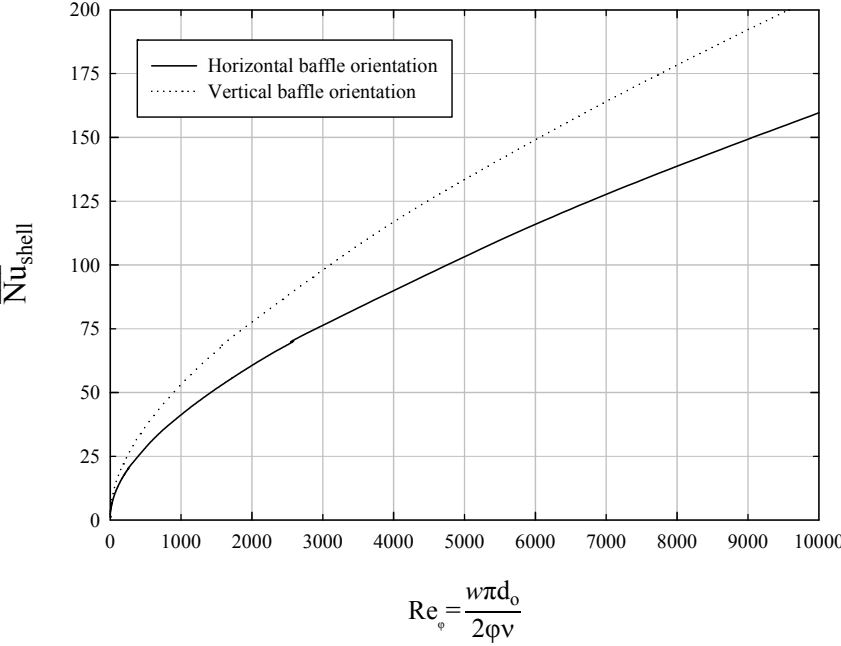
Figure 3.4: Average shell-side Nusselt number versus modified Reynolds number for horizontal and vertical baffle orientation and 24% baffle cut according to the VDI method. The shell-side fluid is water and the heat transfer process is heating.

18

Both shell-side pressure drop and average Nusselt number are calculated for horizontal and vertical baffle orientation. The shell-side pressure drop and heat transfer coefficient for the vertical baffle orientation is greater than the shell-side pressure drop and heat transfer coefficient for the horizontal baffle orientation, as it is shown in Figures 3.3 and 3.4.

The effect of baffle orientation on the pressure drop and heat transfer coefficient of the shell-side are analyzed by representing the values of the pressure drop ratio $\Delta p_{horizontal}/\Delta p_{vertical}$ and the Nusselt number ratio $(\overline{Nu}_{shell})_{horizontal}/(\overline{Nu}_{shell})_{vertical}$ at different Reynolds numbers. The Reynolds number is based on the conditions at the inlet nozzle.

$$Re_{inlet} = \frac{u_{inlet}D_n}{\nu} \tag{3.1}$$

In Equation (3.1) u_{inlet} and D_n is the fluid velocity at the inlet nozzle and the inside diameter of the inlet nozzle, respectively.

The shell-side pressure drop ratio $\Delta p_{horizontal}/\Delta p_{vertical}$ versus Re_{inlet} is plotted in Figure 3.5.
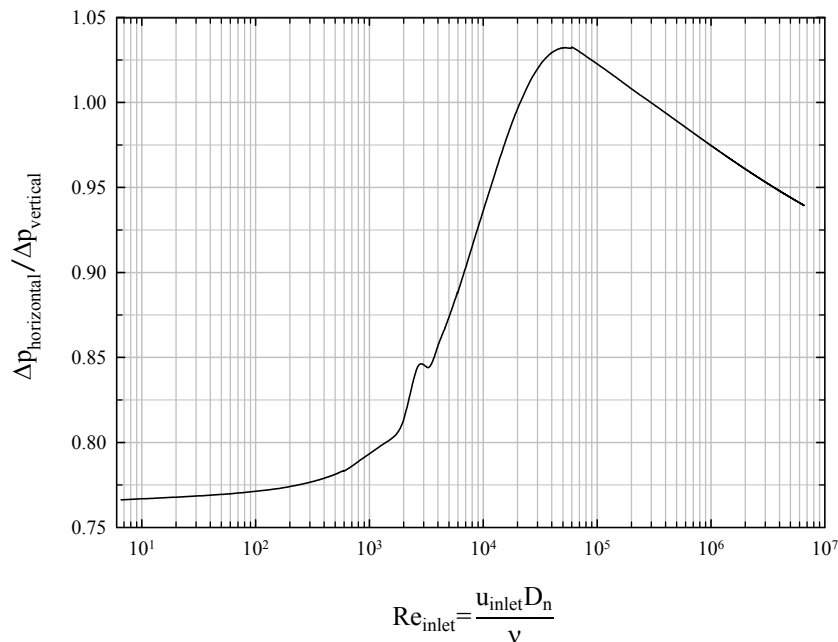
Figure 3.5: $\Delta p_{horizontal}/\Delta p_{vertical}$ versus Re_{inlet} for 24% baffle cut according to the VDI method. The shell-side fluid is water and the heat transfer process is heating.

Figure 3.5 indicates that the shell and tube heat exchanger with vertical baffle orientation presents higher pressure drop than that with horizontal baffle orientation. A comparable behavior for the heat transfer coefficient should be expected due to the analogy between the pressure drop and the heat transfer coefficient. The local maximums of graph in Figure 3.5 are due to the mathematical formulation presented in VDI heat atlas [VDI, 2006].

Figure 3.6 represents the shell-side Nusselt number ratio $(\overline{Nu}_{shell})_{horizontal}/(\overline{Nu}_{shell})_{vertical}$ as a function of Re_{inlet}.

The shell-side pressure drop behaviour according to the Delaware method corresponds with the VDI method. However, the value of $(\overline{Nu}_{shell})_{horizontal}/(\overline{Nu}_{shell})_{vertical}$ is equal to 1 for all Reynolds numbers according to the Delaware method.
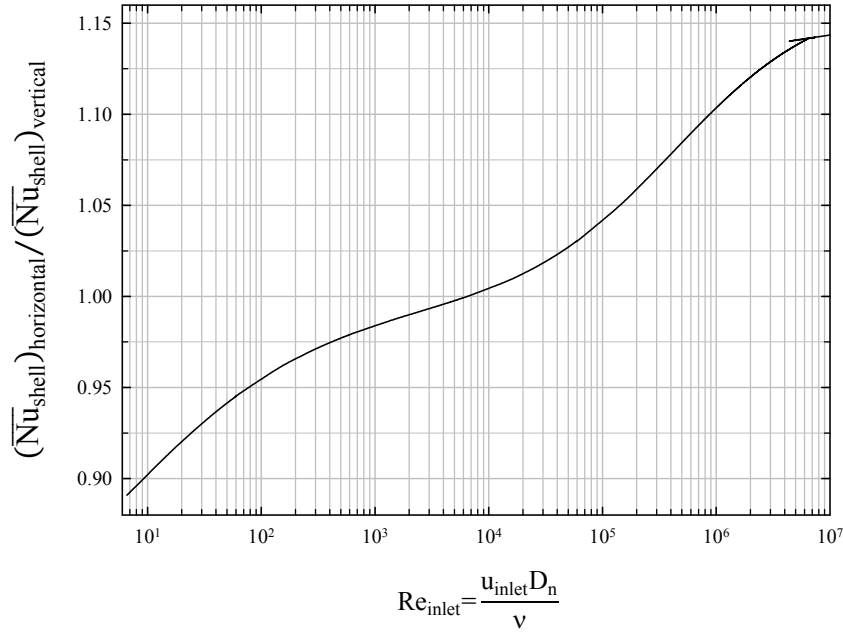
Figure 3.6: $(\overline{Nu}_{shell})_{horizontal}/(\overline{Nu}_{shell})_{vertical}$ versus Re_{inlet} for 24% baffle cut according to the VDI method. The shell-side fluid is water and the heat transfer process is heating.

3.2 Definition of Baffle Orientation

The baffle orientation is not a flow property, but a geometrical characteristic which declares the orientation of the baffles with respect to the nozzles. Therefore, it is important to state clearly and mathematically the definition of the baffle orientation.
In order to define the baffle orientation of a heat exchanger, reference planes and vectors are introduced as given in Figure 3.7.

- The "baffle-orientation-plane" is parallel to the tube-bundle axis and touches the baffle edge.
- The "inlet (outlet)-plane" contains the inlet (outlet) area of the inlet (outlet) nozzle.
- The "tube-sheet-plane" contains the tube-sheet at the inlet zone.
- "Face-vectors" are normal to the planes considered and directed to the centre of the shell.
- The "baffle-vector" is normal to the baffle-orientation-plane and directed towards the outside of the shells.

The description of the abovementioned system will be in Cartesian coordinates with y-axis being in opposite direction of the face-vector of the inlet-plane and z-axis in direction of the face-vector of the tube-sheet-plane. If $\vec{j}$ and $\vec{k}$ denote the unit vectors of y and z axes, respectively, the positive direction of x-axis can be found by its unit vector $\vec{i}$ according to the following equation:

$$\vec{i} = \vec{j} \times \vec{k} \qquad (3.2)$$

In the x-y plane of this Cartesian coordinates, the counter-clockwise angle between the "baffle-vector" and the "face-vector" of the "inlet-plane" characterizes the baffle orientation in each baffle zone.
In the typical sketch shown in Figure 3.7, $\angle$("baffle-vector", "face-vector" of "inlet-plane") represents the counter-clockwise angle between the "baffle-vector" and the "face-vector" of the "inlet-plane".

20

In the present work two different baffle orientations will be considered: horizontal and vertical. In the heat exchanger with horizontal baffle orientation, $\angle$("baffle-vector", "face-vector" of "inlet-plane") at the inlet and outlet zone is equal to 0º, and at the central baffle spacing zones is equal to 180º or 0º. In the heat exchanger with vertical baffle orientation, $\angle$("baffle-vector", "face-vector" of "inlet-plane") at the inlet and outlet zone is equal to 270º, and at the central baffle spacing zones is equal to 90º or 270º.

Now it is possible to define the horizontal and vertical baffle orientation by use of a set of angles. Thereby the first angle refers to the inlet zone, the second angle refers to the first central baffle spacing zone and ditto. The last angle refers to the outlet zone.

Figure 3.8 represents schematically two E type shell and tube heat exchangers with three central baffle spacing zones. Using the aforementioned definition, the shell and tube heat exchanger with horizontal baffle orientation (see Figure 3.8) has a set of angles $\angle=\{0°,180°,0,180°,0°\}$. In the same manner, the shell and tube heat exchanger with vertical baffle orientation presented in Figure 3.8, has a set of angles $\angle=\{270°,90°,270°,90°,270°\}$.

The abovementioned mathematical definition could be considered as an appropriate method to define the other baffle orientations for a segmentally baffled shell and tube heat exchanger.
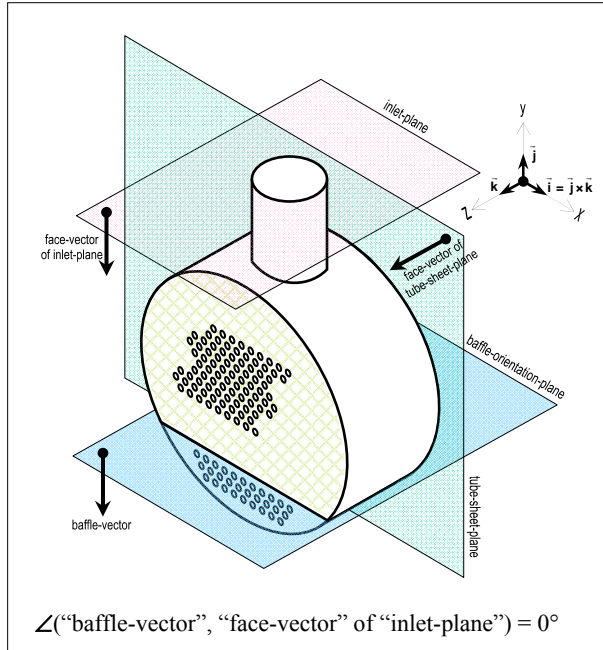
Figure 3.7: System definition of Cartesian coordinates, baffle orientation and outlet nozzle arrangement

3.3 Minimum Shortcut Distance

The residence time of the working fluid in the inlet zone of the shell and tube heat exchanger depends on baffle orientation, baffle cut, and number of tubes.

The comparison of residence times of the inlet zone of two shell and tube heat exchangers with identical number of tubes and baffle cut but with different baffle orientation is done by contrasting the rectilinear distance between the inlet nozzle and the baffle window of these two inlet zones. In the present work, the rectilinear distance between the inlet nozzle and the baffle window will be termed as minimum shortcut distance (MSD). Since there are infinite numbers of MSDs, it is meaningful to present an average or normalized distance. Figure 3.9 illustrates the variables used to calculate the normalized minimum shortcut distance (NMSD). Equation (3.3) presents the integral form of NMSD based on the variables shown in Figure 3.9.

$$\text{NMSD} = \frac{\int_{\Theta_{min}}^{\Theta_{max}} \text{MSD}(\Theta)\,d\Theta}{\int_{\Theta_{min}}^{\Theta_{max}} d\Theta} \tag{3.3}$$
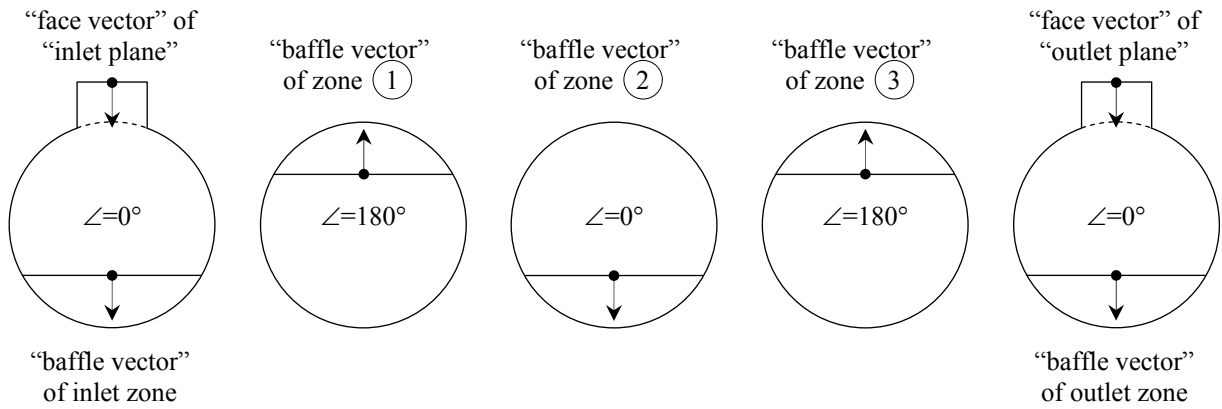
(a) E type shell and tube heat exchanger with horizontal baffle orientation: $\angle = \{0°,180°,0°,180°,0°\}$.
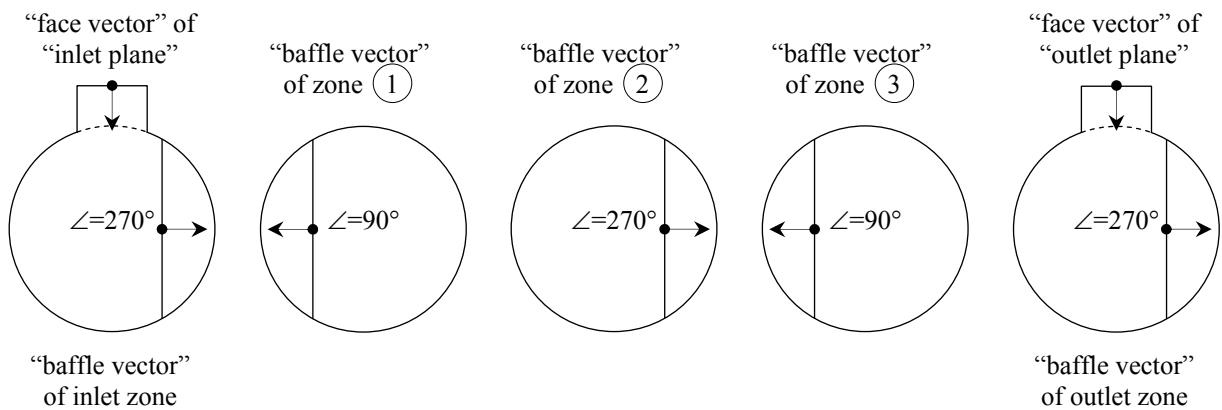
(b) E type shell and tube heat exchanger with vertical baffle orientation: $\angle = \{270°,90°,270°,90°,270°\}$.

Figure 3.8: Presentation of E type shell and tube heat exchanger with three central baffle spacing zones and two different baffle orientations: (a) horizontal baffle orientation and (b) vertical baffle orientation. The value presented in $\angle$ refers to the counter-clockwise angle between the presented vectors and the "face-vector" of the "inlet-plane".
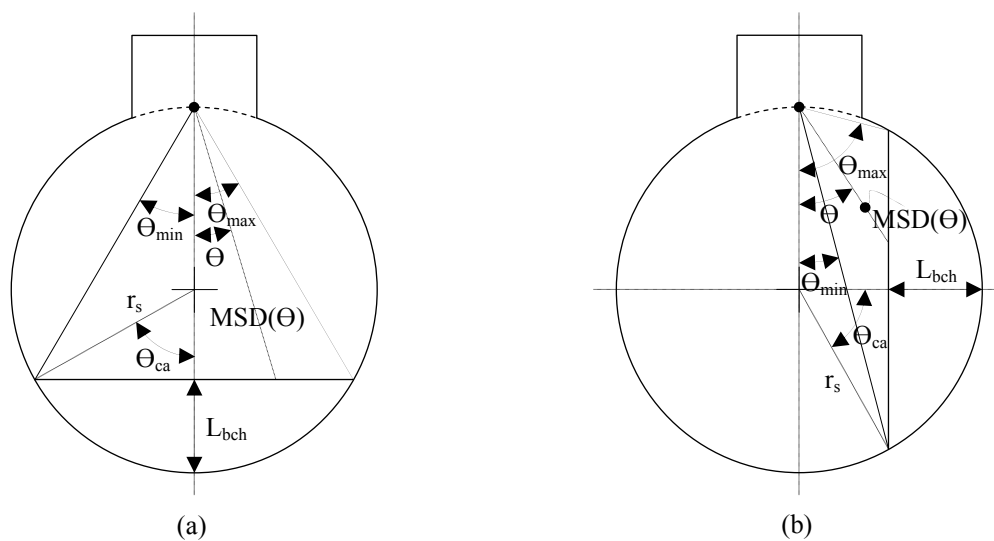
Figure 3.9: The variables used to calculate the normalized minimum shortcut distance or NMSD for the inlet zone. Case (a) and (b) represents the horizontal and vertical baffle orientation, respectively.

22

The integral form above is solved and expressed as a function of Θ_{ca}. Θ_{ca} is the centri-angle of the baffle cut intersection with the inside shell wall, and depends on the baffle cut height L_{bch} and the shell inside radius r_s.

$$\Theta_{ca}= \arccos\left(\frac{r_s-L_{bch}}{r_s}\right)=\arccos\left(1-\frac{B_C}{50}\right) \tag{3.4}$$

In Equation (3.4), B_C is the segmental baffle cut percentage.

$$B_C=50\frac{L_{bch}}{r_s} \tag{3.5}$$

The mathematical function of NMSD for horizontal and vertical baffle orientation is given by the following equations:

$$(NMSD)_{horizontal}=\frac{2\sin\Theta_{ca}}{\Theta_{ca}\tan\left(\Theta_{ca}/2\right)}\ln\left[\sec\left(\Theta_{ca}/2\right)+\tan\left(\Theta_{ca}/2\right)\right]r_s \tag{3.6}$$

$$(NMSD)_{vertical}=\frac{\cos\Theta_{ca}}{\Theta_{ca}}\ln\left[\frac{1+\sin\Theta_{ca}+\sqrt{2(1+\sin\Theta_{ca})}}{1-\sin\Theta_{ca}+\sqrt{2(1-\sin\Theta_{ca})}}\right]r_s \tag{3.7}$$

The comparison between $(NMSD)_{horizontal}$ and $(NMSD)_{vertical}$ is done by introducing the normalized minimum shortcut distance ratio or NMSDR.

$$NMSDR=\frac{(NMSD)_{horizontal}}{(NMSD)_{vertical}}=\frac{4}{1-\tan^2\left(\Theta_{ca}/2\right)}\frac{\ln\left[\sec\left(\Theta_{ca}/2\right)+\tan\left(\Theta_{ca}/2\right)\right]}{\ln\left[\frac{1+\sin\Theta_{ca}+\sqrt{2(1+\sin\Theta_{ca})}}{1-\sin\Theta_{ca}+\sqrt{2(1-\sin\Theta_{ca})}}\right]} \tag{3.8}$$

Figure 3.10 represents the plot of NMSDR versus B_C for segmental baffle cut percentage less than 45. Figure 3.10 confirms that the value of NMSD for horizontal baffle orientation is greater than the value of NMSD for vertical baffle orientation. Therefore, the residence time in a shell and tube heat exchanger with horizontal baffle orientation is more than the residence time in a shell and tube heat exchanger with vertical baffle orientation. This means that a shift in baffle orientation from vertical to horizontal will increase the mixing level and consequently the rate of heat transfer and the value of pressure drop. Hence, the ratio of $(\overline{Nu}_{shell})_{horizontal}/(\overline{Nu}_{shell})_{vertical}$ shown in Figure 3.6 seems to be rational, at least for $Re_{inlet}\gtrsim 6\times 10^3$. However, the behaviour of $\Delta p_{horizontal}/\Delta p_{vertical}$ represented in Figure 3.5 is not logical.

It is important to restate the assumption of no leakages in the aforementioned analysis. However, the concept of NMSDR is useful to explain the effect of baffle orientation on performance of a real shell and tube heat exchanger with leakage streams.
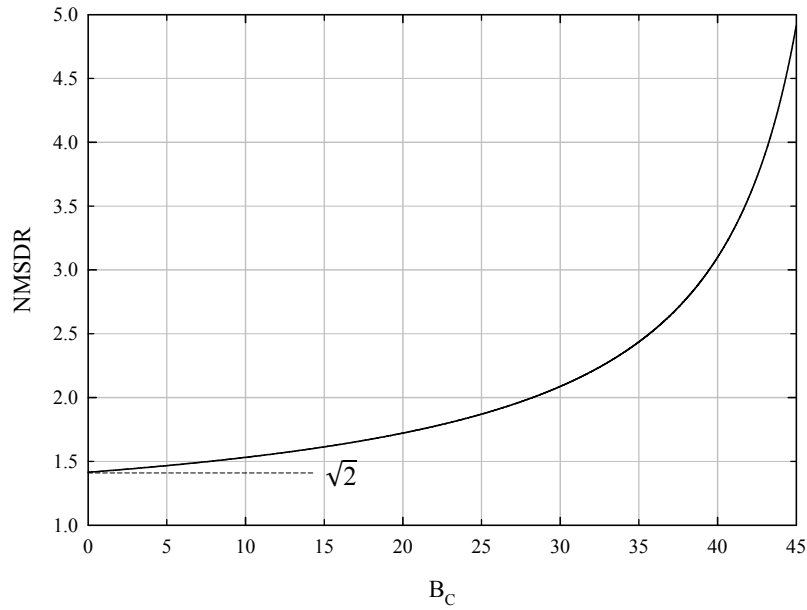
Figure 3.10: NMSDR versus B_c for baffle cuts less than 45% of shell inside diameter. This graph shows that the value of NMSD for horizontal baffle orientation is greater than the value of NMSD for vertical baffle orientation.

3.4 The Necessity of the Investigation of the Effect of Baffle Orientation

The discussions in Sections 3.1 and 3.3 confirm that the effect of baffle orientation is not taken into account yet. In fact, all the available investigations and methods are only based on one baffle orientation, namely horizontal.

Moreover, NMSDR shows that both heat transfer and pressure drop will increase when the baffle orientation changed from horizontal to vertical. Therefore, it is important to investigate the effect of baffle orientation on the performance of shell and tube heat exchangers.

4. Application of CFD for the Present Heat Exchanger Investigations

The technological value of computational fluid dynamics (CFD) has become undisputed in the last decade. CFD allows to compute flows that can be investigated experimentally only at reduced Reynolds numbers, or at greater cost, or not at all. Another significant feature of CFD is to evaluate and quantify the data in a high level of details without changing the geometry. This is similar to an ideal experimental method in which measuring all the required data without inserting or installing a set of measurement devices is possible. Measuring the necessary data in a high level of detail without changing the real geometry is an ultimate tool in research and development [Ferziger, 2002].

A distinguishing feature of the present state of computational fluid dynamics is that large commercial CFD codes have arisen, and have found widespread use in industry.

One of the most powerful commercial CFD tools is the state-of-the-art computer program Fluent which offers different and suitable solutions and models and provides valuable geometrical tools for modelling fluid flow and heat transfer in complex geometries [Fluent, 2008]. In the present work, Fluent is applied as CFD tool for the heat exchanger investigations.

4.1 Model Characteristics

In order to build up a CFD model, it is necessary to find a suitable spatial discretization for the geometrical calculation domain which is in the present work the shell-side geometry of the considered shell and tube heat exchanger.

Based on the requirement to reduce numerical errors (numerical diffusion, mesh independence and the alignment of the mesh elements with the main flow direction), the applied mesh scheme is a conformal, non-hybrid, structured mesh, that is, a grid scheme with quadrilateral-faced hexahedral elements [Thompson, 1985; Ruppertt, 1995; Wesseling, 2001; Russell, 2002; Shewchuk, 2005]. A brief description of some important features of this grid scheme is given in the following subsections 4.1.1 and 4.1.2.

4.1.1 Mesh Qualification

The mesh quality has a considerable impact on the computational analysis in terms of the quality of the solution and the required computational time.

The evaluation of the quality of the mesh is very useful because it provides some indication of how suitable a particular discretization is for the analysis type under consideration [Babuska and Aziz, 1976; Křížek, 1992].

For the present work two quality ratios have been applied namely the aspect ratio which defines the dilation of a mesh element and the equiangular skewness which measures the skewness of a mesh element.

For hexahedral elements, the aspect ratio Q_{AR} is defined as:

$$Q_{AR} = \frac{\max\{l_i\}}{\min\{l_i\}} \tag{4.1}$$

where l_i is the average length of the edges in a coordinate direction i local to the element. $Q_{AR}=1$ describes an equilateral element. However, the mesh structure for the shell-side of a medium size heat exchanger could have mesh elements with aspect ratio up to 15.

The equiangular skewness, or EquiAngle, is a normalized measure of the distortion of a mesh element. For hexahedral elements, the EquiAngle skewness Q_{EAS} is expressed as follow:

$$Q_{EAS} = \max \left\{ \frac{2\vartheta_{max}\text{-}\pi}{\pi}, \frac{\pi\text{-}2\vartheta_{min}}{\pi} \right\} \qquad (4.2)$$

where ϑ_{max} and ϑ_{min} are the maximum and minimum angle in radian between the edges of a element, respectively. A hexahedral element with $Q_{EAS}=0$ is a cuboid, while $Q_{EAS}=1$ describes a completely degenerate element. In general, high quality three dimensional meshes contain elements which show an average Q_{EAS} value of 0.4 [Gambit, 2007].

4.1.2 Determination of Mesh Size and Structure
The required computational memory for solving the governing equations (see section 4.2) at each mesh element is about 1.5 Kbyte [Fluent, 2008]. Hence, the maximum number of elements which can be solved is about 1,400,000, since the available computational memory for the present work is limited to 2GB.

A midsize heat exchanger with one tube pass typically consists of about 500 tubes. Hence the question has to be answered how it is possible to mesh the shell-side inlet zone of a medium size shell and tube heat exchanger with 1,400,000 quadrilateral-faced hexahedral elements.

For this reason, preliminary grid investigations for different ideal (without leakages) shell and tube heat exchangers (baffle cut 15%, horizontally orientated baffles, triangular tube layout 30°) are carried out. For a shell and tube heat exchanger consisting of 140 tubes (tube outside diameter 19.05 mm, shell inside diameter 304.8 mm), source faces are introduced in order to mesh the inlet zone. Figure 4.1 (a) represents schematically the inlet zone of the heat exchanger with 140 tubes. The source faces are two-dimensional surfaces between the tubes which construct the tube sheet. Figure 4.2 (a) shows a typical source face. The source faces are meshed using a quad-pave meshing scheme in a manner that the 2D aspect ratio of cells will be around 1, and at least 10 elements will be located between two adjacent tubes. This ensures the compatibility of the mesh structure with the turbulent flow. Figure 4.2 (b) represents a meshed source face. Figure 4.1 (b) shows a part of the meshed tube sheet obtained by juxtaposing the meshed source faces.

Finally, the cooper mesh scheme is applied in order to generate the three dimensional mesh for the inlet zone. In the cooper scheme, the meshed source faces are swept along the tube length with a certain extrusion number or size. The quad-faced hexahedral elements of the 3D mesh structure have an aspect ratio less than 2 and the maximum EquiAngle skewness equal to 0.53. The application of the mesh procedure described results in 60,000,000 mesh elements for the inlet zone of the shell and tube heat exchanger with 140 tubes.

The same meshing procedure as described for the heat exchanger with 140 tubes is applied for the grid generation for the inlet zone of two smaller ideal heat exchangers with 10 and 24 tubes, respectively (see Figures 4.3 and 4.4). The baffle cut, the baffle orientation and the tube layout are identical with heat exchanger with 140 tubes. The tubes outside diameter and the shell inside diameter are 16 mm and 90 mm for the heat exchanger with 10 tubes and 19.05 mm and 205 mm for the heat exchanger with 24 tubes. The resulting mesh structures contain 1,200,000 and 1,500,000 elements for the heat exchangers with 10 and 24 tubes, respectively. About 99.6% of the mesh elements of both grids have an EquiAngle skewness less than 0.5.

The number of 3D elements required for meshing the inlet zone can be expressed as a function of the tube number, as it can be concluded from the mesh structure generated for the inlet zone of the heat exchangers with 140, 10 and 24 tubes. The function that will estimate the number of mesh cells is named as the mesh number estimation function or MNEF. Besides the tube number, MNEF depends on the shell inside diameter, the number of 2D elements between two adjacent tubes, the 2D and the 3D aspect ratios. In Figure 4.5 the curves of MNEF as a function of the tube number with the shell inside diameter as a

parameter are depicted. In Figure 4.5, the 2D and 3D aspect ratios are 2 and 4, respectively, and the number of mesh elements between two adjacent tubes is 10.

<div align="center">(a)   (b)</div>
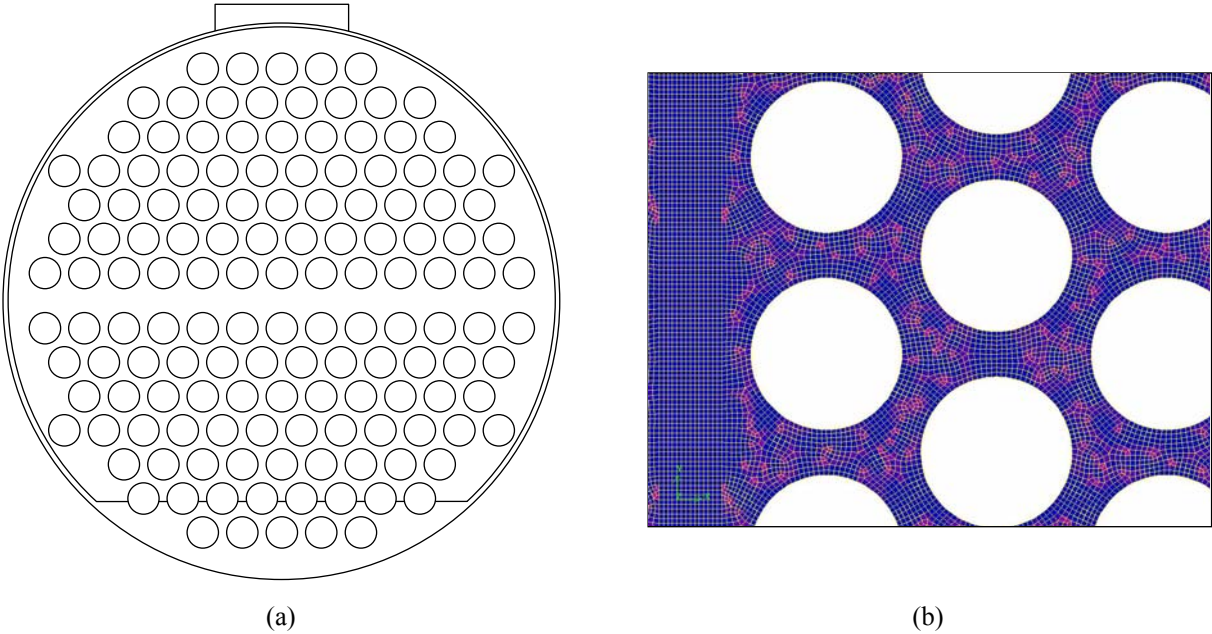
Figure 4.1: TEMA shell and tube heat exchanger with 140 tubes: (a) inlet zone (b) two dimensional mesh structure. 10 elements are located between two adjacent tubes. The 2D aspect ratio is about 1. Approximately, 99.7% of elements have the EquiAngle skewness less than 0.3, and the rest of elements have the skewness less than 0.53. The elements with blue colour have the best skewness, i.e. 0, and the red elements have the maximum skewness, 0.53.

<div align="center">(a)   (b)</div>
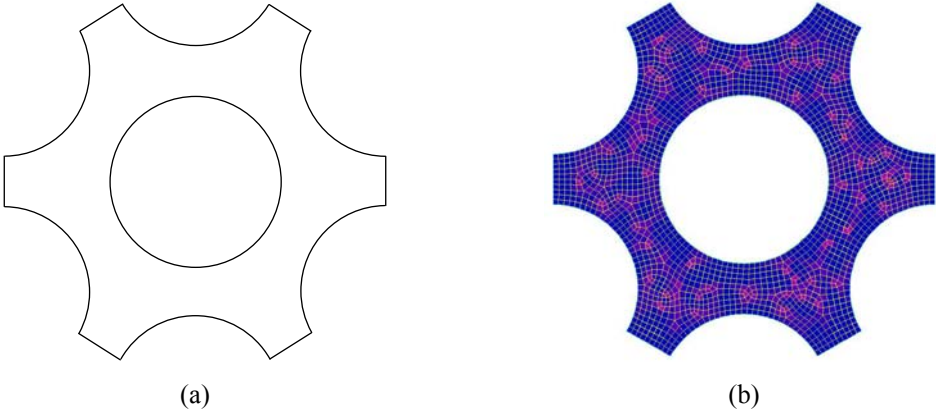
Figure 4.2: Basic two dimensional surface: (a) source face (b) meshed source face using the pave scheme.

The analysis of MNEF for the TEMA shell and tube heat exchangers shows that the value of MNEF is proportional to the square of the tube number, the cube of the number of 2D elements between two adjacent tubes, and the inverse of the 2D and 3D aspect ratios.

<div align="right">27</div>
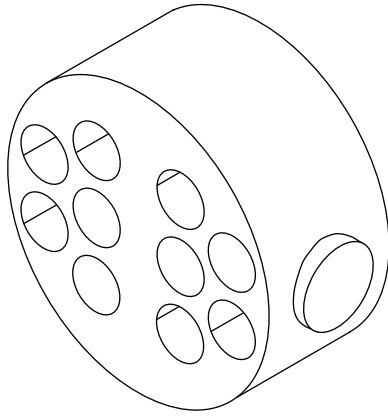
Figure 4.3: Inlet zone of a shell and tube heat exchanger with 10 tubes.
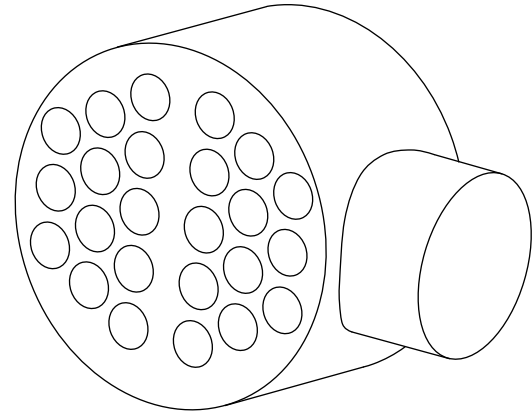
Figure 4.4: Inlet zone of a shell and tube heat exchanger with 24 tubes.
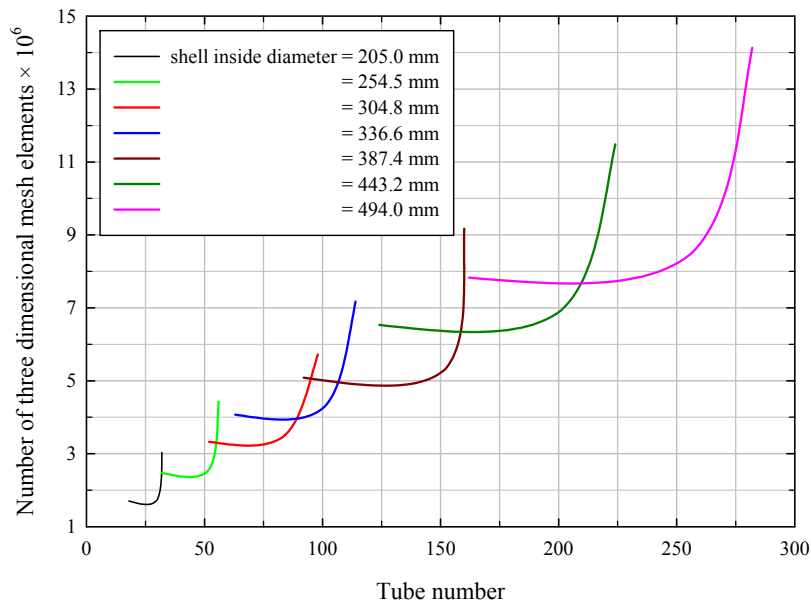
Figure 4.5: Estimated number of three dimensional elements required for meshing the inlet zone versus tube number. The tube layout is triangular 30°. The number of cells between two adjacent tubes is 10 and the 2D and 3D aspect ratios are about 2 and 4, respectively.

Considering Figure 4.5, the only way to mesh the inlet zone of a medium size shell and tube heat exchanger with 1,400,000 cells hence is to reduce the number of elements between tubes and to increase the 2D and 3D aspect ratios. A simple analysis on MNEF shows that the inlet zone of an ideal shell and tube heat exchanger consisting of around 600 tubes can be meshed with 1,200,000 cells by inserting 8 elements between two adjacent tubes and by applying the 2D and 3D aspect ratios equal to 10 and 15, respectively. This will be presented and discussed in chapter 5.

4.2 Numerical Model

4.2.1 Governing Equations
In a steady state study, as the present work, CFD uses basically the Eulerian formulation for analysis and computation. That is, the conservation equations will be solved at every fixed

point of the domain. The steady state governing equations in the Cartesian coordinate are as follows [Ferziger, 2002; Fluent, 2008]:

$$\vec{\nabla}\cdot(\rho\vec{u})=0 \qquad (4.3)$$

$$\vec{\nabla}\cdot(\rho u_i\vec{u})=-\frac{\partial}{\partial x_i}\left(p+\frac{2}{3}\mu\vec{\nabla}\cdot\vec{u}\right)+\vec{\nabla}\cdot\left[\mu\left(\frac{\partial u_i}{\partial x_j}+\frac{\partial u_j}{\partial x_i}\right)\vec{i}_j\right] \qquad (4.4)$$

$$\frac{\partial}{\partial x_i}\left[u_i\left(\rho e_s+\rho\frac{u_i^2}{2}\right)\right]=\frac{\partial}{\partial x_i}\left[(k_f+k_{f,turb})\frac{\partial T}{\partial x_i}+u_j(\mu+\mu_{turb})\left(\frac{\partial u_i}{\partial x_j}+\frac{\partial u_j}{\partial x_i}-\frac{2}{3}\frac{\partial u_j}{\partial x_j}\right)\right] \qquad (4.5)$$

Equation (4.3) is the continuity or mass conservation equation. Equation (4.4) is the momentum conservation equation in the direction i of the non-accelerating Cartesian frame for Newtonian fluids and without body forces. In Equation (4.4), $\vec{i}_j$ represents the Cartesian unit vector in the direction of the coordinate x_j. Equation (4.5) describes the energy equation for a one-component fluid in the direction i of the Cartesian coordinate. In Equation (4.5) e_s is the sensible enthalpy, $k_{f,turb}$ is the turbulent thermal conductivity and μ_{turb} is the turbulent or eddy viscosity.

4.2.2 Turbulence
The Reynolds stress model (RSM), the standard k-ω model, the renormalization group k-ε (RNG k-ε), the realizable k-ε and the standard k-ε models are the most suitable turbulence models for the present work [Wilcox, 1998; Ferziger, 2002; Fluent, 2008]. Compared with the k-ε models, the RSM requires additional memory and CPU time due to the increased number of transport equations for Reynolds stresses. On average, the RSM requires 50-60% more CPU time per iteration and 15-20% more memory compared to the k-ε models [Fluent, 2008]. In order to find the difference between the RSM, the k-ω and the k-ε models, the inlet zone of the shell and tube heat exchanger shown in Figure 4.4 is meshed and then solved by applying different turbulence models. The comparison between the final results of the RSM, the k-ω and the k-ε models does not show any significant qualitative and quantitative difference. However, the k-ε models are more satisfactory since the k-ω model are fairly new and have not been examined as well as the k-ε models. Moreover, the RSM needs more memory than k-ε models.
Both the realizable and RNG k-ε models have shown substantial improvements over the standard k-ε model where the flow features include strong streamline curvature, vortices, and rotation. However, the realizable k-ε model is still relatively new and it is not clear in exactly which instances the realizable k-ε model consistently outperforms the RNG model. On the other hand, the RNG theory provides an analytically-derived differential formula for effective viscosity that accounts for low-Reynolds-number effects [Fluent, 2008]. Hence, the RNG k-ε model is the preferred turbulence model implemented in the present work.

4.2.3 Near Wall Treatment of the Flow
Turbulent flows are significantly affected by the presence of walls. Obviously, the mean velocity field is affected through the no-slip condition that has to be satisfied at the wall. However, the turbulence is also changed by the presence of the wall in non-trivial ways. Very close to the wall, viscous damping reduces the tangential velocity fluctuations, while kinematic blocking reduces the normal fluctuations. Toward the outer part of the near-wall region, however, the turbulence is rapidly augmented by the production of turbulence kinetic energy due to the large gradients in mean velocity [Bradshaw, 1971; Tennekes, 1972].

Numerous experiments have shown that the near-wall region can be largely subdivided into three layers. In the innermost layer, called the viscous sublayer, the flow is almost laminar, and the molecular viscosity plays a dominant role in momentum and heat or mass transfer. In the outer layer, called the fully-turbulent layer, turbulence plays a major role. Finally, there is an interim region between the viscous sublayer and the fully turbulent layer where the effects of molecular viscosity and turbulence are equally important. This interim region is called blending region or buffer layer. The important parameter to distinguish the different viscous layers in a flow is the dimensionless sub-layered distance y^+. The value of y^+ depends on the friction velocity u_τ. The friction velocity u_τ is defined as $\sqrt{\tau_W/\rho}$ where τ_W is the surface or wall shear stress. The friction velocity can be interpreted as the disturbance velocity induced by shear stress of the solid walls. The subdivisions of the near-wall region can be presented as the plot of u/u_τ versus y^+ in a semi-log coordinates [Kutateladze, 1964].

One common approach to model the near-wall region is the usage of so-called "wall functions". In doing so, the viscosity-affected inner region, i.e. viscous sublayer and buffer layer, is not resolved. Instead, semi-empirical formulas called "wall functions" are used to bridge the viscosity-affected region between the wall and the fully-turbulent region. The use of wall functions obviates the need to modify the turbulence models to account for the presence of the wall.

Depending on the turbulence model, three choices of wall function approaches are available: standard wall functions which are based on the proposal of Launder and Spalding, non-equilibrium wall functions, and enhanced wall treatment [Kutateladze, 1964; Launder and Spalding, 1974; Kader, 1981; Fluent, 2008]. Since both non-equilibrium wall functions and enhanced wall treatment require sufficiently fine mesh structure near the walls, the standard wall functions is implemented in the present work.

5. Effect of Baffle Orientation, Baffle Cut and Fluid Viscosity on Pressure Drop and Heat Transfer Coefficient in the Inlet Zone of Shell and Tube Heat Exchangers without Leakages

As shown in the previous chapter, it is possible to mesh the inlet zone of a medium size ideal shell and tube heat exchanger with around 1,200,000 cells. The meshed domain then will be solved numerically by applying the RNG k-ε turbulence model and standard wall functions. This procedure makes it feasible to study the influence of baffle cut and baffle orientation on the shell-side performance of a shell and tube heat exchanger. In the present chapter, a shell and tube heat exchanger consisting of 660 tubes is considered. The geometrical data according to the HTRI data sheet is presented in Appendix B. Additional information regarding the tube layout may be found in Appendix D.

5.1 Geometry and Mesh Structure

Three baffle cuts and two baffle orientations are considered for the inlet zone of the shell and tube heat exchanger with 660 tubes. The baffle cuts are 20%, 24% and 30% of the shell inside diameter, and the baffle orientations are horizontal and vertical. The heat exchanger has equal baffle spacing. No leakage flows are taken into account. Figure 5.1 represents the inlet zone of the shell and tube heat exchanger with horizontal baffle orientation.

Figure 5.2 shows schematically the tube partition width for the heat exchanger and the configuration of tube pitch.

Table 5.1 provides the geometrical layout of the shell and tube heat exchanger in more detail.

For shell and tube heat exchangers with single-segmental baffles, the most frequently used baffle cut is 25% [Kara and Güraras, 2004]. Since a baffle cut of 25% introduces mesh elements with skewness more than 0.7 around the baffle tips, a baffle cut of 24% is taken into account instead of 25%.

5.2 CFD Model for the Study of Inlet Zone Effects

In addition to the geometry for the inlet zone with horizontal baffle orientation, a corresponding geometry is also prepared for the shell and tube heat exchanger with vertical baffle orientation.

The geometry with horizontal baffle orientation consists of 1,198,478 three dimensional
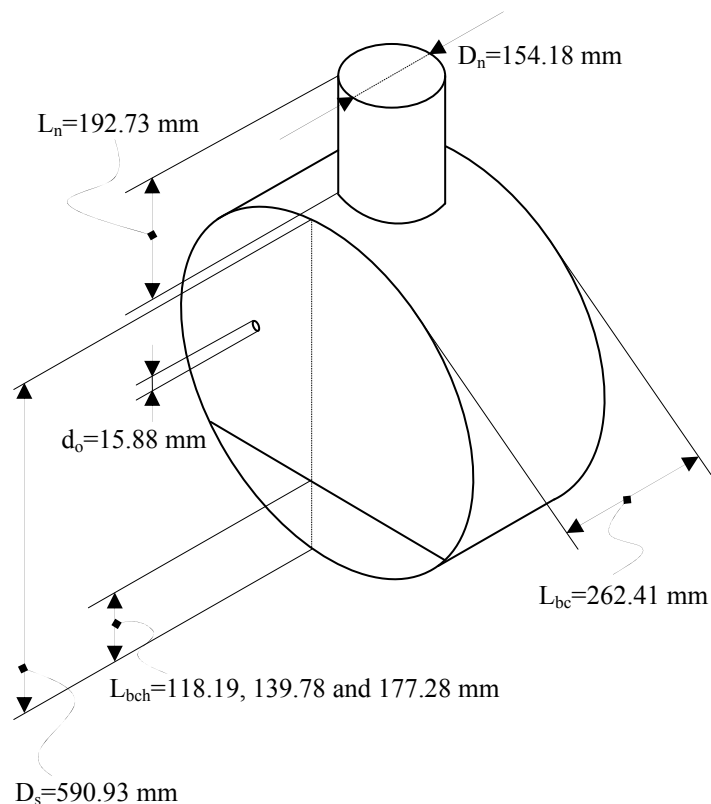
Figure 5.1: Main dimensions of the inlet zone of the shell and tube heat exchanger consisting of 660 tubes. The baffle thickness (6.35 mm), the tube pitch (3.20 mm) and the tube partition width (1.97 mm) are not indicated in this figure.

D_n=154.18 mm

L_n=192.73 mm

d_o=15.88 mm

L_{bc}=262.41 mm

L_{bch}=118.19, 139.78 and 177.28 mm

D_s=590.93 mm

control elements, while the vertical baffle orientation includes 1,187,508 elements.

The mesh structure is generated by use of the cooper mesh scheme (see subsection 4.1.2) and includes only quadrilateral-faced hexahedral elements. Figure 5.3 represents the source faces near the baffle and baffle window. The combination of source faces looks like a honeycomb, as can be seen in Figure 5.3. Figure 5.4 shows the surface meshes of the shell wall and the baffle window. The cooper mesh scheme aligns the mesh elements with the tube length and consequently reduces the numerical errors.

| (a) Vertical baffle orientation | (b) Horizontal baffle orientation | (c) Configuration of tube pitch |
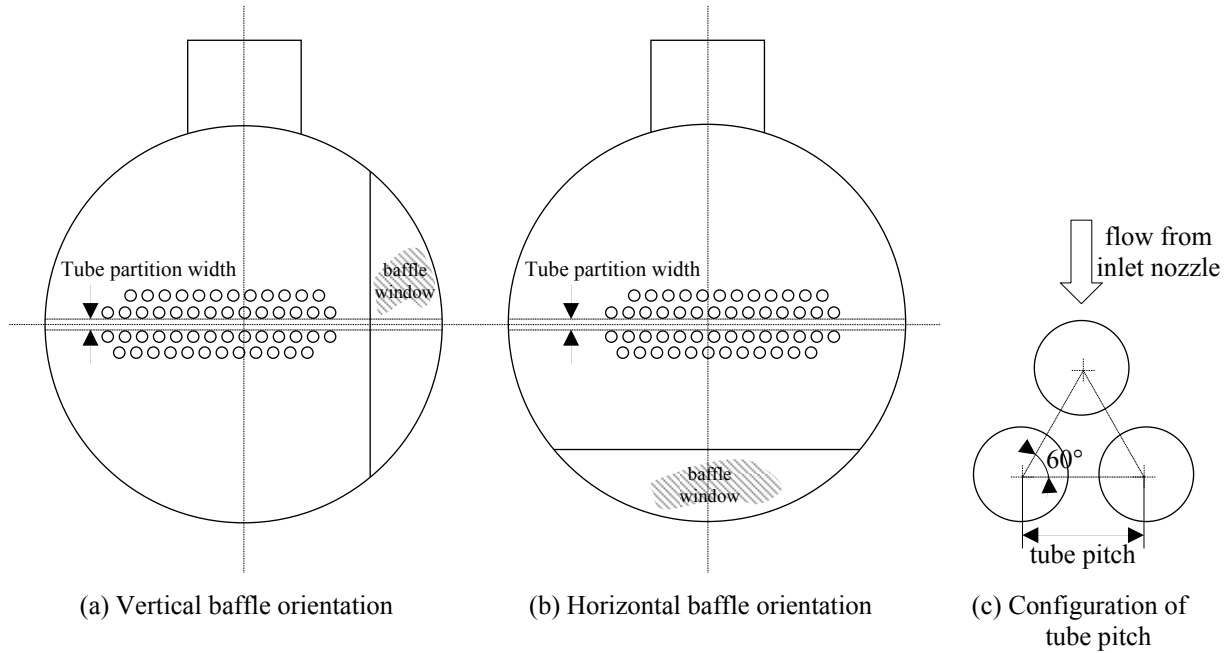
Figure 5.2: Configuration of the tube partition width for the shell and tube heat exchanger with (a) vertical baffle orientation and (b) horizontal baffle orientation, and also the tube pitch.

Item	Symbol	Size
Tube number	n_t	660
Tube outside diameter	d_o	15.875 mm ($^5/_8$ in)
Nozzle inside diameter	D_n	154.178 mm (6.07 in)
Nozzle minimum length	L_n	192.786 m (7.59 in)
Tube partition width	--	9.525 mm (0.375 in)
Baffle spacing (for the inlet, outlet and intermediate regions)	L_{bc}	262.407 mm (10.331 in)
Baffle thickness	--	6.350 mm (¼ in)
Shell inside diameter	D_s	590.931 mm (23.265 in)
Baffle cut height	L_{bch}	118.19, 139.78 and 177.28 mm
Baffle cut percentage	B_C	20%, 24% and 30%
Tube pitch	l_{tp}	20.638 mm ($^{13}/_{16}$ in)

Table 5.1: Geometrical measurements of the inlet zone of the shell and tube heat exchanger with 660 tubes.

Reduction of mesh number under 1,200,000 elements is achieved by inserting 8 elements between tubes and by adjusting the two dimensional and the three dimensional aspect ratios

32

about 10 and 15, respectively. Figure 5.5 shows the meshed geometries with horizontal and vertical baffle orientations.
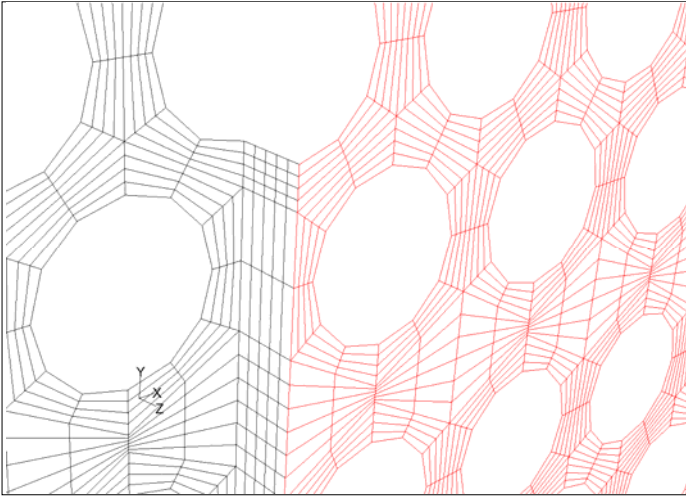
Figure 5.3: Meshed source faces around the tubes. The red region shows the baffle window.
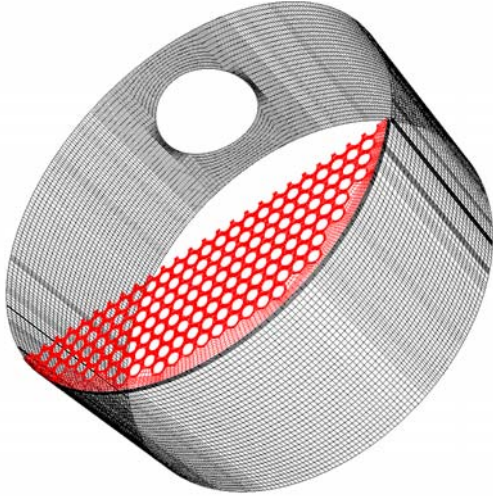
Figure 5.4: Surface meshes in baffle window and shell wall.

In both geometries, approximately 98% of the total mesh elements have EquiAngle skewness less than 0.4. Figure 5.6 shows the distribution of EquiAngle skewness for these two geometries.
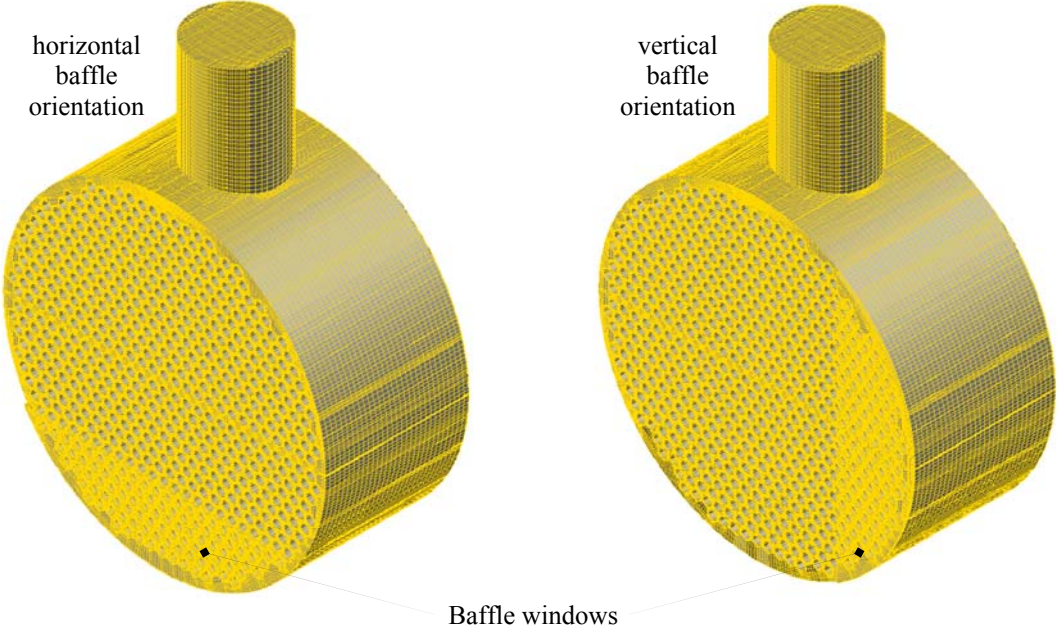
Figure 5.5: Meshed inlet zone of shell and tube heat exchanger with 660 tubes for both horizontal and vertical baffle orientation. The shell side fluid is meshed by use of the cooper mesh scheme. The total number of quadrilateral-faced hexahedral elements is 1,198,478 and 1,187,508 for horizontal and vertical baffle orientation, respectively.

5.2.1 Boundary Conditions

The conjugate heat transfer boundary condition for tube walls is more realistic than the constant temperature boundary condition. However, the conjugate boundary condition requires excessive mesh elements on the tube side. Therefore, a constant temperature boundary condition is considered for the tube walls. All other solid walls, i.e. the baffle, the tube sheet, the nozzle and the shell wall, are defined as adiabatic walls.
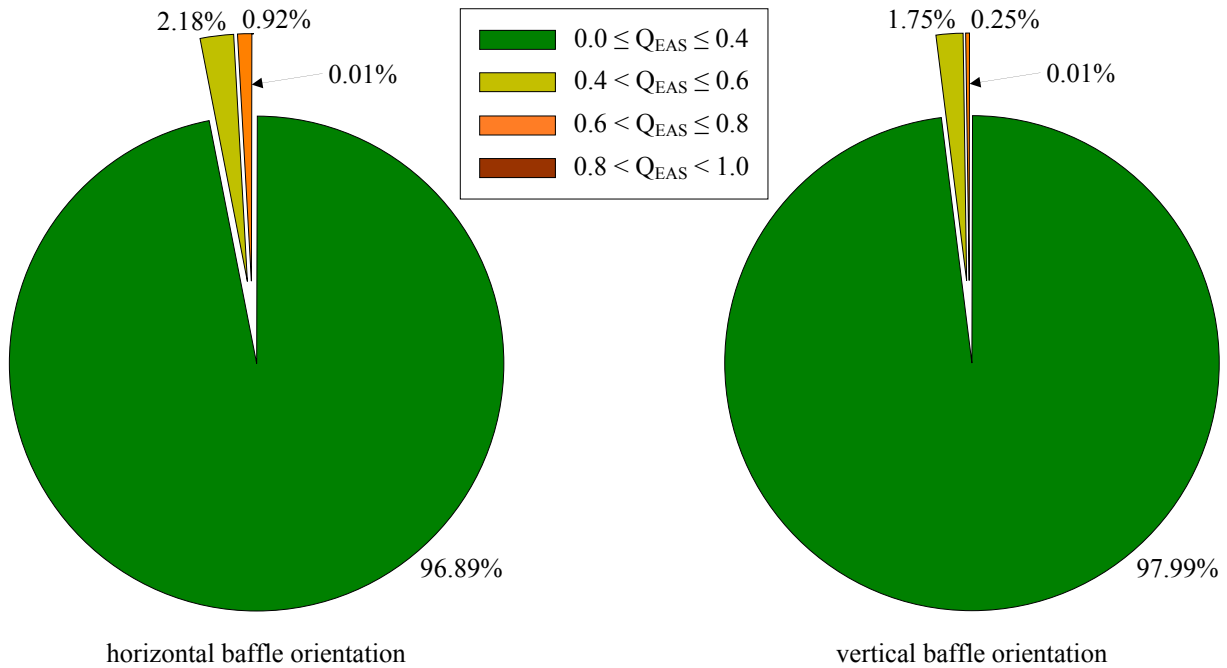
Figure 5.6: Distribution of EquiAngle skewness of hexahedral mesh structure generated for the inlet zone.

The boundary condition for the inlet, i.e. the inlet nozzle, is the velocity inlet boundary condition since the velocity vectors and the temperature at inlet are known. Moreover, the shell-side flow is incompressible and the first solid obstruction, i.e. the first tube row, is not too close to the inlet boundary. This makes the velocity inlet boundary condition for the inlet more applicable [Fluent, 2008].

Appropriate boundary conditions for the outlet, i.e. the baffle window, are the outlet pressure boundary condition and the outflow boundary condition [Fluent, 2008]. The outlet pressure boundary condition requires the specification of a static gauge pressure at the outlet boundary. This boundary condition is also used if the flow reverses direction at the outlet. The reverse flow or backflow at outlet will cause difficulties in the numerical solution. The outlet pressure boundary condition will minimize these numerical difficulties. The simulation results obtained by applying the outlet pressure boundary condition have shown that the backflow behaviour at outlet is negligible (less than 3% of the total flow reverses direction at outlet). On the other hand, the static gauge pressure at the outlet boundary is not faithfully known. Therefore, the outlet boundary condition is not defined for the outlet.

The outflow boundary condition is used to model flow exits where the details of the flow velocity and pressure are not known prior to solution of the flow problem. From the numerical point of view, all required information for outflow boundary condition will be extrapolated from the interior. The outflow boundary conditions consist of zero normal derivatives at the boundary for all quantities. The zero-derivative condition is intended to represent a smooth continuation of the flow through the boundary. Hence, the outflow boundary conditions can

be considered as a Dirichlet boundary condition and are derived following an approach analogous to the Dirichlet-to-Neumann method [Ol'shanskii, 2000]. Importantly, the outflow boundaries cannot be used if the flow is compressible or if the modelling encounters unsteady flows with varying density. However, when the Mach number is less than 0.1, compressibility effects are negligible and the variation of fluid density with pressure can safely be ignored in flow modelling [Jin and Barza, 1993]. In the present work, the fluid velocity is less than 33 m/s. Moreover, the flow velocity and pressure at the outlet are not known, and the outlet backflow is negligible. Hence, the outflow boundary condition is the appropriate boundary condition for the outlet.

The boundary conditions used for the present stage of study are summarized in Table 5.2.

Boundary	Boundary condition
Tube outside walls	Constant temperature equal to 370K
Tube sheet wall	Adiabatic
Baffle wall	Adiabatic
Nozzle wall	Adiabatic
Shell wall	Adiabatic
Inlet at inlet nozzle	Velocity inlet: defined velocity, all velocity vectors are normal to the boundary.
	The inlet temperature is 30 K more than the tube wall temperature, i.e. 400 K.
Outlet at baffle window	Outflow: zero normal derivatives for all quantities, Mach number < 0.1

Table 5.2: Boundary conditions for the inlet zone of the heat exchanger with 660 tubes and without leakages.

5.2.2 Thermophysical Properties of Working Fluids

Three fluids with constant physical properties are considered as shell-side fluids: air, liquid water and engine oil. The physical properties are obtained at 8 bar and 385 K [Touloukian, 1972; Rohsenow, 1998; Incropera, 2006; VDI, 2006]. Operating pressure 8 bar is an arbitrary high pressure that will facilitate minimization of the difficulties in numerical solution [Fluent, 2008].

As it is shown in Table 5.2, the tube wall temperature and the inlet temperature are equal to 370 K and 400 K, respectively. The temperature of the tube walls and the inlet temperature are selected based on typical operating conditions of shell and tube heat exchangers in oil refineries [Gary and Handwerk, 2001]. Therefore, the average bulk temperature, which is the operating temperature, is equal to 385 K.

Table 5.3 shows the physical properties of the shell-side fluids.

Physical property	Symbol	Unit	Shell side fluid			Variation
			Gaseous air	Liquid water	Liquid engine oil	
Density	ρ	kg/m³	7.25	998.20	828.96	Constant
Dynamic viscosity	μ	kg/(m.s)	2.250×10^{-5}	1.003×10^{-3}	1.028×10^{-2}	Constant
Thermal Conductivity	k_f	W/(m.K)	0.032	0.600	0.135	Constant
Heat capacity surface	c_p	J/(kg.K)	1018.63	4182.00	2307.00	Constant
Prandtl number	Pr	--	0.716	6.991	175.674	Constant

Table 5.3: Physical properties of three shell-side fluids. All physical properties are assumed to be constant and are obtained at 8 bar 385 K.

35

5.2.3 Settings

The overall numerical setup for the present investigation is summarized in Table 5.4 [Torrance, 1986; Shyy, 1994; Anderson, 1995; Wesseling, 2001; Ferziger, 2002; Fluent, 2008].

Model/Treatment	Algorithm/Theorem	Formulation/Method/Discretization
Turbulence model	k-ε Model	RNG with following constants: C_μ=0.0845, $C_{\varepsilon 1}$=1.42, $C_{\varepsilon 2}$=1.68, σ_ε =0.85
Near wall treatment	Wall function	Standard wall function base on Launder and Spalding
Flow solver	Pressure-base	Segregated / Implicit
Velocity coupling method	Pressure-base	SIMPLE
Other sources of heat	Radiation Viscous heating	Neglected For engine oil with inlet velocity more than 20 m/s (Br ≥ 1)
Gradients and Derivatives	Green-Gauss	Green-Gauss cell-based gradient evaluation
Discretization	Taylor	First-order

Table 5.4: CFD setup

5.2.4 Mesh Validations

5.2.4.1 Mesh Dependency

Ignorance of mesh dependency can sometimes be an embarrassment in numerical calculations. The numerical results are not trustworthy when the numerical simulation depends on the mesh size. Mesh structures need to be developed to eradicate the mesh dependency.

The inlet zone of a shell and tube heat exchanger with 140 tubes, presented in Figure 4.1 (a), is meshed with different mesh sizes. Herein, the mesh size is the total number of quadrilateral-faced hexahedral elements.

The main parameters that define the mesh size are: the number of elements between two tubes, the number of elements on the tube perimeter, and the number of elements on the tube length. The mesh structure characterised by 8×12×30 indicates that 8 elements are between two tubes, 12 elements are on the tube perimeter, and 30 elements are on the tube length. The mesh 8×12×30 is similar to the mesh presented in Figure 5.3 and Figure 5.4.

The total number of mesh elements, i.e. the mesh size, for the inlet zone of the heat exchanger with 140 tubes is 250,000 when the mesh is 8×12×30. A refined and a coarse mesh are also generated for the inlet zone of the heat exchanger with 140 tubes. The refined mesh is characterized by 10×24×45 with the mesh size of around 1,000,000. The coarse mesh is a 6×12×25 mesh and includes about 160,000 elements.

All three meshes (8×12×30, 10×24×45 and 6×12×25) are used to perform calculations applying the CFD setup presented in Table 5.4 and the boundary conditions shown in Table 5.2. The shell-side fluid was liquid water with the physical properties as presented in Table 5.3. The qualitative results of these three simulations were very similar. Moreover, the deviation of the quantitative results of these simulations, i.e. the outlet temperatures and pressures, were less than 0.10%. This means that the numerical simulation is mesh-independent.

The mesh structure generated for the inlet zone of the shell and tube heat exchanger with 660 tubes (described in section 5.2) is 8×12×30 mesh. A refined and a coarse mesh are also generated for this mesh. The refined mesh is 8×12×33 with about 1,300,000 elements. This is the maximum possible level of refinement because refining the mesh structure with 10×24×45

36

mesh will produce around 4,500,000 elements. The coarse mesh is 6×12×25 mesh and included about 750,000.

The numerical results obtained from the simulations of the refined mesh, i.e. 8×12×33 mesh, and the coarse mesh, i.e. 6×12×25 mesh, are compared with the numerical results obtained from the simulation of the original mesh, i.e. 8×12×30 mesh. The relative absolute difference between the outlet temperature of the original mesh and the refined mesh is less than 0.002%, while the same difference for the coarse mesh is less than 0.117%. For the outlet pressure, the maximum relative absolute difference between the original mesh and the refined mesh is 0.054%. The same difference for the coarse mesh amounts to 0.129%. The comparison of the outlet temperature and pressure obtained from the simulations of the refined, coarse and original meshes at seven different Reynolds numbers are presented in Figure 5.7.
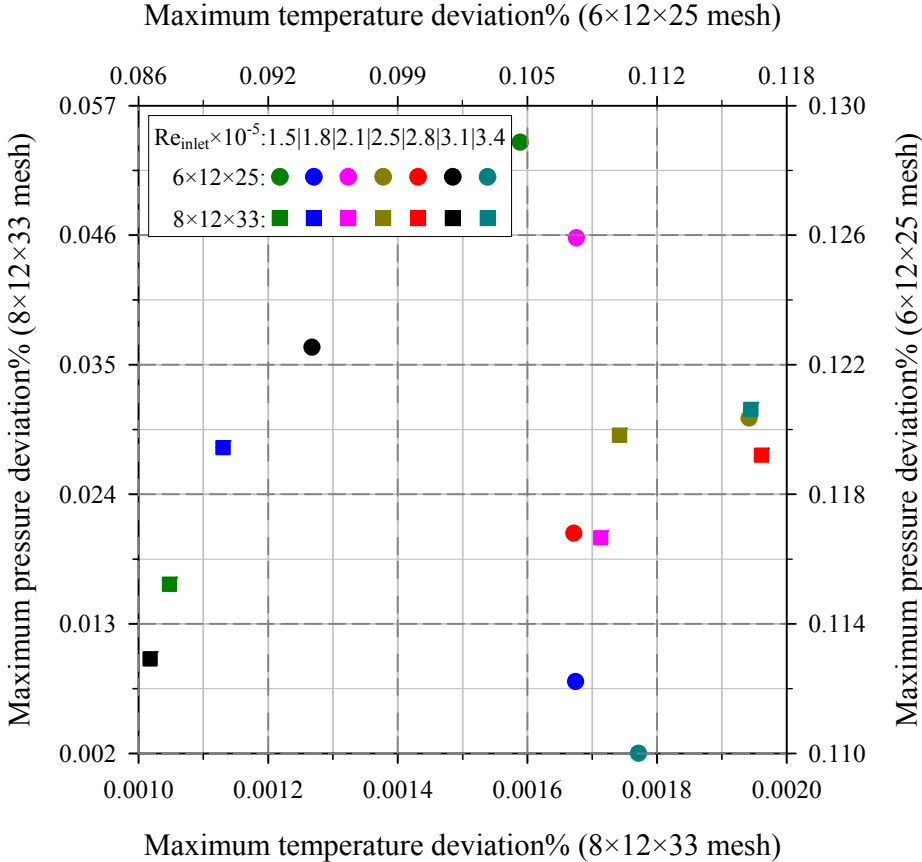
Figure 5.7: Comparison of the outlet temperature and pressure obtained from the simulations of the refined, coarse and original meshes at seven different Reynolds numbers. The refined mesh is characterised by 8×12×33 and the coarse mesh is described by 6×12×25.

The identical numerical results obtained from the simulations of the refined, coarse and original meshes show that the mesh structure generated for the inlet zone (described in section 5.2) guarantees the mesh independency of the simulation.

5.2.4.2 Reliability of Mesh Structure for Wall Function Treatment

As it is described in subsection 4.2.5 and shown in Table 5.1, a semi-empirical function based on the proposal of Launder and Spalding, bridges the viscosity-affected region between the wall and the fully turbulent region [Launder and Spalding, 1974]. This semi-empirical function comprises laws for mean velocity and temperature, which yields:

$$\frac{\rho\overline{U}}{\tau_W}\sqrt[4]{C_\mu k^2}=\frac{1}{\kappa}\ln(Ey^*) \tag{5.1}$$

with

$$y^*=\frac{\rho y}{\mu}\sqrt[4]{C_\mu k^2} \tag{5.2}$$

In Equation (5.1) and (5.2), κ is the von Kârmân constant equal to 0.4187, E is the empirical constant in the law of the wall (equal to 9.81 for RNG k-ε model), y* is the dimensionless sublayer-scaled wall distance, k is the turbulent kinetic energy, τ_W is the surface or wall shear stress, $\overline{U}$ is the mean velocity of the fluid at the distance y from the wall, and C_μ is the constant coefficient in the k-ε eddy viscosity formulation.

The distance from the wall at the wall-adjacent cells is usually measured in the wall unit y* or y+, where y+ is another type of the dimensionless sublayer-scaled wall distance.

$$y^+=\frac{y\sqrt{\rho\tau_W}}{\mu} \tag{5.3}$$

The logarithmic law for mean velocity is known to be valid for y*>30 ~ 60 [Hinze, 1959; Bradshaw, 1971; Wilcox, 1998; Pope, 2000; Ferziger, 2002]. For the RNG k-ε model, logarithmic law is employed when y* is greater than 11.225 [Kutateladze, 1964; Launder and Spalding, 1974; Ferziger, 2002]. Moreover, the comparable values of y* and y+ show that the first cell is placed in the fully turbulent region [Ferziger, 2002].

Figure 5.8 shows the values of y+ and y* as a function of the inlet Reynolds number obtained from 25 numerical simulations. In these simulations, which will be discussed in section 5.8, the shell-side fluid is liquid water, the baffle orientation is horizontal, and the baffle cut is 24%. It can be seen from Figure 5.8 that the values of y+ are similar to the values of y*. The turbulent flow occurs at $Re_{inlet} \approx 10^5$. At $Re_{inlet} > 10^5$ the value of y+ exceeds 11.225. y+ versus the inlet Reynolds number in the domain of turbulent flow for three baffle cuts and three shell-side fluids are presented in Figure 5.9. Although the shell-side fluids are air, liquid water and engine oil, the values of y+ are independent of the shell-side viscosity. Since the values of y+ are more than 14 for all Reynolds numbers, the mesh structure is satisfactory for implementing the standard wall function.

5.3 Performance of the Inlet Zone in the Domain of Laminar and Turbulent Flow

25 simulations are accomplished for the inlet zone of the shell and tube heat exchanger with 660 tubes. The baffle cut is equal to 24% and the shell side fluid is liquid water. The inlet fluid velocities are between 0.1 and 2.2 m/s, which cover an inlet Reynolds number range in the laminar and turbulent flow domains ($4.6\times10^3 \le Re_{inlet} \le 3.4\times10^5$).

The results of the shell-side pressure drop and the shell-side heat transfer coefficients are presented by the shell-side Kârmân number and the shell-side Nusselt number, respectively.

$$Nk=\frac{\rho d_{Hsp}^3\left(\Delta p_{shell}/L_{bc}\right)}{\mu^2} \tag{5.4}$$

$$Nu=\frac{h_{shell}d_{Hsh}}{k_f} \tag{5.5}$$
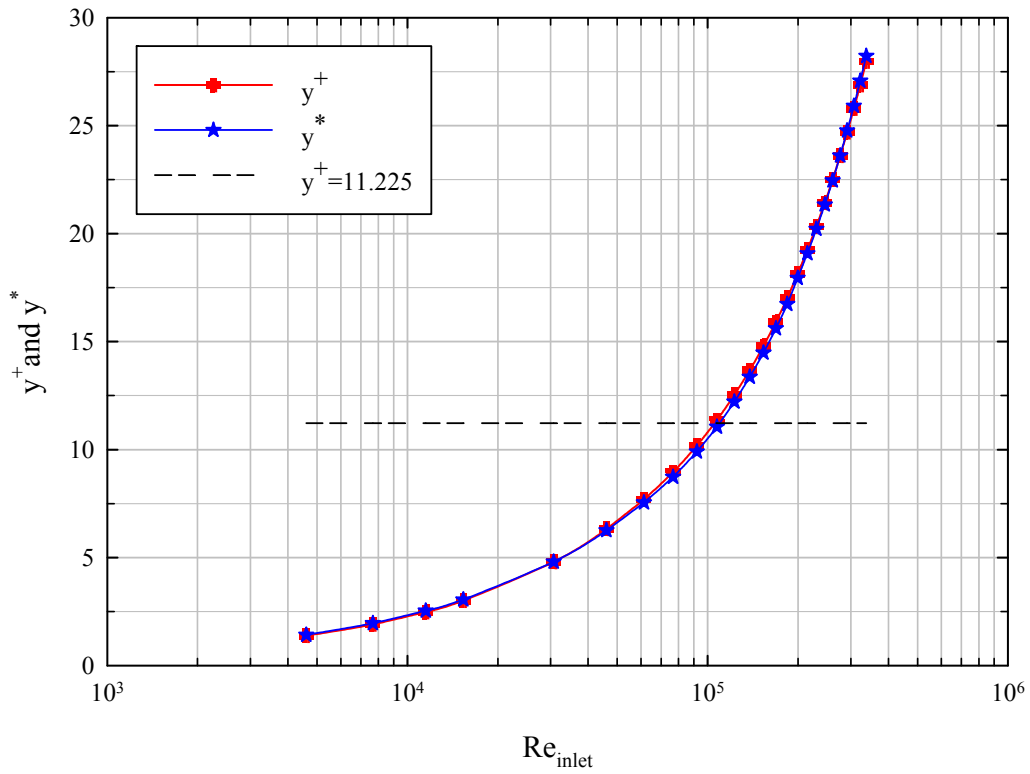
Figure 5.8: Values of y+ and y* versus the inlet Reynolds number for horizontally orientated baffles (baffle cut 24%).
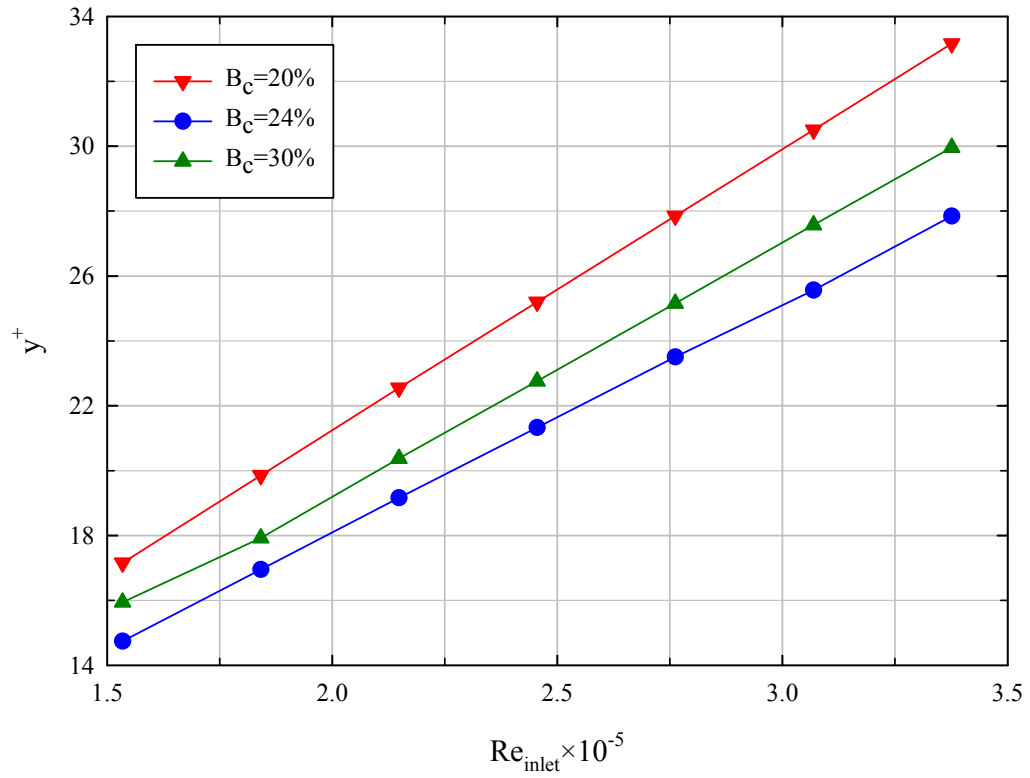
Figure 5.9: Values of y+ versus the inlet Reynolds number for horizontal baffle orientation and for baffle cuts 20%, 24% and 30%.

In Equations (5.4) and (5.5), d_{Hsp} is the hydraulic diameter for shell-side pressure drop and d_{Hsh} is the hydraulic diameter for shell-side heat transfer.

$$d_{Hsp} = \frac{D_s^2 - n_t d_o^2}{D_s + n_t d_o} \tag{5.6}$$

$$d_{Hsh} = \frac{D_s^2 - n_t d_o^2}{n_t d_o} \tag{5.7}$$

Equations (5.4) and (5.5) yield $d_{Hsh}=1.099d_o$ and $d_{Hsp}=1.041d_o$ for the present investigation. The shell-side Kârmân number, Nk, and the shell-side Nusselt number, Nu, are presented in Figure 5.10 as a function of the Reynolds number of the inlet.
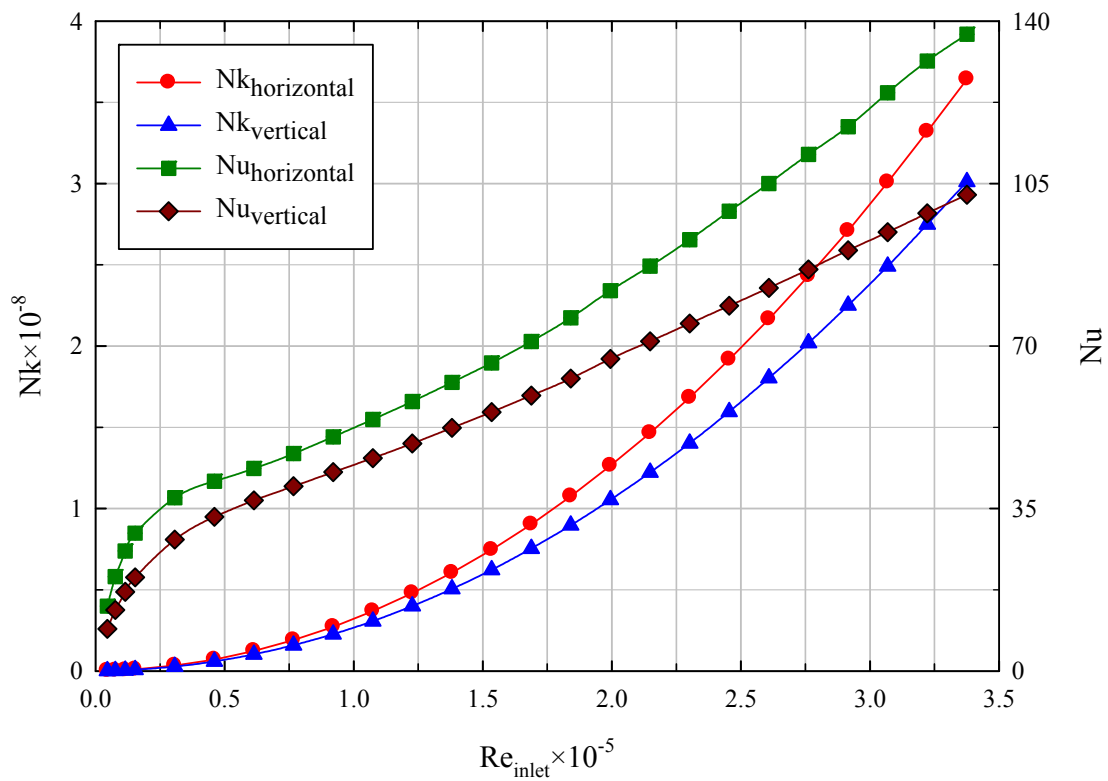
Figure 5.10: The effect of baffle orientation on the shell-side pressure drop and heat transfer coefficient for the inlet zone of the shell and tube heat exchanger with 660 tubes. The baffle cut is 24% and the shell-side fluid is water.

As it is shown in Figure 5.10, the shell-side pressure drop and the shell-side heat transfer coefficient for horizontal baffle orientation are greater than for vertical baffle orientation. This can be explained by considering the effect of baffle orientation on the residence time and the mixing level of the shell-side fluid. As it is explained in section 3.3, at baffle cut 24% the value of NMSD for horizontal baffle orientation is approximately 84% greater than the value of NMSD for vertical baffle orientation (see Equation (3.8) and Figure 3.10). Therefore, the residence time and mixing level of the shell-side fluid for horizontal baffle orientation are greater than for vertical baffle orientation. Consequently, the horizontal baffle orientation will result greater values of pressure drop and heat transfer coefficient than the vertical baffle orientation.

40

The static pressure distribution in the inlet zone for horizontal and vertical baffle orientation is presented in Figure 5.11. In order to have a better view of pressure gradients, the static pressure distribution on the tube walls is also presented in Figure 5.12. In Figures 5.11 and 5.12, the heat transfer processes is heating.

Figure 5.11: Pressure field in the inlet zone for horizontally (left) and vertically (right) orientated baffles (water, baffle cut 0.24%, $Re_{inlet}=3.4\times10^5$). The heat transfer processes is heating.
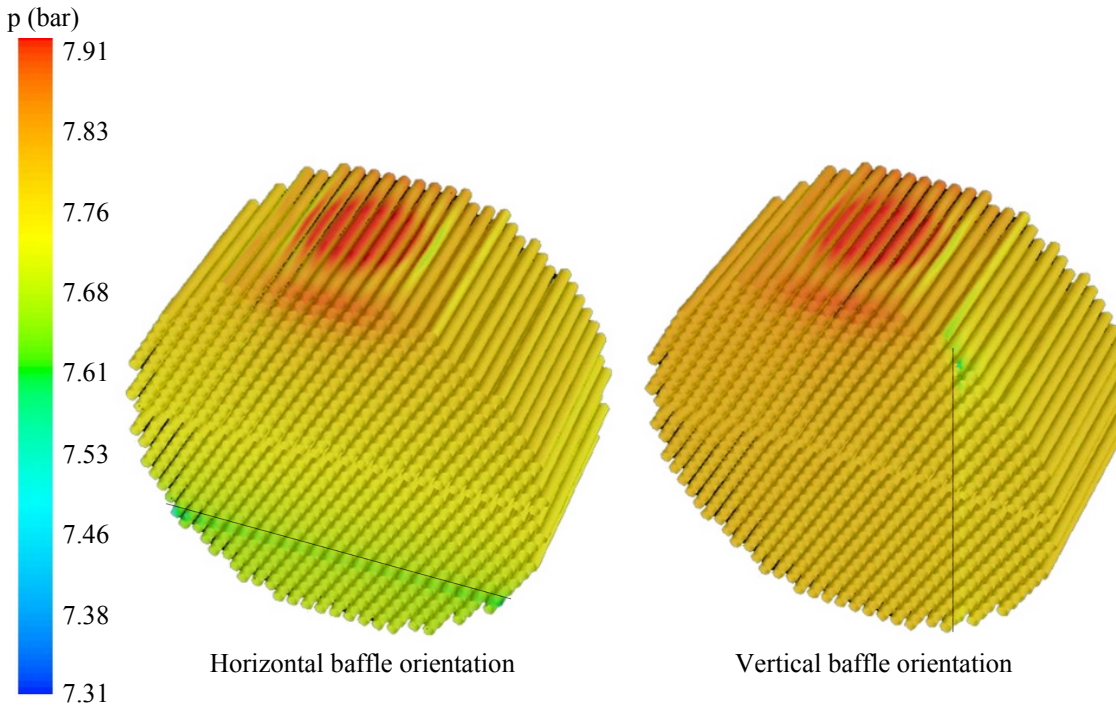
Figure 5.12: Pressure field on the tube walls of the inlet zone for horizontally (left) and vertically (right) orientated baffles (water, baffle cut 0.24%, $Re_{inlet}=3.4\times10^5$). The heat transfer processes is heating.

The horizontal baffle orientation and vertical baffle orientation have closely comparable values of pressure drop near the inlet nozzle, as it is shown in Figures 5.11 and 5.12. However, the overall pressure drop, especially near the baffle window, for horizontal baffle orientation is significantly greater than the overall pressure drop for vertical baffle orientation. The static temperature distribution in the inlet zone for horizontal and vertical baffle orientation is presented in Figure 5.13. The static temperature distribution on the tube walls is also shown in Figure 5.14. In Figures 5.13 and 5.14, the heat transfer processes is heating.

Figure 5.13: Temperature field in the inlet zone for horizontally (left) and vertically (right) orientated baffles (water, baffle cut 0.24%, $Re_{inlet}=3.4\times10^5$). The heat transfer processes is heating.
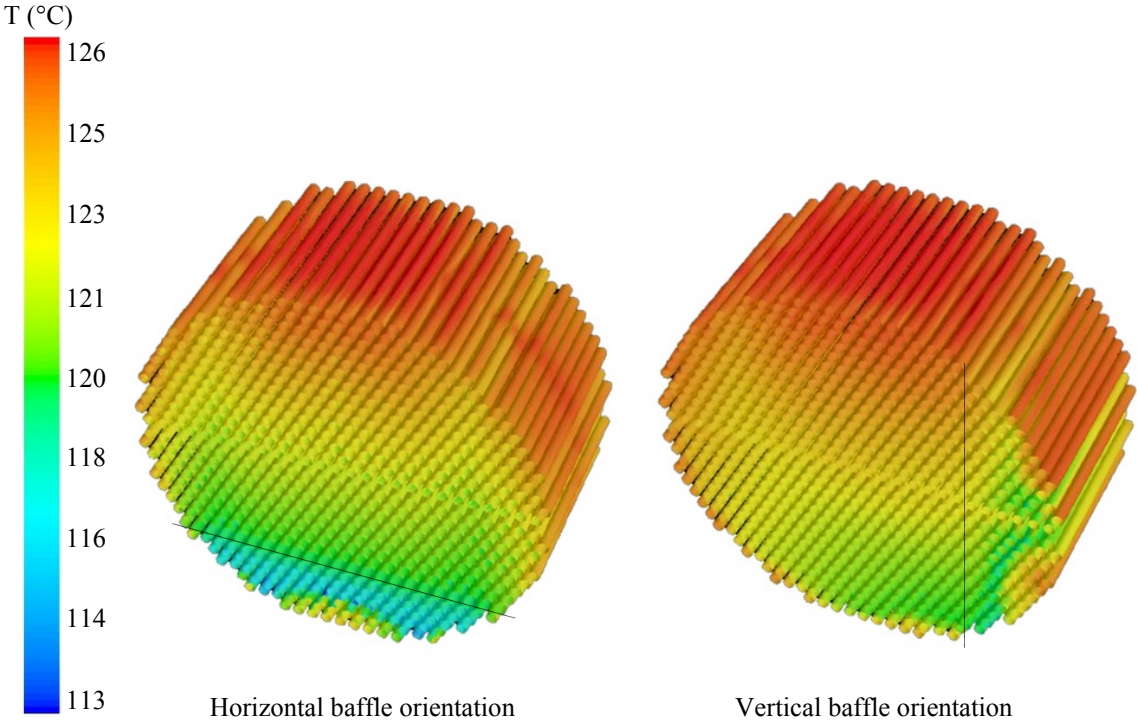
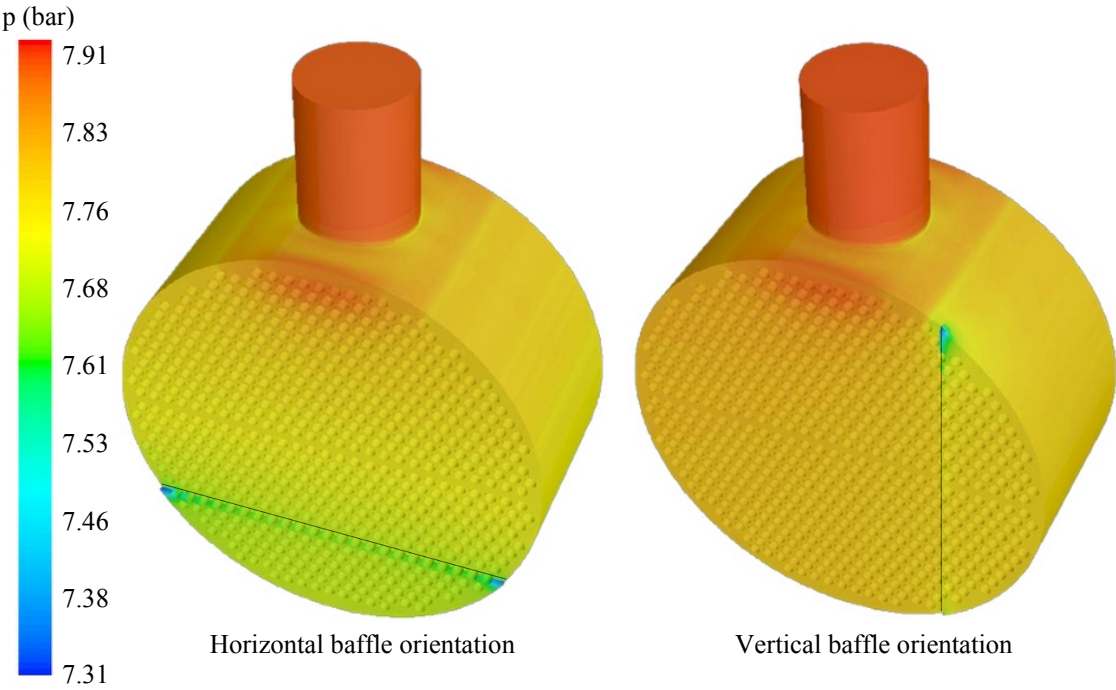Figure 5.14: Temperature field on the tube walls of the inlet zone for horizontally (left) and vertically (right) orientated baffles (water, baffle cut 0.24%, $Re_{inlet}=3.4\times10^5$). The heat transfer processes is heating.
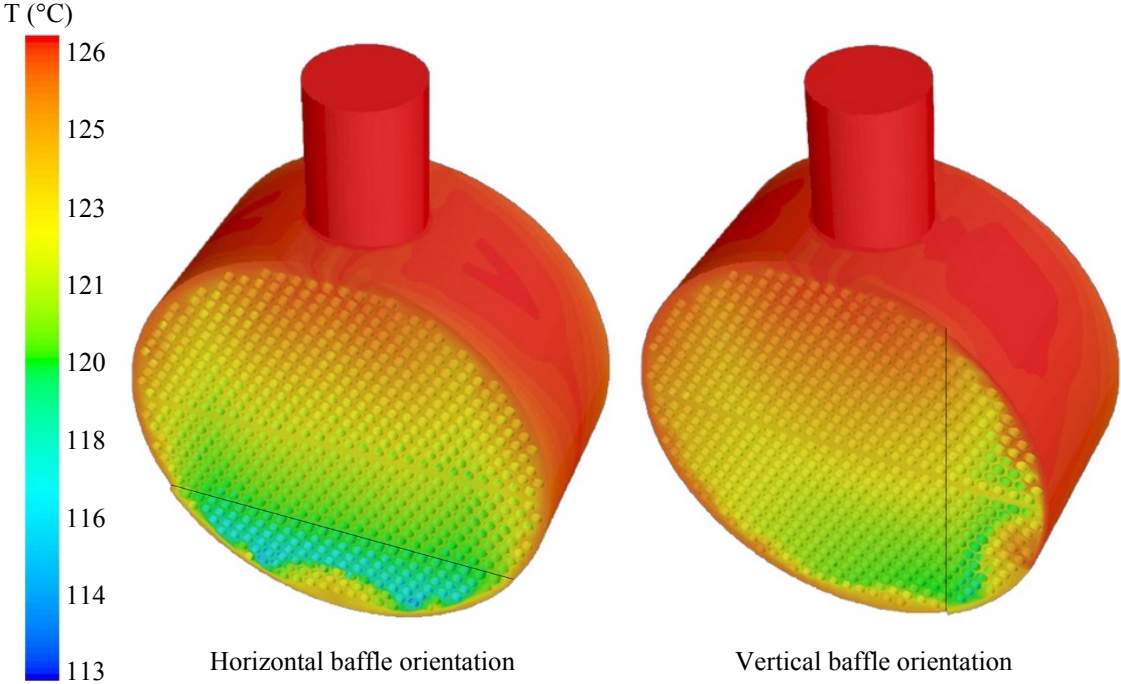
42

From Figures 5.13 and 5.14 it can be seen that the heat transfer is greater for the arrangement with horizontally orientated baffle than for the arrangement with vertical baffle orientation. Moreover, the baffle window for horizontal baffle orientation is significantly more effective in heat transfer than the baffle window for vertical baffle orientation. In the heat exchanger with horizontal baffle orientation, about 89% of the baffle window area is up to 8 °C colder than the inlet temperaure. However, only 33% of the baffle window area is 6 °C colder than the inlet temperature for the heat exchanger with vertical baffle orientation.

In order to have a better understanding of the effect of baffle orientation on the shell-side heat transfer and pressure drop, the profiles of temperature, pressure and velocity are determined at the middle of the inlet zone. The middle of the inlet zone is presented by a plane shown in Figure 5.15. The temperature, pressure and velocity profiles of the heat exchangers with horizontal and vertical baffle orientation are obtained on this plane.
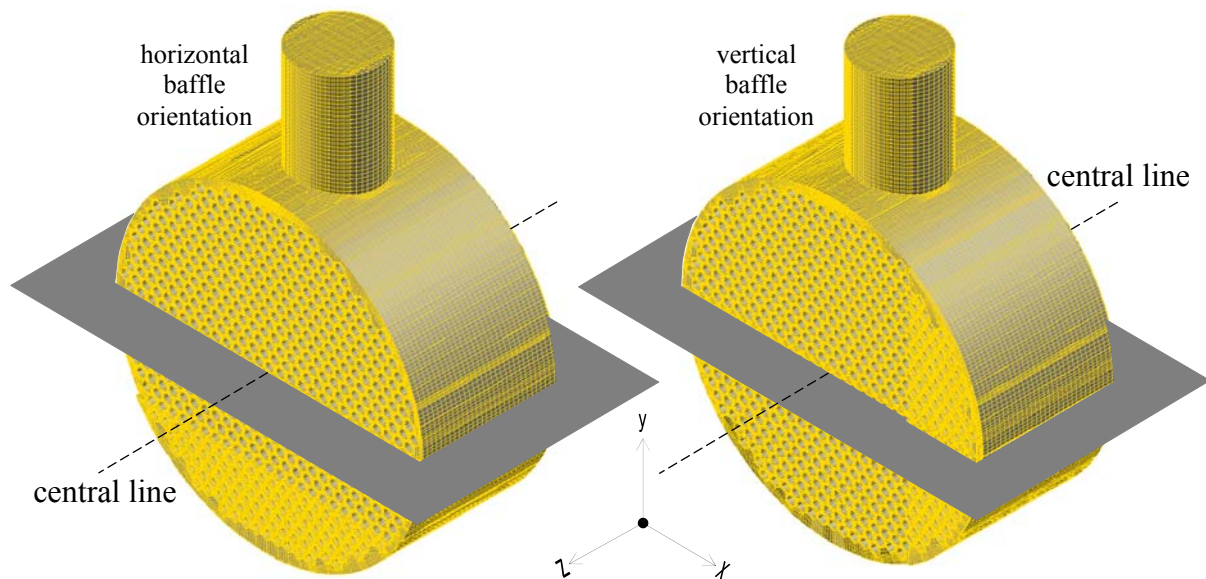
Figure 5.15: The plane which presents the middle of the inlet zone of the shell and tube heat exchanger with horizontal baffle orientation (left) and vertical baffle orientation (right).

Figure 5.16 shows the temperature profile at the middle of the inlet zone of the shell and tube heat exchanger with horizontal and vertical baffle orientaion. For the shell and tube heat exchanger with horizontal baffle orientation, the baffle window is located isobilateral with respect to the inlet nozzle. Therefore, the temperature profile at the middle of the inlet zone with horizontal baffle orientation is symmetrical. However, the asymmetrical profile of temperature in the shell and tube heat exchanger with vertical baffle orientation is due to the lopsided positioning of the baffle window with respect to the inlet nozzle.

The effect of the baffle orientation on the pressure drop, presented in Figure 5.17, is very perspicuous. For the inlet zone with horizontal baffle orientation, the highest pressure drop is observed near the shell wall due to the the bypass flow. However, the highest pressure drop is observed in the baffle window for the inlet zone with vertical baffle orientation.

The velocity magnitude profile for the inlet zone with horizontal and vertical baffle orientation is shown in Figure 5.18. The velocity magnitude |u| is an scalar value and is equal to $\sqrt{|\vec{u}_x|^2 + |\vec{u}_y|^2 + |\vec{u}_z|^2}$ where $\vec{u}_x$, $\vec{u}_y$ and $\vec{u}_z$ are the x, y and z components of velocity vector in Cartesian coordinates.
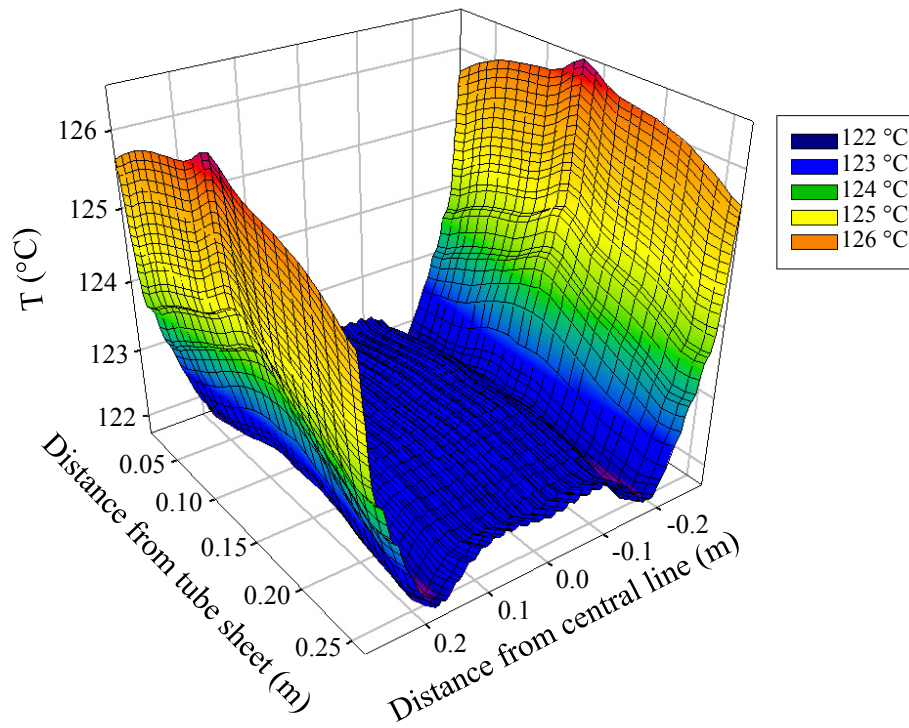
Figure 5.16: Temperature profile at the centre of the inlet zone for both horizontally (top) and vertically (bottom) orientated baffles of a shell and tube heat exchanger with 660 tubes (Re_{inlet}=3.4×10^5).

Figure 5.17: Pressure profile at the centre of the inlet zone for both horizontally (top) and vertically (bottom) orientated baffles of a shell and tube heat exchanger with 660 tubes (Re_{inlet}=3.4×10^5).

Figure 5.18: Velocity magnitude profile at the centre of the inlet zone for both horizontally (top) and vertically (bottom) orientated baffles of a shell and tube heat exchanger with 660 tubes ($Re_{inlet}=3.4\times10^5$).

For the inlet zone with horizontal baffle orientation, the highest velocity magnitude is observed in the bypass region. However, the highest velocity magnitude is observed in the baffle window for the inlet zone with vertical baffle orientation. In order to have a more comprehensible analysis of the velocity profile, the profiles of $\vec{u}_x$, $\vec{u}_y$ and $\vec{u}_z$ are presented in Figures 5.19, 5.20 and 5.21, respectively. The x, y and z axes of the Cartesian coordinate system are presented in Figure 5.15 and defined in subsection 3.2.

At the middle of the inlet zone with horizontal baffle orientation, the x-velocity profile, i.e. $\vec{u}_x$ profile, is asymmetrical, however, the profile of the magnitude of the x-velocity, i.e. $|\vec{u}_x|$ profile, is symmetrical. Mathematically, the x-velocity profile at the middle of the inlet zone with horizontal baffle orientation can be expressed as $\vec{u}_x(x, z) \sim -\vec{u}_x(2x_{cl}-x, z)$, where x_{cl} defines the location of the central line presented in Figure 5.15 on the x-axis. This can be explained only by considering the existence of vortices. Therefore, the x-velocity profile shows intensive vortices in the inlet zone of the shell and tube heat exchanger with horizontal baffle orientation. In contrast to this, the x-velocity profile at the middle of the inlet zone with vertical baffle orientation shows redirection of the flow to the baffle window without effective vortices.

The y-velocity profile at the middle of the inlet zone is presented in Figure 5.20. The profile of $\vec{u}_y$ for horizontal baffle orientation shows an intensive bypass flow and an effective flow in the tube bank region toward the baffle window. The profile of $\vec{u}_y$ for vertical baffle orientation indicates that the y-velocity flow in the tube bank region is not as effective as the y-velocity flow for horizontal baffle orientation. Therefore, the tubes located far from the inlet nozzle for horizontal baffle orientation are more effective in transferring heat and generating pressure drop than for vertical baffle orientation.

The z-velocity profile at the middle of the inlet zone is presented in Figure 5.21. The magnitude of $\vec{u}_z$ is negligible compared to the magnitude of $\vec{u}_x$ and $\vec{u}_y$ for horizontal baffle orientation. However, the profile of $\vec{u}_z$ represents a high level of mixing in the inlet zone when using the horizontal baffle orientation. The profile of $\vec{u}_z$ at the middle of the inlet zone with vertical baffle orientation confirms the redirection of the flow to the baffle window without effective vortices.

The profiles presented in Figures 5.16 to 5.20 explain the behaviour shown in Figure 5.10, that is the heat transfer rate and the pressure drop of the inlet zone with horizontal baffle orientation is greater than the heat transfer rate and the pressure drop of the inlet zone with vertical baffle orientation.

Since the heat transfer coefficient relates to the energy recovered by the heat exchanger and the pressure drop refers to the work which is necessary to maintain the shell-side fluid flow, a shell-side gain factor suitable for the assessment of shell and tube heat exchangers may be introduced as ratio of the shell-side heat transfer coefficient to the shell-side pressure drop:

$$\Gamma_{shell} = \frac{Nu_{shell}}{Nk_{shell}} \propto \frac{h_{shell}}{\Delta p_{shell}}$$ (5.8)

To facilitate the judgment between the horizontal and vertical baffle orientation, a performance factor is defined as:

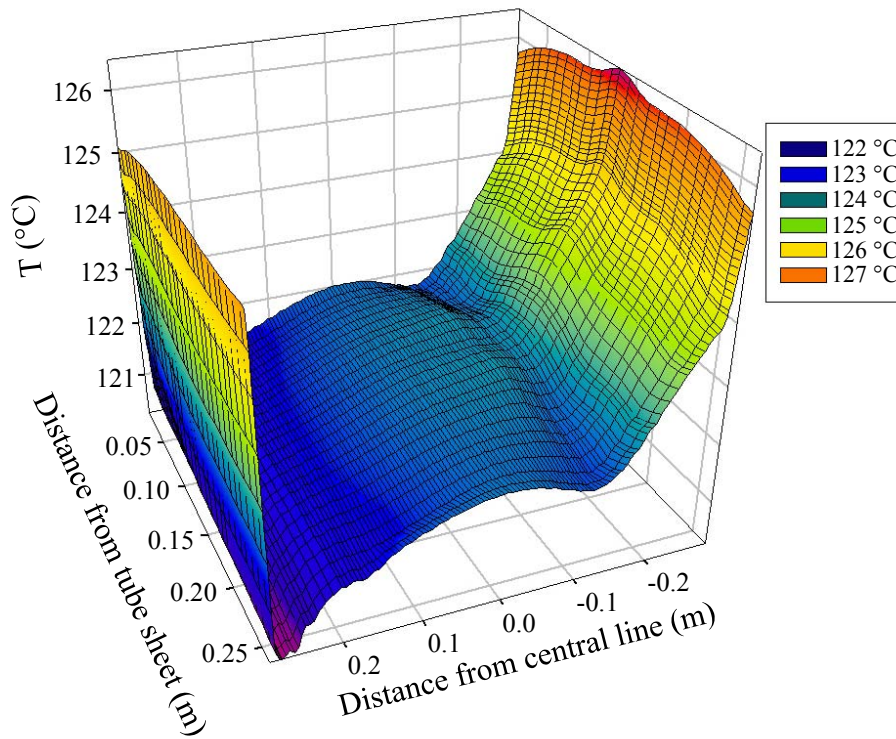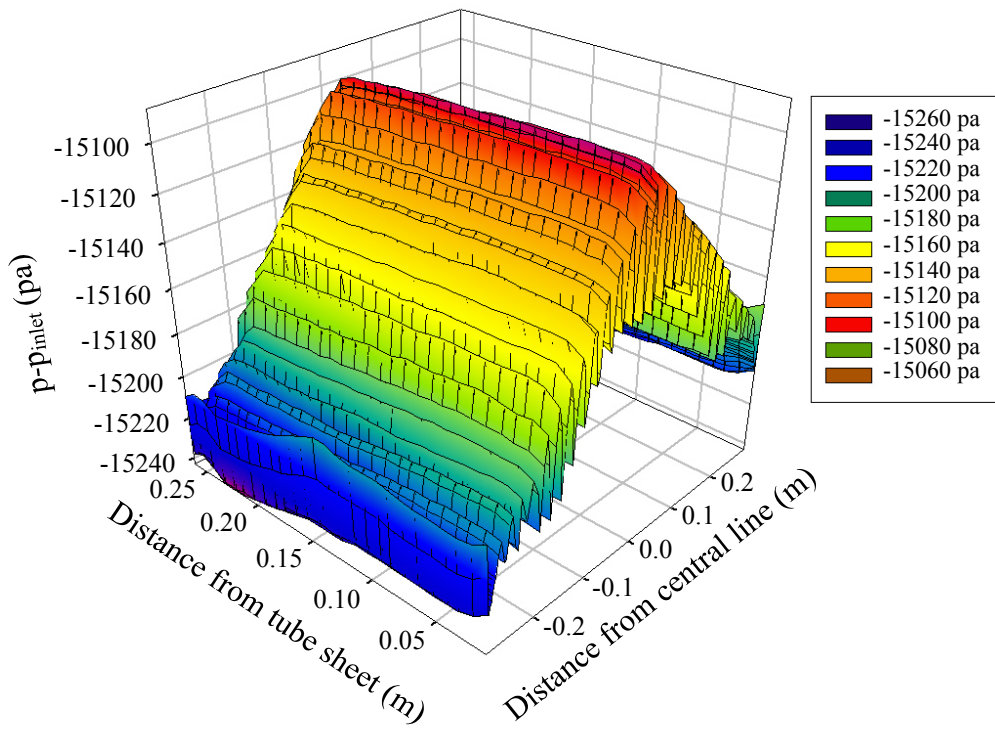$$\Phi = \frac{(\Gamma_{shell})_{hor.}}{(\Gamma_{shell})_{ver.}}$$ (5.9)
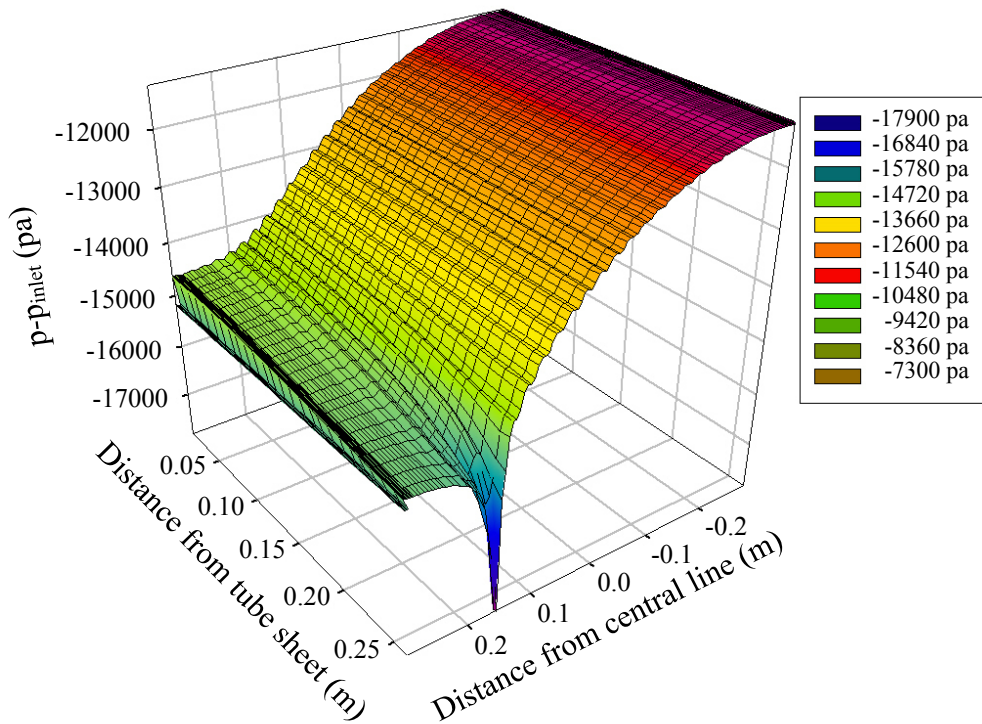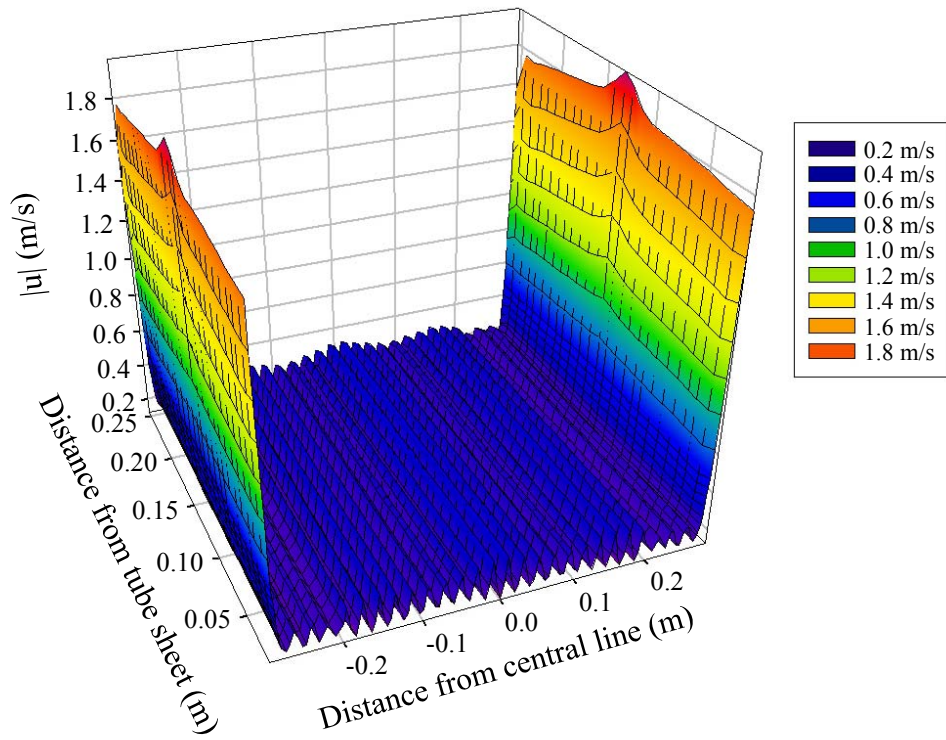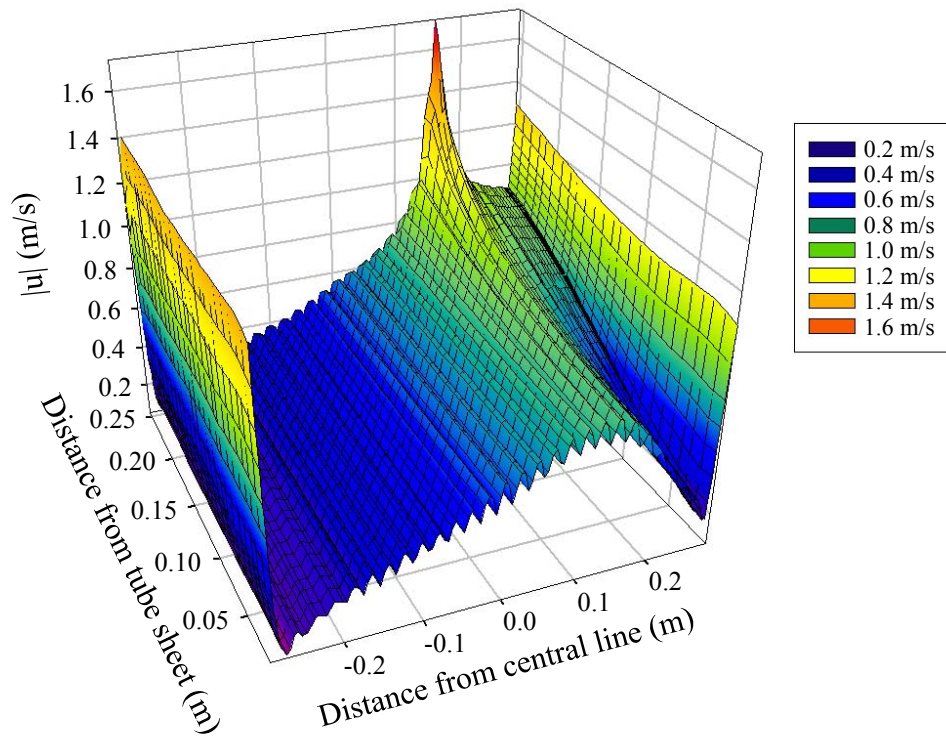
Figure 5.19: x-velocity profile at the centre of the inlet zone for both horizontally (top) and vertically (bottom) orientated baffles of a shell and tube heat exchanger with 660 tubes (Re_{inlet}=3.4×10^5).
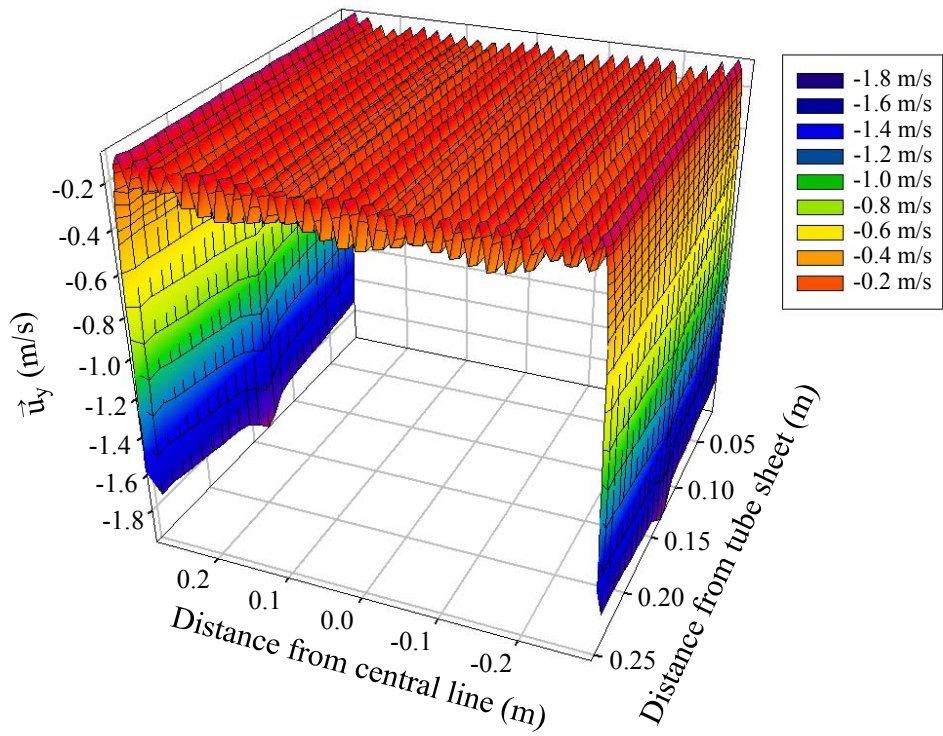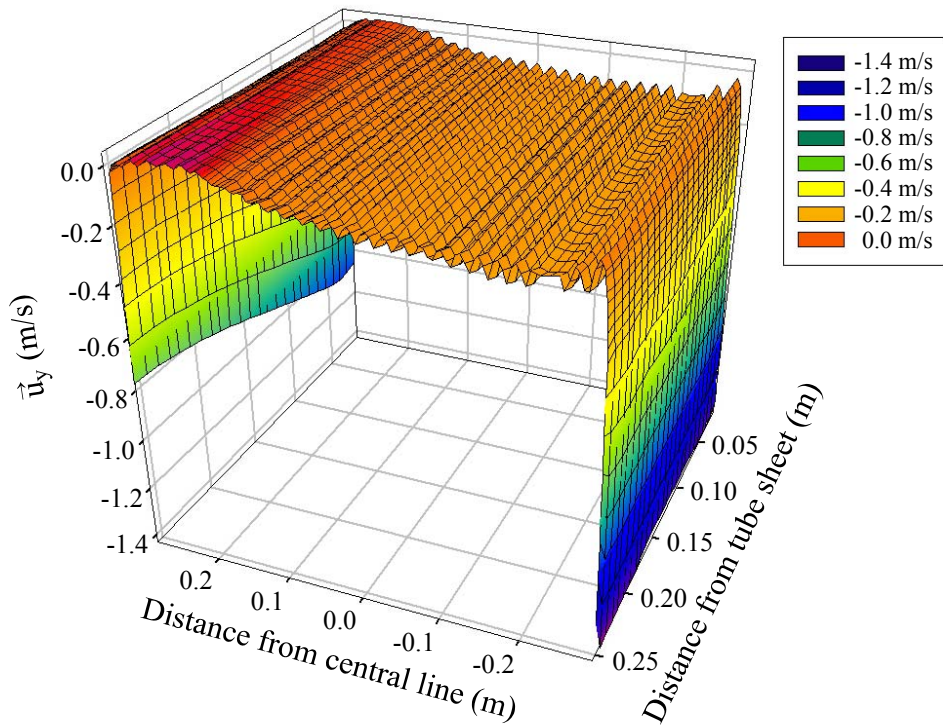
Figure 5.20: y-velocity profile at the centre of the inlet zone for both horizontally (top) and vertically (bottom) orientated baffles of a shell and tube heat exchanger with 660 tubes ($Re_{inlet}=3.4\times10^5$).

Figure 5.21: z-velocity profile at the centre of the inlet zone for both horizontally (top) and vertically (bottom) orientated baffles of a shell and tube heat exchanger with 660 tubes ($Re_{inlet}=3.4\times10^5$).

Applying the Equation (5.8) in Equation (5.9), the performance factor is simply as:

$$\Phi = \frac{\left(h_{shell}/\Delta p_{shell}\right)_{hor.}}{\left(h_{shell}/\Delta p_{shell}\right)_{ver.}} = \frac{\left(h_{hor.}/h_{ver.}\right)_{shell}}{\left(\Delta p_{hor.}/\Delta p_{ver.}\right)_{shell}} = \frac{\left(Nu_{shell}/Nk_{shell}\right)_{hor.}}{\left(Nu_{shell}/Nk_{shell}\right)_{ver.}} = \frac{\left(Nu_{hor.}/Nu_{ver.}\right)_{shell}}{\left(Nk_{hor.}/Nk_{ver.}\right)_{shell}} \quad (5.10)$$

A performance factor Φ greater than one indicates that a heat exchanger with horizontally orientated baffles is more desirable than one with vertical baffle orientation. Rationally, no advantage exists between different baffle orientations when the performance factor is equal or near to one.

Figure 5.22 shows the performance factor Φ at baffle cut 24% for liquid water. As it is shown in Figure 5.22, at Reynolds number 4.6×10^3 the value of Φ is about 1.22 and then at Reynolds number 7700 it reaches a maximum value about 1.24. Next to this local maximum, the performance Φ decreases as the Reynolds number increases. The minimum value for Φ is approximately 0.98 at Reynolds number 92000. In this range of Reynolds number ($4.6 \times 10^3 \leq Re_{inlet} \leq 9.2 \times 10^4$), the value of y+ is near 10.

Next to this Reynolds number range, the value of Φ increases with increasing the Reynolds number. At $Re_{inlet} \approx 1.7 \times 10^5$ the value of Φ is equal to 1. In this range, y+ is between 11.225 and 16. Next to it, the performance Φ ascends continuously with increasing the Reynolds number. At $Re_{inlet} \approx 3.4 \times 10^5$ the value of Φ reaches 1.1. It seems that the trend of Φ at high Reynolds number approaches to a constant value around 1.1.
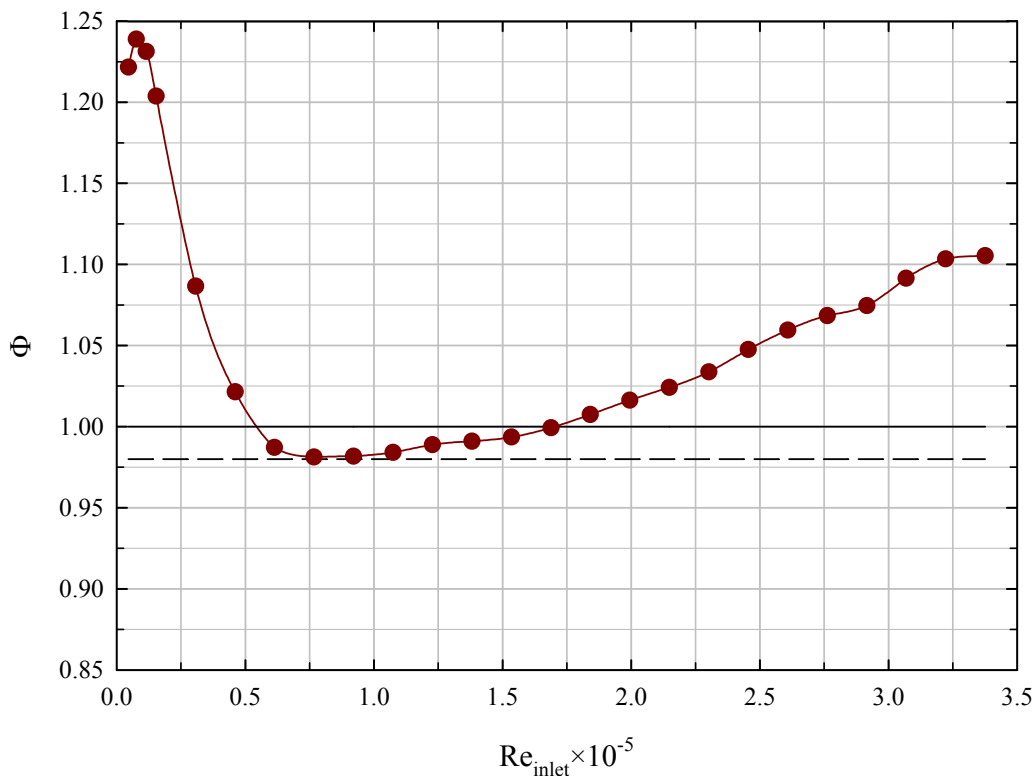
Figure 5.22: Inlet zone performance factor Φ at baffle cut 24% for liquid water as a function of Reynolds number. The heat transfer processes is heating.

Figure 5.22 shows the benefit of using horizontal baffle orientation compared to the vertical baffle orientation. Even though the results confirm the predicted behaviour discussed in

subsection 3.3, the CFD resuls have to be compared with experimental data in order to ensure the validation of the numerical results.

5.4 Validation and Sensibility Analysis

The numerical results are based on a set of convergence criteria. The nature of discretization makes it impossible to have an exact conformity between the numerical results and the hypothetical exact analytical solution. Therefore, an error analysis of the numerical results is required. Moreover, it is necessary to compare the numerical results with experimental data. On the other hand, any design parameter is obtained from the measurement of fundamental quantities. For example, the heat transfer coefficient is obtained from the heat capacity rate, the heat transfer area and the inlet and outlet temperatures. The evaluation of the heat transfer coefficient depends on the measurement of the outlet temperature if the capacity rate, the heat transfer area and the inlet temperature are considered as known variables. Any deviation on the basic quantities will cause deviations on the pertinent parameters. Therefore a sensibility analysis is performed which is suitable to explain the exactness of the results achieved.

5.4.1 Validation with Experimental Data for Ideal Tube Banks
A CFD model is implemented for different ideal tube banks. The mesh structure is based on the mesh scheme explained in section 5.2 and the numerical setup is according to Table 5.4. The ideal tube banks are based on the studies presented by Kays and London [1954]. The numerical results obtained from the simulation of these different ideal tube banks are compared with the experimental data published by Kays and London [1954]. These experimental data are also used by Martin [2002]. The comparison between the experimental data of pressure drop and the pressure drops obtained from the CFD simulations is shown in Figure 5.23. The pressure drop is presented as modified Fanning friction factor f. The CFD simulation can predict the pressure drop of 52 experimental data with a relative absolute error less than 10%, as it is shown in Figure 5.23.
Additionally the experimental data of the heat transfer coefficient, presented as Colburn j-factor for heat transfer j_H, are compared with the results obtained from CFD simulations (see Figure 5.24). An absolute relative error less than 10% for heat transfer coefficient confirms the validation of the simulation.
Even though the flow on the shell-side of an ideal shell and tube heat exchanger is not simillar to the flow on an ideal tube bank, the presented validation proves the reliability and trustworthiness of the CFD setup and simulation procedure.

5.4.2 Error Analysis
The convergence of the numerical calculation is presented as the residuals of continuity, velocities, k, ε and energy. A typical convergence progress for the present investigation is depicted in Figure 5.25.
The horizontal branch of the convergence progress shows that the iterative error is very low and in fact very near to zero. The maximum order of the iterative error is 10^{-5}%. Hence, the numerical error base on the convergence criteria is adequately satisfactory.
The other two important parameters for error analysis are the unbalanced values of mass and energy. The unbalanced value of mass is always equal to zero, since the outflow boundary condition is in some manner a mirror of the velocity inlet boundary condition due to the mass rate. The maximum unbalanced value for energy conservation, however, is about 0.2%. Figure 5.26 presents the unbalanced value of energy as a function of the inlet Reynolds numbers.
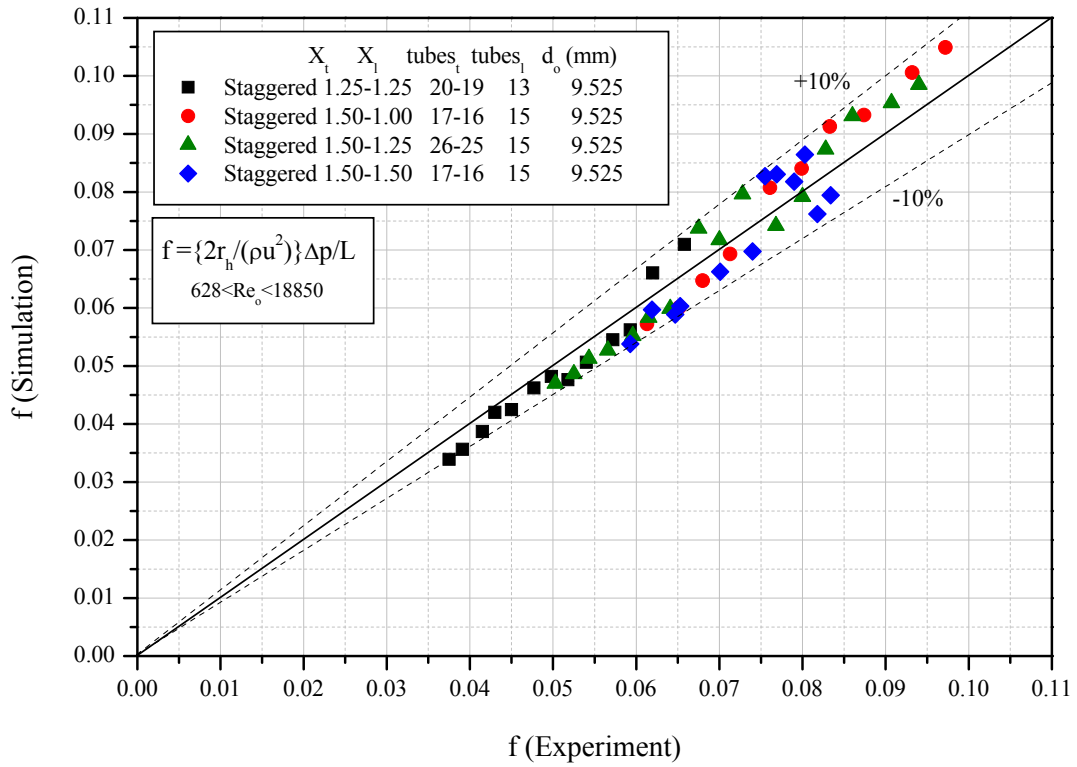
Figure 5.23: Comparison between the experimental data of pressure drop and the pressure drops obtained from the CFD simulations.
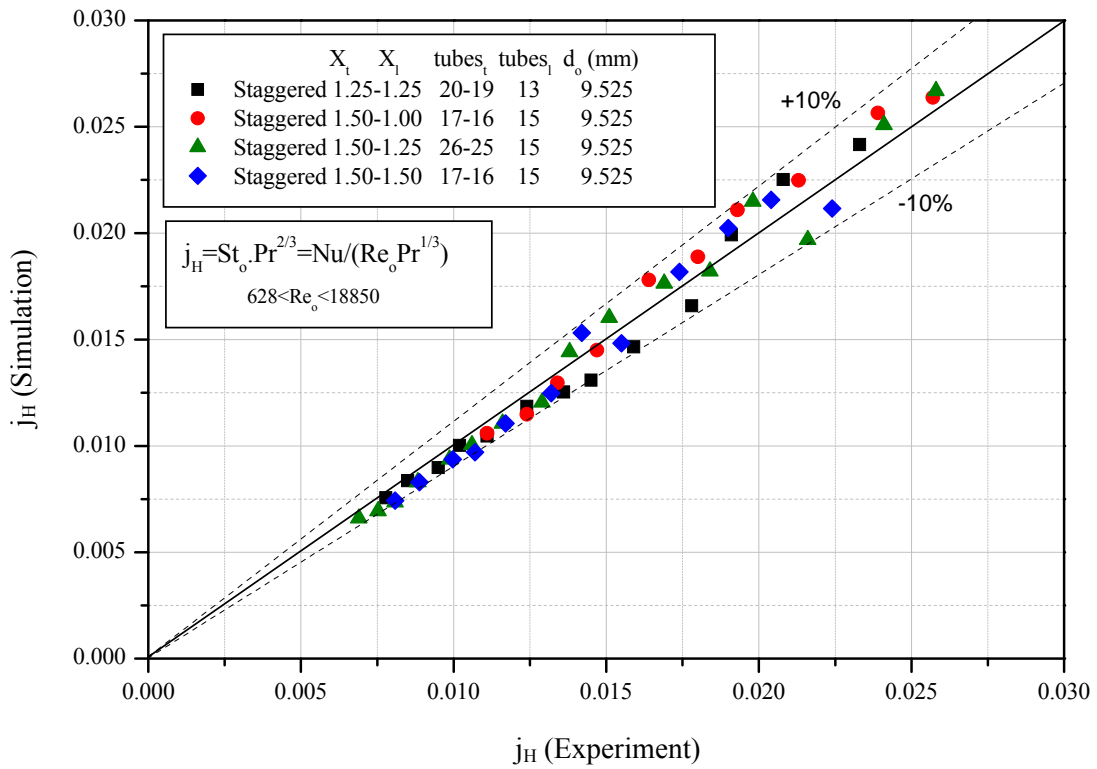
Figure 5.24: Comparison between the experimental data of heat transfer coefficient and the heat transfer coefficients obtained from the CFD simulations.
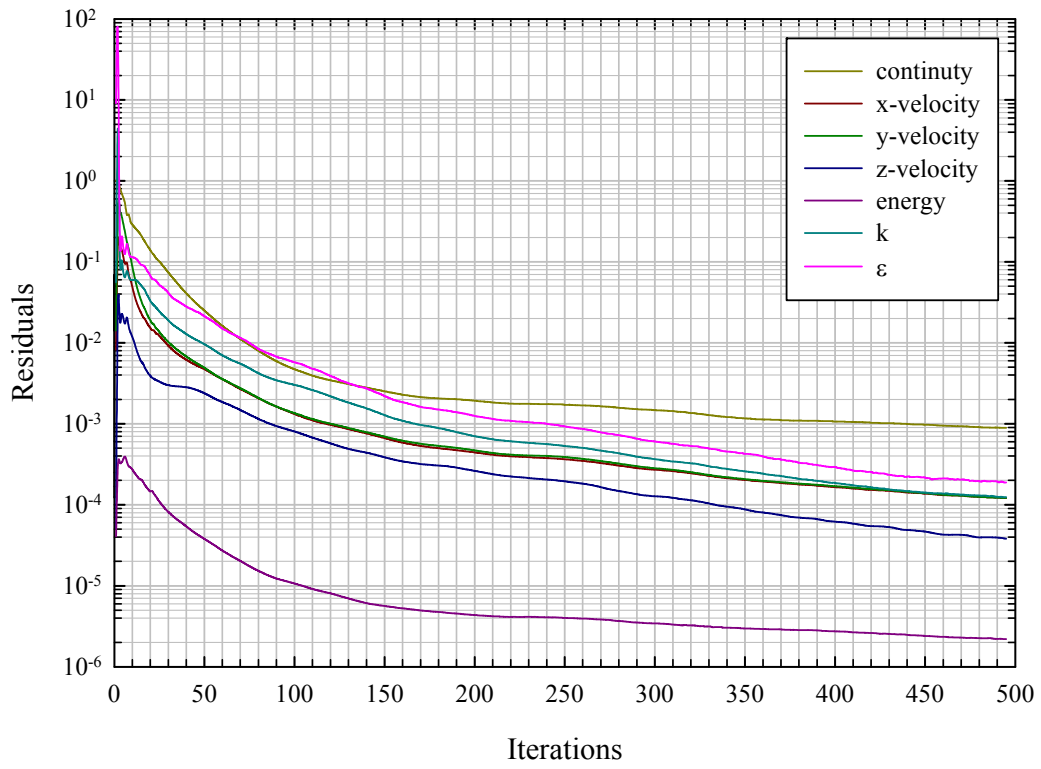
Figure 5.25: Convergence progress for the present investigation as residuals for continuity, velocities, energy, k and ε.
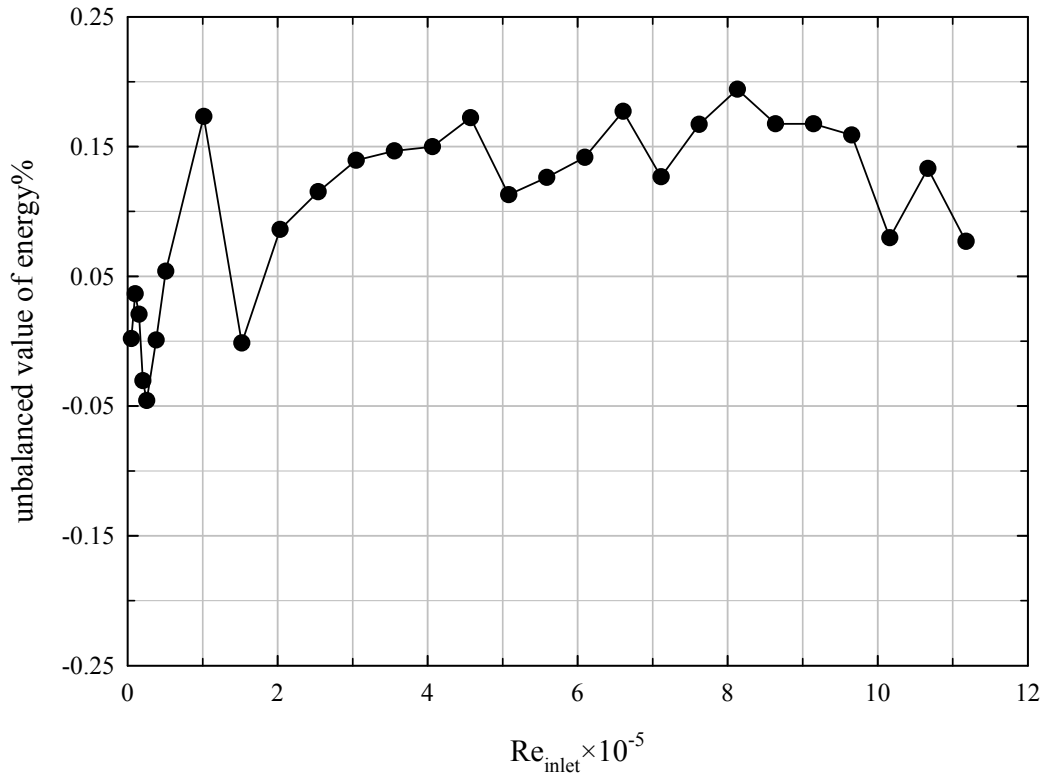
Figure 5.26: Maximum unbalanced value of energy as a function of the inlet Reynolds number.

54

5.4.3 Sensibility Analysis

The relative error of the Nusselt number, i.e. $\|\varepsilon_{Nu}\|$, can be represented as a function of the relative error of the outlet temperature, i.e. $\|\varepsilon_T\|$.

$$\|\varepsilon_{Nu}\|=\pm\frac{\theta_o}{|\theta\text{-}1|}\frac{\gamma}{St_{inlet}}\exp\left(\frac{St_{inlet}}{\gamma}\right)\|\varepsilon_T\| \qquad (5.11)$$

with $\theta=T_{wall}/T_{in}$, $\theta_o=T_{out}/T_{in}$. The inlet Stanton number St_{inlet} is equal to $Nu/\left(Re_{inlet}\overline{Pr}\right)$ and the dimensionless parameter γ is equal to $(\mu_{in}/\overline{\mu})(\ell_H/D_n)(A_{in}/A_H)$. T_{wall} is the average temperature at the tube walls. T_{in} and T_{out} are the inlet and outlet temperatures, respectively. Nu is the shell-side Nusselt number, Re_{inlet} is the inlet Reynolds number and $\overline{Pr}$ is the average shell-side Prandtl number. The shell-side dynamic viscosity at inlet is denoted with μ_{in} and $\overline{\mu}$ is the average shell-side dynamic viscosity. The heat transfer characteristic length of the heat exchanger is denoted with ℓ_H and D_n is the inside diameter of the inlet nozzle. A_{in} is the cross sectional area of the inlet nozzle and A_H is the total heat transfer area. The derivation of Equation (5.11) is given in Appendix C.

The relative error of the shell-side pressure drop, i.e. $\|\varepsilon_{\Delta p}\|$, can be represented as a function of the relative error of the outlet temperature, i.e. $\|\varepsilon_T\|$.

$$\|\varepsilon_{\Delta p}\|=\pm 2.5\frac{\theta_o}{|\theta\text{-}1|}\frac{\gamma}{St_{inlet}}\exp\left(\frac{St_{inlet}}{\gamma}\right)\|\varepsilon_T\| \qquad (5.12)$$

The derivation of Equation (5.12) is also presented in Appendix C.

Equation (5.12) shows that the absolute relative error of the shell-side pressure drop is 2.5 times higher than the absolute relative error of the shell-side Nusselt number.

Figure 5.27 represents the relative error of the Nusselt number as a function of γ/St_{inlet} with the relative temperature deviation for $\theta=T_{wall}/T_{in}=400K/370K\cong1.08$ as a parameter.
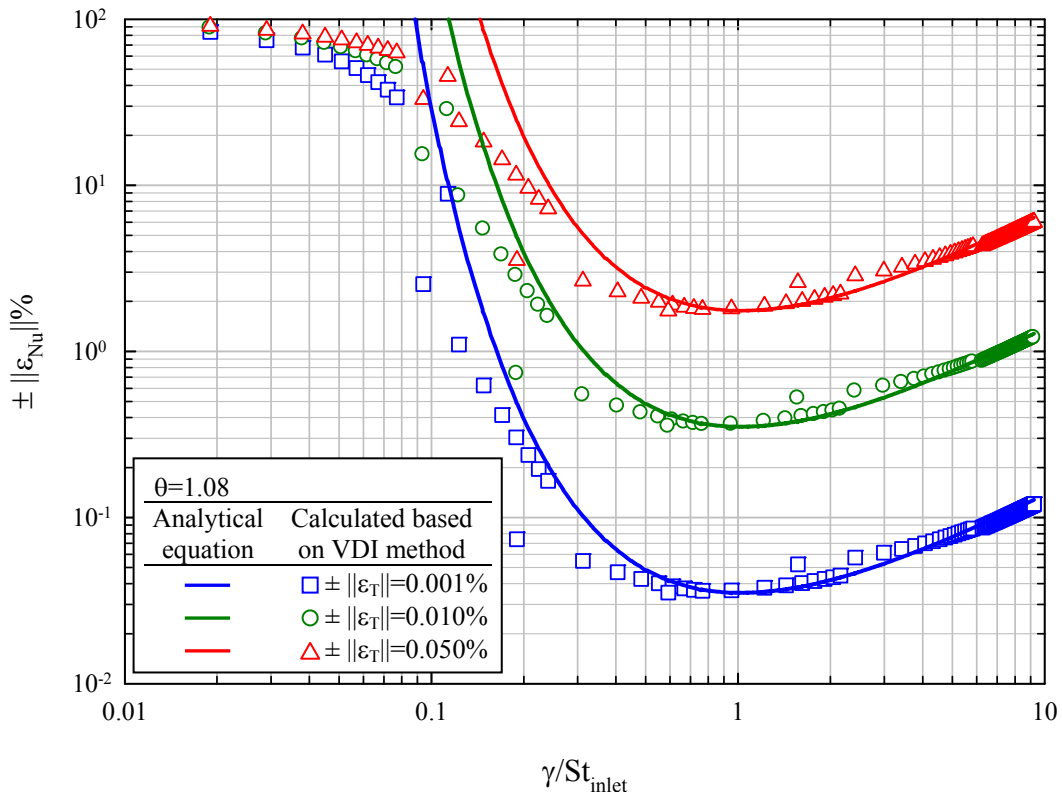
Figure 5.27: Relative deviation of the Nusselt number obtained from Equation (5.11) as a function of γ/St_{inlet}.

The relative deviation calculated from Equation (5.11) is presented by solid lines while, the relative deviation obtained by applying the VDI method is shown by symbols.

From Figure 5.27 and Equations (5.11) and (5.12) it can be seen that a small deviation in the measurement of the outlet temperature will cause a significant deviation in the calculation of the shell-side heat transfer coefficient and pressure drop. This deviation decreases by increasing the Reynolds number and/or the heat transfer area A_H. Figure 5.27 proves that the semi-analytical equation (5.11) can be used as a suitable method to find the sensibilty of the Nusselt number calculation regarding outlet temperature. It is obvious from Figure 5.27 that at high inlet Stanton number and/or heat transfer area A_H, the Nusselt number is very sensible to the measured temperature. Hence, at low Reynolds numbers the confirmation of the CFD results with the experimental data and/or the data obtained form a calculation method, like VDI and Delaware methods, is very difficult. This is especially important for shell-side fluids with low Prandtl numbers, i.e. gases. However, at high Reynolds numbers, a low deviation between the experimental Nusselt numbers and the Nusselt numbers obtained from the CFD simulation shows a negligible difference between the temperatures measured in the experiment and the temperatures calculated by the CFD simulation. This attests a significant satisfactory agreement of the CFD simulation with the measurement data.

5.4.4 Validation with VDI Method

The CFD results for the shell-side heat transfer coefficient are compared with the shell-side heat transfer coefficient calculated according to the VDI method. The comparison between the two sets of results is illustrated in Figure 5.28, where the shell-side heat transfer coefficient is presented in a dimensionless form as shell-side Nusselt number. For the calculation water as shell-side fluid, cooling as heat transfer process and 24% as baffle cut were used.
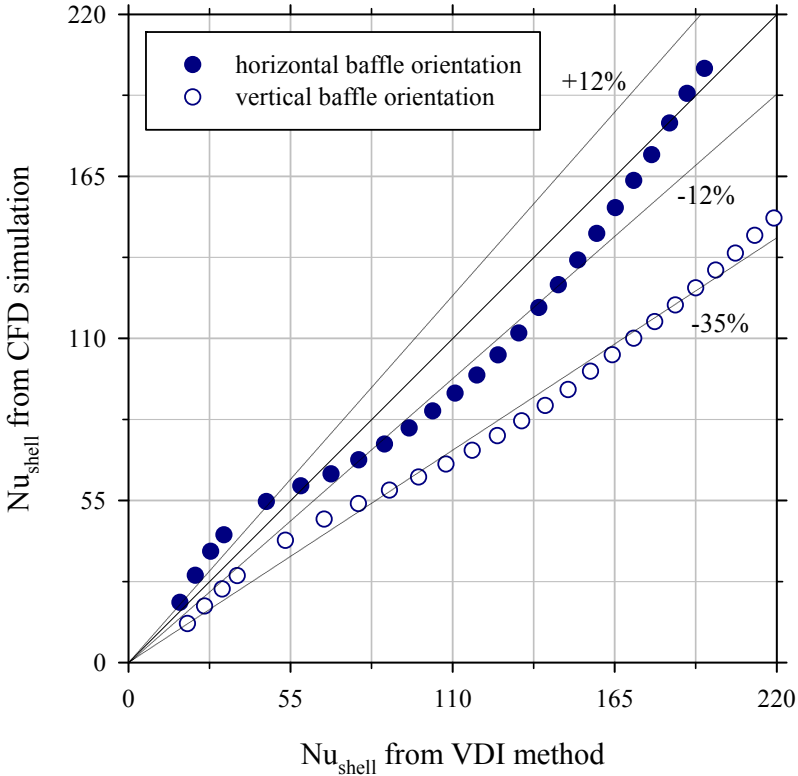
Figure 5.28: Comparison between the CFD results for the shell-side Nusselt number, and the shell-side Nusselt numbers obtained by the VDI method.

The Reynolds number is in the range $4.6 \times 10^3 \leq Re_{inlet} \leq 3.4 \times 10^5$. This corresponds to $0.14 \leq \gamma/St_{inlet} \leq 0.78$.

The absolute average deviation of the CFD results from the results obtained by the VDI method is about 12% for the horizontal baffle orientation. Based on the sensibility analysis discussed in subsection 5.9.3, 12% deviation in the Nusselt number corresponds to a deviation between 0.006% and 0.190% in the temperature, i.e. a temperature deviation between 0.02 and 0.7 °C. This confirms the significant agreement between the CFD results and the VDI method.

However, for the vertical baffle orientation, the deviation in the Nusselt numbers is up to 35% which corresponds to a temperature deviation of more than 1%, i.e. a temperature deviation of about 4 °C. This considerable deviation confirms that the VDI method cannot predict the shell-side heat transfer coefficient (and pressure drop as well) in arbitrary baffle orientations in a satisfactory manner, and that only for the horizontal baffle orientation good results are achieved.

5.5 Performance of the Inlet Zone Subject to Different Shell-Side Fluid Viscosities

In order to study the effect of baffle orientation on the performance factor, cp. Equation (5.10), at different baffle cuts and different shell-side viscosities, three shell-side fluids and three baffle cuts are considered. The shell-side fluids are presented in Table 5.3 and the baffle cuts are 20%, 24% and 30%.

Moreover, seven Reynolds numbers in the range $1.5 \times 10^5 \leq Re_{inlet} \leq 3.4 \times 10^5$ are considered for the investigation. Hence, 126 simulations are applied to analyse the performance of the inlet zone at horizontal and vertical baffle orientations.

In the following, the final results of these simulations are presented and discussed.

5.5.1 Pressure Drop

Figure 5.29 shows the shell-side pressure drop as a function of the Reynolds number at the inlet. The baffle cut and the baffle orientation are used as parameters.

The advantages of introducing pressure drop as dimensionless Kârmân number is to reduce the number of curves since at any baffle orientation and any baffle cut, the same curve explains the behaviour of pressure drop for any fluid. The ratio of the pressure drop for two different fluids depends on the ratio of their density and dynamic viscosity according to Equation (5.13).

$$\frac{(\Delta p)_{fluid\,2}}{(\Delta p)_{fluid\,1}} = \left\{ \frac{(\rho)_{fluid\,1}}{(\rho)_{fluid\,2}} \right\} \left\{ \frac{(\mu)_{fluid\,2}}{(\mu)_{fluid\,1}} \right\}^2 \qquad (5.13)$$

For a defined geometry, the pressure drop of engine oil is about 127 times higher than the pressure drop for liquid water and 1758 times higher than the pressure drop for air.

Figure 5.29 shows that for a given baffle cut, the pressure drop for the horizontal baffle arrangement is always higher than the pressure drop for the vertical baffle orientation. The results in detail are as follows:

- The geometry with a vertical baffle orientation and a baffle cut of 30% shows the smallest pressure drop. The same values were found for a baffle cut of 24% (vertical baffle orientation).
- For the geometry with a horizontal baffle orientation and a baffle cut of 30%, 8% higher pressure drop is observed compared to the geometry with the same baffle cut but vertical baffle orientation.

- The geometry with horizontal baffle orientation (24% baffle cut) and the geometry with vertical baffle orientation (20% baffle cut) show the same pressure drop. This pressure drop is about 20% higher than the pressure drop observed for vertical orientated baffle with a cut of 30%.
- The highest pressure drop is calculated for horizontal orientated baffle with a baffle cut 20%.
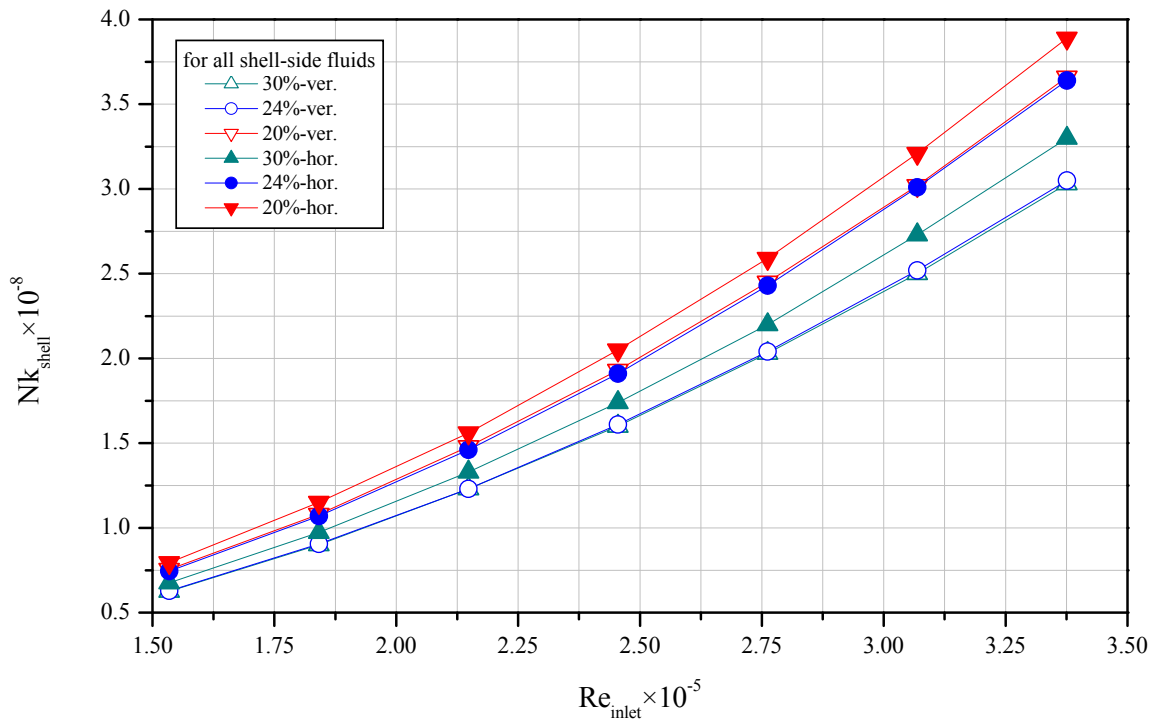
Figure 5.29: The effect of baffle cut and baffle orientation on the shell-side pressure drop presented as shell-side Kârmân number Nk_{shell} as a function of inlet Reynolds.

The shell-side pressure drop as a function of the baffle cut is presented in Figure 5.30. According to Figure 5.30, the value of the pressure drop decreases with increasing baffle cut. The dependency of pressure drop on the baffle cut seems to be linear for the horizontal baffle orientation and shows a decrease from baffle cut 20% to 30%. A decrease from baffle cut 20% to 24% can also be seen for the vertical baffle orientation while in the range from 24% to 30% the change of the pressure drop is negligible.

Moreover, the pressure drop increases as the Reynolds number increases, which is an expected behaviour.

Figure 5.31 represents the ratio of the dimensionless Kârmân number for the horizontal and vertical arrangement as a function of the Reynolds number at the inlet. This ratio is always greater than 1 which confirms that the horizontal baffle orientation produces more pressure drop than the vertical baffle orientation.

As can be seen from Figure 5.31, at baffle cut 24% the horizontal baffle orientation produces a pressure drop nearly 1.19 times higher than the pressure drop evaluated for the vertical baffle orientation. This value is about 1.06 and 1.08 at baffle cut 20% and 30%, respectively.
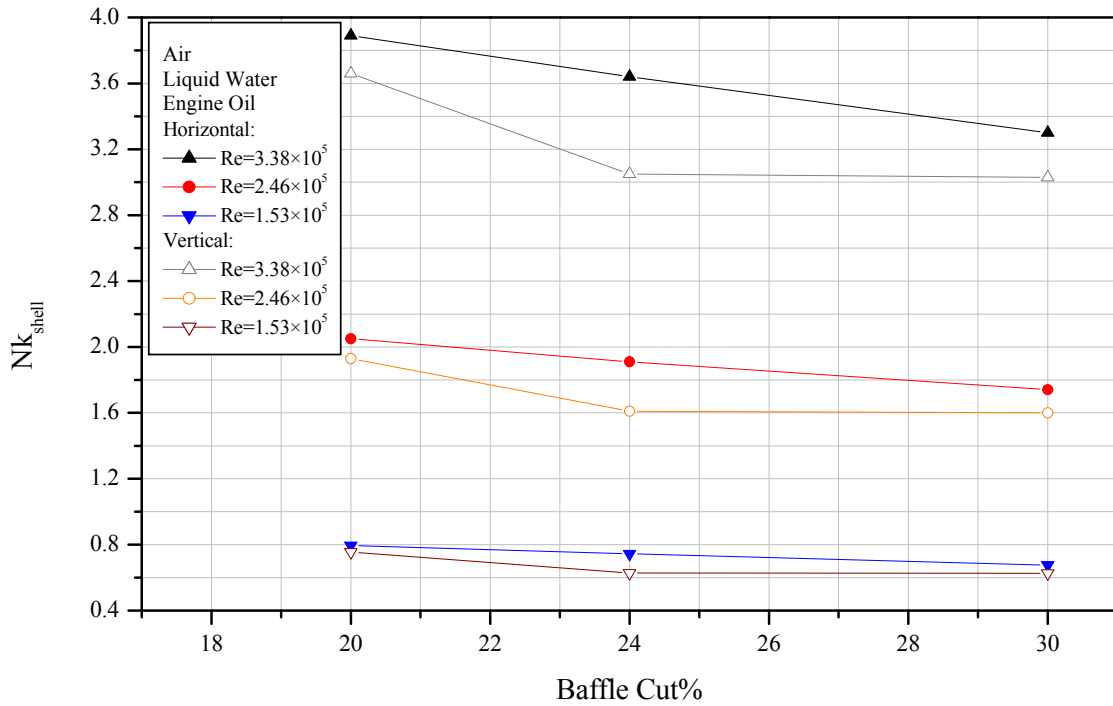
Figure 5.30: Shell-side pressure drop as a function of baffle cut at low, middle and high Reynolds numbers.
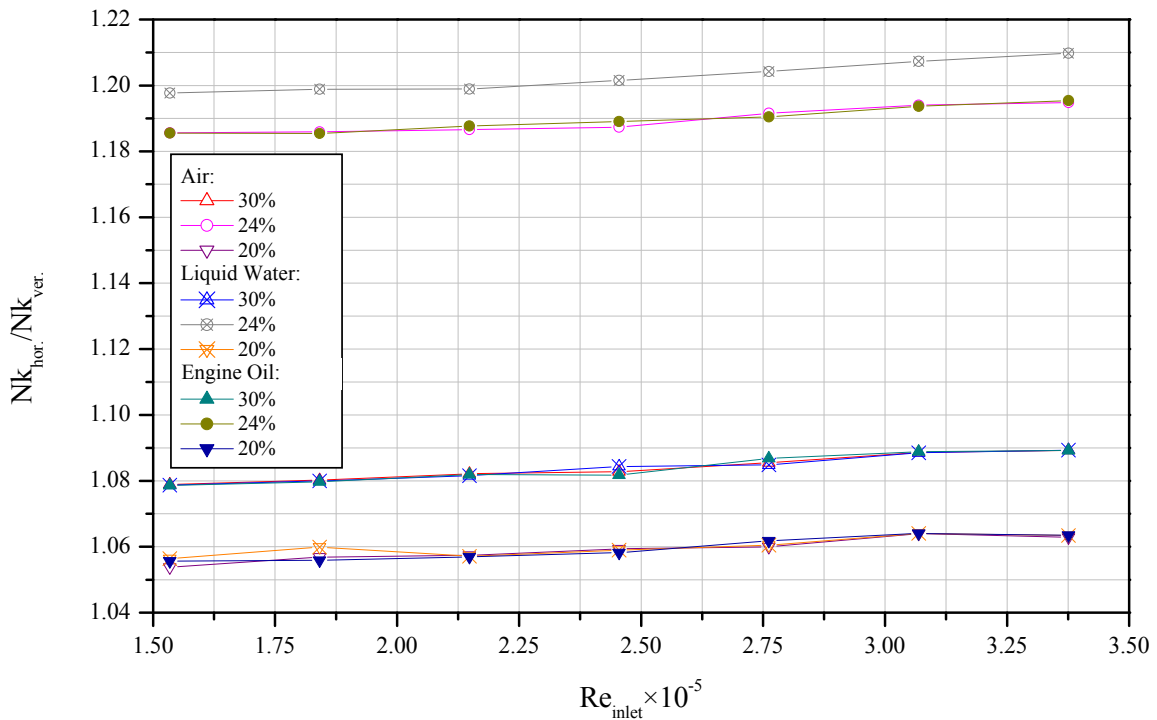
Figure 5.31: The effect of baffle cut on ratio of shell-side pressure drop for horizontal and vertical baffle orientation at different Reynolds number.

5.5.2 Heat Transfer Coefficient

In Figure 5.32 the dimensionless shell-side heat transfer coefficient is shown as a function of the Reynolds number with the baffle cut, the baffle orientation and the working fluids as parameters.

Figure 5.32 shows that the overall shell-side heat transfer coefficient increases with increasing Reynolds number. In general the heat transfer in the shell and tube heat exchanger with horizontal baffle orientation is better than the heat transfer in a heat exchanger with vertical baffle orientation.
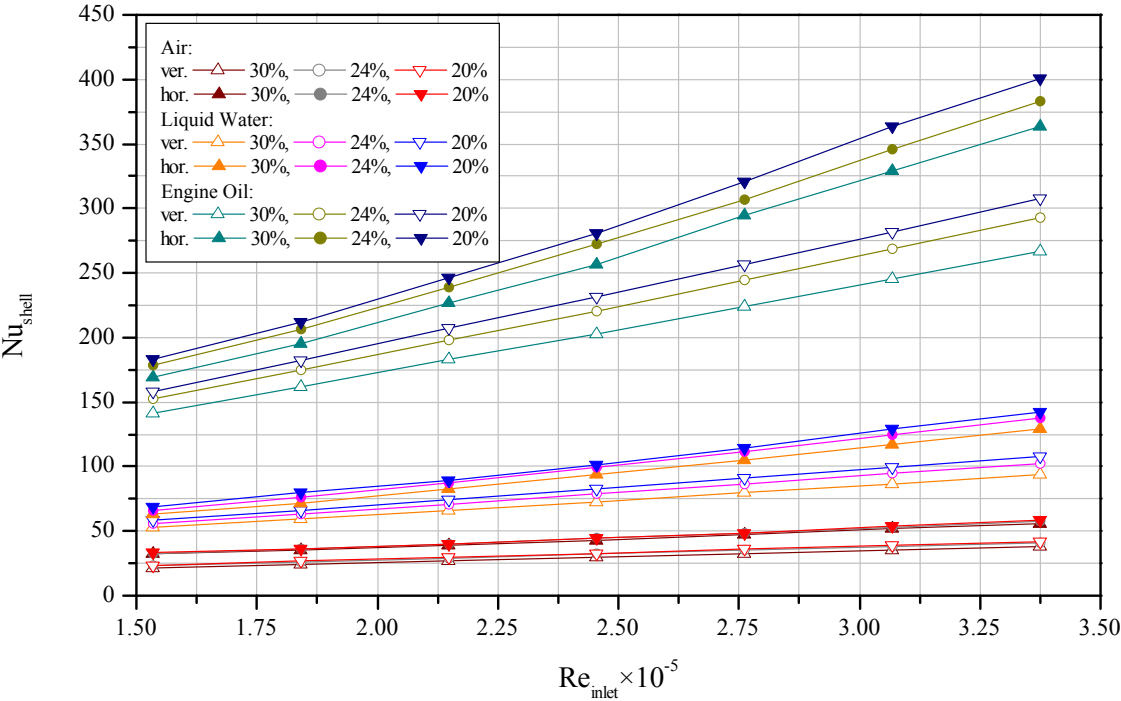
Figure 5.32: The effects of baffle cut and baffle orientation on the shell-side heat transfer coefficient at different Reynolds numbers and for different working fluids.

Increasing the viscosity of the working fluid in the shell side at constant Reynolds number causes an increase of the heat transfer coefficient. For instance, at horizontal baffle orientation, the shell side heat transfer coefficient using liquid water is about 2.2 times higher than the shell side heat transfer coefficient using air as working fluid. The heat transfer coefficient at the shell sides is found to be 6.9 times higher for engine oil as the working fluid, compared to air as working fluid. In the same geometries, the shell-side heat transfer coefficient using liquid water is only 2.5 times more than the value obtained for air.

Figures 5.33 (a) to 5.33 (c) present the shell-side heat transfer coefficient for horizontal and vertical baffle orientation as a function of the baffle cut. As it is shown in Figure 5.33, the heat transfer in a geometry with horizontal baffle orientation is always better than the heat transfer in a geometry with vertical baffle orientation.

In Figure 5.34 the effect of the baffle cut on the shell-side heat transfer coefficient for different working fluids is shown.

Figure 5.35 shows the ratio of the dimensionless heat transfer coefficient (horizontal/vertical) as a function of the Reynolds number with the baffle cut and the working fluid as parameters. Results for the horizontal baffle orientation shows 15% to 50% higher heat transfer coefficients compared to the vertical baffle orientation.

When the dynamic viscosity of the working fluid decreases, the momentum transport also decreases. In this case the effect of baffle orientation on the heat transfer is more significant. For gas air, the performance ratio $Nu_{hor.}/Nu_{ver.}$ is then higher than the performance ratio for liquid water. Consequently, the performance ratio $Nu_{hor.}/Nu_{ver.}$ for liquid water is higher than the performance ratio for engine oil.
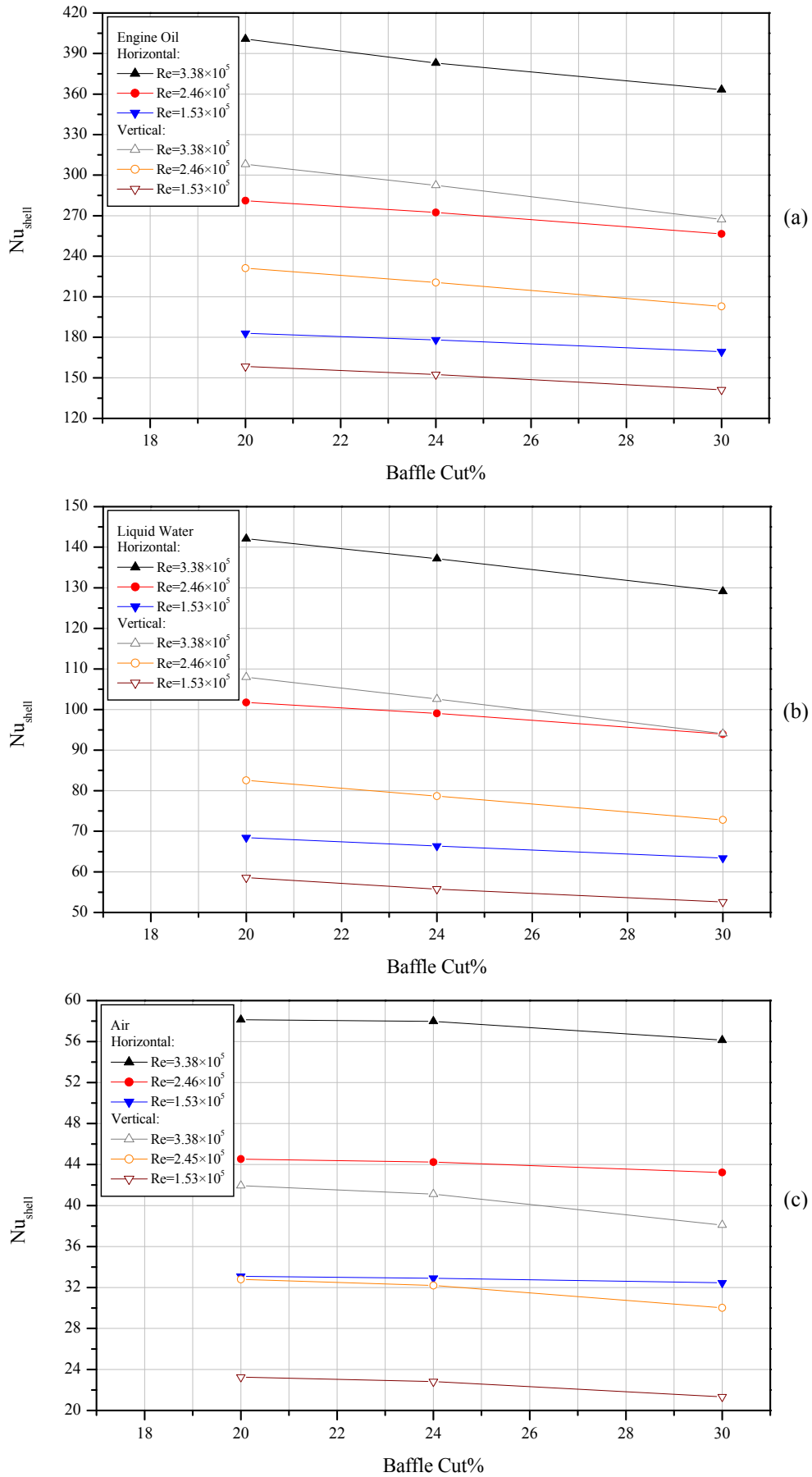
Figure 5.33: Shell-side heat transfer coefficient for horizontal and vertical baffle orientation as a function of baffle cut at low, middle and high Reynolds number. The working fluids are engine oil (a), liquid water (b) and air (c).

61

Increasing the Reynolds number increases the performance ratio $Nu_{hor.}/Nu_{ver.}$ for liquid water and engine oil. For air a minimum performance ratio $Nu_{hor.}/Nu_{ver.}$ is detected at a Reynolds number near 2.4×10^5.
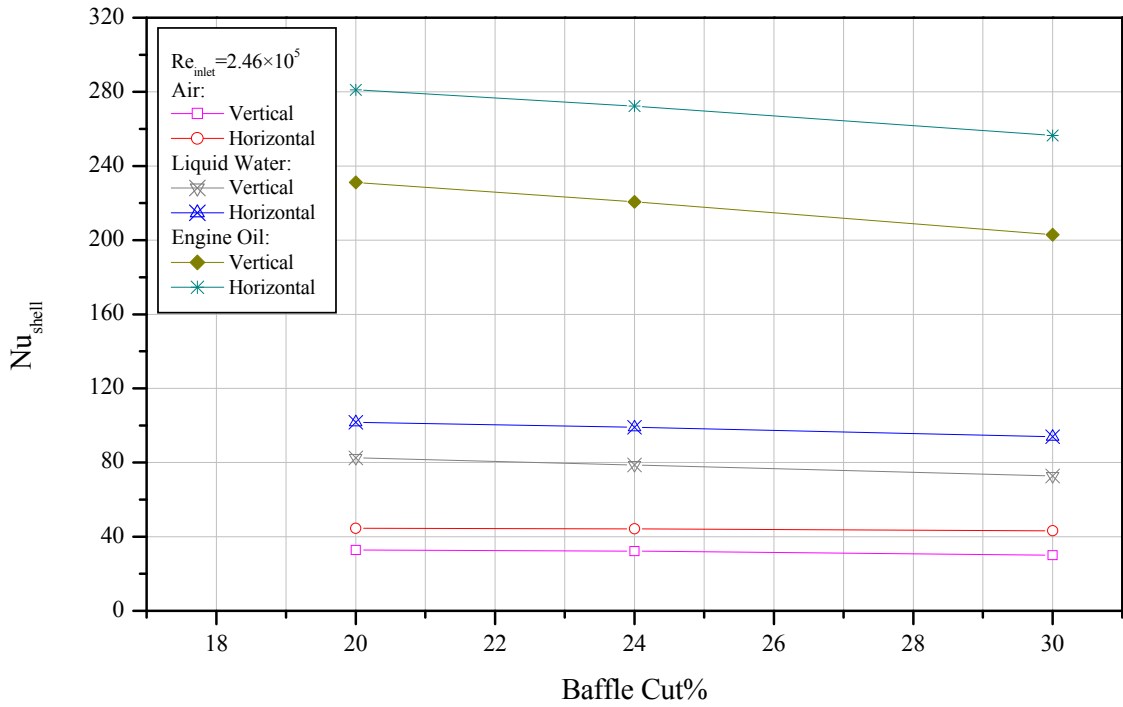
Figure 5.34: The effect of baffle cut on shell-side heat transfer coefficient for different working fluids at $Re_{inlet}=2.46 \times 10^5$.
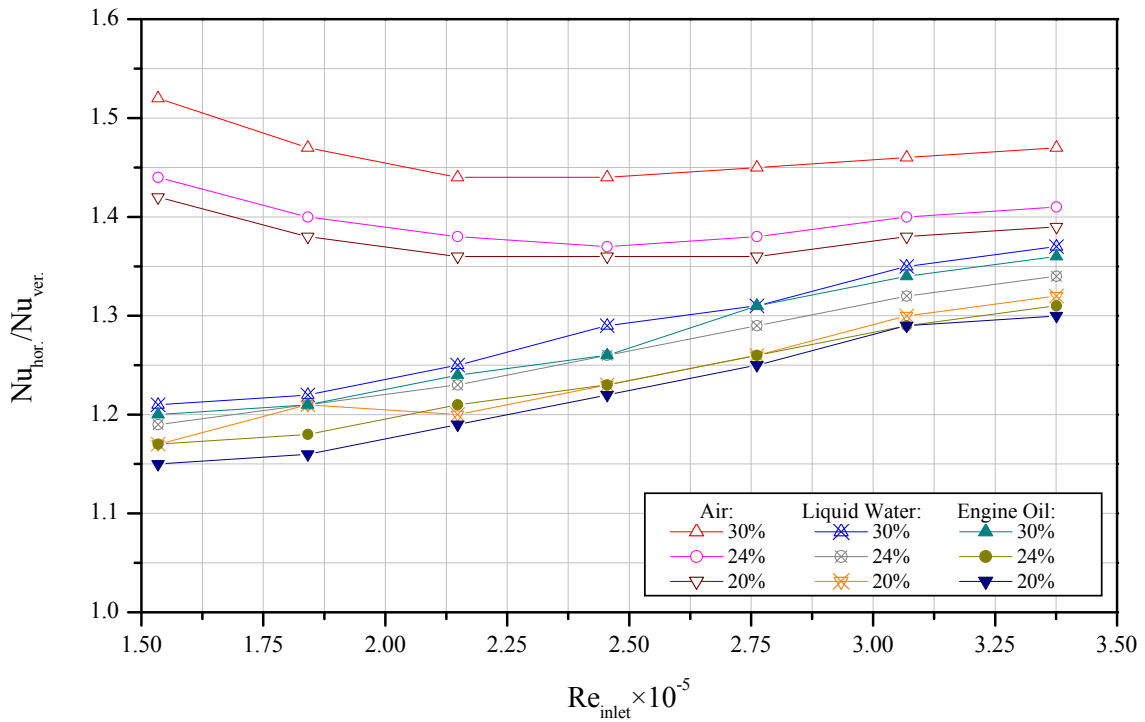
Figure 5.35: The effect of baffle orientation on heat transfer coefficient which is presented as performance ratio $Nu_{hor.}/Nu_{ver.}$ as a function of Reynolds number for different fluid in shell side.

To evaluate the advantages of horizontal baffle orientation over vertical baffle orientation, the performance Φ defined in Equation (5.10) is depicted in Figure 5.36.
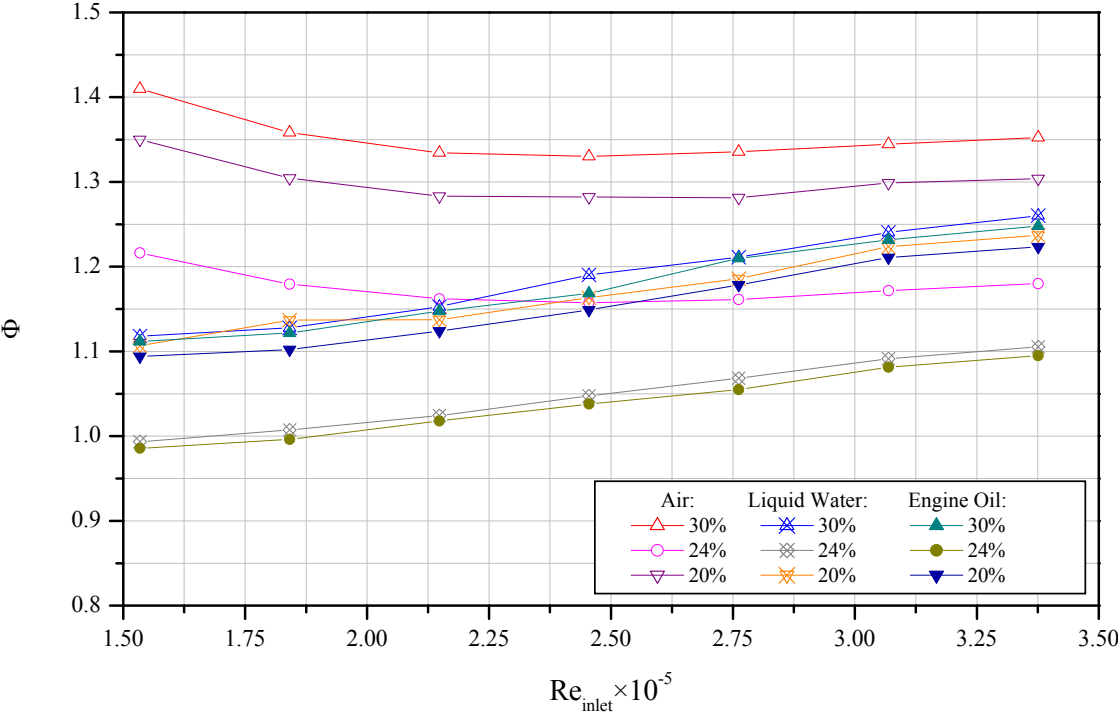
Figure 5.36: The performance factor Φ as a function of Reynolds number for different shell-side fluids.

The analysis of the behaviour of the performance factor Φ as a function of the Reynolds number (see Figure 5.36), can be summarized as follows:

1. Independent from the baffle cut considered, the Φ value for air has the highest value. Smallest values for Φ are obtained for engine oil. Hence, an increase of the dynamic viscosity of the working fluid results in a decreasing of the Φ value.

2. The value of Φ for the baffle cuts 20% and 30% are about 11% and 14% higher than the value of Φ for the baffle cut 24%.

3. An increase of the Reynolds number causes an increase of the Φ values when liquid water and engine oil were used as working fluids. On the other hand, a minimum value for Φ is detected at Reynolds numbers near 2.4×10^5 when air is used as working fluid.

Figures 5.37 (a) to 5.37 (c) show the behaviour of the performance Φ subjected to the Reynolds number for each shell-side fluid, separately. These figures are presented in order to show the different behaviour of air as compared to the other two liquids more clearly. Looking at these figures, the same behaviour of liquid water and engine oil can be observed.

It is possible to predict the value of the performance factor Φ for different shell-side fluids at different baffle cuts by using the data for one particular working fluid at one specified baffle cut. The particular working fluid is called reference working fluid or reference shell-side fluid and the specified baffle cut is called the reference baffle cut.

In the following section this idea will be explained and a semi-analytical model for determination of the performance factor Φ will be introduced.
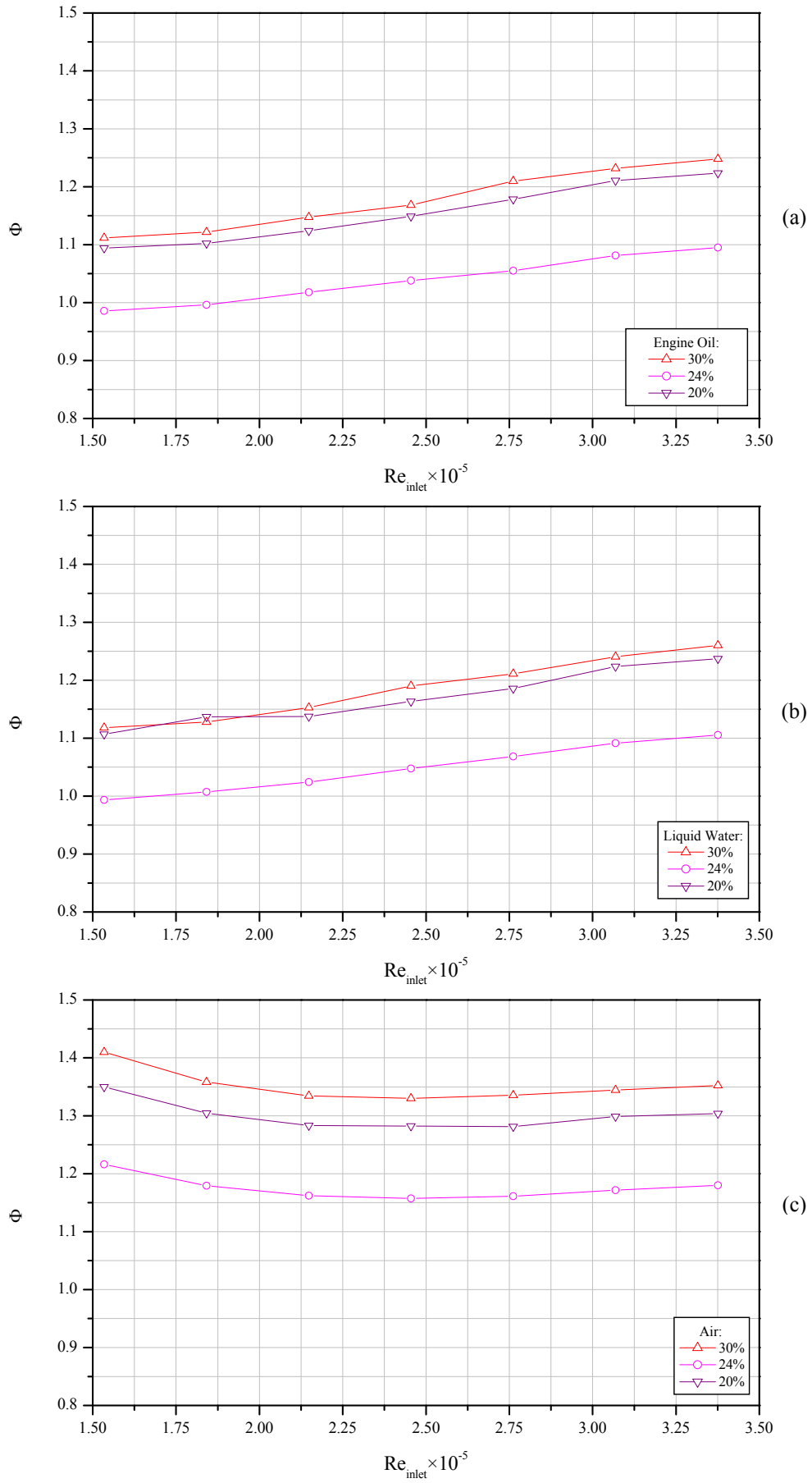
Figure 5.37: The advantage of horizontal baffle orientation: Φ, as a function of Reynolds number for working fluids engine oil (a), liquid water (b) and air (c).

5.6 Semi-Analytical Model for the Performance of the Inlet Zone of Shell and Tube Heat Exchangers without Leakages

In the following sections a semi-analytical model is described for the calculation of the performance factor Φ of the inlet zone of shell and tube heat exchangers with arbitrary baffle cut and without leakages.

5.6.1 Performance Factor of Water at Baffle Cut 24%

It is possible to introduce a function that explains the performance factor Φ of the inlet zone of a shell and tube heat exchanger without leakage flows. This function has the following properties:

1. At very low Reynolds numbers, the performance factor Φ tends to a constant value. This constant value depends on the values of NMSD for horizontal and vertical baffle orientations, i.e. Equations (3.6) and (3.7). In fact, at very low Reynolds numbers, the shell-side fluid will flow in the paths that minimize the energy dissipation and the energy loss of the flow. Moreover, the fluid can flow from the nozzle to the bottom of the shell, directly. This is true especially for dense fluids at very low Reynolds numbers. Hence for dense shell-side fluids the following extreme value condition may be stated:

$$\lim_{Re_{inlet}\to 0}(\Phi) = \Phi|_{Re_{inlet}=0} = \frac{(NMSD)_{horizontal}/r_s + 2}{(NMSD)_{vertical}/r_s + 2} \tag{5.14}$$

2. The kinematic energy of the shell-side fluid increases with Reynolds number. It means that, the shell-side fluid has enough energy to compensate its dissipation rate at higher Reynolds numbers. Therefore, the dispersion of the shell-side fluid will increase with Reynolds number. Hence, the performance factor Φ decreases with increasing Reynolds number. This is true in laminar flow domain:

$$\frac{d\Phi}{dRe_{inlet}} < 0 : \forall Re_{inlet} \in Laminar \tag{5.15}$$

3. In the transition from laminar to turbulent flow, the mixing level of the shell-side fluid will increase with increasing Reynolds number. Therefore, the effect of any geometrical change on the performance factor Φ will be more significant at higher Reynolds numbers. Introducing two limits $Re_{trans,ll}$ (low limit) and $Re_{trans,ul}$ (upper limit) for the description of the transition region yields:

$$\exists ! Re_{inlet} \leq Re_{trans,ll} \mid \frac{d^2\Phi}{dRe_{inlet}^2} = 0 \tag{5.16}$$

$$\exists ! Re_{inlet} \geq Re_{trans,ul} \mid \frac{d^2\Phi}{dRe_{inlet}^2} = 0 \tag{5.17}$$

$$\exists Re_{inlet} \in (Re_{trans,ll}, Re_{trans,ul}) \mid \frac{d\Phi}{dRe_{inlet}} = 0 \tag{5.18}$$

65

4. The energy dissipation rate is approximately independent of the Reynolds number at very high velocities [Boffetta and Romano, 2002]. Moreover, based on the asymptotic invariance approach, turbulent flows will be almost independent of the viscosity. Therefore, at very high Reynolds numbers the performance factor tends to a constant value which has to be controlled mainly by the geometry. On the other hand, in the turbulent flow domain, the pressure drop is approximately proportional to Re^2, while the heat transfer coefficient is proportional roughly to $Re^{0.8}$. Therefore, any geometrical change that enhances the mixing level of the shell-side fluid will increase the heat transfer coefficient much more than the pressure drop. Hence the following condition fits:

$$\left| \frac{d(h_{hor.}/h_{ver.})_{shell}}{dRe_{inlet}} \right| \gg \left| \frac{d(\Delta p_{hor.}/\Delta p_{ver.})_{shell}}{dRe_{inlet}} \right| : \forall Re_{inlet} \in \text{High Turbulent} \quad (5.19)$$

Equation (5.19) shows that the ratio of shell-side heat transfer coefficients will control the performance factor Φ at high Reynolds numbers. The enhancement of the shell-side heat transfer coefficient increases with increasing Reynolds number:

$$\frac{d\Phi}{dRe_{inlet}} \geq 0 : \forall Re_{inlet} \in \text{High Turbulent} \quad (5.20)$$

Moreover, the mixing level of the shell-side fluid depends on the shortest and the longest distance between the inlet nozzle and the baffle window. The shortest distance is proportional to the NMSD and the longest distance depends on the inside shell diameter. Therefore, for extremely high Reynolds numbers it may be hypothesized that:

$$\lim_{Re_{inlet} \to \infty} (\Phi) = \frac{(NMSD)_{horizontal}/r_s + 2}{(NMSD)_{vertical}/r_s + 2} \quad (5.21)$$

5. Since the infinite Reynolds number has only a mathematical interpretation, a Reynolds number will be defined in which the value of Φ reaches 95% of its ultimate value. If this Reynolds number is denoted with $Re_{inlet,95\%\Phi\infty}$, one obtains:

$$\Phi|_{Re_{inlet,95\%\Phi_\infty}} = 0.95 \times \frac{(NMSD)_{horizontal}/r_s + 2}{(NMSD)_{vertical}/r_s + 2} \quad (5.22)$$

A lognormal distribution function satisfies the properties described in Equations (5.14) to (5.22):

$$\Phi = \frac{(NMSD)_{horizontal}/r_s + 2}{(NMSD)_{vertical}/r_s + 2} + \frac{C_1}{Re_{inlet}} \exp\left\{ -0.5 \left(\frac{\ln\left(\frac{Re_{inlet}}{C_2}\right)}{C_3} \right)^2 \right\} \quad (5.23)$$

It is assumed that the constant values of Equation (5.23), i.e. C_1, C_2 and C_3, depend on viscosity, $Re_{trans,ll}$, $Re_{trans,ul}$ and $Re_{inlet,95\%\Phi\infty}$:

$$C_n = f_n\left(\mu, \ Re_{trans,ll}, \ Re_{trans,ul}, \ Re_{inlet,95\%\Phi_\infty} \right) : n \in \{1, 2, 3\} \quad (5.24)$$

For water with constant physical properties, i.e. the physical properties at 20 °C and 1 atm, the hypothetical function that satisfies Equations (5.14) to (5.22) is as follow:

$$\Phi_{24\%\,|\text{Water,ISO}} = \frac{(\text{NMSD})_{\text{horizontal}}/r_s + 2}{(\text{NMSD})_{\text{vertical}}/r_s + 2} - \frac{\text{Re}_{\text{trans,ll}}}{\text{Re}_{\text{inlet}}} \exp\left\{-0.5\left(\frac{\ln\left(\frac{2\text{Re}_{\text{inlet}}}{\text{Re}_{\text{inlet,95\%}\Phi_\infty}}\right)}{\ln\left(\frac{\text{Re}_{\text{inlet,95\%}\Phi_\infty}}{2\text{Re}_{\text{trans,ul}}}\right)}\right)^2\right\} \quad (5.25)$$

with

$$\text{Re}_{\text{trans,ll}} = 5.0\times10^4, \ \text{Re}_{\text{trans,ul}} = 1.1\times10^5, \ \text{Re}_{\text{inlet,95\%}\Phi_\infty} = 6.5\times10^5$$

In Equation (5.25), $\Phi_{24\%\,|\text{Water,ISO}}$ refers to the performance factor Φ at a baffle cut of 24% for water as shell-side fluid with constant physical properties at 20 °C and 1 atm.
The average absolute error between the data presented in Figure 5.22 and the semi-analytical function suggested in Equation (5.25) is less than 1%. The comparison between the CFD results and the semi-analytical model is presented in Figures 5.38 and 5.39 and shows that the semi-analytical function of the performance factor Φ at baffle cut 24% for water can predict the CFD results with a significant accuracy. The absolute relative error of the model with respect to the CFD results ranges between 0.06% and 2.15%.
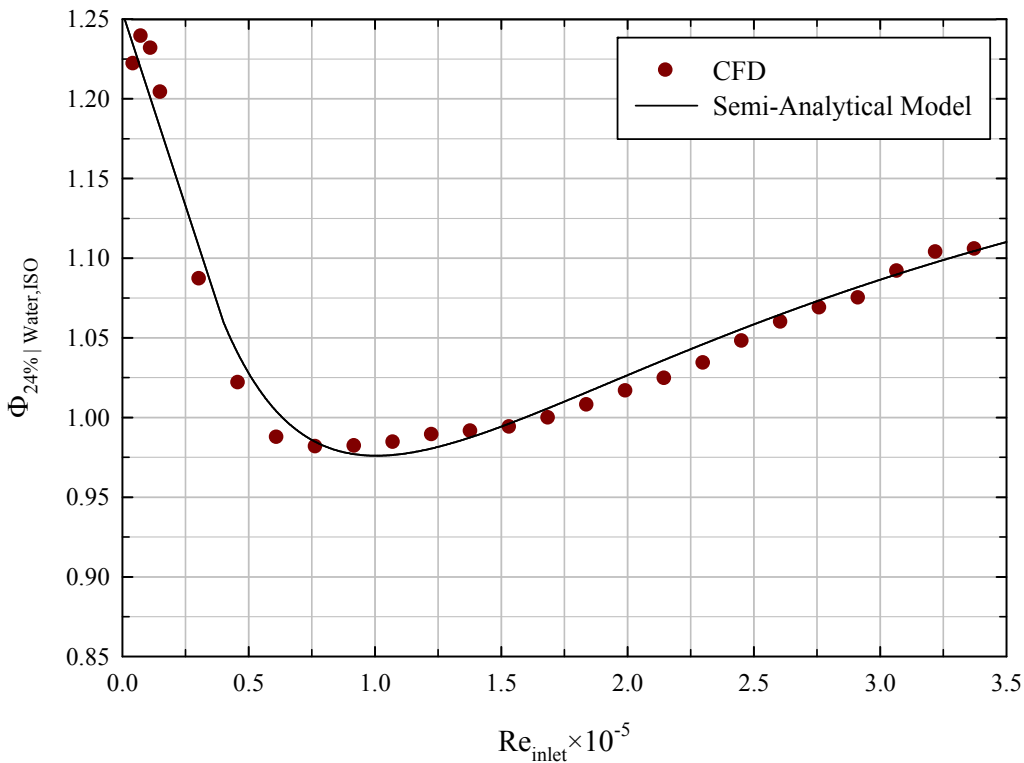
Figure 5.38: Comparison of CFD results and the semi-analytical model presented in Equations (5.25).

5.6.2 Consideration of Different Working Fluids
In order to consider different working fluids for the semi-analytical description, a working fluid preference Θ_{WF} is introduced as follows:
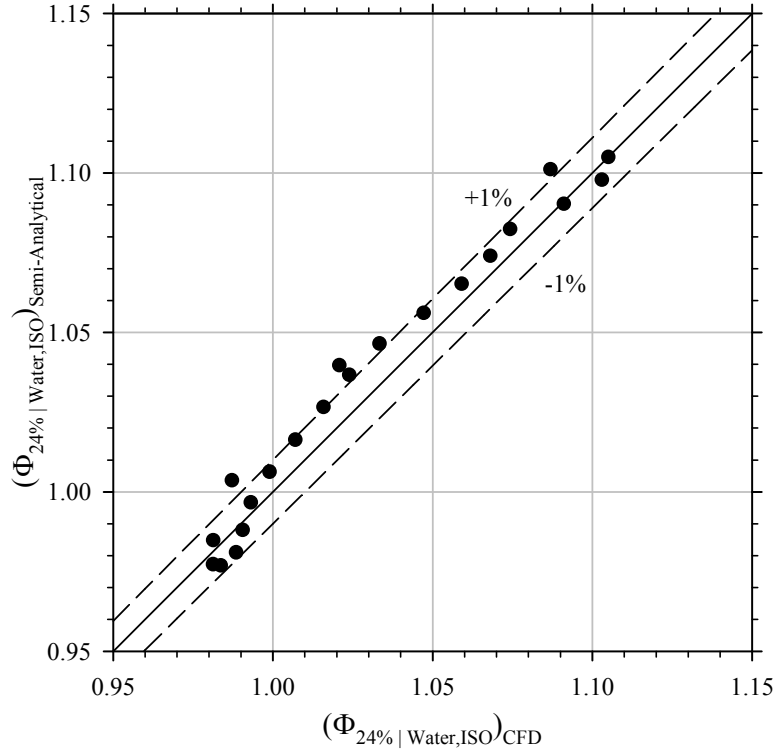
Figure 5.39: The comparison between the CFD and the semi-analytical model.

$$\Theta_{WF} = \left. \frac{\Phi_{WF}}{\Phi_{Water}} \right|_{BC} \tag{5.26}$$

The subscript WF refers to the desired working fluid. For water as the working fluid, Θ_{WF} is equal to one. It is difficult to introduce a function that can explain the behaviour of the working fluid preference Θ_{WF} in the whole Reynolds number domain. An analytical approach for the description of Θ_{WF} has to satisfy the following conditions at high Reynolds numbers:

1. The value of Θ_{WF} for water is equal to one, hence:

$$\Theta_{WF} = 1 : WF \equiv Water \tag{5.27}$$

2. The value of the mixing level and the dissipation rate depends on the viscosity. Therefore, any geometrical change that increases the mixing level and the energy transfer rate is more effective for the low viscous fluids than for the viscous fluids. As a result, the effect of the baffle orientation on the performance factor is more significant for shell-side fluids with low viscosity:

$$\frac{d\Theta_{WF}}{d\mu} \leq 0 : \forall Re_{inlet} \in High \ Reynolds \ Numbers \tag{5.28}$$

3. According to the large-Reynolds-number asymptotic theory, the performance factor is independent of the viscosity in the range of very high Reynolds numbers:

$$\lim_{Re_{inlet} \to \infty} (\Theta_{WF}) = 1 \tag{5.29}$$

In order to satisfy the conditions (5.28) and (5.29), the value of Θ_{WF} has to be inversly proportional to the Reynolds and Prandtl numbers:

$$\Theta_{WF} = f\left(\frac{1}{Re_{inlet}}, \frac{1}{Pr_{WF}}\right) \tag{5.30}$$

In Figure 5.40, the working fluid preference Θ_{WF} is plotted as a function of Reynolds number for different shell-side fluids.
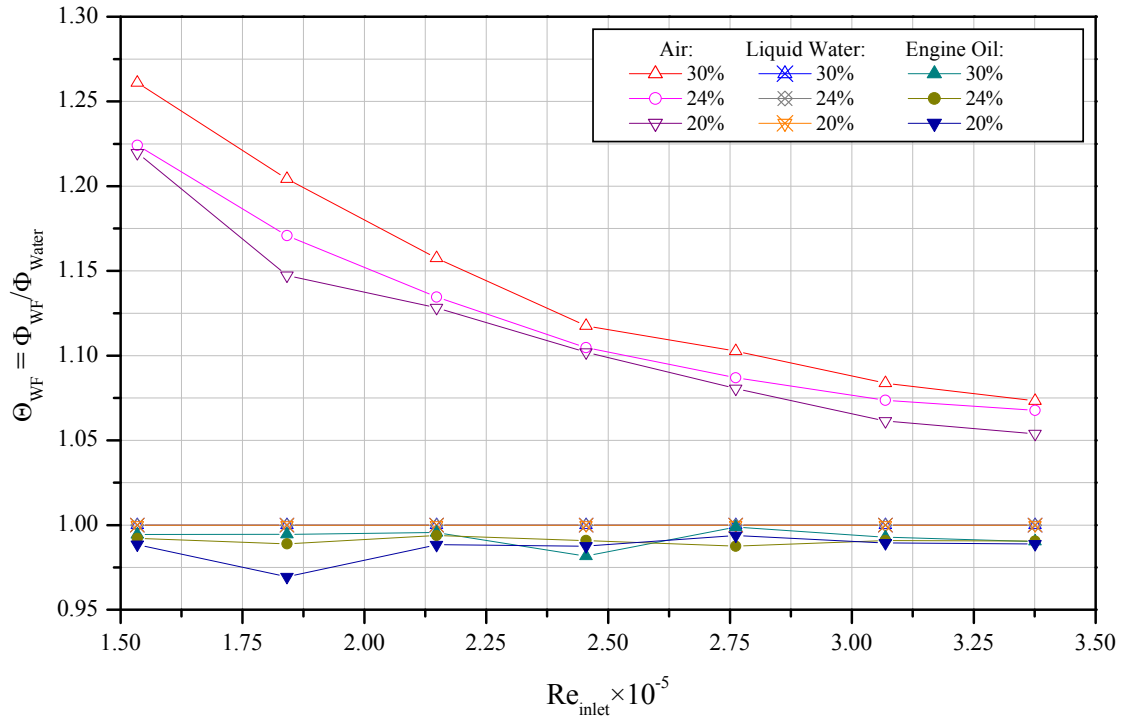
Figure 5.40: Working fluid preference Θ_{WF} as a function of Reynolds number for different shell-side fluids and different baffle cuts.

From Figure 5.40 it can be seen that the working fluid preference for engine oil is approximately constant and near to 1 for all baffle cuts and Reynolds numbers. The behaviour of air is different from the behaviour of engine oil, however. Θ_{Air} decreases with increasing Reynolds number. The value of Θ_{Air} does not change very much with the baffle cut; the absolute relative deviation of Θ_{Air} at different baffle cuts is less than 5%. Therefore, it may be postulated that the value of Θ_{WF} is independent of the baffle cut. The hypothetical function that satisfies Equations (5.27)-(5.30), and is independent of the baffle cut and describes the behaviour of Θ_{WF} for air and engine oil is:

$$\Theta_{WF} = \exp\left\{\left(\frac{5}{2}\frac{\left(\frac{Pr_{Water,ISO}}{Pr_{WF}}\right)^2 - 1}{Re_{inlet}^{\frac{1}{2}}}\right)^3\right\} \tag{5.31}$$

69

The semi-analytical function of Θ_{WF} according to Equation (5.31) predicts the CFD results with a relative absolute error less than 3.15%.
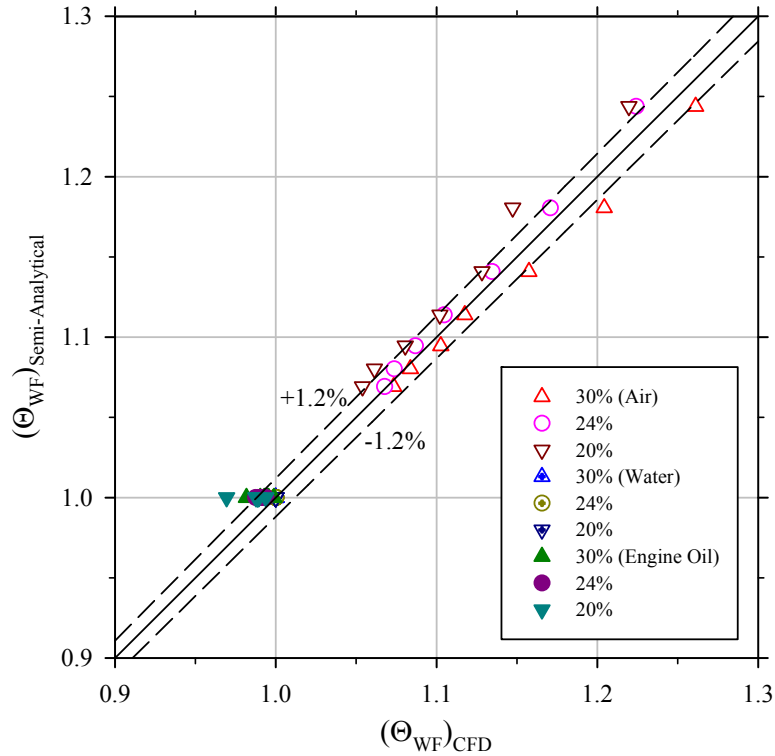
Figure 5.41: Comparison between the CFD results of Θ_{WF} and the values of Θ_{WF} obtained from Equation (5.31).

5.6.3 Effect of Different Baffle Cuts

In order to consider the influence of different baffle cuts, a baffle cut preference Θ_{BC} is introduced as follows:

$$\Theta_{BC}= \frac{\Phi_{BC}}{\Phi_{24\%}} \qquad (5.32)$$

In Equation (5.32), Φ_{BC} and $\Phi_{24\%}$ denote the performance factor at baffle cut BC and at baffle cut 24%, respectively. Therefore, the baffle cut preference Θ_{BC} is the ratio of the performance factor Φ at any baffle cut to the performance factor Φ at the reference baffle cut of 24%. The behaviour of Θ_{BC} for three shell-side fluids as a function of the inlet Reynolds number is presented in Figure 5.42.

The absolute relative deviation of Θ_{BC} at different shell-side fluids is less than 4%, as it can be seen from Figure 5.42. Therefore, at each baffle cut, an average value of Θ_{BC} is adequate to describe the value of baffle cut preference for all shell-side fluids. The average value of Θ_{BC} is depicted in Figure 5.43.

The shell-side heat transfer coefficinet and pressure drop depend on the normalized minimum shortcut distance or NMSD, as it is described before. Therefore, the performance factor Φ_{BC} could be presented as a function of NMSDR. Consequently, the baffle cut preference Θ_{BC} is:

$$\Theta_{BC}=f(\text{NMSDR}) \qquad (5.33)$$
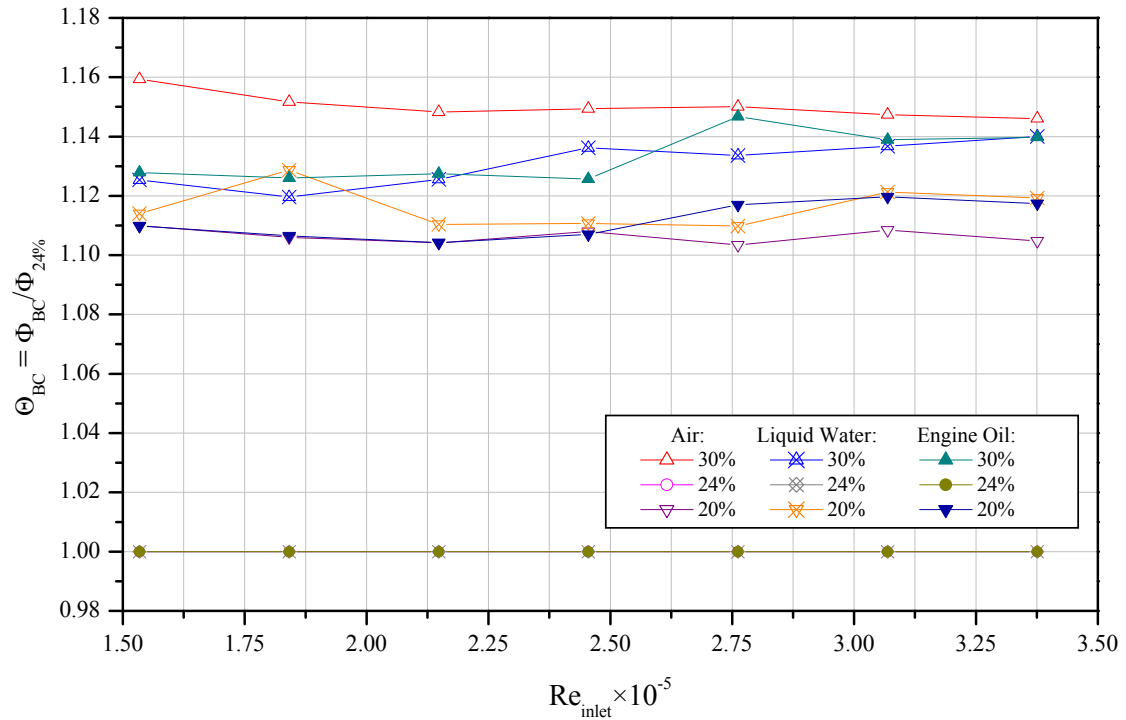
Figure 5.42: Baffle cut preference Θ_{BC} as a function of the inlet Reynolds number for three shell-side fluids.
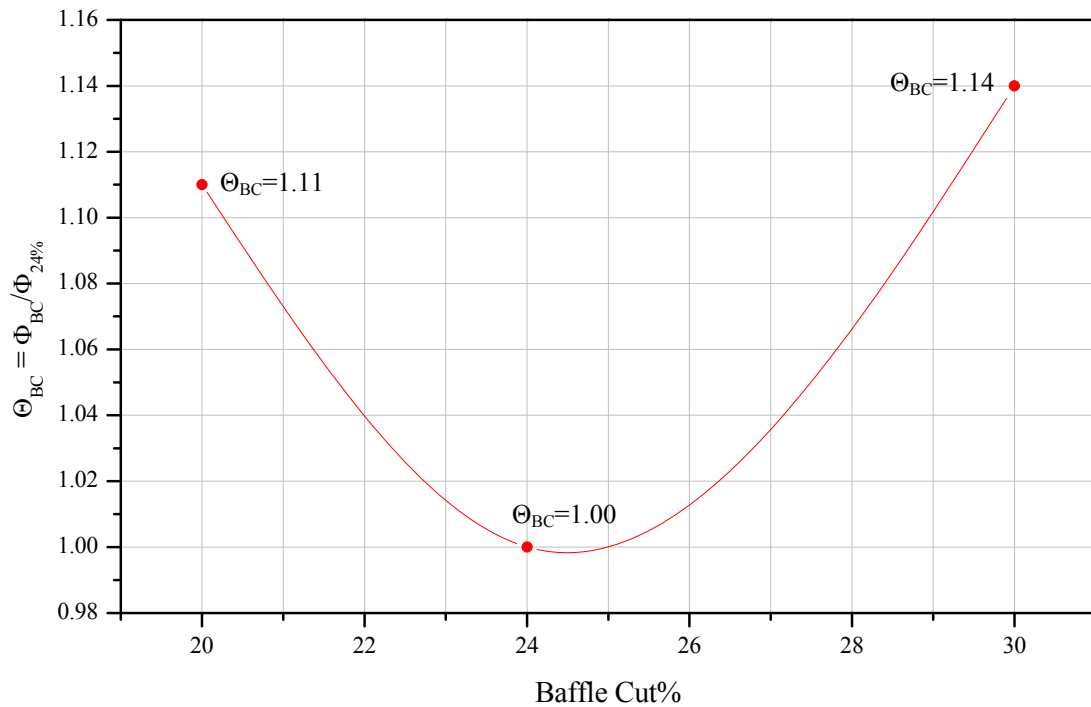
Figure 5.43: Average baffle cut preference Θ_{BC} as a function of Reynolds number.

When the baffle cut approaches to zero, the value of NMSDR tends to $\sqrt{2}/2$. On the other hand, when the baffle cut is very close to zero, which is in fact a hypothetical situation, the residence time of the shell-side fluid in the inlet zone with horizontal baffle orientation will be nearly equal to the residence time of the shell-side fluid in the inlet zone with vertical baffle orientation. This means that at baffle cut 0%, the performance factor of the inlet zone with

71

horizontal baffle orientation will be equal to the performance factor of the inlet zone with vertical baffle orienatation. Hence:

$$\lim_{B_C \to 0}(\text{NMSDR}) = \frac{\sqrt{2}}{2} \quad , \quad \lim_{B_C \to 0}(\Phi_{BC}) = 1 \tag{5.34}$$

Applying Equation (5.34) on (5.32) yields:

$$\lim_{\text{NMSDR} \to \frac{\sqrt{2}}{2}}(\Theta_{BC}) = \lim_{B_C \to 0}(\Theta_{BC}) = \frac{1}{\Phi_{24\%}} \tag{5.35}$$

The value of NMSDR at a baffle cut of 50% approaches to infinity. The physical interpretation prefigures that Θ_{BC} has a finite value at baffle cut 50%:

$$\lim_{\text{NMSDR} \to \infty}(\Theta_{BC}) = \lim_{B_C \to 50\%}(\Theta_{BC}) = \text{finite} \tag{5.36}$$

On the other hand, for a shell and tube heat exchanger without leakages, the heat transfer and pressure drop depend on the cross sectional flow area of the baffle window as well. The cross sectional flow area of the baffle window, or $A_{\text{window}}^{\text{csf}}$, is proportional to the void factor of the baffle window. With increasing values of $A_{\text{window}}^{\text{csf}}$, the fluid velocity will decrease and consequently, the heat transfer coefficient and pressure drop will reduce in the baffle window. Moreover, as the number of tubes in the baffle window decreases, the effective cross-flow resistance of the shell will increase. In fact, the effective cross-flow resistance of the shell is proportional to the difference between the total tube number and the number of tubes located in the baffle window. $A_{\text{window}}^{\text{csf}}$ changes with the baffle orientation and the baffle cut. The ratio of $\left(A_{\text{window}}^{\text{csf}}\right)_{\text{horizontal}} / \left(A_{\text{window}}^{\text{csf}}\right)_{\text{vertical}}$ depends on the baffle cut and tube layout. Figure 5.44 shows the ratio $\left(A_{\text{window}}^{\text{csf}}\right)_{\text{horizontal}} / \left(A_{\text{window}}^{\text{csf}}\right)_{\text{vertical}}$ as a function of the baffle cut for the triangular tube layout of 30°.

The value of $\left(A_{\text{window}}^{\text{csf}}\right)_{\text{horizontal}} / \left(A_{\text{window}}^{\text{csf}}\right)_{\text{vertical}}$ for the triangular tube layout 60° is the inverse value of $\left(A_{\text{window}}^{\text{csf}}\right)_{\text{horizontal}} / \left(A_{\text{window}}^{\text{csf}}\right)_{\text{vertical}}$ for the triangular tube layout 30°. This is due to the fact that the tube layout 60° is the 90° axial rotation of the tube layout 30° around the axis parallel to the tube length.

The value of $\left(A_{\text{window}}^{\text{csf}}\right)_{\text{horizontal}} / \left(A_{\text{window}}^{\text{csf}}\right)_{\text{vertical}}$ is equal to one for tube layouts square 90° and rotated square 45° since these tube layouts have a 90° rotational symmetry about the axis parallel to tube length.

Considering Equations (5.35) and (5.36) and Figure 5.44, the hypothetical function of Θ_{BC}, i.e. Equation (5.33), can be presented by a wave-form-damped-sine function. An exact form of this function results by applying the average values of Θ_{BC}:

$$\Theta_{BC} = \frac{\sqrt{5}}{2} + \frac{6}{5}\exp\left\{-\frac{5}{4}(\text{NMSDR})\right\}\sin\left\{-5\pi(\text{NMSDR}) + \frac{9}{5}\right\} \tag{5.37}$$

The recommended function for Θ_{BC} versus the baffle cut is presented in Figure 5.45. Equation (5.37) can predict the value of Θ_{BC} with an absolute relative error less than 1.4%. Nevertheless, Equation (5.37) has to be proven for all baffle cuts and tube layouts. In fact, more investigations have to be carried out for other baffle cuts and tube layouts in order to obtain a general function for Θ_{BC}.
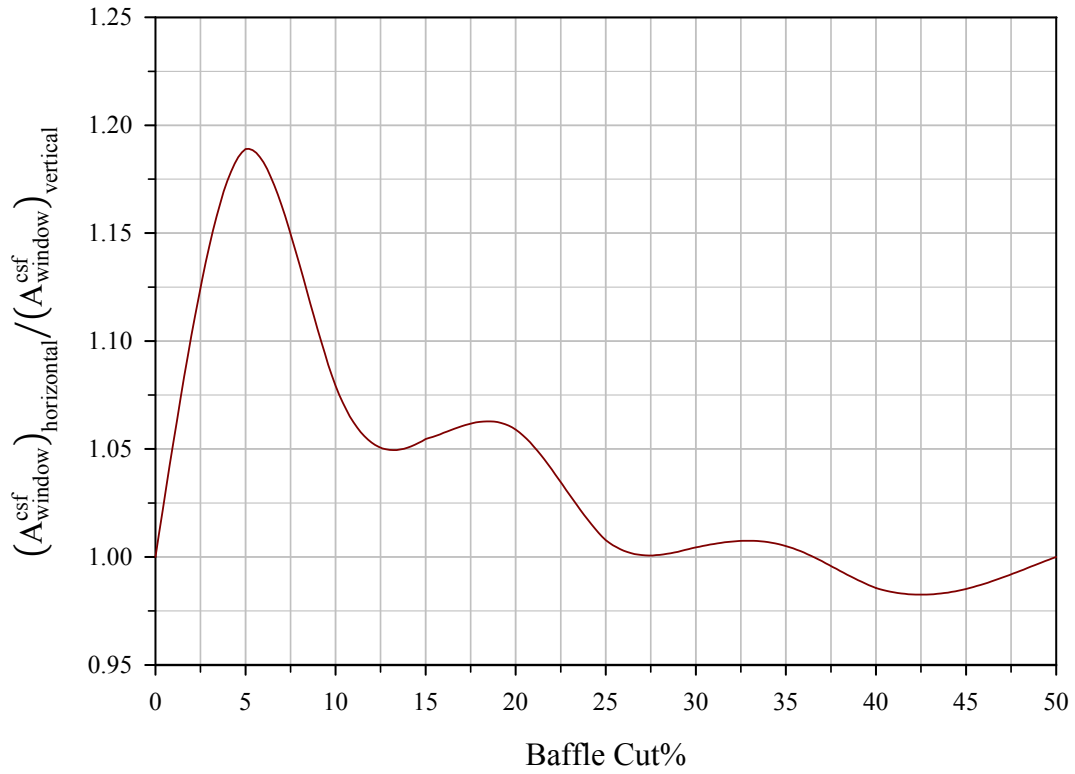
Figure 5.44: $\left(A_{window}^{csf}\right)_{horizontal}/\left(A_{window}^{csf}\right)_{vertical}$ as a function of baffle cut for the triangular tube layout 30°.

Legend:
$$\frac{\sqrt{5}}{2}+\frac{6}{5}\exp\left\{-\frac{5}{4}(\text{NMSDR})\right\}\sin\left\{-5\pi(\text{NMSDR})+\frac{9}{5}\right\}$$
● Average value from CFD results
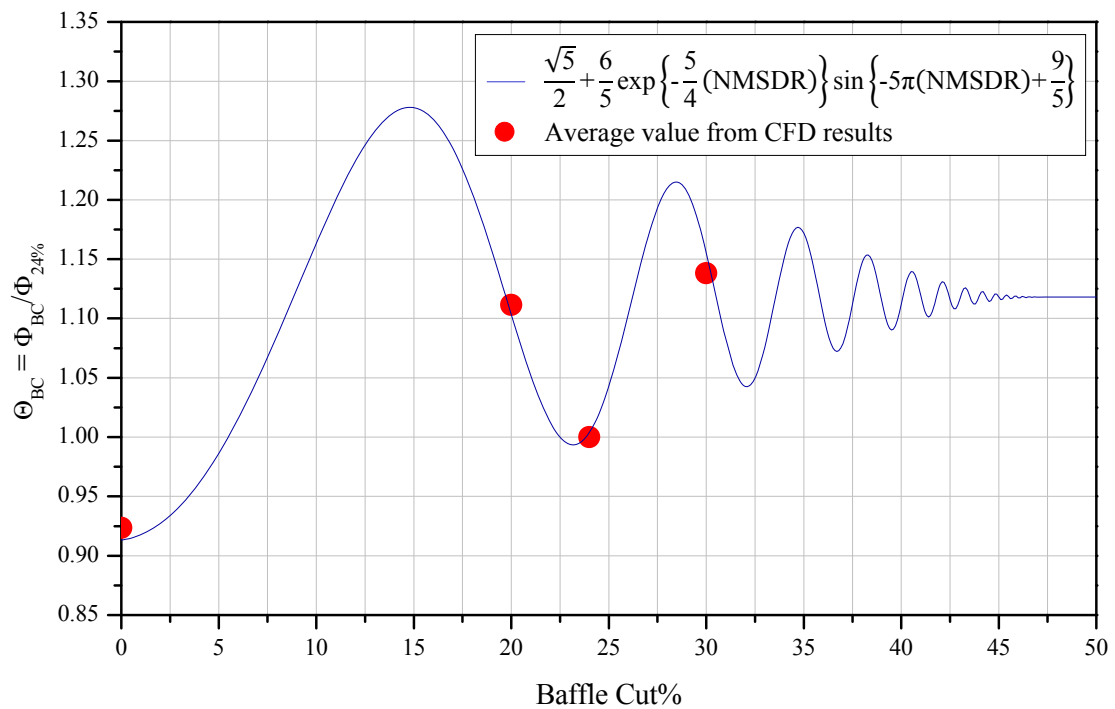
Figure 5.45: Recommended baffle cut preference Θ_{BC} as a function of baffle cut for the triangular tube layout 30°.

Knowing the functions of $\Phi_{24\%\,|Water,ISO}$, Θ_{WF} and Θ_{BC}, the value of the performance factor Φ for the working fluid WF at a baffle cut BC can be calculated as follow:

$$\Phi=\Phi_{BC}|_{WF}=\Phi_{24\%}|_{Water,ISO}\times\frac{\Phi_{BC}}{\Phi_{24\%}}\times\frac{\Phi_{WF}}{\Phi_{Water}}\times\left(\frac{Pr_{WF,wall}}{Pr_{WF,bulk}}\right)^{\left(1+\frac{1}{7}\right)} \qquad (5.38)$$

or

$$\Phi=\Phi_{24\%}|_{Water,ISO}\times\Theta_{BC}\times\Theta_{WF}\times\left(\frac{Pr_{WF,wall}}{Pr_{WF,bulk}}\right)^{\left(1+\frac{1}{7}\right)} \qquad (5.39)$$

In Equations (5.38) and (5.39), the subscripts "wall" and "bulk" refer to the properties of the working fluid at the tube wall temperature and at the fluid bulk temperature, respectively.

In order to compensate the effects of nonisothermal condition in the fluid on the performance factor, the correction factor $(Pr_{WF,wall}/Pr_{WF,bulk})^{(1+1/7)}$ is introduced.

When the Prandtl number near the tube wall decreases, the thickness of the thermal boundary layer near the tube wall will decrease. On the other hand, the mixing level in the fluid bulk increases with viscosity. Therefore, the enhancement in the heat transfer is proportional to $Pr_{WF,bulkl}/Pr_{WF,wall}$. This effect is more significant for the geometry with low level of mixing, i.e for the inlet zone with vertical baffle orientation. Hence, the performance factor Φ is proportional to $(Pr_{WF,bulkl}/Pr_{WF,wall})^{-1}$. The exponent 1/7 is based on Kârmân-Prandtl 1/7 power law for velocity distribution of a turbulent flow in a circular pipe. In fact, the flow between tubes is considered to be similar to the flow inside a tube. The exponent 1 is due to this fact that the mixing level is proprtional to the Prandtl number.

The comparison between the CFD results of the performance factor and the performance factor calculated from the semi-analytical model is presented in Figure 5.46. The semi-analytical model introduced for Φ predicts the CFD results with a relative absolute error in the range of 0.02% and 4.66%.

Equation (5.39) is a recommended semi-analytical function to evelute the performance factor of the inlet zone of an ideal E type shell and tube heat exchanger at different baffle cuts and for different shell-side fluids.
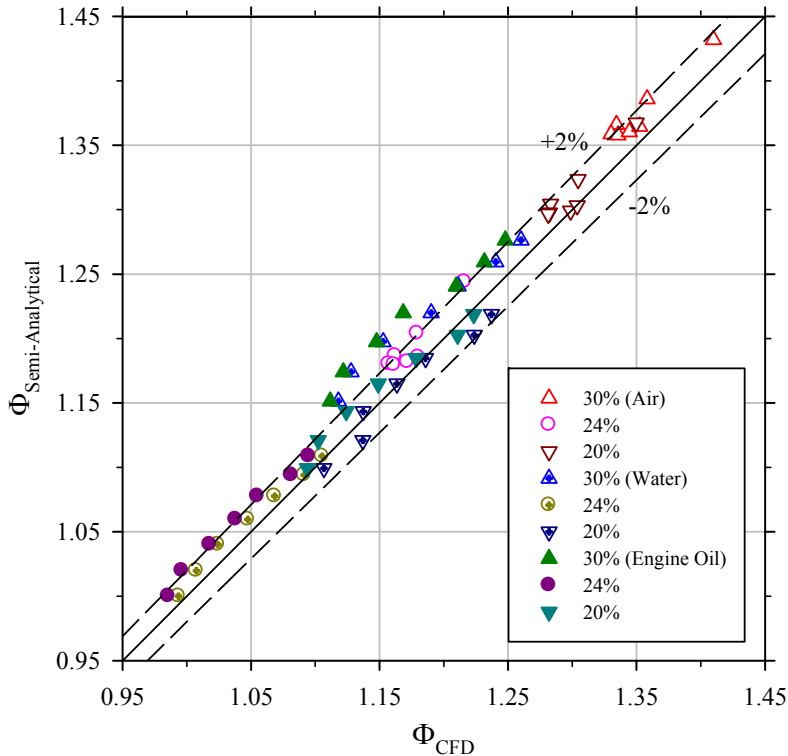
Figure 5.46: The comparison between the CFD results of Φ and the values of Φ obtained from the semi-analytical model.

6. Effect of Baffle Orientation and Fluid Viscosity on Shell-Side Pressure Drop and Heat Transfer Coefficient in a Complete Shell and Tube Heat Exchanger without Leakages

6.1 Geometry

In the following chapter, an E type shell and tube heat exchanger consisting of 660 tubes is considered. The geometrical data are according to the HTRI data sheet, presented in Appendix B, and the TEMA design method [TEMA, 1999].

One baffle cut (24% of the shell inside diameter) and two baffle orientations (horizontal and vertical) are considered for the heat exchanger investigations. The tubes of the heat exchanger are arranged in triangular tube layout of 30°. The baffles are equally spaced.

The heat exchanger is subdivided into one inlet zone, one outlet zone and six central baffle spacing zones. No leakage flows are considered. Figure 6.1 shows schematically the shell and tube heat exchanger.

Table 6.1 provides the geometrical layout of the shell and tube heat exchanger in more detail.
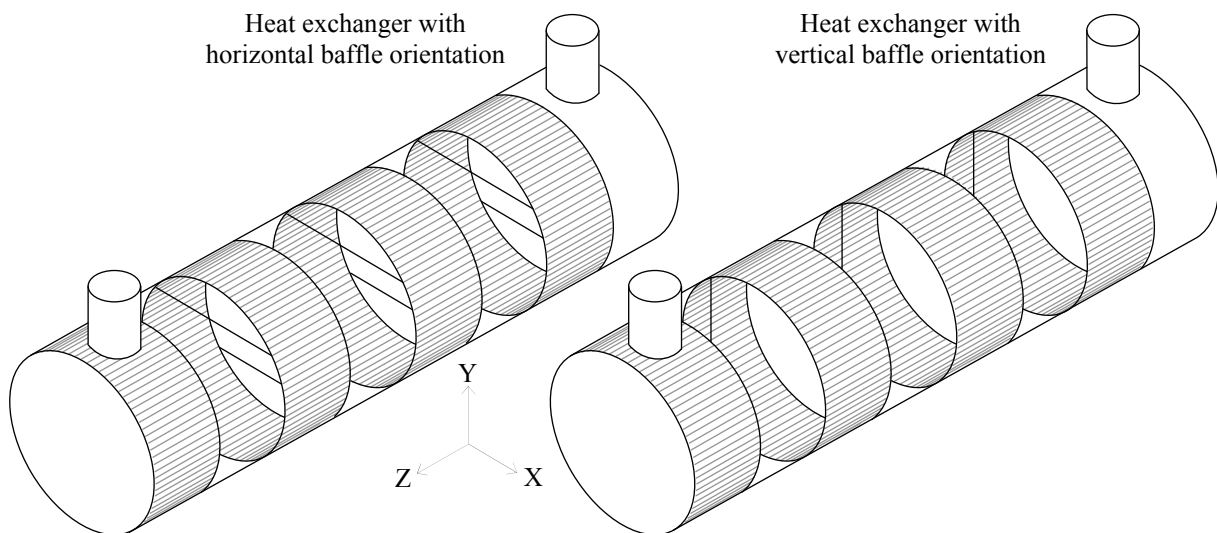
Figure 6.1: Two shell and tube heat exchangers with horizontal and vertical baffle orientation. Each heat exchanger consists of 660 tubes, is without leakage and has equal baffle spacing.

6.2 Meshing and Grid Configuration

Due to the limitation of the computational memory required for the calculation, each heat exchanger consists of eight discrete geometries: one inlet zone, six central baffle spacing zones and one outlet zone. Figure 6.2 shows the discretized shell and tube heat exchanger with horizontal baffle orientation.

The meshing procedure and the final mesh structure for each descrete zone is similar to the procedure and the mesh structure described in subsection 5.2. A set of prism-like volumes defines the mesh structure for the inlet, outlet and central baffle spacing zones. Figure 6.3 represents the typical source faces near the baffle and baffle window.The aspect ratio of around 99% of the total mesh elements is less than 15. Approximately 98% of the total mesh elements have EquiAngle skewness less than 0.4. However, the maximum skewness in the

central baffle spacing zones is 0.62 for the heat exchanger with horizontal baffle orientation and 0.53 for the heat exchanger with vertical baffle orientation. The detail of the mesh structure is presented in Table 6.2.

Item	Symbol	Size
Tube number	n_t	660
Tube outside diameter	d_o	15.875 mm ($^5/_8$ in)
Inlet/Outlet nozzle inside diameter	D_n	154.178 mm (6.07 in)
Inlet/Outlet nozzle minimum length	L_n	192.786 m (7.59 in)
Tube partition width	--	9.525 mm (0.375 in)
Number of central baffle spacing zone	n_{baffle}-1	6
Baffle spacing (inlet, outlet and central baffle spacing)	L_{bc}	262.407 mm (10.331 in)
Baffle thickness	--	6.350 mm (¼ in)
Shell inside diameter	D_s	590.931 mm (23.265 in)
Baffle cut height	L_{bch}	139.78 mm
Baffle cut percentage	B_C	24%
Inside shell-to-baffle clearance (diametral)	L_{sb}	0.00 mm
Diametral clearance between tube outside diameter and baffle hole	L_{tb}	0.00 mm
Tube pitch	l_{tp}	20.638 mm ($^{13}/_{16}$ in)
Tube layout	--	30° triangular

Table 6.1: Geometrical details of the complete shell and tube heat exchanger with 660 tubes.

	Horizontal baffle orientation			Vertical baffle orientation		
Skew value	Inlet zone	Outlet zone	Central baffle spacing zone	Inlet zone	Outlet zone	Central baffle spacing zone
0.0-0.4	96.88%	96.89%	97.18%	97.99%	97.96%	99.42%
0.4-0.6	2.18%	2.19%	1.47%	1.75%	1.78%	0.55%
0.6-0.8	0.92%	0.91%	1.35%	0.25%	0.25%	0.03%
0.8-0.9	0.01%	0.01%	0.00%	0.01%	0.01%	0.00%
0.9-1.0	0.00%	0.00%	0.00%	0.00%	0.00%	0.00%
Total mesh	1198478	1165628	1200420	1187508	1153508	1166380
Skew value min.	6.33×10^{-4}	6.33×10^{-4}	6.33×10^{-4}	6.33×10^{-4}	6.33×10^{-4}	6.33×10^{-4}
Max.	0.94	0.94	0.62	0.94	0.94	0.53

Table 6.2: Details of the grid skew value for the inlet, outlet and central baffle spacing zones of both shell and tube heat exchangers with horizontal and vertical baffle orientation.

6.3 Boundary Conditions

A constant temperature boundary condition is considered for the tube walls. In order to study the heating process and compare the final results with the cooling process, the tube wall temperature is set to 400 K. All other solid walls, i.e. the baffle, the tube sheet, the nozzles and the shell wall, are defined as adiabatic walls.
The boundary condition for the flow at the inlet is the velocity inlet boundary condition since the velocity vectors and the temperature at the inlet are known. Five inlet velocities describe

the velocity vectors at the inlet nozzle. The resulting inlet Reynolds numbers are in the range of 1.02×10^4 to 3.05×10^5. The temperature of the inlet stream is set to 370 K.
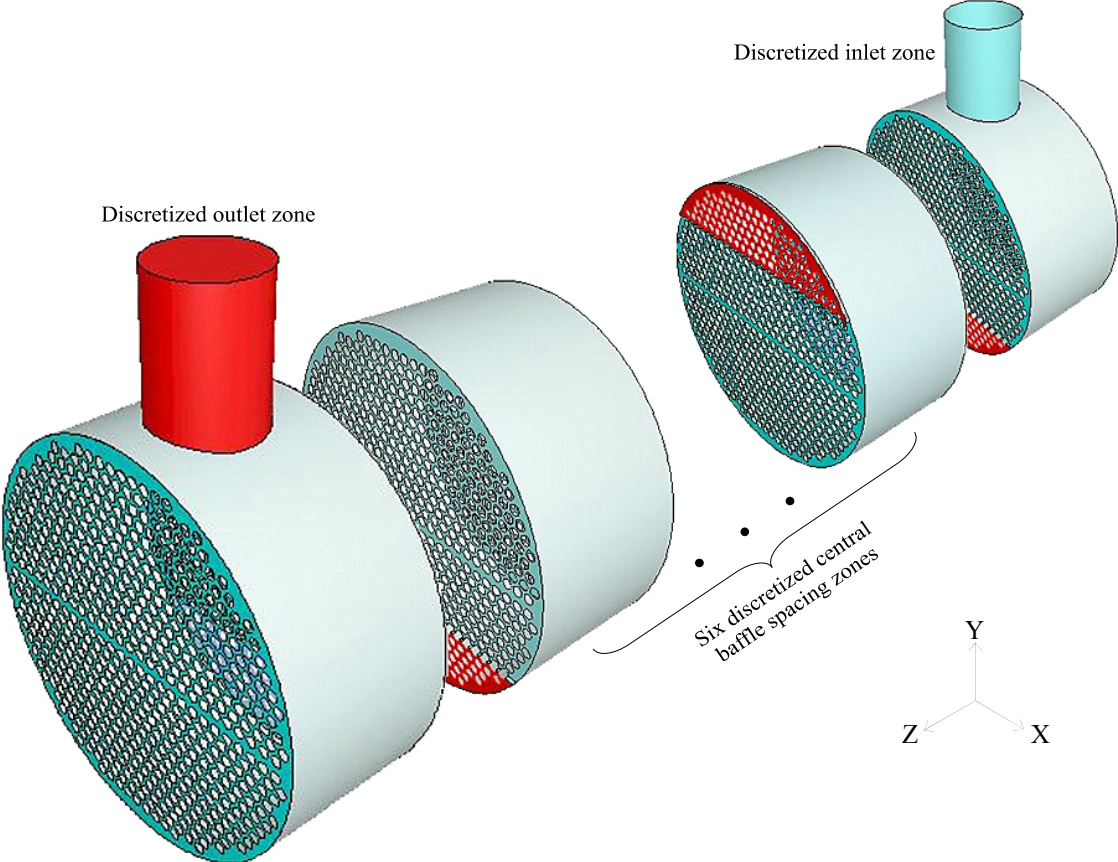
Figure 6.2: Discretized shell and tube heat exchanger with horizontal baffle orientation.
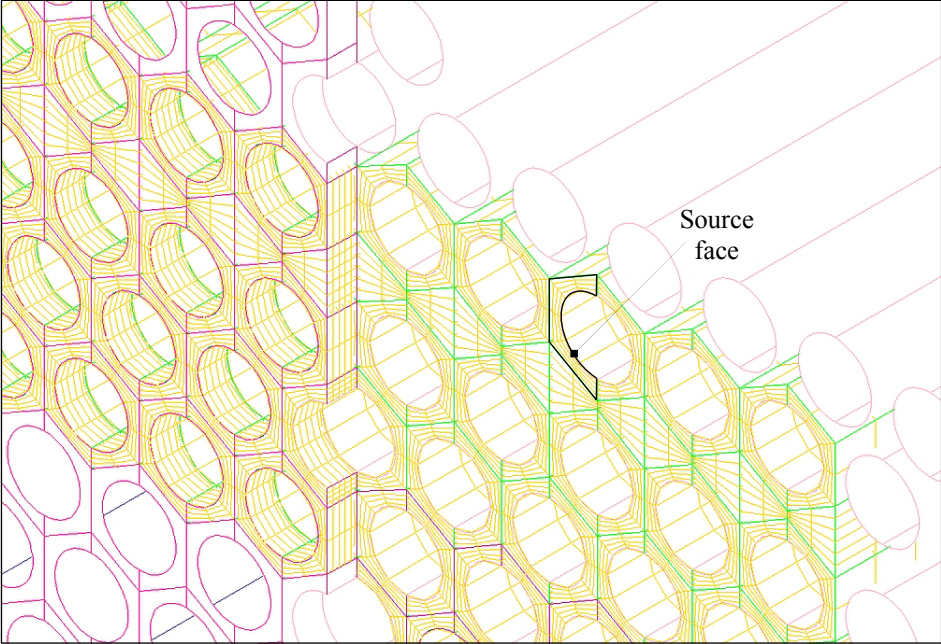
Figure 6.3: Meshed source faces and prism-like volumes around the tubes.

The outflow boundary condition models the flow exit in each discretized zone. For the inlet zone and for the central baffle spacing zones, the outlet boundary is the baffle window. However, for the outlet zone, the outlet boundary is the outlet nozzle.

For the outflow boundary condition fully developed flow is assumed, where the diffusion fluxes in the direction normal to the exit plane are assumed to be zero. For the complete shell and tube heat exchanger, this is not fully achieved, since the hydraulic resistance of the downstream baffle zone causes a backflow at each baffle window.

By assigning an outflow boundary condition to each discrete zone, the effect of the downstream portion of the shell and tube heat exchanger on the flow is neglected. Moreover, the Navier-Stokes equations form a coupled parabolic-elliptic set, hence arbitrary divorcing of one portion of the simulation domain from another one and an enforcement of a boundary condition for the region where the simulation domin is split is not recommended [Torrance, 1986; Jin and Barza, 1993; Shyy, 1994; Anderson, 1995; Wesseling, 2001].

One solution is to represent the downstream baffle zone by a porous medium which could characterize the hydraulic resistant of the downstream zone. Coupling the discretized zone with this porous medium and simultaneously simulating them, could model the back flow in the baffle window. A crude mesh structure without substantial mesh requirements is enough for the downstream zone. In this case, skewness is not a significant issue since the pressure drop per unit length is specified for the porous medium. However, the computational memory essential for the calculation of the coupled zones will exceed the available physical memory.

The most appropriate boundary condition which could define the flow exit is the outflow boundary condition [Wesseling, 2001].

When a discrete zone is simulated, the velocity and temperature profiles will be obtained at the outlet. These profiles will provide the necessary information for the inlet of the next discrete zone.

The boundary conditions used for the present stage of study are listed in Table 6.3.

Item / Boundary zone	Boundary condition
Tube outside walls	Constant temperature equal to 400K
Tube sheets, baffle walls, inlet and outlet nozzle walls and shell wall	Adiabatic
Inlet at inlet nozzle	Velocity inlet: Five plug flows normal to the inlet cross-sectional area $(1.02 \times 10^4 \leq \mathrm{Re}_{inlet} \leq 3.05 \times 10^5)$, and constant stream temperature equal to 370 K, i.e. 30ºC colder than the tube wall.
Flow exit at inlet zone	Neglecting the effect of downstream zone on the flow
Inlet at central baffle spacing zones and outlet zone	Characterize the velocity and temperature profiles which is obtained from the prior zone
Flow exit at central baffle spacing zones	Neglecting the effect of downstream zone on the flow
Flow exit at outlet nozzle zone	Outflow: Fully developed flow normal to the outlet cross-sectional area without back flow and with zero normal derivatives for all quantities. The Mach number is less than 0.1

Table 6.3: Boundary conditions for the discrete zones of the heat exchanger with 660 tubes and without leakages.

6.4 Modelling Options and Numerical Setups

The modelling options and the numerical setups for this part of the investigation is according to the numerical setups described in Chapter 5 and summarized in Table 5.4. However, with the aim of achieving a higher order of accuracy at the cell faces, the second-order upwind scheme is implemented for the discretization of the governing equations.

6.5 Validity of Wall Function Treatment

The values of y* versus y+ for all simulations is presented in Figure 6.4. The values of y* are in the range from 11.225 to 50. The relative deviation between y* and y+ is less than 25%. This confirms the correctness of the mesh structure and the use of the standard wall function.
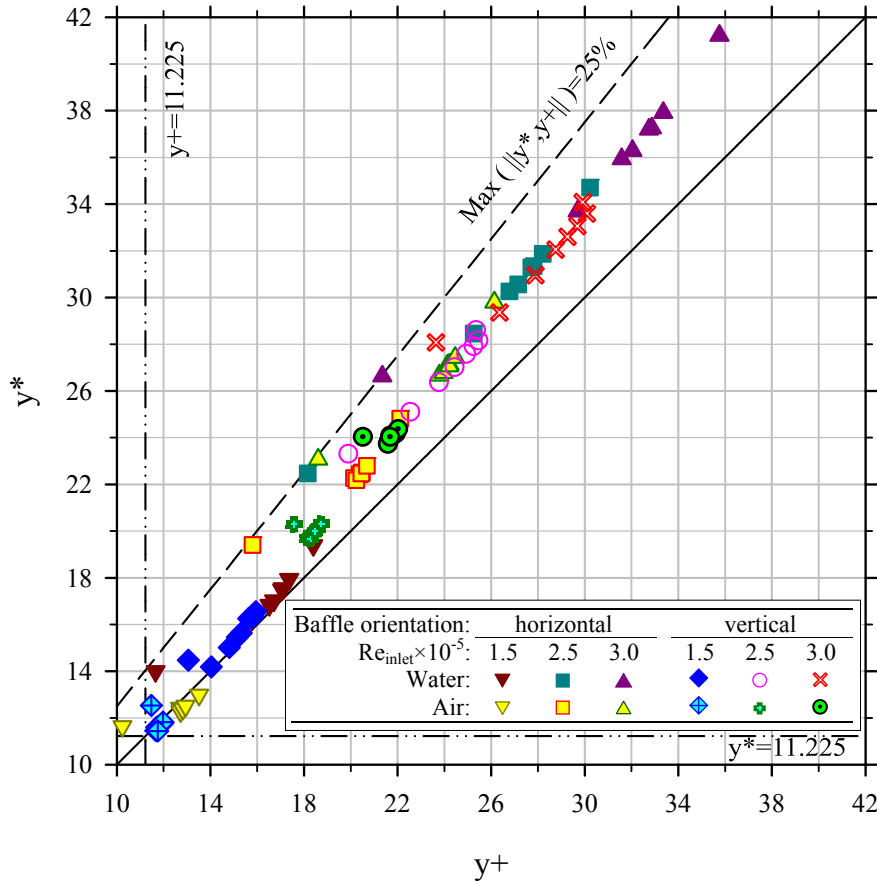
Figure 6.4: y* versus y+ for all simulations.

6.6 Shell-Side Fluids

The shell-side fluids for this part of the investigation are air and liquid water. Polynomial functions of temperature define the physical properties of these two working fluids at an operating pressure equal to 8 bar. The polynomial functions are obtained as curve-fits of experimental data [VDI, 2006; Touloukian, 1972]. Equation (6.1) represents the polynomial function for physical property η_{ph}.

$$\eta_{ph}(T) = \sum_{m=0}^{3} C_m T^m \quad , \quad 370\,K \leq T \leq 400\,K \tag{6.1}$$

In Equation (6.1) η_{ph} refers to the intensive physical property of the shell-side fluid, i.e. density, dynamic viscosity, thermal conductivity and constant-pressure specific heat, in SI units and T is the temperature in Kelvin. The constant coefficients C_0, C_1, C_2 and C_3 are presented in Table 6.4.

79

Physical property	Liquid water at 8 bar				Air at 8 bar			
	C_0	C_1	C_2	C_3	C_0	C_1	C_2	C_3
ρ (kg/m³)	823.010	1.67552	-0.00413	1.649×10^{-6}	25.82170	-0.08958	1.360×10^{-4}	-7.635×10^{-8}
μ (kg/m.s)	0.01441	-9.734×10^{-5}	2.253×10^{-7}	-1.766×10^{-10}	9.514×10^{-7}	7.220×10^{-8}	-5.070×10^{-11}	2.240×10^{-14}
k_f (W/m.K)	-1.3891	0.01368	-2.961×10^{-5}	2.092×10^{-8}	0.00521	7.088×10^{-5}	9.020×10^{-9}	-2.406×10^{-11}
C_p (J/kg.K)	3790.617	4.90568	-0.02053	2.797×10^{-5}	1178.863	-1.09887	0.00229	-1.340×10^{-6}

Table 6.4: Coefficients of the polynomial functions according to Equation (6.1).

The physical properties calculated from the polynomial functions presented in Equation (6.1) and Table (6.4) are consistent with the experimental data.

6.7 Stability and Iterative Error of Calculation

The residual of an intensive property computed by the segregated solver is the imbalance in the discretized equation of that intensive property. The total residual, or the un-scaled residual, is the sum of the residuals over all cells in the computational domain.
In general, it is difficult to judge the convergence by examining the un-scaled residuals. The scaled residual is a more convenient and appropriate indicator of the convergence which is obtained by scaling the residuals using a scaling factor.
The numerical method converges when the truncation error is zero. For a method to be consistent, the truncation error must become zero when the mesh spacing tends to zero. Consistency does not imply convergence. In addition to consistency, stability is required [Wesseling, 2001; Ferziger, 2002].
A numerical solution method is stable if it does not magnify the errors that appear in the course of the numerical solution process. Stability guarantees that the method produces a bounded solution whenever the solution of the exact equation is bounded. For iterative methods, a stable method is one that does not diverge. The stability means that the perturbation of an intensive property in the iterative procedure remains bounded as the iteration tends to infinity. Two useful definitions of stability are the zero-stability and the absolute-stability. The absolute-stability has a minor importance, but the zero-stable scheme is an iterative procedure if the residuals are always less than a descending order function. According to Lax's equivalence theorem, convergence implies zero-stability, and zero-stability plus consistency imply convergence [Ferziger, 2002].
An analysis over the scaled residuals of the present work shows that all the numerical schemes are stable with a zero-stability. Moreover, the perturbation of any intensive property remains bounded as the iteration tends to infinity. The zero-stability can be described by applying a periodic Gaussian-type function. The analysis proves a satisfactory perturbation with an absolute average convergence error less than 0.004%.
As an example, the perturbation and the absolute average convergence error of x-velocity for a typical simualtion is presented in Figure 6.5

6.8 Final Results and Discussion

The momentum transport is proportional to the dynamic viscosity and the mixing level. Therefore, as the dynamic viscosity of the shell-side fluid decreases, the effect of geometry on the performance factor becomes more significant.
The shell-side pressure drop and heat transfer coefficient for horizontal and vertical baffle orientations as a function of inlet Reynolds number are presented in Figure 6.6. The shell-side fluids are water and air. The influence of different baffle spacing zones is also shown in

Figure 6.6. The shell-side pressure drops at inlet and outlet zones are higher than for the other baffle spacing zones, as can be seen from Figure 6.6. However, the outlet zone produces the highest shell-side pressure drop. For the different central baffle spacing zones, the shell-side pressure drops are comparable.

The behaviour of the shell-side heat transfer coefficient differs significantly from the behaviour of shell-side pressure drop.
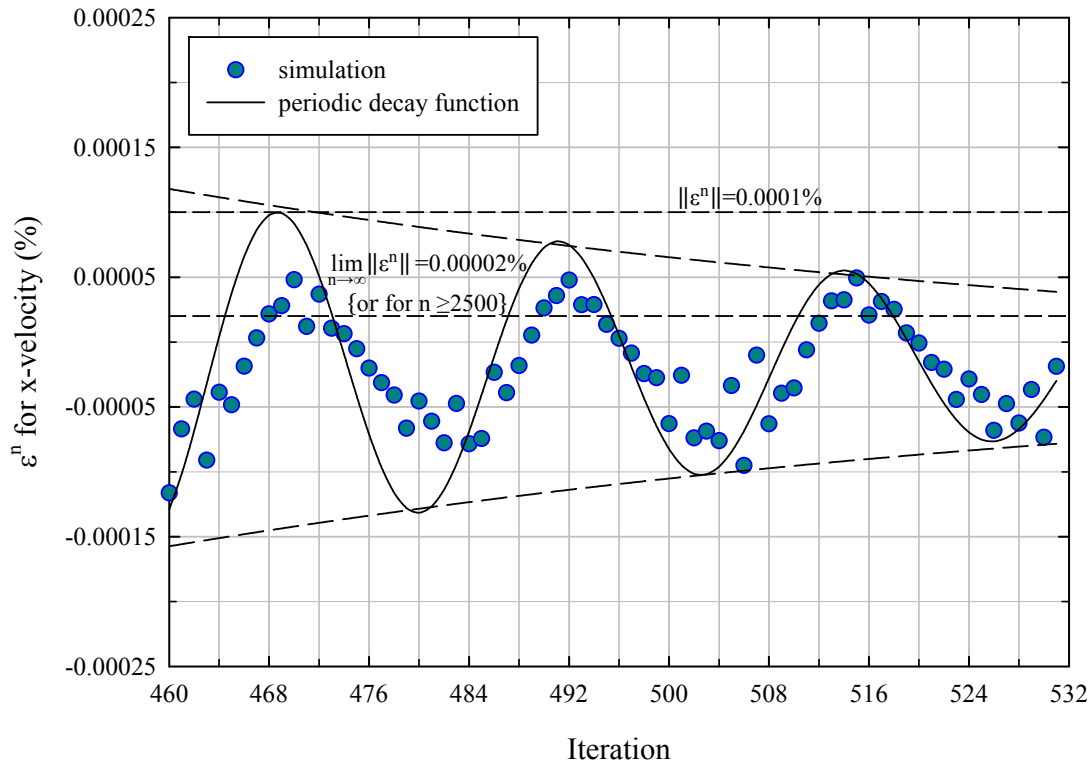
Figure 6.5: Perturbation and convergence error of x-velocity for a typical simulation with $\|\varepsilon^n\|$ as the absolute convergence error and n as number of iteration.

The temperature gradient decreases along the heat exchanger from the inlet zone to the outlet zone. On the other hand, the temperature gradient and the mixing level of the shell-side fluid increase with velocity. Therefore, the shell-side heat transfer coefficient increases with increasing inlet Reynolds number. The effect of geometry on the shell-side heat transfer coefficient is more significant for the shell-side fluids with low dynamic viscosity. Hence, the shell-side heat transfer coefficient for water does not change significantly in different baffle spacing zones except for the outlet zone. For water as shell-side fluid, the average relative difference between the shell-side heat transfer coefficient at the inlet zone and the shell-side heat transfer coefficient at the outlet zone is 13% for the horizontal baffle orientation and 17% for the vertical baffle orientation.

For air as shell-side fluid, the variation in shell-side heat transfer coefficient at different baffle spacing zones is more visible, especially at the outlet zone. In fact, the effect of viscosity on the shell-side heat transfer coefficient is very significant at the outlet zone. For air, the average relative difference between the shell-side heat transfer coefficient at the inlet zone and the shell-side heat transfer coefficient at the outlet zone is 76% for the horizontal baffle orientation and 71% for the vertical baffle orientation.
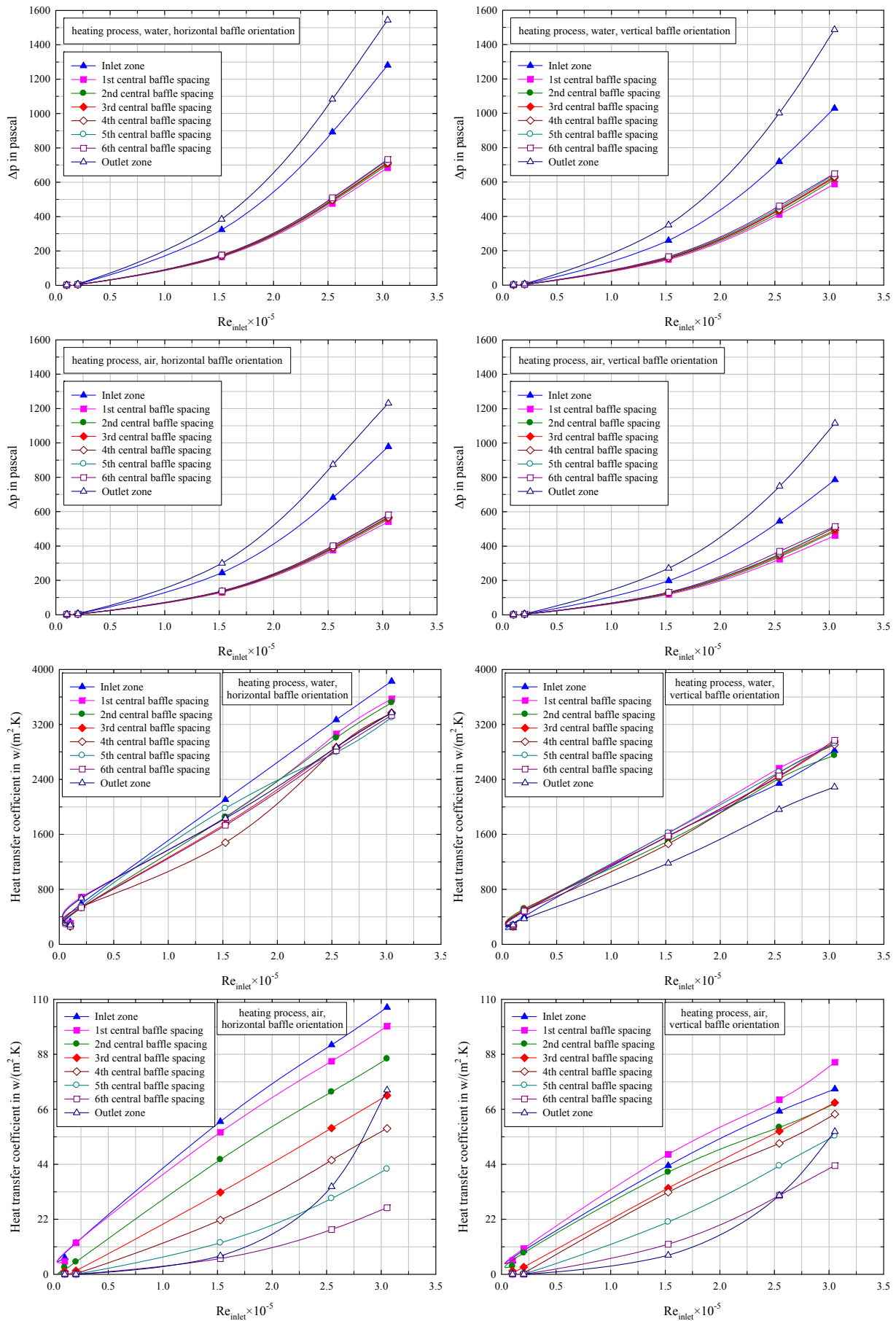
Figure 6.6: Shell-side pressure drop and heat transfer coefficient for horizontal and vertical baffle orientations as a function of inlet Reynolds number at different baffle spacing zones. The shell-side fluids are water and air. The heat transfer process is heating and the baffle cut is 24%.

With the same approach as discussed in Chapter 5, the effect of baffle orientation on the performance factor at the outlet zone can be predicted. However, this does not mean that the performance factor has to be always more than one. In fact, the effect of the intermediate baffle spacing zones on the performance factor has to be considered.

The distance between two baffle windows at each intermediate zone does not change with the baffle orientation. Hence, the effect of the upstream zone on the velocity distribution plays an important role. For a heat exchanger with horizontal baffle orientation the velocity profile at the first baffle window is symmetrical. Contrariwise, a heat exchanger with vertical baffle orientation shows an irregular velocity distribution which might increase the residence time of the shell-side fluid downstream of the intermediate baffle zones. Therefore, the performance factor might decrease. This effect is more noticeable for lower velocities. At the inner intermediate baffle spacing zones, the effect of upstream baffle zone on the velocity distribution will diminish and consequently the performance factor will be constant. However, the performance factor for the lower velocities could decrease.

The conceptual behavior of the performance factor can be summarized as following:

$$\Phi = \begin{cases} \geq 1 & : \quad \text{inlet zone} \\ \text{decreases} \downarrow & : \quad \text{next intermediate baffle spacing zone(s)} \\ \text{might become constant} \rightarrow & : \quad \text{remaining intermediate baffle spacing zones} \\ \text{increases} \uparrow & : \quad \text{outlet zone} \end{cases} \quad (6.2)$$

The local performance factor at each zone for liquid water and air are presented in Figure 6.7 and 6.8, respectively. The conceptual behaviour presented in Equation (6.2) is confirmed by the results given in Figures 6.7 and 6.8.
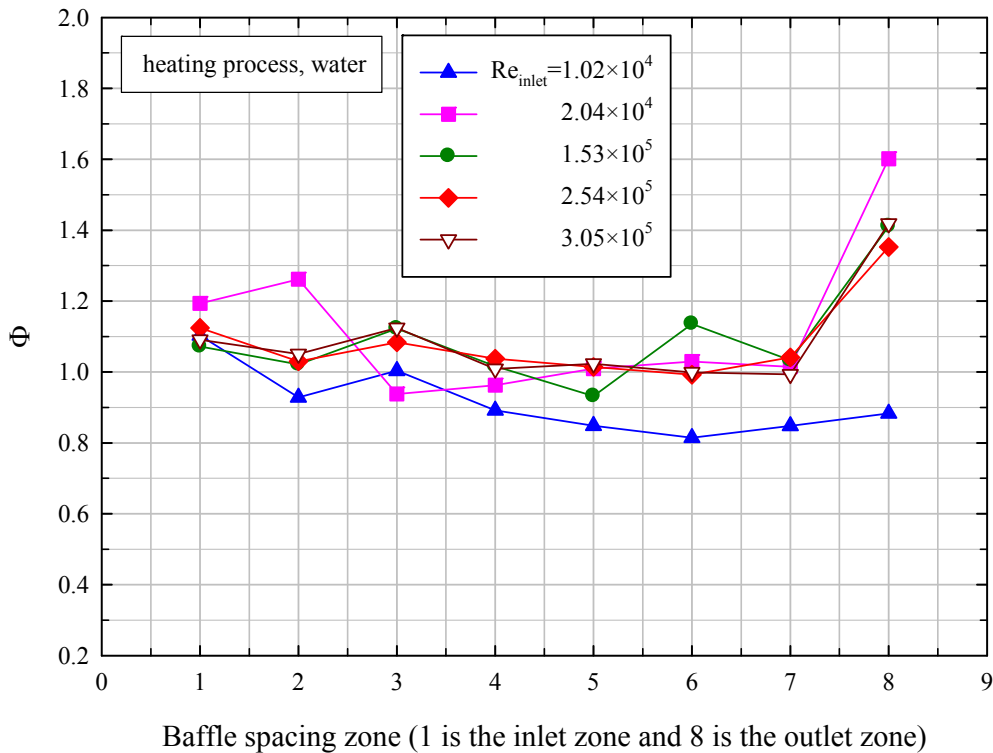
Figure 6.7: Local performance factor at each baffle spacing zone for liquid water as shell-side fluid. The heat transfer process is heating and the baffle cut is 24%.
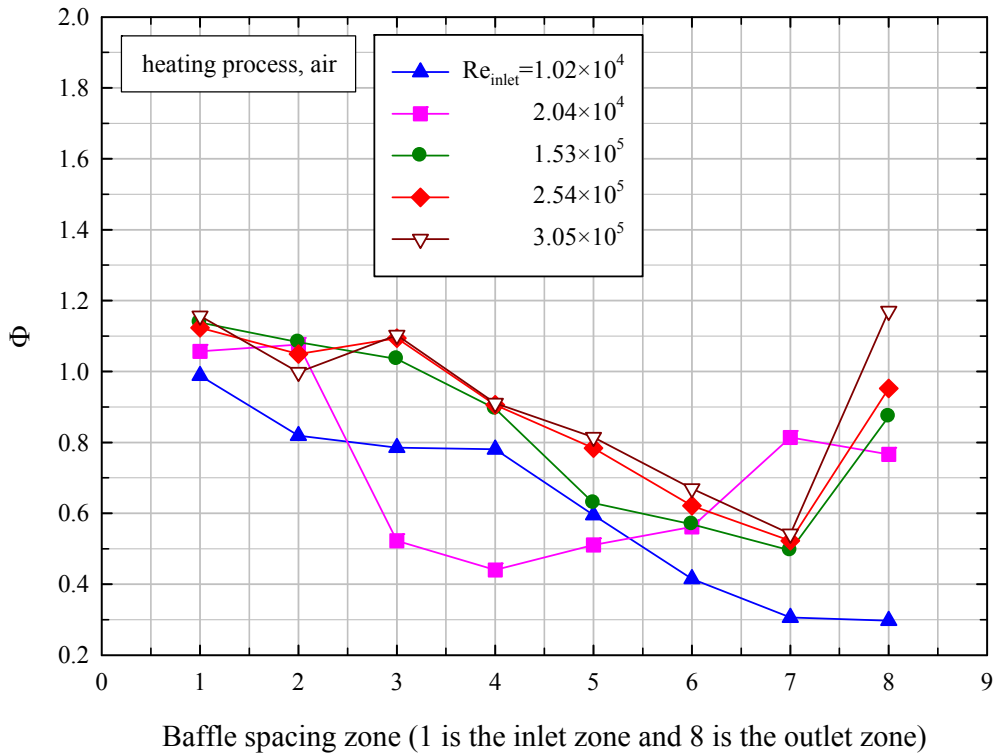
Figure 6.8: Local performance factor at each baffle spacing zone for gas air as shell-side fluid. The heat transfer process is heating and the baffle cut is 24%.

At the intermediate baffle spacing zone, the decay of the performance factor of air is greater than the decay of the performance factor of water. However, the overall trend is the same. The performance factor falls below a value of one at the intermediate baffle zones and reaches a value of 0.8 for water and a value of 0.3 for air at the lowest Reynolds number, i.e. $Re_{inlet} \approx 1.02 \times 10^4$. After the third baffle zone the performance factor falls under the value 1.0 for all inlet velocities. Finally, the performance factor increases at the outlet zone. This is due to the effect of the distance between the last baffle window and the outlet nozzle on the residence time and the mixing level of the shell-side fluid.

7. Effect of Baffle Orientation and Fluid Viscosity on Shell-Side Pressure Drop and Heat Transfer Coefficient in a Complete Shell and Tube Heat Exchanger with Leakages

7.1 Geometry: Complete Shell and Tube Heat Exchanger with Leakages

In this part of the investigation, a standard E type shell and tube heat exchanger consisting of 76 tubes and 6 baffle zones is considered. By reducing the number of tubes from 660 to 76, it became possible to simulate the complete shell-side domain including tube-to-baffle and baffle-to-shell leakages. By simulating the complete shell and tube heat exchanger, the effect of down-stream zones discussed in subsection 6.3, will be considered and the simulation will overcome the weakness of simulating the discrete zones.

The geometrical features of the shell and tube heat exchanger with 76 tubes are outlined in Table 7.1.

Item	Symbol	Size
Tube number	n_t	76
Tube outside diameter	d_o	19.05 mm (¾ in)
Inlet nozzle inside diameter	$(D_n)_{inlet}$	81.20 mm (3.197 in)
Outlet nozzle inside diameter	$(D_n)_{outlet}$	105.56 mm (4.156 in)
Inlet/Outlet nozzle minimum length	L_n	113.00 m (4.449 in)
Tube partition width	--	22.194 mm ($\approx$0.874 in)
Number of central baffle spacing zone	n_{baffle}-1	4
Baffle spacing (inlet, outlet and central baffle spacing)	L_{bc}	112.06 mm (4.412 in)
Baffle thickness	--	3.20 mm ($\approx^1/_8$ in)
Shell inside diameter	D_s	254.00
Baffle cut height	L_{bch}	50.80 mm (2.00 in)
Baffle cut percentage	B_C	20%
Inside shell-to-baffle clearance (diametral)	L_{sb}	1.13 mm
Diametral clearance between tube outside diameter and baffle hole	L_{tb}	0.19 mm
Tube pitch	l_{tp}	23.81 mm ($\approx^{15}/_{16}$ in)
Tube layout	--	30° triangular

Table 7.1: Geometrical features of the complete shell and tube heat exchanger with 76 tubes.

The complete shell and tube heat exchanger with 76 tubes and horizontal baffle orientation is presented in Figure 7.1 (a). The leakage areas of the shell and tube heat exchanger with horizontal baffle orientation and 76 tubes are indicated in Figure 7.1 (b).

7.2 Mesh Structure

The heat exchanger shown in Figure 7.1 is meshed by applying the meshing method explained in Chapters 5 and 6. In total about 1,200,000 mesh elements are used for the shell-side fluid volume of the complete heat exchanger. Almost 99% of the three-dimensional elements have

aspect ratio less than 15. About 97% of all mesh elements are less-skewed elements with values less than 0.4 for the skewness factor.

The surface mesh structure around the tubes for the complete shell and tube heat exchangers with horizontal and vertical baffle orientations are presented in Figures 7.2 (a) and 7.2 (b), respectively.

(a)   (b)
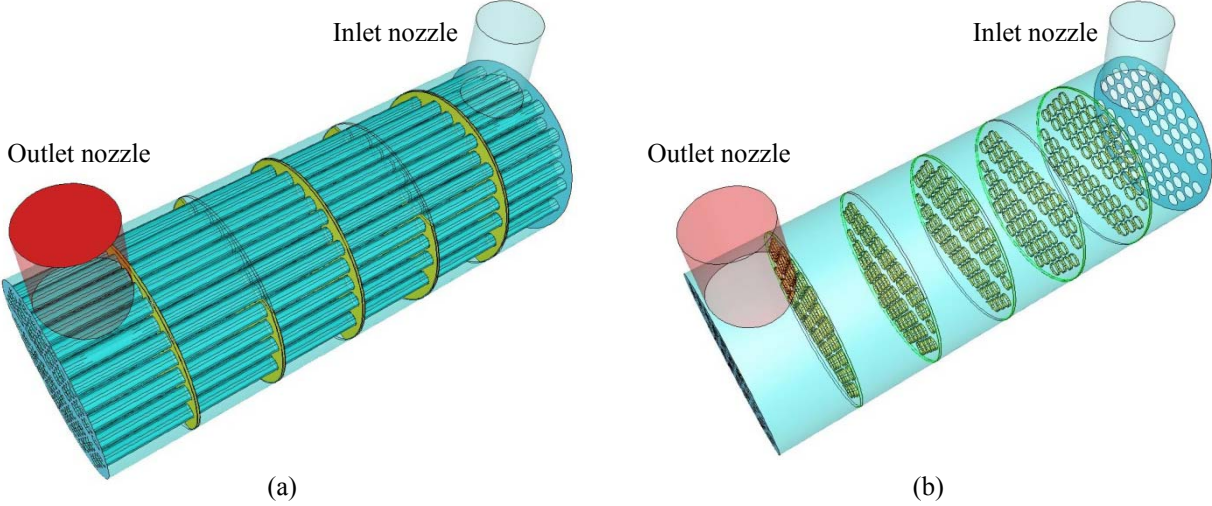
Figure 7.1: Complete shell and tube heat exchanger with horizontal baffle orientation and 76 tubes: (a) the geometry of baffle zones and tubes and (b) the areas of tube-to-baffle and baffle-to-shell leakages.

(a)   (b)
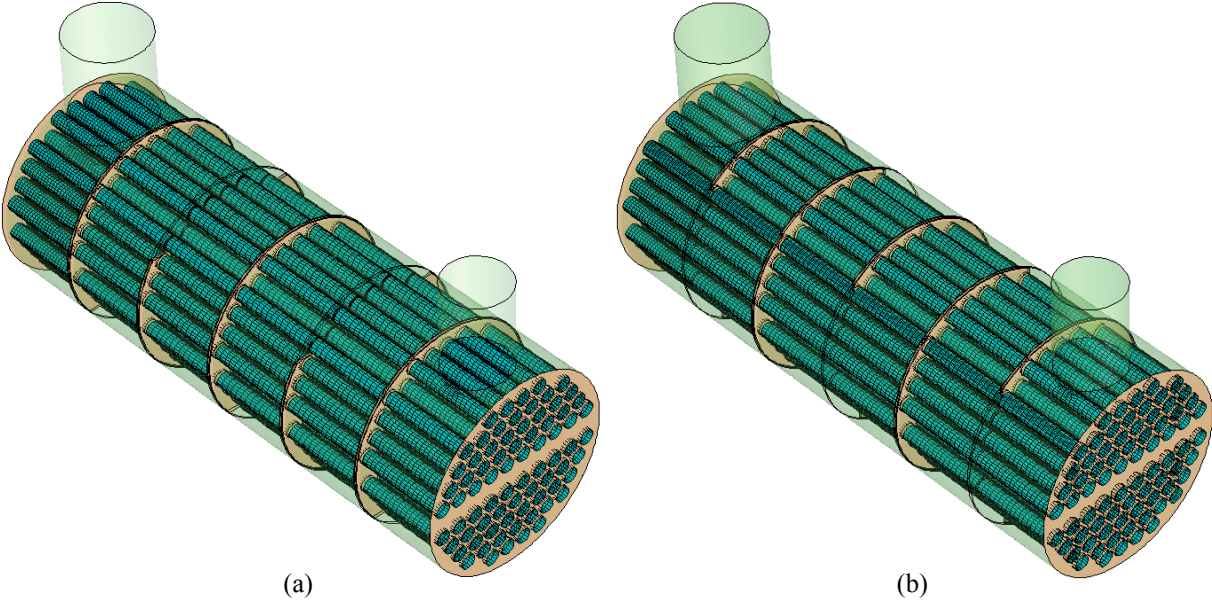
Figure 7.2: Surface mesh structure around the tubes for the shell and tube heat exchangers with (a) horizontal baffle orientation and (b) vertical baffle orientation.

7.3 Boundary Conditions and Physical Properties of Shell-Side Fluids

The boundary conditions for simulating the shell and tube heat exchanger with 76 tubes are presented in Table 7.2. Since the heat exchanger is not subdivided into different discrete

zones, the outflow boundary is the appropriate boundary condition for the outlet, i.e. the outlet nozzle. Moreover, two heat transfer processes are taken into account: heating and cooling.

Item / Boundary zone	Phase	Boundary condition
Tube outside walls	Solid	Constant temperature equal to 400 K for heating and 370 K for cooling
Tube sheets, baffle walls, inlet and outlet nozzle walls and shell wall	Solid	Adiabatic
Inlet at inlet nozzle	Fluid	Velocity inlet: Five plug flows normal to the inlet cross-sectional area ($2.0 \times 10^4 < Re_{inlet} < 10^5$. The temperature at the inlet is equal to 370 K for heating and 400 K for cooling. Hence, the absolute temperature difference between the tube walls and the inlet stream is 30ºC.
Flow exit at outlet nozzle zone	Fluid	Outflow: Fully developed flow normal to the outlet cross-sectional area without back flow and with zero normal derivatives for all quantities. The Mach number is less than 0.1

Table 7.2: Boundary conditions used for simulating the complete shell and tube heat exchangers with leakages.

Air, liquid water and engine oil are considered as shell-side fluids. Polynomial functions of temperature, i.e. Equation (6.1), define the physical properties of the shell-side fluids at operating pressure equal to 8 bar. For air and liquid water, the coefficients of the polynomial functions, i.e. C_0, C_1, C_2 and C_3, are presented in Table 6.4 (see subsection 6.6). For engine oil, the coefficients are listed in Table 7.3.

Physical property	Liquid engine oil at 7.9 bars			
	C_0	C_1	C_2	C_3
ρ (kg/m³)	1081.936	-0.71211	0.000173	-1.0417×10^{-9}
μ (kg/m.s)	4.925282	-0.035006	8.3285×10^{-5}	-6.6245×10^{-8}
k_f (W/m.K)	0.10895	0.000381	-1.2108×10^{-6}	1.0417×10^{-9}
C_p (J/kg.K)	578.1535	4.3932	0	0

Table 7.3: Coefficients for the polynomial functions of temperature define the physical properties of liquid engine oil.

The polynomial functions presented in Equation (6.1) with the coefficients listed in Table 7.3, calculate the physical properties of liquid engine oil with an absolute relative error of less than 7×10^{-2}%.

7.4 Comparison

The comparison between the CFD results and the values obtained by the VDI method is presented in Figures 7.3 and 7.4. For the shell and tube heat exchanger with horizontal baffle orientation, the comparison shows a satisfying level of agreement for the prediction of the shell-side Nusselt number and pressure drop. However, the comparison indicates that the VDI method may under- or oversize a shell and tube heat exchanger with vertical baffle orientation, significantly.

The average absolute deviation for Nusselt number is 15% for horizontal baffle orientation and 89% for vertical baffle orientation. For pressure drop, the average absolute deviation is 20% for horizontal baffle orientation and 52% for vertical baffle orientation.
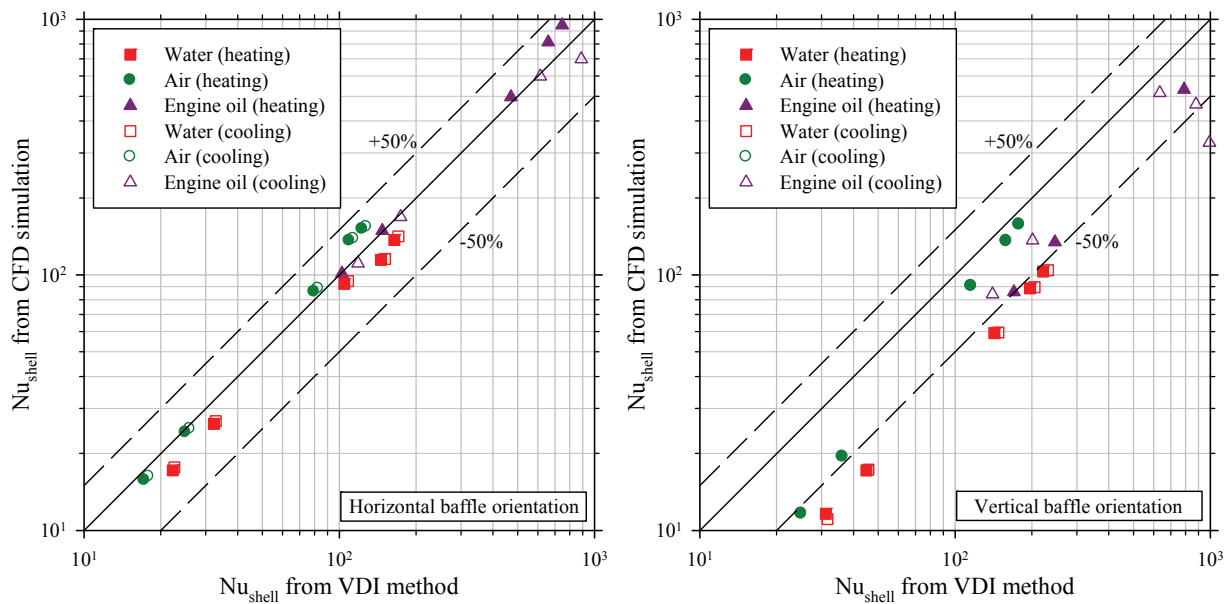
Figure 7.3: Comparison of shell-side Nusselt number, CFD calculation versus VDI method, left: horizontal baffle orientation, right: vertical baffle orientation.
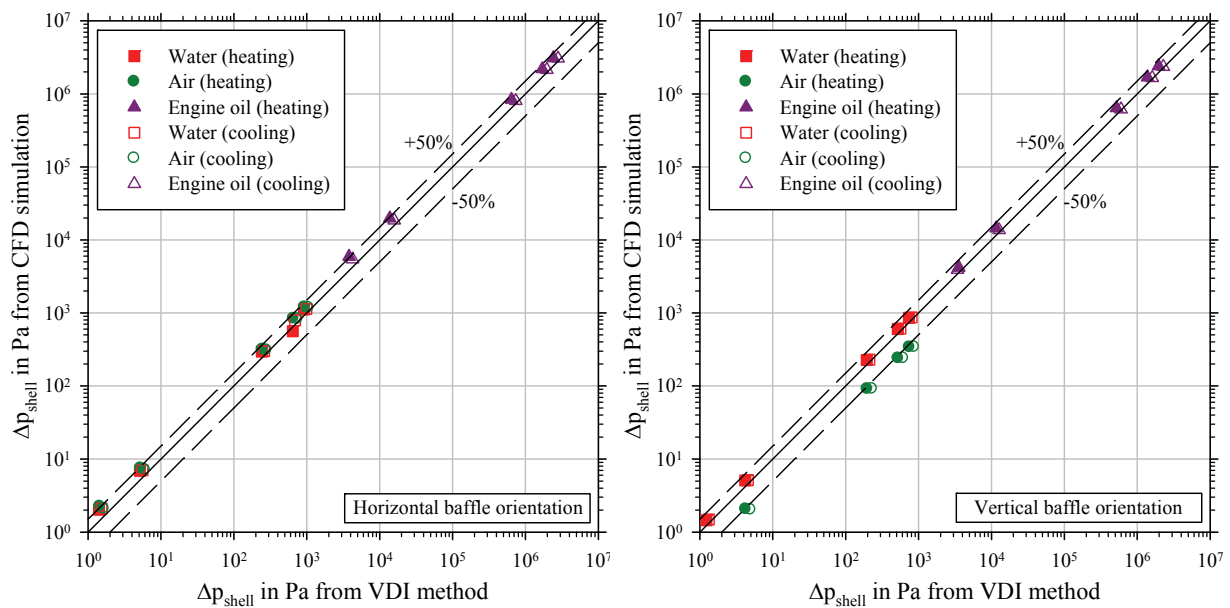
Figure 7.4: Comparison of shell-side pressure drop, CFD calculation versus VDI method, left: horizontal baffle orientation, right: vertical baffle orientation.

7.5 Effect of Leakages on Performance

7.5.1 Stream Analysis
As it is described in subsection 2.3.2, the baffled shell-side flow is very complex. The stream analysis method states that only part of the fluid takes the desired path through the tube nest, whereas a potentially substantial portion flows through the leakage and bypass areas.

The effect of cross-flow stream B on tube-baffle leakage streams A and baffle-shell leakage stream E is schematically presented in Figures 7.5 and 7.6. The pressure drop distribution developed by stream B in the region of the baffles plays an important role in the explanation of the effect of leakages on the performance of shell and tube heat exchanger with vertical and horizontal baffle orientations. As it is shown in Figures 7.5 and 7.6, the relatively intensive flow of stream B in the baffle window induces a lower pressure drop for leakages near the baffle tip, while the pressure drop is higher for leakages near the baffle-shell region. Consequently, the flow rate and mixing in leakages near the baffle-shell region will be higher than the flow rate and mixing in leakages near baffle tip.
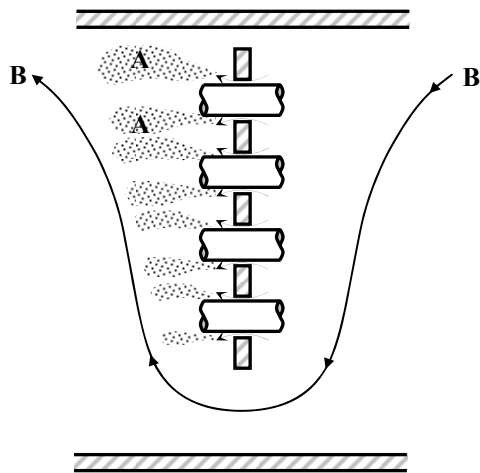
Figure 7.5: Schematic picture of the effect of cross-flow stream B on tube-baffle leakage stream A.
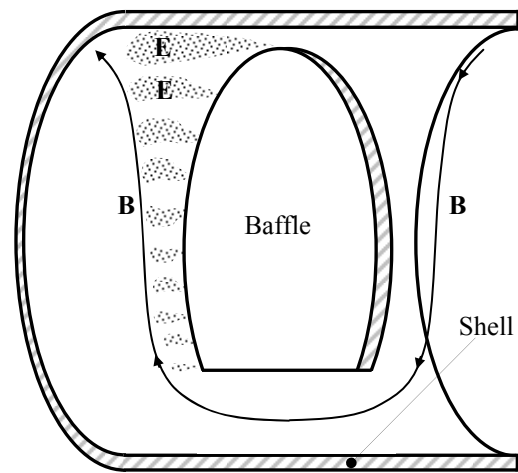
Figure 7.6: Schematic picture of the effect of cross-flow stream B on baffle-shell leakage stream E.

Flow visualization studies in baffled flow significantly demonstrated the broadly varying effectiveness of the various streams [Kopp, 1947]. The effect of baffle cut to baffle spacing ratio is illustrated schematically in Figure 7.7. The ratio of baffle cut to baffle spacing, i.e. L_{bch}/L_{bc}, is very important since it describes conceptually the eddy density and the mixing intensity, and consequently the pressure drop, in the baffle region.

$L_{bch}/L_{bc} < 1$
$(B_C < 30\%)$

$L_{bch}/L_{bc} \approx 1$
$(B_C \approx 40\%)$
or very low Reynolds number
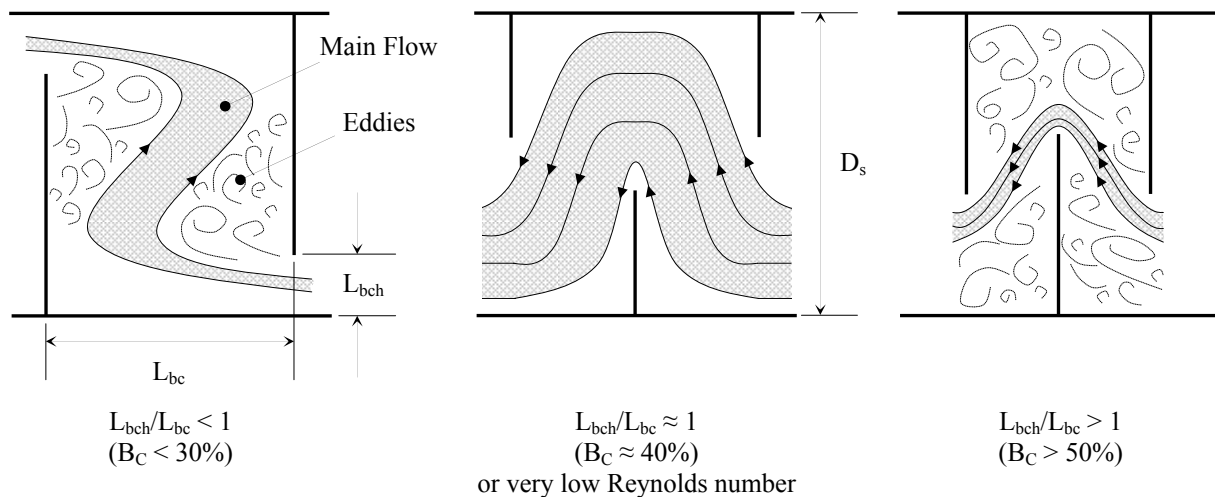
$L_{bch}/L_{bc} > 1$
$(B_C > 50\%)$

Figure 7.7: Schematic presentation of the effect of L_{bch}/L_{bc} and baffle cut B_C on the shell-side flow pattern.

As it is denoted in Figure 7.7, the main flow stream B crosses the tube bank and generates intensive eddies around the baffle walls for $B_C < 30\%$. The intensive eddies around the baffle walls stimulate the turbulent momentum diffusion and cause rapid mixing in the region near the baffle walls. Hence, the rates of momentum, heat, and mass transfer will increase in the baffle region [Tennekes, 1972].

The main stream B will produce blowing or suction for tube-baffle leakages, which consequently will develop a jet-kind stream flow. The flow of stream B near the baffles can be compared with a pure shear flow over a porous wall.

Thus, for $B_C < 30\%$, the effect of tube-baffle leakages on the performance factor is indisputable due to the substantial rates of momentum and heat transfer around the baffle walls and the noticeable pressure drop in the tube-baffle leakages.

Figure 7.8 and 7.9 show the path lines coloured by velocity magnitude for the shell and tube heat exchanger with 76 tubes. The baffle orientation is horizontal and the baffle cut equals 20% of the shell inside diameter. These figures are comparable with the conceptual flow for baffle cut less than 30% of the shell inside diameter (see Figure 7.7).

The main stream B crossing the tube bundle as well as the tube bundle bypass stream C is presented in Figure 7.8. The flow in tube-baffle leakages as well as the bypass stream C is shown in Figure 7.9. In Figures 7.8 and 7.9, the heat transfer process is heating, the shell-side fluid is water and the inlet Reynolds number is about 10^5.

The bypass streams C and F cause a non-uniform flow distribution over the heat transfer surface. In fact, only a portion of the total stream will flow through the active tube surface including the tube-baffle leakages and another portion of the total stream will flow through inactive flow regions, i.e. bypass regions and baffle-shell leakages. Hence, the velocity and the heat transfer coefficient will decrease. This is the negative effect of bypass streams C and F. Another adverse effect of bypasses is when the bypass stream reaches the outlet without a significant change in temperature or, in the worst plausible case, with the same temperature as at the inlet. Considering the negligible change in physical properties with temperature and pressure, the effect of bypasses on the outlet temperature can then be simply represented as:

$$T_{outlet} = T_{outlet}^{ms} + \frac{\dot{M}_{bp}}{\dot{M}}(T_{inlet} - T_{outlet}^{ms}) \tag{7.1}$$

In Equation (7.1), the subscript "bp" refers to the bypass streams and the superscript "ms" refers to a portion of the stream flow without bypasses, i.e. main stream flow.

Taking into the account the cooling and heating processes yields:

$$\begin{cases} \text{for cooling} & : \quad T_{inlet} > T_{outlet}^{ms} \Rightarrow T_{outlet} > T_{outlet}^{ms} \\ \\ \text{for heating} & : \quad T_{inlet} < T_{outlet}^{ms} \Rightarrow T_{outlet} < T_{outlet}^{ms} \end{cases} \tag{7.2}$$

The bypasses may reduce the effective shell-side heat transfer coefficient, depending on extent of the bypass fraction and the inlet temperature, as can be concluded from Equations (7.1) and (7.2). Therefore, the bypasses, especially between tube bundle and shell wall, have to be minimized.

However another important cause of degradation of the shell-side heat transfer coefficient and consequently the shell-side gain factor Γ_{shell} is the existence of stationary eddies. These eddies energize the main stream and are not swept away. Such zones appear where the normal fluid escape routes through the annular orifices between baffles and tubes are blocked. Under such circumstances, not only the heat transfer coefficient and effective temperature difference suffer, but the pressure drop as well. Nevertheless, the reduction on the gain factor can be drastic due to the tube-baffle leakages.
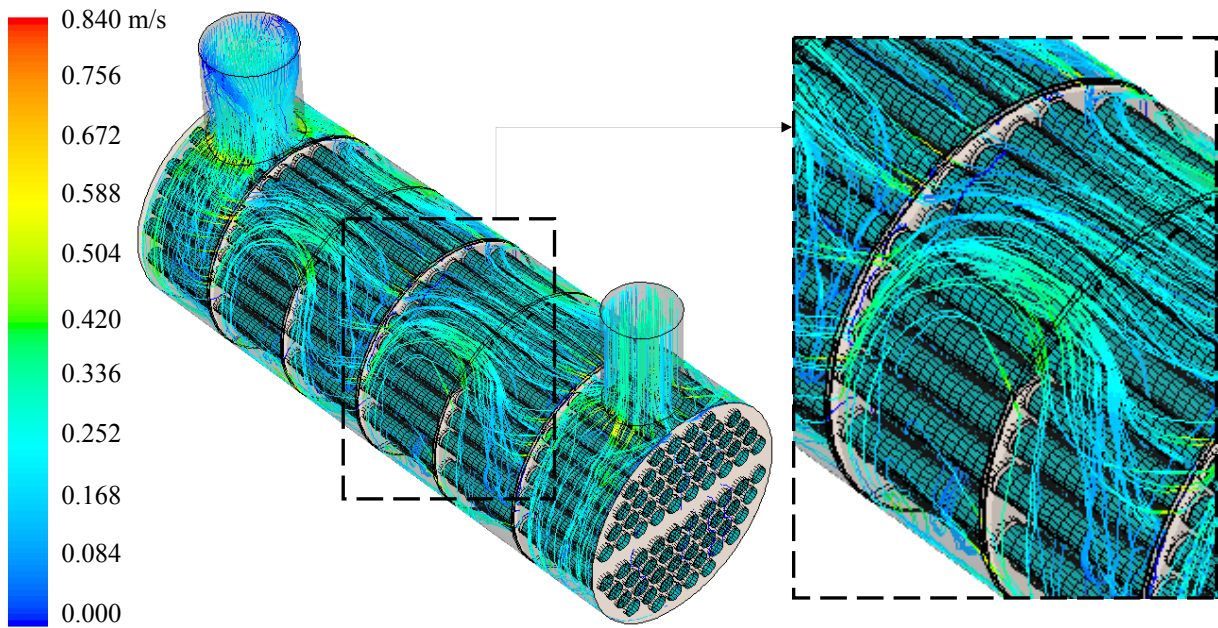
Figure 7.8: Path lines in the tube bundle coloured according to the velocity magnitude for the shell and tube heat exchanger with horizontal baffle orientation.
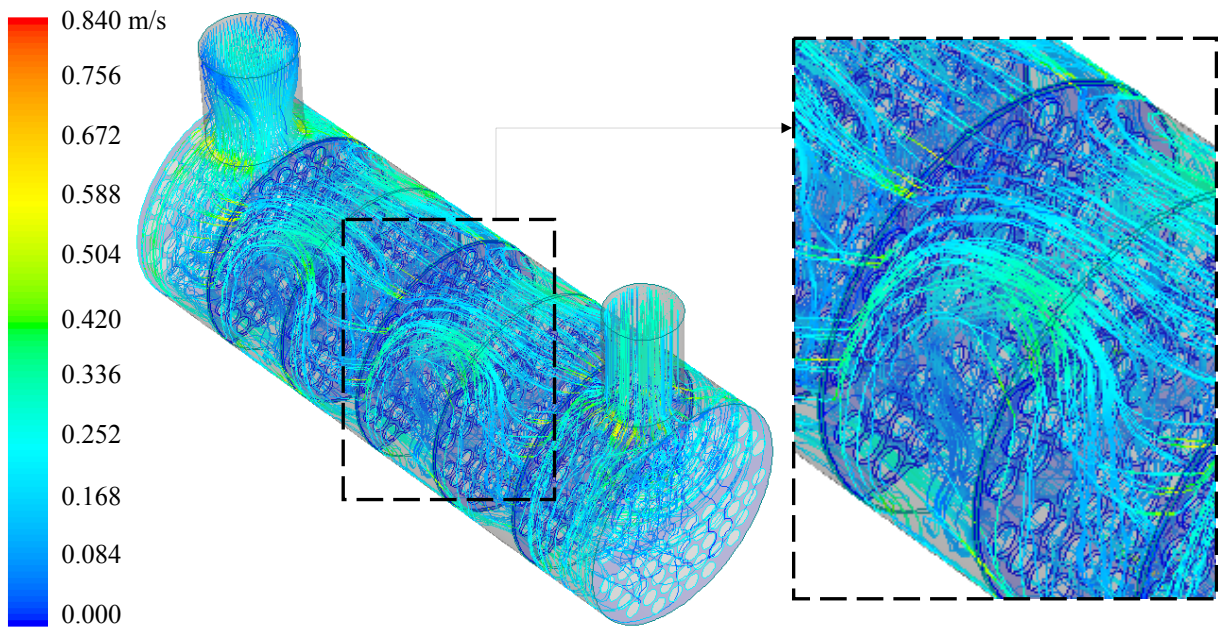
Figure 7.9: Path lines in the tube-baffle leakages coloured according to the velocity magnitude for the shell and tube heat exchanger with horizontal baffle orientation.

The fraction of the total shell-side flow allocated to each stream is presented in Table 7.4 [Palen and Taborek, 1969], based on a large data bank from test heat exchangers.
Table 7.4 shows the importance of the tube bundle bypass stream on the performance of shell and tube heat exchangers in laminar flow. As the shell-side Reynolds number increases, the contribution of leakage streams to the behavior of a shell and tube heat exchanger becomes more significant. A noteworthy fact is that in turbulent flow, the contribution of tube bundle bypass stream to the behavior of a shell and tube heat exchanger is comparable to the corresponding contribution of leakage streams, as can be seen from Table 7.4.

91

The physical mechanism of leakages and bypasses and the relationship between the various streams, their associated resistances and the resulting pressure drop can be represented schematically by Figure 7.10 [Palen and Taborek, 1969].

Stream	Stream designation	Typical stream flow fractions	
		Turbulent	Laminar
Tube-baffle leakage	A	9%-23%	0%-10%
Main effective cross-flow	B	30%-65%	10%-50%
Tube bundle bypass	C	15%-35%	30%-80%
Baffle-shell leakage	E	6%-21%	6%-48%
Tube pass partition bypass	F	(Not in Tinker's model)	

Table 7.4: The fraction of the total shell-side flow allocated to each stream according to Palen and Taborek, determined by applying the HTRI stream analysis method [Palen and Taborek, 1969].

In Figure 7.10, the stream flow resistance specific to any flow channel geometry and Reynolds number, is expressed by a resistance R. The cross flow, bypass, and pass partition streams (B, C, and F) are shown flowing in parallel across each baffle space, joining in the windows, and splitting again at the next baffle space. The tube baffle and baffle shell leakage streams (A and E) are depicted flowing in parallel from a hypothetical nodal point in one baffle space to a corresponding point in the next.

A simplified model which is well-known as piping network flow technique, can be used to explain the effect of leakages, particularly tube-baffle leakage, and tube bundle bypass on the shell-side gain factor for horizontal and vertical baffle orientations. This will facilitate the description of the behaviour of the performance factor and its dependency on the dynamic viscosity of the shell-side fluid and the shell-side Reynolds number.
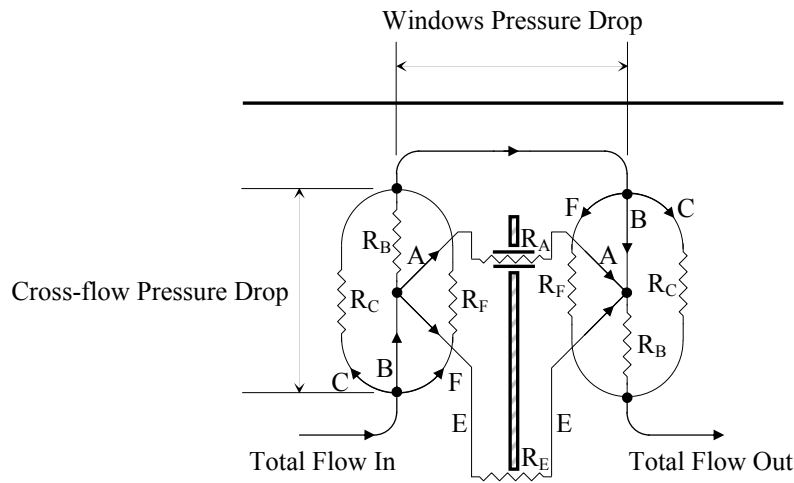
Figure 7.10: Schematic model of shell-side flow branches and their resistances across one baffle

7.5.2 Discussion of the Numerical Results

As described in previous chapters, the judgment between the horizontal and vertical baffle orientation is done by evaluation of the performance factor. The performance factor, indeed, is the ratio of gain factors for horizontal and vertical baffle orientation, as described in Equations (5.8) to (5.10). Therefore, the study of quantities $h_{hor.}/h_{ver.}$ and $\Delta p_{hor.}/\Delta p_{ver.}$ is used to clarify the behavior of the performance factor.

92

Figure 7.11 illustrates the ratio of the shell-side heat transfer coefficient of a heat exchanger with horizontal baffle orientation to the shell-side heat transfer coefficient of a heat exchanger with vertical baffle orientation, as a function of baffle spacing and inlet Reynolds number for a heating process and water as shell-side fluid. Likewise, Figures 7.12 and 7.13 represent the quantities $h_{hor.}/h_{ver.}$ for baffle window and tube-baffle leakages in each baffle window or baffle region.

Figure 7.11: Local ratio $h_{hor.}/h_{ver.}$ at each baffle spacing zone for liquid water as shell-side fluid and heating process.

Figure 7.11 shows that a shell and tube heat exchanger with horizontal baffle orientation has in the inlet region a greater shell-side heat transfer coefficient than a shell and tube heat exchanger with vertical baffle orientation. The inlet region is the region consisting of the inlet baffle spacing and the first central baffle spacing. Moreover, the value of $h_{hor.}/h_{ver.}$ increases with increasing Reynolds number. However, the advantage of horizontal baffle orientation over vertical baffle orientation decreases along the heat exchanger as the value of $h_{hor.}/h_{ver.}$ reaches a value less than one, and even about 0.5 for low Reynolds numbers.
The descending order curves of $h_{hor.}/h_{ver.}$ along the heat exchanger from the inlet to the outlet may be explained by use of Figures 7.12 and 7.13 and considering the influence of the mainly effective cross-flow stream B on other flow streams.
Figure 7.12 shows that $h_{hor.}/h_{ver.}$ is about 35% and 75% for low and high Reynolds numbers, respectively. The shell-side Nusselt number is proportional to Re^m, where $0.6 \leq m \leq 0.8$. Hence, the ratio of the mass flow rate in the baffle windows of the shell and tube heat exchanger with horizontal baffle orientation to the mass flow rate in the baffle window of the shell and tube heat exchanger with vertical baffle orientation is about 25% at low Reynolds numbers. The corresponding mass flow rate ratio at high Reynolds numbers is approximately 65%. This means that the portion of the total shell-side flow passing through the tube-baffle leakages for horizontal baffle orientation is considerably larger than the flow moving through

the tube-to-baffle leakages for vertical baffle orientation. This potentially increases the value of $h_{hor.}/h_{ver.}$ for tube-baffle leakages to a value greater than one, as it is illustrated in Figure 7.13.
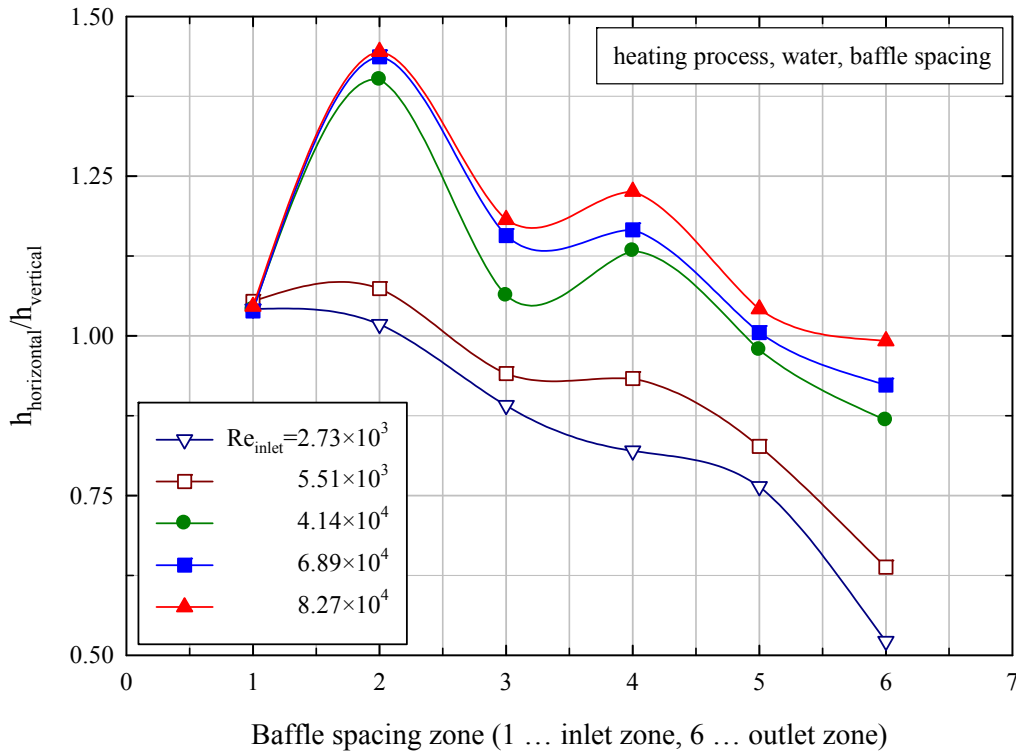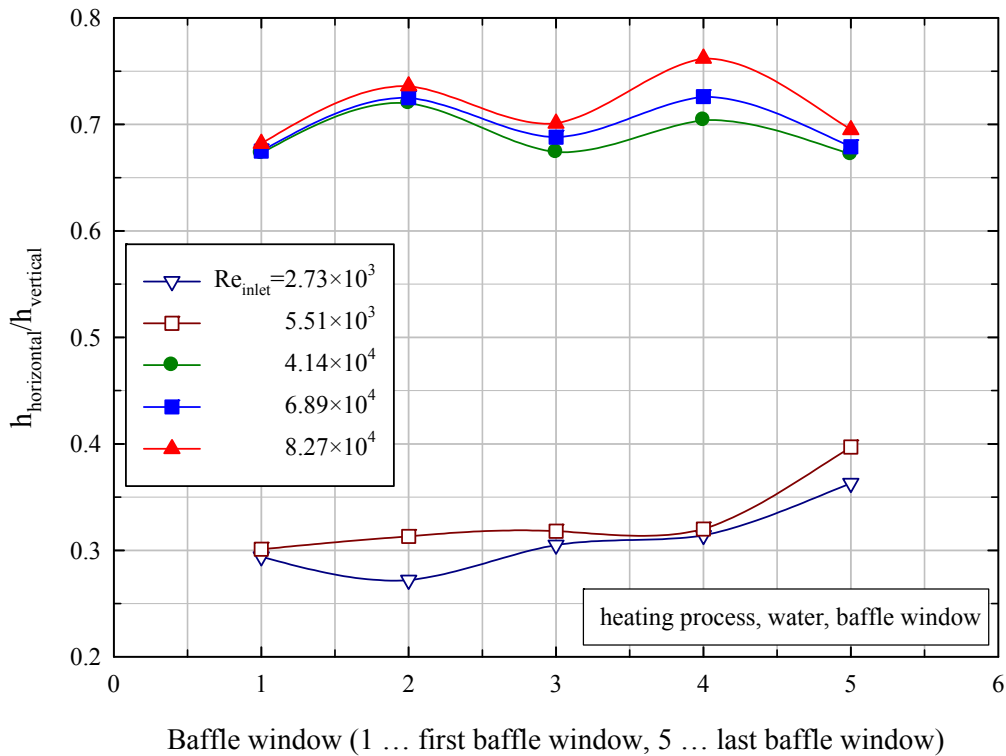

Figure 7.12: Local ratio $h_{hor.}/h_{ver.}$ at each baffle window for liquid water as shell-side fluid and heating process.

The minimum average distance, or the average shortcut distance, between the inlet nozzle and the first baffle window plays an important role in the explanation of the performance factor of the inlet zone. Since in the shell and tube heat exchanger with horizontal baffle orientation this distance is longer than the corresponding distance for the heat exchanger with vertical baffle orientation, the number of possible shortcut streamlines in vertical baffle orientation is greater than the number of possible shortcut streamlines in horizontal baffle orientation. Hence, the proportion of fluid moving over the baffle wall in horizontal baffle orientation is larger than the proportion of fluid passing over the baffle wall in vertical baffle orientation. This increases the likelihood for flow of the shell-side fluid through the tube-baffle leakages in a heat exchanger with horizontal baffle orientation. This phenomenon is illustrated schematically in Figure 7.14.

In the first central baffle spacing, due to the effect of stream B, the fraction of shell-side fluid passing over the baffle wall in the heat exchanger with horizontal baffle orientation is more than the corresponding fraction in the shell and tube heat exchanger with vertical baffle orientation.

This will increase the suction from tube-baffle leakages of the first baffle located in the first central baffle spacing in the horizontal baffle orientation compared to the vertical baffle orientation. As a result, in the first baffle of the shell and tube heat exchanger, the portion of shell-side fluid which is pushed into and sucked from tube-baffle leakages is more significant in the horizontal baffle orientation compared to the vertical baffle orientation.

The influence of the inlet nozzle zone on the downstream baffle spacing zones depends on the inlet Reynolds number and the geometrical aspects of the shell and tube heat exchanger,

94

especially tube length and central baffle spacing distance, tube number, tube layout and baffle cut. This is due to the fact that the time and length scales of turbulent flow may vary slowly downstream, but in sufficiently far distance from the inlet the turbulence time scales are small enough to permit adjustment to the gradually changing environment. As a result, the turbulence is dynamically similar everywhere if non-dimensionalized with local length and time scale. On the other hand, turbulent flows are characterized by very high Reynolds numbers. This means that any proposed description of turbulence should behave properly in the limit as Reynolds number approaches infinity [Tennekes, 1972]. The main characteristics of turbulence such as irregularity and randomness, dissipation, diffusivity and mixing level and consequently the rates of momentum and heat transfer will be the same in downstream zones for both horizontal and vertical baffle orientation, and the only difference is due to the effect of the inlet region. This fact is represented clearly in Figure 7.13, where for high Reynolds numbers the ratio of $h_{hor.}/h_{ver.}$ for tube-baffle leakages in all baffle spacing is about 1.15.
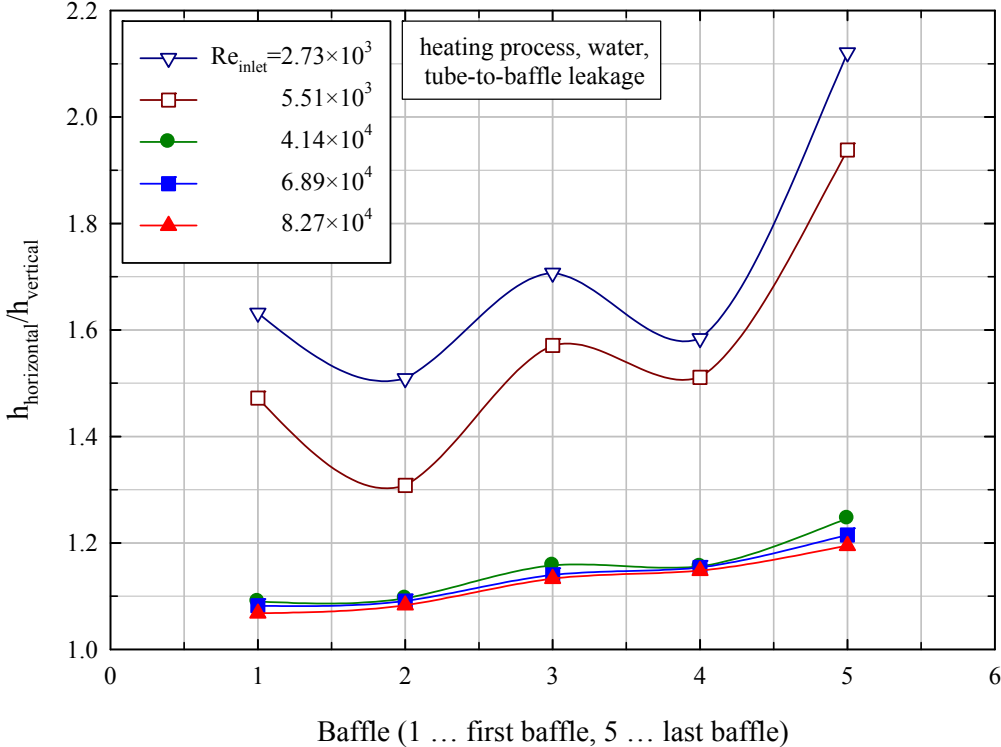
Figure 7.13: Local ratio $h_{hor.}/h_{ver.}$ for tube-baffle leakages at each baffle (shell-side fluid … liquid water and, heat transfer process … heating).

Depending on the Reynolds number and the dynamic viscosity of the shell-side fluid, the fraction of tube-baffle leakage can vary. For low Reynolds numbers, the portion of fluid which could possibly flow as tube-baffle leakages may be more than the corresponding portion at high Reynolds numbers because of the higher static pressure on the baffle wall. On the other hand, the pressure drop increases with increasing Reynolds number. Hence the possibility of the fluid suction from the tube-baffle gaps on the opposite side of the baffle wall will increase with increasing Reynolds number. The fraction of fluid passing through as tube-baffle leakage increases with increasing Reynolds number, as it is presented in Table 7.4. However, the ratio tube-baffle leakages for horizontal baffle orientation to the tube-baffle leakages for vertical baffle orientation decreases with Reynolds number, see Figure 7.13 and 7.14.

95
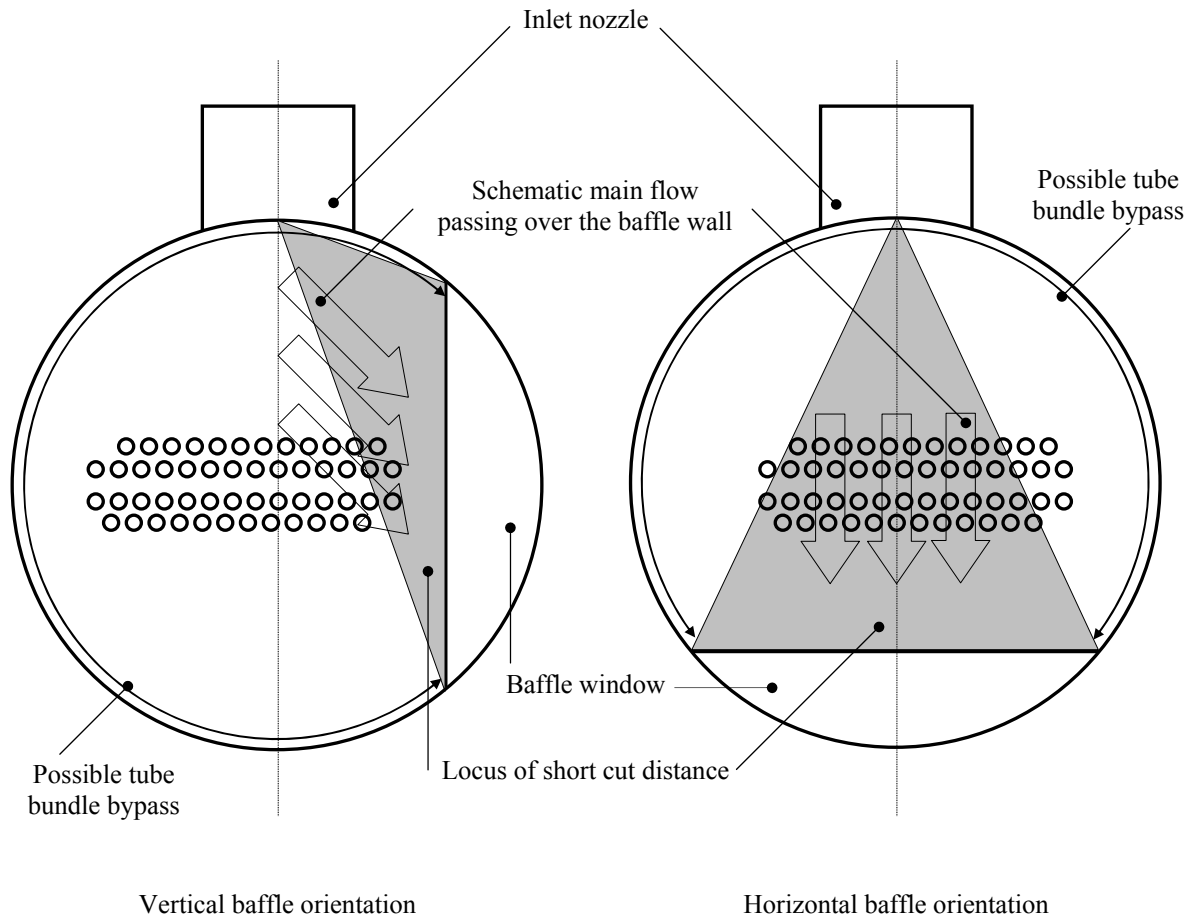
Figure 7.14: Schematic illustration of the fraction of the shell-side fluid passing over the baffle wall in the inlet zone for vertical and horizontal baffle orientation.

The effect of shell-side fluid viscosity on the tube bundle bypass stream C has to be considered, as well. As the shell-side fluid viscosity increases, the portion of the total stream that takes the less viscous bypass route increases [Tinker, 1951]. As illustrated schematically in Figure 7.14, the possible less viscous bypass route is more accessible in the shell and tube heat exchanger with horizontal baffle orientation than in the heat exchanger with vertical baffle orientation. As a consequence, the adverse effect of the bypass stream C described in Equation (7.1) is observable in the heat exchanger with horizontal baffle orientation.

The tube bundle bypass and tube-baffle leakage streams C and A are depicted and compared for horizontal and vertical baffle orientation in Figures 7.15 and 7.16. In Figures 7.15 and 7.16 the shell-side fluid is water, the process is heating and the inlet Reynolds number is around 10^5.

The unfavorable effects of tube bundle bypass and tube-baffle leakage streams on the heat transfer rate causes that the ratio of overall heat transfer coefficient in horizontal baffle orientation to the heat transfer coefficient in vertical baffle orientation to be about 0.8 for $Re_{inlet} \approx 3 \times 10^3$ and around 1.15 for $Re_{inlet} \approx 10^5$.

The jet-like flow through tube-baffle leakage streams (stream A) will increase the pressure drop. This effect is illustrated in Figure 7.17. Since at lower Reynolds numbers the difference between stream A in horizontal baffle orientation and stream A in vertical baffle orientation is more visible, the value of $\Delta p_{hor.}/\Delta p_{ver.}$ in tube baffle leakages increases with decreasing Reynolds number.

96

Figure 7.15: Path lines in the tube bundle coloured according to the static temperature for the shell and tube heat exchanger with 76 tubes. The baffle cut is equal to 20% of the shell inside diameter. The heat transfer process is heating, the shell-side fluid is water and the inlet Reynolds number is about 10^5.

The same arguments apply for baffle-shell leakages, keeping in mind that the heat transfer rate for stream E is negligible especially when the baffle walls are adiabatic. The slight temperature change in the baffle-shell gaps is due to the shear work.

The value of $\Delta p_{hor.}/\Delta p_{ver.}$ in baffle windows as a function of baffle window position and Reynolds number is presented in Figure 7.18.

The bypass stream has not played an important role to distinguish the pressure drop difference between horizontal and vertical baffle orientation. Since the pressure drop is roughly proportional to the second order of velocity, the difference between the pressure drop for horizontal baffle orientation and for vertical baffle orientation does not vanish rapidly with

increasing Reynolds number, as it is described by the concept of similarity of turbulence at high Reynolds number.

The local ratio of pressure drop for horizontal baffle orientation to the pressure drop for vertical baffle orientation as a function of Reynolds number in the baffle spacing is shown in Figure 7.19.

Horizontal Baffle Orientation
$\{\Delta T_{overall}=22.1 \text{ K}, \ln(\Delta T_{in}/\Delta T_{out})=1.33\}$

Vertical Baffle Orientation
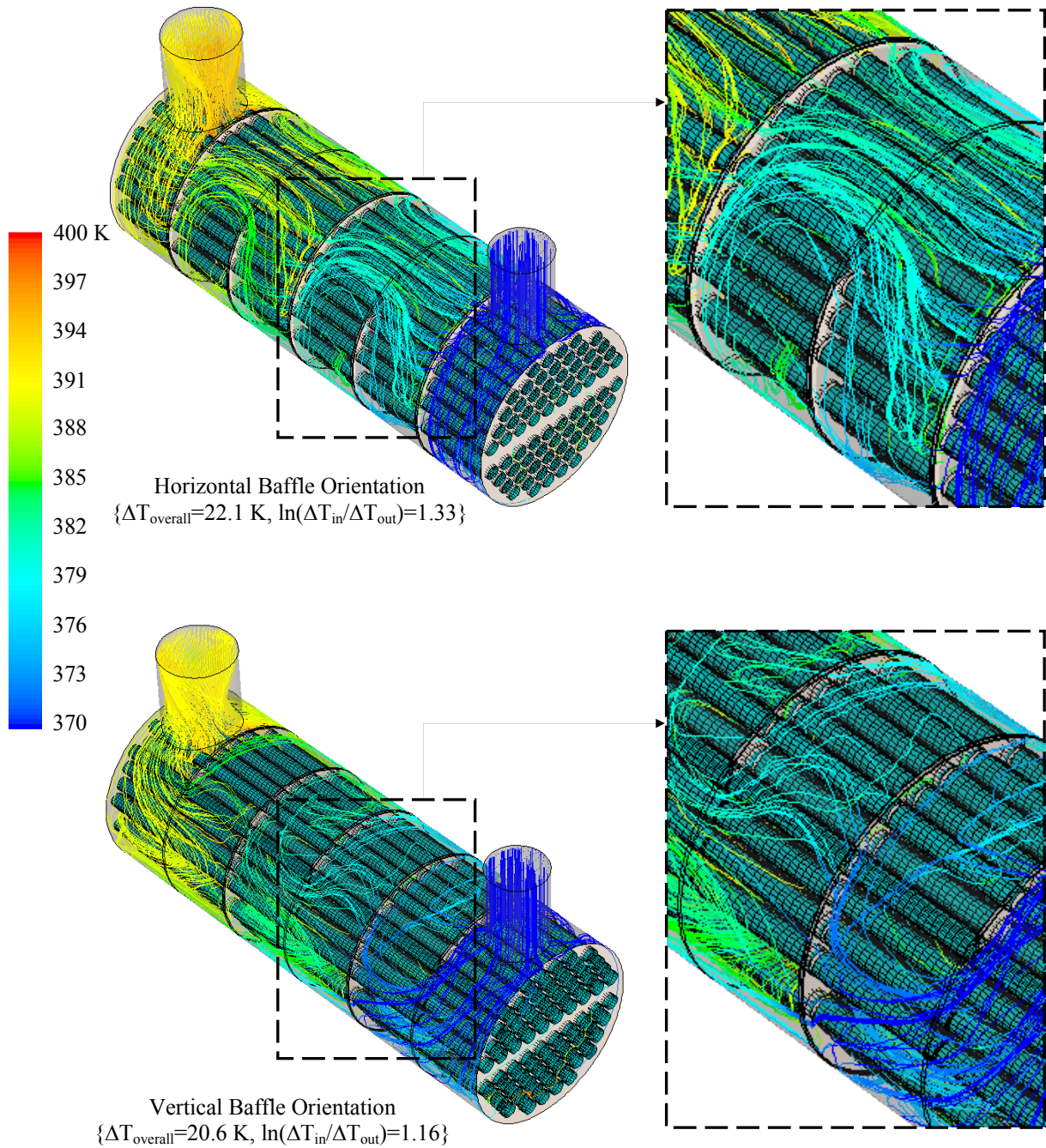$\{\Delta T_{overall}=20.6 \text{ K}, \ln(\Delta T_{in}/\Delta T_{out})=1.16\}$
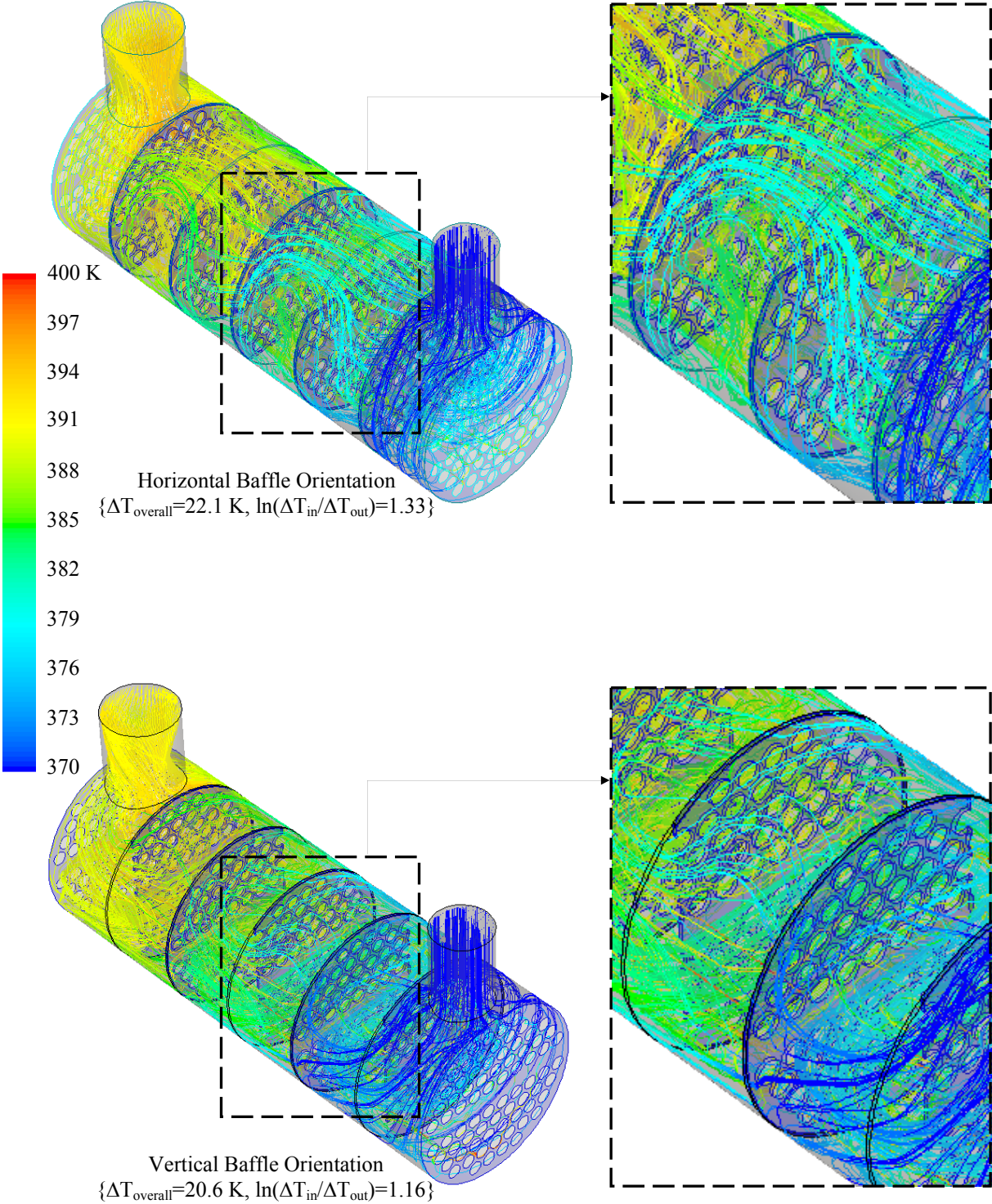
Figure 7.16: Path lines in the tube-baffle gaps coloured according to the static temperature for the shell and tube heat exchanger with 76 tubes. The baffle cut is equal to 20% of the shell inside diameter. The heat transfer process is heating, the shell-side fluid is water and the inlet Reynolds number is about 10^5.

The results in Figure 7.11 and 7.19 explain why the performance factor decreases along the shell and tube heat exchanger from inlet to outlet. It is because of the effect of end zones, which can be characterized as the average shortcut distance between the nozzle and its neighboring baffle window, on the main effective cross-flow stream B and its influence on the leakage streams A and E and consequently on tube bundle bypass stream C.

When the average shortcut distance between the nozzle and its nearest baffle window increases, then:

- The pressure drop in the tube-baffle leakages increases. This causes a better heat transfer in the tube-baffle gap. However, since the pressure drop is proportional to the velocity squared, whereas the heat transfer coefficient depends on $Re^{0.6 \sim 0.8}$, the increase in pressure drop is more significant than the enhancement in heat transfer coefficient.
- The pressure drop in the baffle-shell gaps rises. Since the stream flow E does not influence the heat transfer rate, particularly when the baffle walls are assumed to be adiabatic, the baffle-shell leakages will increase only the overall pressure drop.
- The portion of fluid passing through the less viscous bypass route increases. This stream, i.e. stream C, has a significant and undesirable effect on the heat transfer rate. Since the bypass stream C reaches the outlet without significant change in temperature, it will reduce the effective temperature gradient in the heat exchanger. This will decrease the overall heat transfer.
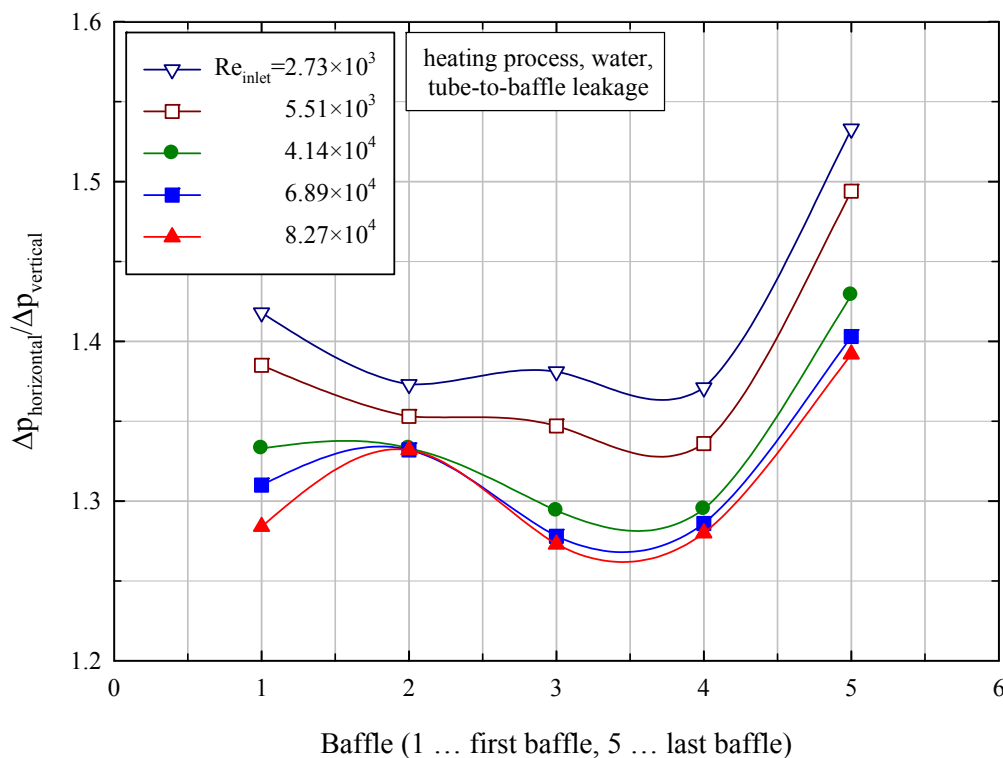
Figure 7.17: $\Delta p_{hor.}/\Delta p_{ver.}$ for tube-baffle leakages at each baffle (water as the shell-side fluid, heating).

Figures 7.20 and 7.21 compare the tube bundle pressure drops ($\Delta p = p - p_{inlet}$) in the baffle window and tube-baffle gaps in a shell and tube heat exchanger with horizontal and vertical baffle orientation. In these Figures the shell-side fluid is water, the process is heating and the inlet Reynolds number is around 10^5.
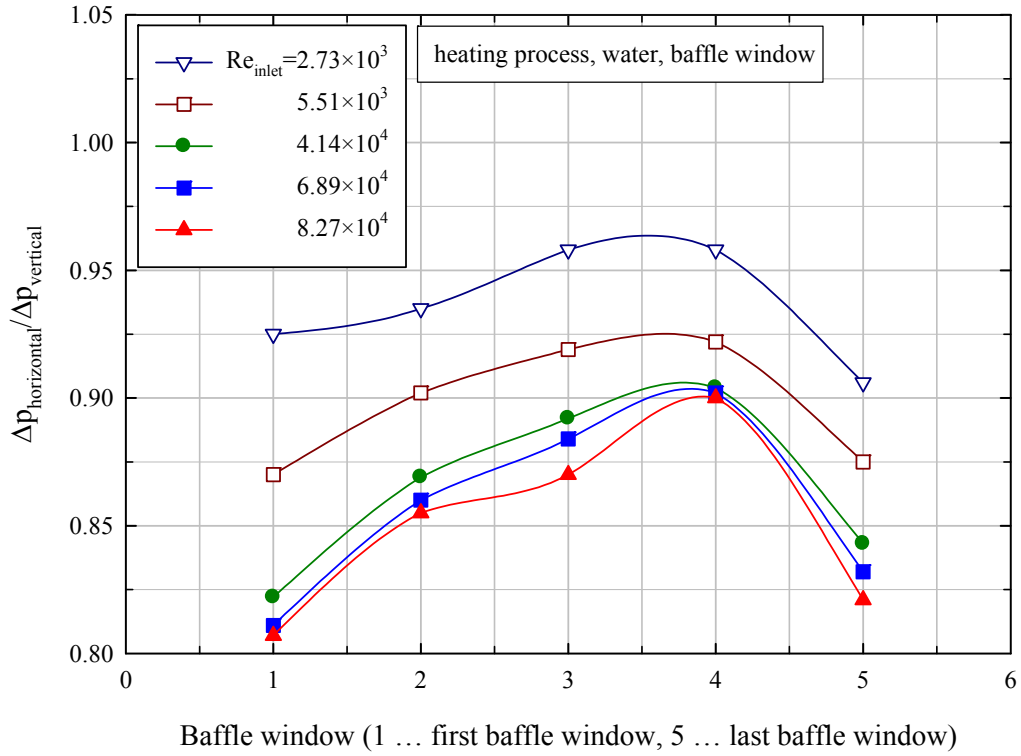
Figure 7.18: Local ratio $\Delta p_{hor.}/\Delta p_{ver.}$ for baffle windows (water as the shell-side fluid, heating).

Figure 7.19: Local ratio $\Delta p_{hor.}/\Delta p_{ver.}$ for baffle spacing (water as the shell-side fluid, heating).
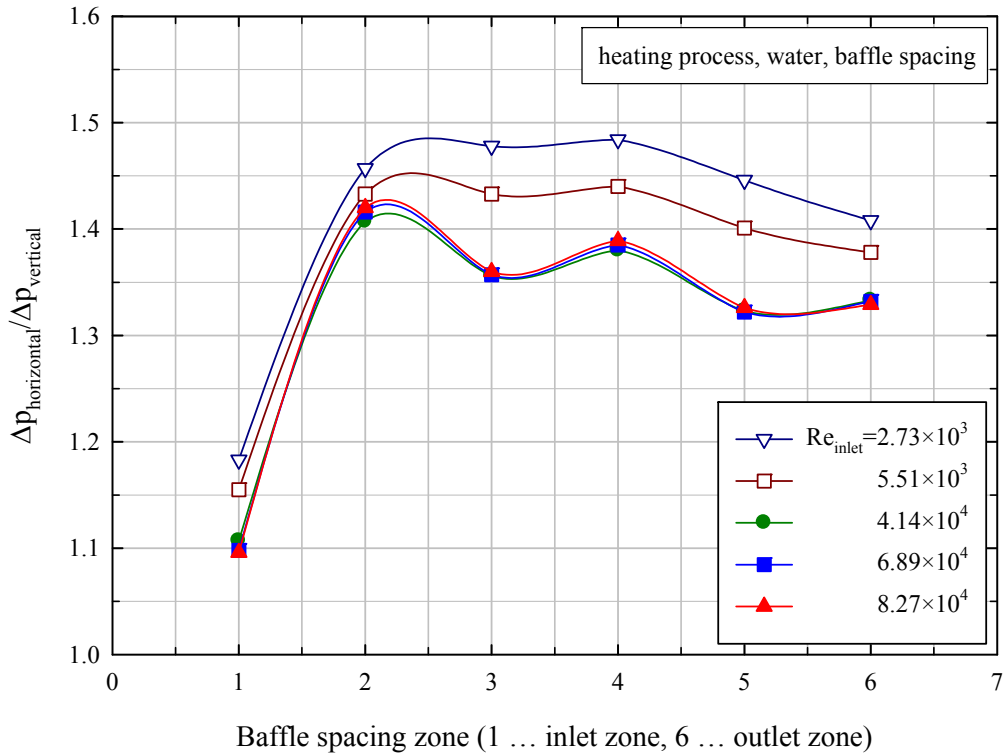
The effect of baffle orientation on streams A and C can be postulated as:

$$R_s = G(\{X\}) \times F_s(R_B) \times Tr(\mu, Re) \times O_s\left(B_C, \angle(\overrightarrow{bf}, \overrightarrow{nz})\right) \qquad (7.3)$$

100

with

$$R_s \equiv \text{Resistance of stream s}$$

$$s \equiv \text{Stream A or stream C}$$

$G(\{X\}) \equiv$ Geometrical function of the shell and tube heat exchanger with the set of parameters $\{X\}=\{$tube layout, tube outside diameter, tube length$\}$

$F_s(R_B) \equiv$ Function describing the influence of main cross-flow stream B with resistance parameter R_B on stream s

$Tr(\mu, Re) \equiv$ Function explaining the transfer rate of heat and momentum which depends on the dynamic viscosity of the shell-side fluid and the Reynolds number

$O_s\left(B_C, \angle(\overrightarrow{bf}, \overrightarrow{nz})\right) \equiv$ Orientation function. This function explains the effect of the baffle orientation and baffle cut on stream s. The orientation function depends on the segmental baffle cut percentage and the angle between baffle vector and face vector of the inlet plane.

$\overrightarrow{bf} \equiv$ Baffle vector

$\overrightarrow{nz} \equiv$ Face vector of the inlet plane

Figure 7.22 illustrates the behaviour of the performance factor for heating and cooling and for different shell-side fluids. In Figure 7.22, the superscript SATP refers to the physical properties at Standard Ambient Temperature and Pressure (T=25 °C, p=100 kPa). The interaction between the different streams decreases the value of the performance factor as depicted in Figure 7.22. For water as shell-side fluid the performance factor is about 0.6 for low Reynolds number and around 0.9 for high Reynolds number, for both cooling and heating processes.

In order to describe the effect of viscosity on the performance factor, the origin of turbulence has to be considered. Turbulence arises from instabilities and cannot maintain itself but depends on its environment to obtain energy. The instabilities which make the flow turbulent are related to the interaction of viscous terms and nonlinear inertia term in the equation of motion.

A common source of energy for turbulent velocity fluctuations is shear in the mean flow. Turbulent flows are generally shear flows. If turbulence arrives in an environment where no shear appears, it decays: the Reynolds number decreases and the flow tends to become laminar again. The outstanding characteristic of turbulent motion is its ability to transport or mix momentum, kinetic energy, and "contaminants" such as heat, particles and moisture.

Moreover, the fluid dynamics of flows at high Reynolds numbers are characterized by the existence of several length scales. In turbulent flows a wide range of length scales exist, bounded from above by dimensions of the flow field and bounded from below by the diffusive action of molecular viscosity.

Turbulence consists of a continuous spectrum of scales. For the purpose of visualizing a turbulent flow by aid of a spectrum of scales, a discussion in terms of eddies is often helpful. A turbulent eddy can be thought of as a local swirling motion whose characteristic dimension is the local turbulence scale. Eddies overlap in space, large ones carrying smaller ones. Turbulence features a cascade process whereby, as the turbulence decays, its kinetic energy transfers from larger eddies to smaller eddies. Ultimately, the smallest eddies dissipate into heat through the action of molecular viscosity. Thus, turbulent flows are always dissipative.

A striking feature of a turbulent flow is the way large eddies migrate across the flow, carrying small-scaled disturbances with them. The arrival of these large eddies near the interface between the turbulent region and the non-turbulent fluid distorts the interface into a highly convoluted shape. Hence, the state of turbulent flow at a given position depends upon

upstream history and cannot be uniquely specified in term of local strain-rate tensor as in laminar flow [Wilcox, 1998].

Nevertheless, the smallest scales of turbulence are many orders of magnitude smaller than the larger scales of turbulence. Furthermore, the ratio of smallest to largest scales decreases rapidly as the Reynolds number increases.

Figure 7.20: Path lines in the tube bundle coloured according to the pressure drop Δp for the shell and tube heat exchanger with 76 tubes (20% baffle cut, heating, water, $Re_{inlet} \approx 10^5$).

It might be expected that at large Reynolds numbers the relative magnitude of viscosity is so small that viscous effects in a flow tend to become vanishingly small. The nonlinear terms in the Navier-Stokes equations counteract this effect by generating motion at scales small

102

enough to be affected by viscosity. The smallest scale of motion automatically adjusts itself to the value of viscosity. As soon as the scale of the flow field becomes so large that viscosity effects could conceivably be neglected, the flow creates small scale motion, thus keeping viscosity effects at a finite level.
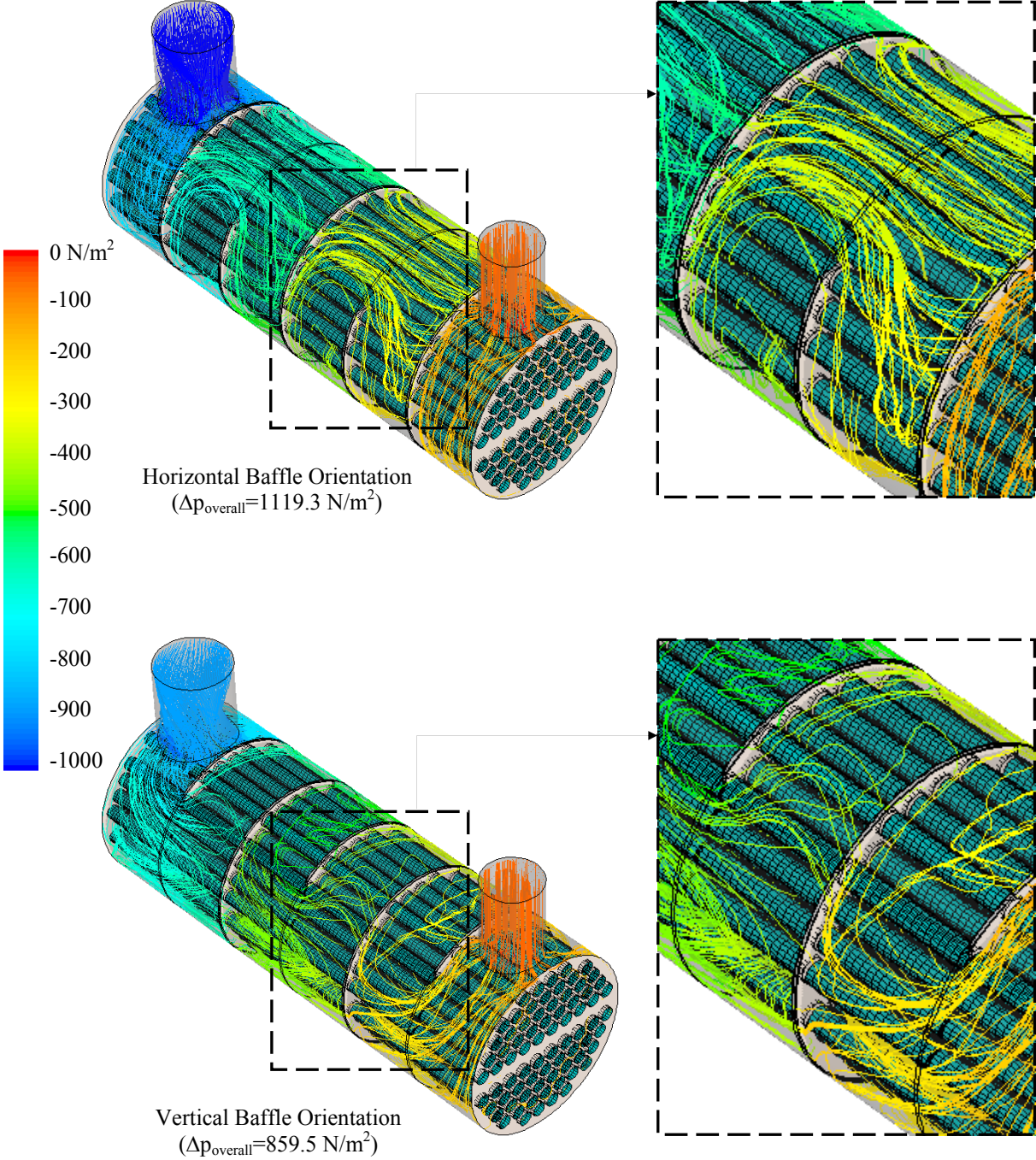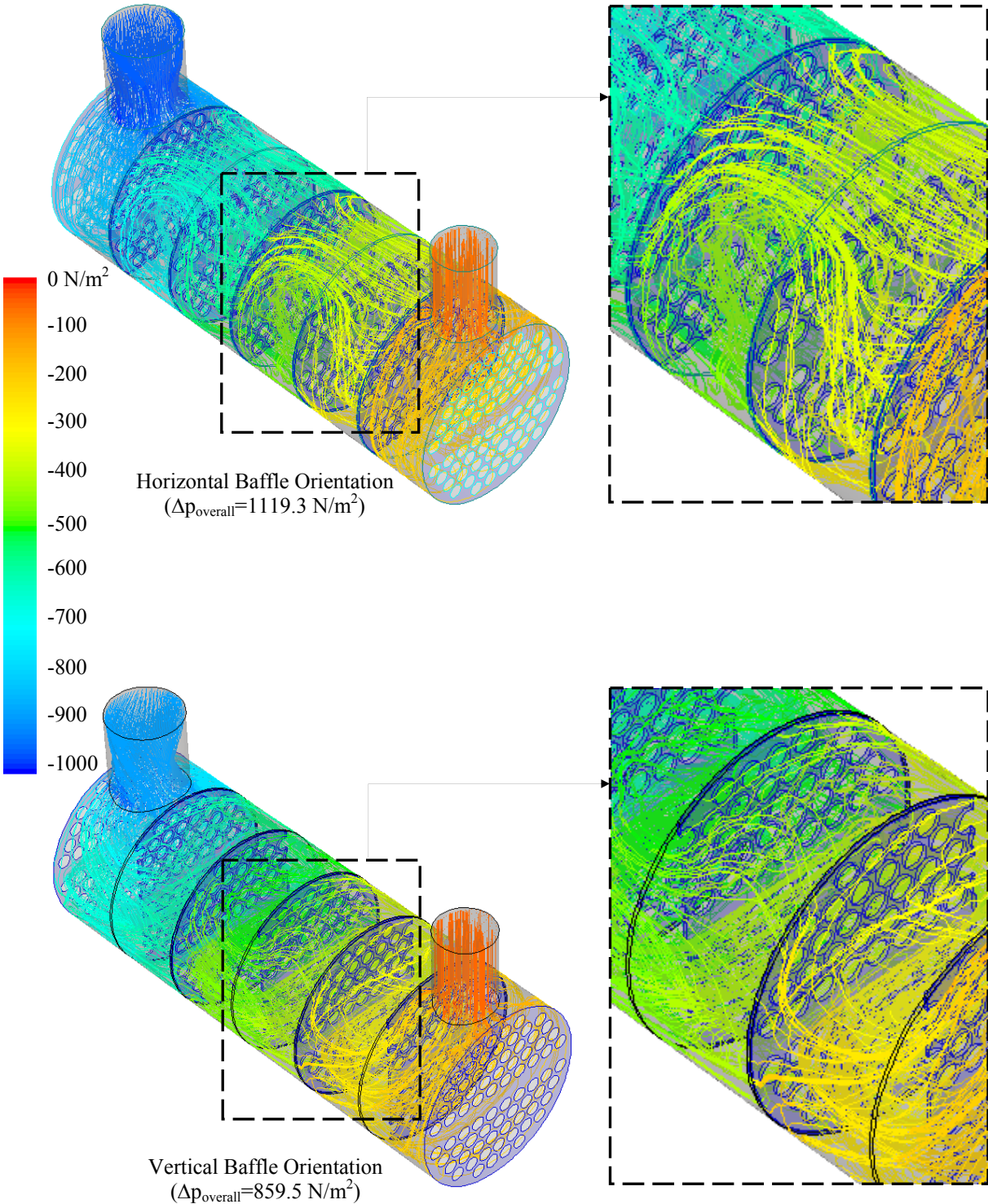

Figure 7.21: Path lines in the tube-baffle gaps coloured according to the pressure drop Δp for the shell and tube heat exchanger with 76 tubes (20% baffle cut, heating, water, $Re_{inlet} \approx 10^5$).
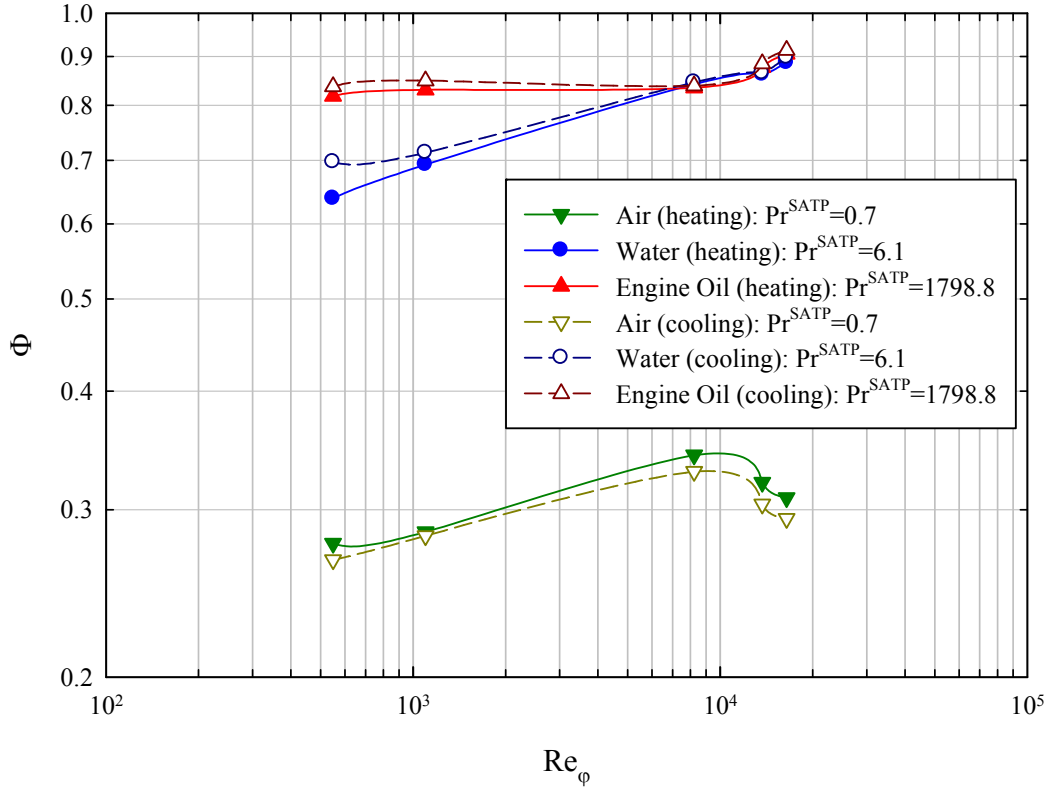
Figure 7.22: Behaviour of the performance factor for different shell-side fluids in heating and cooling processes.

In summary, turbulence is dominated by the large, energy-bearing, eddies. The larger eddies are primarily responsible for the enhanced diffusivity and stresses observed in turbulent flows. Because large eddies persist for long distances, the diffusivity and stresses are dependent upon flow history, and cannot necessarily be expressed as functions of local flow properties. Also, while the small eddies ultimately dissipate turbulence energy through viscous action, the rate at which they dissipate is controlled by the rate at which they receive energy from the largest eddies.

The largest eddy size can be measured as the integral length scale, ℓ [Wilcox, 1998].

$$\ell(\vec{x}, t) = \frac{3}{8} \int_0^\infty \frac{\overline{u_i'(\vec{x}, t) \cdot u_i'(\vec{x}+\vec{\xi}, t)}}{\overline{u_i'(\vec{x}, t) \cdot u_i'(\vec{x}, t)}} d|\vec{\xi}| \qquad (7.4)$$

In Equation (7.4), $\overline{u_i'(\vec{x}, t) \cdot u_i'(\vec{x}+\vec{\xi}, t)}$ is the displacement average of the fluctuating velocities at the same time but at different displacements $|\vec{\xi}|$ and $\overline{u_i'(\vec{x}, t) \cdot u_i'(\vec{x}, t)}$ is the displacement average of the fluctuating velocities at the same time and with zero displacement. Moreover, $\vec{\xi}$ defines the displacement vector between two points in the flow, say $\vec{x}$ and $\vec{x} + \vec{\xi}$.

Equation (7.4) shows that the size of larger eddies depends on the velocity fluctuations which are affected by environment and geometry.

On the other hand, the cascade process present in all turbulent flows involves a transfer of turbulence kinetic energy, k, from larger eddies to smaller eddies. Because small scale motion tends to occur on a short time scale, it is reasonable to assume that such motion is independent of the relatively slow dynamics of the large eddies and of the mean flow. This is one of the

premises of Kolmogorov's universal equilibrium theory. Hence, the motion of the smallest scales should depend only on the rate at which the large eddies supply energy, $\varepsilon=-dk/dt$, and the kinematic viscosity, v. Using these parameters, the length, time, and velocity scales are as follows:

$$\zeta = (v^3/\varepsilon)^{1/4}, \tau = (v/\varepsilon)^{1/2}, \upsilon = (v\varepsilon)^{1/4} \tag{7.5}$$

These scales are referred to as the Kolmogorov micro-scales of length ζ, time τ, and velocity υ [Friedlander and Topper, 1961].
The Reynolds number formed with υ and ζ is equal to one.

$$\upsilon\zeta/v = 1 \tag{7.6}$$

Equation (7.6) illustrates that the small-scale motion is quite viscous and that the viscous dissipation adjusts itself to the energy supply by adjusting length scales.
In turbulent flow, a plausible assumption is to take the rate at which large eddies supply energy to the small eddies to be proportional to the reciprocal of the time scale of the large eddies. The amount of kinetic energy per unit mass in the large scale turbulence is proportional to the square of the characteristic velocity fluctuation of turbulence, i.e. u^2. The rate of transfer of energy is assumed to be proportional to u/ℓ. The rate of energy supply to the small scale eddies is thus of order $(u^2)(u/\ell)$. This energy is dissipated at rate ε, which should be equal to the supply rate [Taylor, 1935]:

$$\varepsilon \approx u^3/\ell \tag{7.7}$$

Substituting Equation (7.7) into Equation (7.5), the Kolmogorov scales could be represents as follow:

$$\zeta = \left(\frac{\ell v^3}{u^3}\right)^{1/4}, \tau = \left(\frac{\ell v}{u^3}\right)^{1/2}, \upsilon = \left(\frac{v}{\ell}u^3\right)^{1/4} \tag{7.8}$$

As it is presented in Equations (7.5) to (7.8), the Kolmogorov scales of length and time decreases with increasing dissipation rates. In gases, high dissipation rates are more likely to occur than in liquids. Equation (7.8) shows that for low viscosity fluids, the change in turbulence length scale has a significant effect on mixing and transfer rate of heat, particles or moisture.
In a shell and tube heat exchanger with horizontal baffle orientation, the velocity fluctuations are significantly more intensive than the velocity fluctuations in a shell and tube heat exchanger with vertical baffle orientation. This is due to the effect of geometry on the rate of shear. Consequently, the rate of energy transfer in a shell and tube heat exchanger with horizontal baffle orientation is higher than the rate of energy transfer in a heat exchanger with vertical baffle orientation.
Moreover, dealing with heat transfer, the heat has to be transferred from or into the bulk of the shell-side fluid to or from the tube walls. In this heat transfer path, two main resistances can be considered: resistance in bulk of fluid and resistance in laminar sub-layer near the tube walls. The mixing level in the bulk of fluid will increase as the viscosity of fluid increases. I.e. the heat transfer resistance in the bulk of fluid will decrease by increasing the viscosity of fluid, whereas the laminar sub-layer will be thicker as the viscosity increases. Consequently, an increase in viscosity will enhance the heat transfer rate in the bulk of fluid, while it will

diminish the heat transfer rate in the region near the tube walls. Hence, the change in eddy sizes due to the geometrical variations may result in a minor enhancement on the overall heat transfer rate for all shell-side fluids.

The improvement in heat transfer rate depends on thermal diffusivity, viscosity, energy dissipation rate and on the portion of tube walls which take part the heat transfer. In the flow domain of low Reynolds numbers, the kinematic viscosity ν plays an important role. On the other hand, since at low Reynolds numbers the mean velocity of the shell-side fluid is not high enough, the change in baffle orientation does not change the effective heat transfer area significantly. This is due the high residence time of the shell-side fluid for low velocities. As a conclusion, at low Reynolds numbers, the main resistance is in the region near the tube walls. In this velocity domain, increasing the turbulent integral length scale will produce larger eddies in the turbulent boundary layer. These larger eddies generated in the region near the tube walls will disturb the sub-layer which will reduce the heat transfer resistance near the wall region and enhance the heat transfer results. The change in turbulent integral length scale depends on the velocity fluctuation originating from the rigid walls, and the grow rate of velocity fluctuation depends on the viscous diffusion rate or kinematic viscosity. At low Reynolds number, on the other hand, the Kolmogorov scales which describe the transfer rate in micro-scales are very important. At this scale, the kinematic viscosity has a significant effect. Convincingly, at low Reynolds number, the disturbance of the sub-layer region and consequently the reduction of heat transfer resistance and the enhancement of heat transfer rate in micro-scales is more perceptible when the kinematic viscosity is higher. Therefore, the effect of baffle orientation on heat transfer at low Reynolds numbers is more apparent for shell-side fluids with higher kinematic viscosity ν. For shell-side fluids with high kinematic viscosity, the effect of baffle orientation on heat transfer at low Reynolds number is more significant for shell-side fluids with low thermal diffusivity, i.e. $\alpha=\nu/Pr$. In fact, the thermal diffusivity defines the heat transfer resistance in the sub-layer region. This behavior is illustrated in Figure 7.23, in which the heat transfer enhancement for air ($\alpha=1.6\times10^{-5}$ m^2/s and $\nu=2.3\times10^{-5}$ m^2/s) and engine oil ($\alpha=8.3\times10^{-8}$ m^2/s and $\nu=1.5\times10^{-4}$ m^2/s) is compared. On the other hand, when the kinematic viscosity is very low while the thermal diffusivity α is not high enough, changing the baffle orientation from horizontal to vertical does not increase the turbulent integral length scale considerably but only changes the effective heat transfer surface slightly. This may either improve the heat transfer rate or reduce it due to the new developed sub-layers around the tube walls and the very low thermal diffusivity. This fact is shown in Figure 7.23: at low Reynolds numbers, the heat transfer coefficient ratio, i.e. $h_{horizontal}/h_{vertical}$, decreases for water ($\alpha=1.5\times10^{-7}$ m^2/s and $\nu=8.9\times10^{-7}$ m^2/s) while it increases for air and engine oil.

As the Reynolds number increases, the thickness of the sub-layer decreases. Consequently, the heat transfer resistance in regions near the tube walls will diminish as the Reynolds number increases. In this case, the dissipation rate ε will be important since it describes the rate of heat transfer in the bulk. In gases, a high dissipation rate is more likely to occur than in liquids [Tennekes, 1972]. Therefore, an increase in the integral length scale ℓ is more effective to decrease the dissipation rate in gases than in liquids. Due to this fact, increasing the Reynolds number will increase the value of $h_{horizontal}/h_{vertical}$ for air more than the values of $h_{horizontal}/h_{vertical}$ for water and engine oil, as it is shown in Figure 7.23.

Moreover, the main difference between two turbulent flows with different Reynolds numbers but with same integral scale is the size of the smallest eddies. Hence, an increase in the integral length scale is more visible in liquids with higher kinematic viscosity than in liquids with lower kinematic viscosity. Therefore, the value of $h_{horizontal}/h_{vertical}$ for engine oil is greater than the value of $h_{horizontal}/h_{vertical}$ for water at high Reynolds numbers. There is another difference between the behavior of $h_{horizontal}/h_{vertical}$ at intermediate Reynolds numbers for

106

water and for engine oil. When the shell-side liquid is water, the heat transfer coefficient ratio, i.e. $h_{horizontal}/h_{vertical}$, increases with increasing Reynolds number, while for engine oil the value of $h_{horizontal}/h_{vertical}$ decreases. This is due to the development of the effective heat transfer area and consequently the formation of a laminar sub-layer around these areas. The development of a new sub-layer may slightly increase the heat transfer resistance. This could decrease the heat transfer coefficient ratio for the liquid with lower thermal diffusivity α to some extent. This fact is clearly distinguishable for the engine oil with lower thermal diffusivity ($\alpha=8.3\times10^{-8}$ m^2/s) in Figure 7.23.

As described previously, it has to be considered that increasing the Reynolds number will intensify the flow of the shell-side fluid in inactive heat transfer zones like tube-pass partition channel, tube bundle bypass, and particularly baffle-shell gaps and tube-baffle gaps. This may diminish the heat transfer rate. Depending on the dynamic viscosity, the dissipation rate and the thermal diffusivity, increasing the Reynolds number may magnify the reduction of heat transfer coefficient ratio, i.e. $h_{horizontal}/h_{vertical}$.
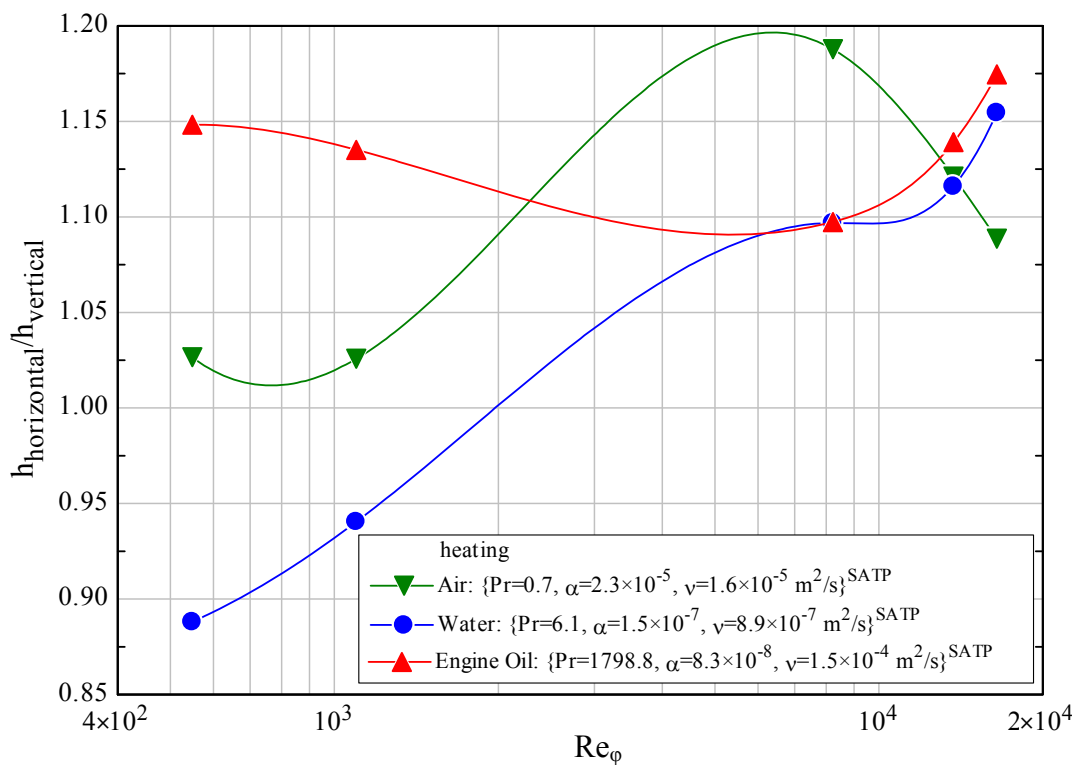
Figure 7.23: Heat transfer coefficient ratio, .i.e. $h_{horizontal}/h_{vertical}$, for different shell-side fluids as a function of Reynolds number (heating process).

At very high Reynolds numbers, the mixing level is rather high and the sub-layer thickness is small. As a result, the possible change in the heat transfer resistances due to the variation in the baffle orientation is negligible at very high Reynolds numbers. At very high Reynolds numbers, turbulent flows tend to be almost independent of viscosity and changing of the baffle orientation from vertical to horizontal will increase the effective heat transfer surface. Since at high Reynolds number the thickness of sub-layer near the tube wall is extreme thin, thermal diffusivity α is not the controlling parameter. At high Reynolds numbers, the value of kinematic viscosity ν is the controlling parameter since at small eddy level, the higher value of kinematic viscosity means higher rate of viscous energy loss. Therefore increasing the effective heat transfer area may enhance the heat transfer more for the liquid with higher

kinematic viscosity. The author believes that increasing the dissipation rate could again force the main effective flow stream to take the less viscous bypass route which could decrease the heat transfer coefficient ratio. This can happen for liquids when the Reynolds number approaches to an extreme high value. Since the gases are much more dissipative than the liquids, a large value of velocity (which corresponds to high Reynolds number) is more likely to occur than in liquids. Hence, the plot of $h_{horizontal}/h_{vertical}$ as a function of Reynolds number seems to be at first ascending until reaching an absolute maximum value. Then, the curves will have a descending order trend. The graph of $h_{horizontal}/h_{vertical}$ has a horizontal asymptote when it is introduced as a function of Reynolds number. Hence, at extremely high Reynolds numbers, $h_{horizontal}/h_{vertical}$ will approach to a constant value. This behavior could happen for liquids at very high Reynolds number. However, since the gases are more dissipative, the abovementioned behavior of $h_{horizontal}/h_{vertical}$ will be observed for gases already at comparatively lower Reynolds numbers. This behavior can be seen in Figure 7.23 at $Re_{\varphi}=8200$.

The influence of the heat transfer process, i.e. cooling or heating, on the heat transfer coefficient ratio is presented in Figure 7.24. Figure 7.24 shows that the behavior and the trend of $h_{horizontal}/h_{vertical}$ in cooling and in heating are exactly correspondent. As it is presented in Figure 7.24, heating increases the value of $h_{horizontal}/h_{vertical}$ for air while for water and engine oil cooling raises the quantity of $h_{horizontal}/h_{vertical}$. This is due to the effect of viscosity on heat transfer. For the heating process, the temperature of shell-side fluid near the tube walls is higher than the temperature of shell-side fluid in the bulk while for the cooling process this fact is reverse. It means that for air (and other gases) the viscosity near the tube walls is higher than the viscosity in the bulk when the process is heating. This is true for liquids like water and engine oil when the process is cooling. High viscosity near the wall increases the heat transfer resistance due to the augmented viscous sub-layer. On the other hand, when the viscosity of the shell-side fluid in the bulk drops due to heat transfer, the effect of baffle orientation with respect to increasing the mixing level will be more visible. Therefore, for gases the enhancement of $h_{horizontal}/h_{vertical}$ during heating is more apparent than the enhancement of $h_{horizontal}/h_{vertical}$ during cooling. For liquids, contrary to gases, the value of $h_{horizontal}/h_{vertical}$ during cooling is more than the value of $h_{horizontal}/h_{vertical}$ during heating. As the Reynolds number increases, the value of heat transfer ratio during cooling operation approaches to the value of heat transfer ratio during heating operation. This fact can be clearly observed in Figure 7.24 for two shell-side liquids, i.e. water and engine oil, at $Re_{\varphi} \geq 1.4 \times 10^4$. However, due to the higher dissipation rate in gases, the equality of cooling and heating on heat transfer ratio will happen at relatively higher Reynolds numbers.

Considering the effect of the heat transfer process on dynamic viscosity of the shell-side fluid, the distinction between the pressure drop ratio $\Delta p_{horizontal}/\Delta p_{vertical}$ in heating and cooling processes is justifiable. Figure 7.25 shows the pressure drop ratio as a function of Re_{φ} for different shell-side fluids during heating and cooling operation. Changing the baffle orientation from vertical to horizontal enhances the heat transfer rate and the pressure drop. This is mainly because of the rise of mixing level and specially the significant intensification of the leakage flows, in tube-baffle holes. Since the pressure drop depends on the dynamic viscosity μ, the effect of baffle orientation on pressure drop is significant for the shell-side fluid with lower viscosity.

For viscous fluids, changing the baffle orientation from vertical to horizontal increases the mixing level and intensifies the flow through the leakages. However, the increase in pressure drop due to the change in baffle orientation, i.e. from vertical to horizontal, for viscous fluids is not as significant as the corresponding pressure drop for low viscous fluids. This means that the influence of baffle orientation on pressure drop is more noteworthy at lower dynamic viscosity. Considering that the pressure drop is approximately proportional to square of the velocity, intensifying the leakage flow streams will increase the pressure drop significantly.

As it is shown in Figure 7.25, the pressure drop for horizontal baffle, i.e. $\Delta p_{horizontal}$, is about 40% more than the pressure drop for vertical baffle orientation, i.e. $\Delta p_{vertical}$, when the shell-side fluid is water or engine oil. For air, $\Delta p_{horizontal}$ is up to 270% more than $\Delta p_{vertical}$.

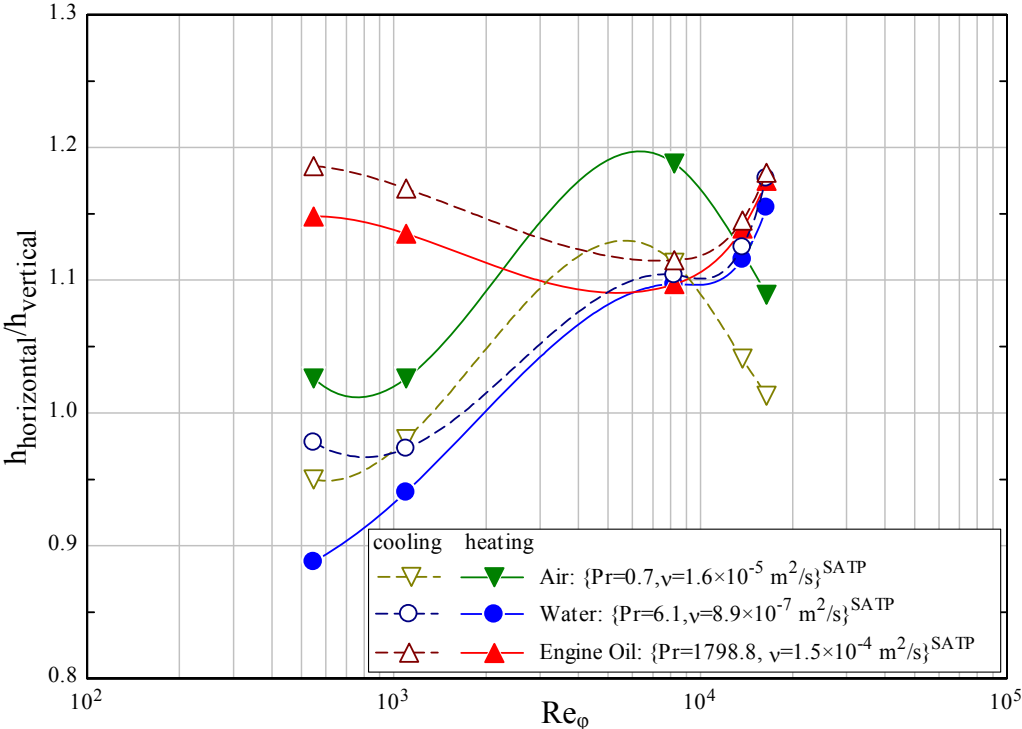Figure 7.24: Behaviour of heat transfer coefficient ratio, .i.e. $h_{horizontal}/h_{vertical}$, for different shell-side fluids in cooling and heating processes.
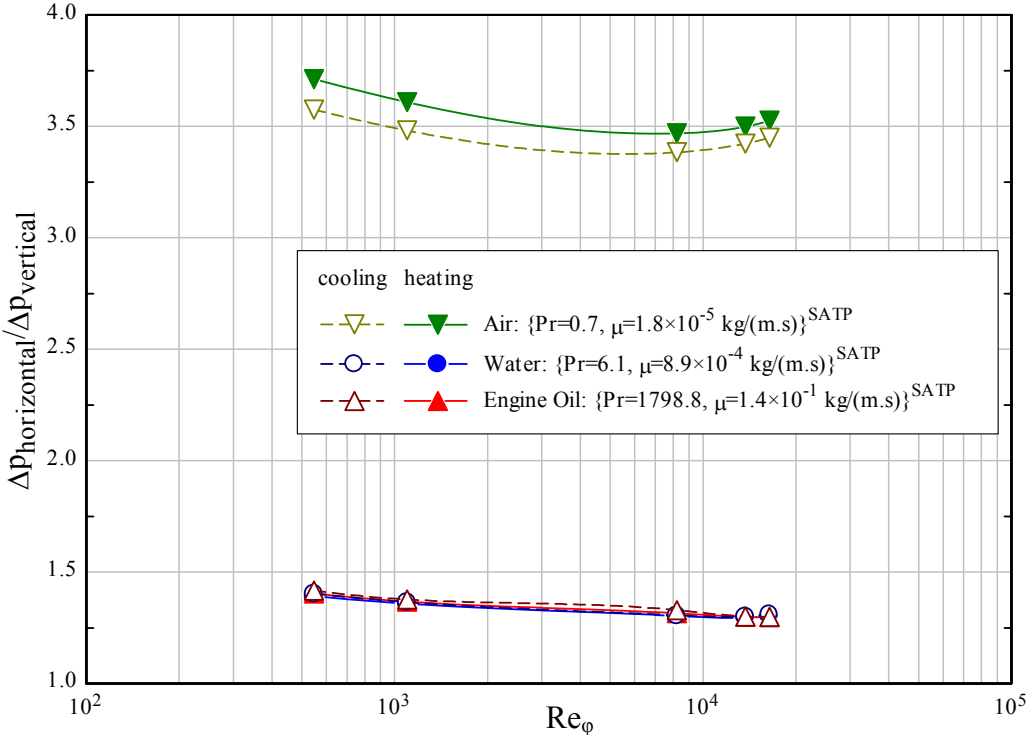
Figure 7.25: Pressure drop ratio $\Delta p_{horizontal}/\Delta p_{vertical}$ for different shell-side fluids in cooling and heating processes.

The very high value of pressure drop ratio $\Delta p_{horizontal}/\Delta p_{vertical}$ in gases is due to the high dissipation rate compared to the dissipation rate in liquids.

In summary, in shell and tube heat exchangers with horizontal baffle orientation the heat transfer rate is not considerably higher than the heat transfer rate in the shell and tube heat exchanger with vertical baffle orientation. But due to the intensification of leakage streams, the pressure drop in shell and tube heat exchangers with horizontal baffle orientation is significantly higher than the pressure drop in shell and tube heat exchangers with vertical baffle orientation. This effect is more noticeable for gases than for liquids, since the dissipation rates in gases are higher than the dissipation rates in liquids. Due to this fact, the gain factor for horizontal baffle orientation, $(\Gamma_{shell})_{hor.}$, is approximately 70% lower than the gain factor of vertical baffle orientation, $(\Gamma_{shell})_{ver.}$, for air as shell-side fluid. For water and engine oil, $(\Gamma_{shell})_{hor.}$ is about 20% lower than $(\Gamma_{shell})_{ver.}$ which represents the difference of performance factor in liquids and in gases. It is important to mention that the effect of heat transfer process, i.e. cooling or heating, on the performance factor is negligible. Moreover, at high Reynolds number, the effect of baffle orientation on the performance factor seems to be independent of physical properties when the shell-side fluid is liquid.

8. Conclusions and Outlook

In the present thesis, it could be shown that the orientation of baffles has a significant influence on the shell-side pressure drop and heat transfer of heat exchangers.

The effect of baffle orientation is not taken into account in common design methods (e.g. the VDI and Delaware methods). In fact, all the available investigations and methods are only based on one baffle orientation, namely horizontal. By introducing a performance factor (Φ), the effects of horizontally and vertically orientated baffles on pressure drop and heat transfer could be compared and assessed.

The tube-baffle leakages and bypass streams play an important role in the explanation of the performance factor of segmentally baffled shell and tube heat exchangers. The comparison of calculated results with and without leakage flows presents different behaviour especially in the end zones of the heat exchanger and underlines the importance of the consideration of tube-baffle leakage and bypass streams for the prediction of the performance factor of technical heat exchangers.

In a shell and tube heat exchanger without leakage flows, advantage of the horizontal baffle orientation over the vertical one has been found in the inlet and outlet zones for all investigated shell-side fluids (air, water, engine oil). The use of vertical baffle orientation seems to be more desirable in the intermediate baffle spacing zones particularly for low viscosity shell-side fluids. The same trend seems to apply for highly viscous shell-side fluids at low Reynolds numbers.

It is possible to introduce a semi-analytical model that explains the performance factor of the inlet zone of shell and tube heat exchangers with arbitrary baffle cut and without leakage flows. The semi-analytical model is presented as a function of the performance factor of water at a baffle cut of 24%, the working fluid preference and the baffle cut preference (as defined on pages 67 to 72). Two important geometrical parameters for the semi-analytical model of the performance factor are the normalized minimum shortcut distance (NMSD) and the normalized minimum shortcut distance ratio (NMSDR).

The concepts of NMSD and NMSDR are useful to explain the effect of baffle orientation on the performance of a real shell and tube heat exchanger with and without leakage streams. NMSDR shows that both heat transfer and pressure drop will be increased in a shell and tube heat exchanger (with or without leakage flows) when the baffle orientation is changed from horizontal to vertical.

For all shell-side fluids (air, water, engine oil) which have been considered in a heat exchanger with leakage flows, the vertical baffle orientation seems to be more advantageous than the horizontal orientation. It was found, that the horizontal baffle orientation produces up to 250% higher pressure drop compared to the pressure drop in vertical baffle orientation. The heat transfer coefficient is up to 20% higher than the heat transfer coefficient for vertical orientation. The local and overall behaviour of the performance factor for liquids as shell-side fluid is comparable and reaches a value of about 0.85 at high Reynolds numbers. With air as shell-side fluid a value of about 0.3 for the overall performance factor was obtained at high Reynolds numbers. The benefit of vertical baffle orientation over horizontal baffle orientation is more noticeable for gases since the dissipation rate in gases is much higher than in liquids.

For single segmental baffle cuts, the performance factor Φ facilitates the judgment between the horizontal and vertical baffle orientation. For horizontal baffle orientation $\angle(\overrightarrow{bf},\overrightarrow{nz}) \in \{0°,180°\}$, while for vertical baffle orientation $\angle(\overrightarrow{bf},\overrightarrow{nz}) \in \{90°,270°\}$. However, in a shell and tube heat exchanger with single segmental baffle cut, the baffle orientation could have any other arbitrary angle $\angle(\overrightarrow{bf},\overrightarrow{nz})$, i.e. inclined baffle orientation. Therefore, a general equation for the performance factor Φ has to be defined as

$$\Phi = \frac{(\Gamma_{shell})_{hor.}}{(\Gamma_{shell}) \text{ for baffle orientation equal to } \angle(\overrightarrow{bf},\overrightarrow{nz})} = \frac{(\Gamma_{shell})_{hor.}}{(\Gamma_{shell})_{\angle(\overrightarrow{bf},\overrightarrow{nz})}} \qquad (8.1)$$

This means that the behaviour of shell-side pressure drop and heat transfer coefficient have to be investigated for other inclined baffle orientations. Consequently, the semi-analytical model for the performance of the inlet zone of shell and tube heat exchangers without leakages has to be modified for other inclined baffle orientations. For this purpose, the performance factor of water at baffle cut 24% has to be remodelled for different inclined baffle orientations.

The semi-analytical model for the performance factor Φ is a function of baffle cut preference Θ_{BC}. However, Θ_{BC} is described as a function of NMSDR and is modelled by applying the data obtained from 3 baffle cuts, i.e. 20%, 24% and 30%. In order to have a better understanding of the effect of baffle cut on Φ, the function of Θ_{BC} has to be generalized for other baffle cuts, e.g. 10%, 15%, 35%, 40% and 45%. Moreover, since NMSDR is defined as $(NMSD)_{horizontal}/(NMSD)_{vertical}$, the baffle cut preference Θ_{BC} has to be remodelled as a function of $(NMSD)_{horizontal}/(NMSD)_{\angle(\overrightarrow{bf},\overrightarrow{nz})}$ for different baffle orientations.

In order to study the effects of nonisothermal conditions in the fluid on the performance factor, the abovementioned investigations have to be performed for the shell-side fluids with variable physical properties. This will verify the correction factor $(Pr_{WF,wall}/Pr_{WF,bulk})^{(1+1/7)}$ which is introduced in the semi-analytical model for the performance factor Φ.

This methodology should be applied for a complete shell and tube heat exchanger without subdividing the heat exchanger into the different discrete zones. In order to generalize the study of the performance factor Φ at the inlet zone for the complete heat exchanger, the shell and tube heat exchanger has to be considered as an ideal heat exchanger, i.e. without leakages. As a final outlook for the presented work, the effect of leakages on the performance factor Φ has to be investigated for

- different tube-baffle leakages and without baffle-shell leakages
- different baffle-shell leakages and without tube-baffle leakages
- different tube-baffle and baffle-shell leakages

In each stage of the investigation, the final results have to be compared with the results of an ideal shell and tube heat exchanger.

It is important to mention that all the aforesaid investigations and procedures are only for one tube layout, i.e. 30° triangular. It seems to be necessary to study the behaviour of the performance factor Φ for different tube layouts, e.g. rotated triangular 60°, square 90° and rotated square 45°.

References

[Achenbach, 1971]   E. Achenbach, On the Cross Flow through In-Line Tube Banks with Regard to the Effect of Surface Roughness, Wärme- und Stoffübertragung, Vol. 4, pp. 152-155, 1971.

[Anderson, 1995]   J. D. Anderson, Jr., "Computational Fluid Dynamics: The Basic with Applications", McGraw-Hill Book Company Inc., New York, 1995.

[ASME, 2004]   American Society of Mechanical Engineers, "2004 ASME Boiler and Pressure Vessel Code-An International Code, Section VIII, Division 3, Alternative Rules for Construction of High Pressure Vessels", New York, 2004.

[Babuska and Aziz, 1976]   I. Babuska and A. K. Aziz, On the Angle Condition in the Finite Element Method, SIAM Journal on Numerical Analysis, Vol. 13, No. 2, pp. 214-226, April 1976.

[Bačlič, 1990]   B. S. Bačlič, ϵ-NTU Analysis of Complicated Flow Arrangements, in "Compact Heat Exchangers: A Festschrift for Alexander L. London", Hemisphere Publishing, Washington DC, USA, pp. 31-91, 1999.

[Ball, 2000]   J. Ball, Construction Basic of Shell and Tube Heat Exchanger, API Heat Transfer, March 2000.

[Bell, 1960]   K. J. Bell, Exchanger Design Based on the Delaware Research Program, Petro/Chem. Engineer, pp. C-26–C-40c, October 1960.

[Bell, 1963]   K. J. Bell, Final Report of the Cooperative Research Program on Shell and Tube Heat Exchanger , Bulletin No. 5, University of Delaware Engineering Experiment Station, Newark, Delaware, November 1963.

[Bergelin, 1950]   O. P. Bergelin, A. P. Colburn and H. L. Hull, Heat Transfer and Pressure Drop During Viscous Flow Across Unbaffled Tube Banks, Bulletin No. 2, University of Delaware Engineering Experiment Station, Newark, Delaware, June 1950.

[Bergelin, 1958]   O. P. Bergelin, M. D. Leighton, W. L. Lafferty and R. L. Pigford, Heat Transfer and Pressure Drop During Viscous and Turbulent Flow Across Baffled and Unbaffled Tube Banks, Bulletin No. 4, University of Delaware Engineering Experiment Station, Newark, Delaware, November 1958.

[Boffetta and Romano, 2002]   G. Boffetta and G. P. Romano, Structure Functions and Energy Dissipation Dependence on Reynolds Number, Physics of Fluids, Vol. 14, Issue 10, pp. 3453-3458, October 2002.

[Bott, 1995]   T. R. Bott, "Fouling of Heat Exchangers", Elsevier Science & Technology Books, 1995.

[Boucher and Lapple, 1948]   D. F. Boucher and C. E. Lapple, Pressure Drop Across Tube Banks, Chemical Engineering Progress, Vol. 44, pp. 117-134, 1948.

[Bradshaw, 1971]   P. Bradshaw, "An Introduction to Turbulence and its Measurement", Pergamon Press, 1971.

[Bressler, 1958]   R. Bressler, Die Wärmeübertragung einzelner Rohrreihen in quer angeströmten Rohrbündeln mit kleinen Versetzungsverhältnissen, Forschung im Ingenieurwesen, Vol. 24, No. 3, pp. 90-103, Mai 1958.

[Chilton and Genereaux, 1933] T. H. Chilton and R. P. Genereaux, Pressure Drop Across Tube Banks, Transactions of the American Institute of Chemical Engineers, Vol. 29, pp. 161-173, 1933.

[Colburn, 1933]   A. P. Colburn, A Method of Correlating Forced Convection Heat Transfer Data and Comparison with Fluid Friction, Trans. AIChE, Vol. 29, pp. 174-210, 1933.

[Colburn, 1942]   A. P. Colburn, Heat Transfer by Natural and Forced Convection, Engineering Bulletin, Purdue University, Research Series No. 84, Volume 26, pp. 47-50, 1942.

[Deng et al., 2009]   J. Deng, X.-M. Shao, X. Fu and Y. Zheng, Evaluation of the Viscous Heating Induced Jam Fault of Valve Spool by Fluid–Structure Coupled Simulations, Energy Conversion and Management, Vol. 50, Issue 4, pp. 947-954, April 2009.

[Donohue, 1949]   D. A. Donohue, Heat Transfer and Pressure Drop in Heat Exchangers, Industrial and Engineering Chemistry, Vol. 41, No. 11, pp. 2499-2511, November 1949.

[Driedger, 1996]   W. C. Driedger, Controlling Shell and Tube Exchangers, Hydrocarbon Processing, Vol. 7, Issue 3, pp. 111-122, March 1996.

[Eckert, 1972]   E. R. G. Eckert, "Analysis of Heat and Mass Transfer", McGraw-Hill, New York, 1972.

[Emerson, 1963]   W. H. Emerson, Shell-Side Pressure Drop and Heat Transfer with Turbulent Flow in Segmentally Baffled Shell and Tube Heat Exchangers, International Journal of Heat and Mass Transfer, Vol. 6, Issue 8, pp. 649-668, August 1963.

[Ferziger, 2002]   J. H. Ferziger and M. Perić, "Computational Methods for Fluid Dynamics", Springer-Verlag, Berlin-Heidelberg, 2002.

[Fluent, 2008]   FLUENT Incorporated, "Fluent 6.3, User's Guide", Fluent Incorporated, 2008.

[Friedlander and Topper, 1961] S. K. Friedlander and L. Topper, "In Turbulence, Classic Papers on Statistical Theory", Interscience, New York, 1961.

[Gaddis and Gnielinski, 1977] E. S. Gaddis and V. Gnielinski, Pressure Drop on the Shell Side of Shell and Tube Heat Exchangers with Segmental Baffles, Chemical Engineering and Processing, Vol. 36, No. 2, pp. 149-159, 1977.

[Gaddis and Gnielinski, 1978] V. Gnielinski and E. S. Gaddis, Berechnung des mittleren Wärmeübergangskoeffizienten im Außenraum von Rohrbündelwärmeaustauschern mit Segmentumlenkblechen, Verfahrenstechnik, Vol. 12, No. 4, pp. 211-217, 1978.

[Gaddis and Gnielinski, 1983] E. S. Gaddis and V. Gnielinski, Druckverlust in quer durchströmten Rohrbündeln, Verfahrenstechnik, Vol. 17, No. 7, pp. 410-418, 1983.

[Gambit, 2007]   FLUENT Incorporated, "Gambit 2.4, User's Guide", Fluent Incorporated, May 2007.

[Gardner, 1945]   K. A. Gardner, Efficiency of Extended Surface, ASME Journal of Heat Transfer, Vol. 67, No. 8, pp. 621-631, 1945.

[Gary and Handwerk, 2001] J. H. Gary and G. E. Handwerk, "Petroleum Refining Technology and Economics", Marcel Dekker Inc., 4th Edition, 2001.

[Gibson and Launder, 1978] M. M. Gibson and B. E. Launder, Ground Effects on Pressure Fluctuations in the Atmospheric Boundary Layer, Journal of Fluid Mechanics, Vol. 86, Issue 3, pp. 491-511, June 1978.

[Gnielinski, 1978]   V. Gnielinski, Gleichungen zur Berechnung des Wärmeübergangs in querdurchströmten einzelnen Rohrreihen und Rohrbündeln, Forschung im Ingenieurwesen, Vol. 44, No. 1, pp. 15-25, Januar 1978.

[Görtler, 1975]   H. Görtler, "Dimensionsanalyse: Theorie der physikalischen Dimensionen mit Anwendungen", Springer-Verlag, Berlin, 1975.

[Grimison, 1937]   E. D. Grimison, Correlation and Utilization of New Data of Flow Resistance and Heat Transfer for Cross-Flow of Gases over Tube Banks, ASME Journal of Heat Transfer, Vol. 59, No. 7, pp. 583-594, 1937.

[Gunter and Shaw, 1945] A. Y. Gunter and W. A. Shaw, A General Correlation of Friction Factor for Various Types of Surfaces in Cross Flow, Transactions of the American Society of Mechanical Engineers, Vo. 67, pp. 643-660, 1945.

[Hesselgreaves, 2001]   J. E. Hesselgreaves, "Compact Heat Exchangers: Selection, Design and Operation", Elsevier Science & Technology Books, 2001.

[Hewitt, 1992]   G. F. Hewitt, "Handbook of Heat Exchanger Design", Begell House Inc., New York, 1992.

[Hinze, 1959]   J. O. Hinze, "Turbulence: An Introduction to its Mechanism and Theory", McGraw-Hill Book Company Inc., New York, 1959.

[Huge, 1937]   E. C. Huge, Experimental Investigation of Effects of Equipment Size on Convection Heat Transfer and Flow Resistance in Cross Flow of Gases Over Tube Banks, Transactions of the American Society of Mechanical Engineers, Vol. 59, pp. 573-581, 1937.

[Incropera, 2006]   F. P. Incropera and D. P. Dewitt, "Introduction to Heat Transfer", John Wiley & Sons, 5th Edition, 2006.

[Jakob, 1938]   M. Jakob, Flow Resistance in Cross Flow of Gases Over Tube Banks: Contribution to a Discussion of Papers by Messrs Pierson, Huge and Grimison, Transactions of the American Society of Mechanical Engineers, Vol. 60, pp. 384-386, 1938.

[Jaluria and Torrance, 1986] Y. Jaluria and K. E. Torrance," Computational Heat Transfer", Hemisphere Publishing Corporation, New York, 1986.

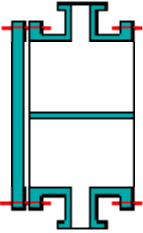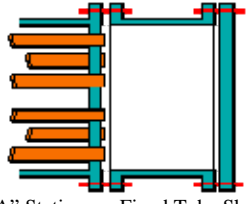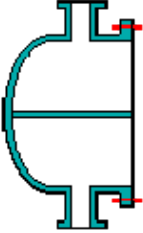| [Jin and Barza, 1993]	G. Jin and M. Braza, A Nonreflecting Outlet Boundary Condition for Incompressible Unsteady Navier-Stokes Calculations, Journal of Computational Physics, Vol. 107, Issue 2, pp 239-253, August 1993.
[Kader, 1981]	B. Kader, Temperature and Concentration Profiles in Fully Turbulent Boundary Layers, International Journal of Heat and Mass Transfer, Vol. 24, Issue 9, pp. 1541-1544, September 1981.
[Kakaç, 1981]	S. Kakaç, A. E. Bergles, and F. Mayinger (Editors), "Heat Exchangers: Thermal-Hydraulic Fundamentals and Design", Hemisphere Publishing, Washington, USA, 1981.
[Kara and Güraras, 2004]	Y. A. Kara and Ö. Güraras, A Computer Program for Designing of Shell and Tube Heat Exchangers, Applied Thermal Engineering, Vol. 24, Issue 13, pp. 1797-1805, September 2004.
[Kays and London, 1984]	W. M. Kays and A. L. London, "Compact Heat Exchangers", McGraw-Hill, 3rd Edition, 1984.
[Kays, 1954]	W. M. Kays, A. L. London and R. K. Lo, Heat Transfer and Friction Characteristics for Gas flow Normal to Tube Banks, Trans. ASME, Vol. 76, pp. 387-396, 1954.
[Kern, 1965]	D. Q. Kern, "Process Heat Transfer", McGraw-Hill, New York, 1965.
[Kopp, 1947]	S. Kopp, H. R. Sennstorm and A. Y. Gunter, A Study of Flow Patterns in Baffled Heat Exchangers, ASME Paper 47-A-103, 1947.
[Kottke, 1998]	V. Kottke and H. Li, Effect of Baffle Spacing on Pressure Drop and Local Heat Transfer in Shell and Tube Heat Exchanger for Staggered Tube Arrangement, International Journal of Heat and Mass Transfer, Vol. 41, Issue 10, pp. 1303-1311, May 1998.
[Kraus and Aziz, 2001]	A. D. Kraus, A. Aziz and J. Welty, "Extended Surface Heat Transfer", John Wiley & Sons, 1st Edition, New York, USA, 2001.
[Křížek, 1992]	M. Křížek, On the Maximum Angle Condition for Linear Tetrahedral Elements, SIAM Journal on Numerical Analysis, Vol. 29, No. 1, pp. 513-520, February 1992.
[Kuppan, 2000]	T. Kuppan, "Heat Exchanger Design Handbook", Marcel Dekker, Inc., Madras-India, 2000.
[Kutateladze, 1964]	S. S. Kutateladze and A. I. Leont'ev, "Turbulent Boundary Layers in Compressible Gases", Edward Arnold (Publishers) Ltd., London, 1964.
[Launder and Spalding, 1972]	B. E. Launder and D. B. Spalding, "Lectures in Mathematical Models of Turbulence", Academic Press, London, England, 1972.
[Launder and Spalding, 1974]	B. E. Launder and D. B. Spalding, The Numerical Computation of Turbulent Flows, Computer Methods in Applied Mechanics and Engineering, Vol. 3, Issue 2, pp. 269-289, March 1974.
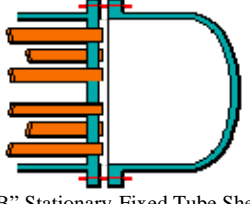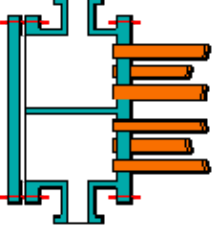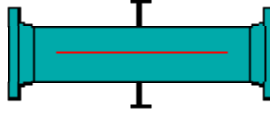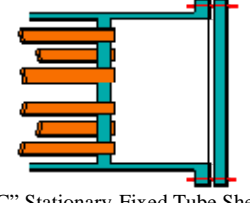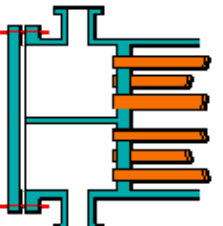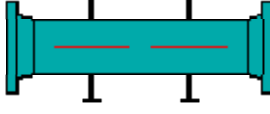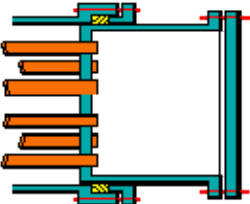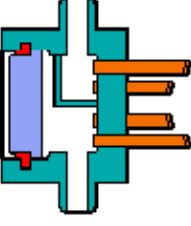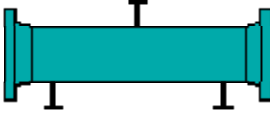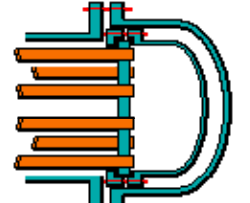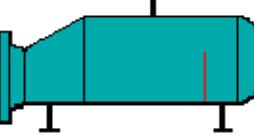
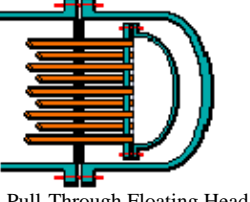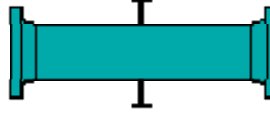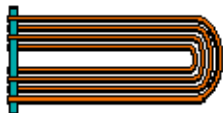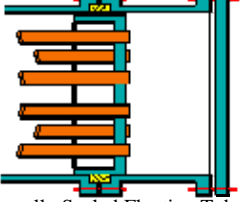| [Launder et al., 1975] | B. E. Launder, G. J. Reece, and W. Rodi, Progress in the Development of a Reynolds-Stress Turbulence Closure, Journal of Fluid Mechanics, Vol. 68, Issue 3, pp. 537-566, April 1975. |
[Launder, 1989]	B. E. Launder, Second-Moment Closure: Present... and Future?, International Journal of Heat and Fluid Flow, Vol. 10, Issue 4, pp. 282-300, December 1989.
[Lienhard, 2002]	J. H. Lienhard IV and J. H. Lienhard V, "A Heat Transfer Textbook", Phlogiston Press, 3rd Edition, Massachusetts, USA, 2002.
[Luben Cabezas-Gómez, 2007]	L. Cabezas-Gómez, H. A. Navarro and J. M. Saiz-Jabardo, Thermal Performance of Multipass Parallel and Counter-Cross-Flow Heat Exchangers, ASME Journal of Heat Transfer, Vol. 129, Issue 3, pp. 282-290, March 2007.
[Martin, 2002]	H. Martin, The generalized Lévêque equation and its practical use for the prediction of heat and mass transfer rates from pressure drop, Chemical Engineering Science, Vol. 57, Issue 16, pp. 3217-3223, August 2002.
[McAdams, 1942]	W. H. McAdams, "Heat Transmission", McGraw-Hill, 2nd Edition, New York, 1942.
[McCabe, 2005]	W. L. McCabe, J. C. Smith and P. Harriott, "Unit Operations of Chemical Engineering", McGraw-Hill Education, New York, 7th Edition, 2005.
[Menter, 1994]	F. R. Menter, Two-Equation Eddy-Viscosity Turbulence Models for Engineering Applications, AIAA Journal, Vol. 32, Issue 8, pp. 1598-1605, August 1994.
[Muniz et al., 2008]	A. R. Muniz, A. R. Secchi and N. S. M. Cardozo, High-Order Finite Volume method for Solving Viscoelastic Fluid Flows, Brazilian Journal of Chemical Engineering, Vol. 25, No. 1, pp. 153-166, January-March 2008.
[Naterer, 2003]	G. F. Naterer, "Heat Transfer in Single and Multiphase Systems", CRC Press LLC, 2003.
[Nellis, 2003]	G. F. Nellis, Effectiveness-NTU Relations for Heat Exchangers With Streams Having Significant Kinetic Energy Variation, ASME Journal of Heat Transfer, Vol. 125, Issue 2, pp. 377-387, 2003.
[Ol'shanskii, 2000]	M. A. Ol'shanskii and V. M. Staroverov, On simulation of outflow boundary conditions in finite difference calculations for incompressible fluid, International Journal for Numerical Methods in Fluids, Vol. 33, Issue 4, pp. 499-534, June 2000.
[Oosthuizen, 1999]	P. H. Oosthuizen and D. Naylor, "Introduction to Convective Heat Transfer Analysis", McGraw-Hill, 1999.
[Özişik, 1988]	M. N. Özişik, "Heat Transfer: A Basic Approach", McGraw-Hill International Editions, New York, 3rd Edition, 1988.
[Palen and Taborek, 1969]	J. W. Palen and J. Taborek, Solution of Shell Side Flow Pressure Drop and Heat Transfer by Stream Analysis Method, Chem. Eng. Prog. Symp. Ser., Vol. 65, No. 92, 1969.

[Palen, 1986]	J. W. Palen, "Heat Exchanger Sourcebook", Hemisphere Publication Corporation, 1986.
[Perry and Chilton, 1999]	R. H. Perry, C. H. Chilton and D. W Green, "Perry's Chemical Engineers' Handbook", McGraw-Hill, 7th Edition, 1999.
[Pierson, 1937]	O. L. Pierson, Experimental Investigation of the Influence of Tube Arrangement on Convection Heat Transfer and Flow Resistance in Cross Flow of Gases Over Tube Banks, Transactions of the American Society of Mechanical Engineers, Vol. 59, pp. 563-572, 1937.
[Pitts, 1998]	D. R. Pitts and L. E. Sissom, "Theory and Problems of Heat Transfer", Schaum's Outline Series, McGraw-Hill, 2nd Edition, 1998.
[Poddar and Polley, 2000]	T. K. Poddar and G. T. Polley, Optimize Shell and Tube Heat Exchanger Design, Chemical Engineering Progress, Vol. 96, No. 9, September 2000.
[Pope, 2000]	S. B. Pope, "Turbulent Flows", Cambridge University Press, Cambridge, 2000.
[Rohsenow, 1998]	W. M. Rohsenow, J. P. Hartnett and Y. I. Cho, "Handbook of Heat Transfer", McGraw-Hill, 3rd Edition, 1998.
[Ruppertt, 1995]	J. Ruppertt, A Delaunay Refinement Algorithm for Quality 2-Dimensional Mesh Generation, Vol. 18, Issue 3, pp. 548-585, May 1995.
[Russell, 2002]	M. B. Russell, P. N. Surendran and S. D. Probert, Quantifying Acceptable Mesh Dependencies for Computational Investigations of Airflows within Rooms, Applied Energy Vol. 72, Issue 1, pp. 409-425, May 2002.
[Saunders, 1988]	E. A. D. Saunders, "Heat Exchangers: Selection, Design and Constructions", John Wiley &Sons, Inc, New York, 1988.
[Schlichting, 1979]	H. Schlichting, "Boundary-Layer Theory", McGraw-Hill, 7th Edition, 1979.
[Sekulić, 1999]	D. P. Sekulić, R. K. Shah, and A. Pignotti, A Review of Solution Methods for Determining Effectiveness–NTU Relationships for Heat Exchangers with Complex Flow Arrangements, Applied Mechanics Review, Vol. 52, No. 3, pp. 97–117, 1999.
[Serth, 2007]	R. W. Serth, "Process Heat Transfer: Principles and Applications", Elsevier Science & Technology Books, April 2007.
[Shah, 2003]	R. K. Shah and D. P. Sekulic, "Fundamentals of Heat Exchanger Design", John Wiley & Sons, Inc., Hoboken, USA, 2003.
[Shames, 1982]	I. H. Shames, "Mechanics of Fluids", McGraw-Hill, 2nd Edition, 1982.
[Shewchuk, 2005]	J. R. Shewchuk, "Lecture Notes on Geometric Robustness", Department of Electrical Engineering and Computer Sciences, University of California at Berkeley, USA, May 2005.

[Shih et al., 1995]   T.-H. Shih, W. W. Liou, A. Shabbir, Z. Yang and J. Zhu, A New k-ε Eddy-Viscosity Model for High Reynolds Number Turbulent Flows-Model Development and Validation, Computers Fluids, Vol. 24, Issue 3, pp. 227-238, March 1995.

[Shyy, 1994]   W. Shyy, "Computational Modeling for Fluid Flow and Interfacial Transport", Elsevier Science Publishers B.V., Amsterdam, 1994.

[Taborek, 1979]   J. Taborek, Evolution of Heat Exchanger Design Techniques, Heat Transfer Engineering, Vol. 1, No. 1, 1979.

[Taylor, 1935]   G. I. Taylor, Statistical Theory of Turbulence, Proceeding of the Royal Society of London, Vol. A151, pp. 421-478, London, 1935.

[TEMA, 1999]   J. Harrison (Editor), "Standards of The Tubular Exchanger Manufacturers Association", Tubular Exchanger Manufacturers Association, Inc., 8th Edition, 1999.

[Tennekes, 1972]   H. Tennekes and J. L. Lumley, "A First Course in Turbulence", The MIT Press, Massachusetts, 1972.

[Ter Linden, 1939]   A. J. Ter Linden, Die Strömungswiderstand eines Rohrbündels, Die Wärme, Vol. 62, pp. 319-323, 1939.

[Thompson, 1985]   J. F. Thompson, Z. U. A. Warsi and C. W. Mastin, "Numerical Grid Generation: Foundations and Applications", Elsevier Science Publishers, 1985.

[Tinker, 1947]   T. Tinker, Shell Side Heat Transfer Characteristics of Segmentally Baffled Shell and Tube Heat Exchangers, Annual ASME Meeting, 1947.

[Tinker, 1951]   T. Tinker, Shell Side Characteristics of Shell and Tube Heat Exchanger, Parts I-III, General Discussion of Heat Transfer, Institution of Mechanical Engineers, London and ASME, pp. 84-110, New York, 1951.

[Tinker, 1958]   T. Tinker, Shell-Side Characteristics of Shell and Tube Heat Exchanger, Journal of Heat Transfer, Vol. 80, pp. 36-52, 1958.

[Touloukian, 1972]   Y. S. Touloukian and C. Y. Ho, Editors, "Thermophysical Properties of Matter", Vol.1-13, Plenum Press, New York, 1972.

[Utamura, 2008]   M. Utamura, K. Nikitin, and Y. Kato, A Generalised Mean Temperature Difference Method for Thermal Design of Heat Exchangers, International Journal of Nuclear Energy Science and Technology (IJNEST), Vol. 4, Issue 1, pp. 11-31, 2008.

[VDI, 2006]   Verein deutsche Ingenieure, Her., "VDI Wärmeatlas", Springer-Verlag, Berlin-Heidelberg, 2006.

[Wesseling, 2001]   P. Wesseling, "Principles of Computational Fluid Dynamics", Springer-Verlag, Berlin-Heidelberg, 2001.

[Wilcox, 1998]   D. C. Wilcox, "Turbulence Modelling for CFD", DCW Industries, Inc., 2nd Edition, 1998.

[Wolverine, 2001]   Wolverine Tube, Inc., Wolverine Tube Heat Transfer Data Book, Wolverine Tube, Inc Research and Development Team, 2001.

[Yakhot and Orszag, 1986]   V. Yakhot and S. A. Orszag, Renormalization Group Analysis of Turbulence: I. Basic Theory, Journal of Scientific Computing, Vol. 1, No. 1, pp. 1-51, March 1986.

[Zhang et al., 2009]   T. Zhang, L. Jia, Z. Wang, C. Li and Y. Jaluria, Fluid Heat Transfer Characteristics with Viscous Heating in the Slip Flow Region, EPL Journal, Vol. 85, No. 4, pp. 40006(p1)-40006(p6), February 2009.

[Zlokarnik, 2002]   M. Zlokarnik, "Scale-up in Chemical Engineering", Wiley-VCH Verlag, 2002.

[Žukauskas, 1972]   A. A. Žukauskas, Heat Transfer from Tubes in Cross Flow, Advanced Heat Transfer, Vol. 8, pp. 93-160, 1972.

[Zwillinger, 2003]   D. Zwillinger, "Standard Mathematical Tables and Formulae", CRC Press LLC, 2003.

Appendix A: TEMA Designation System

Front End Stationary Head		Shell Type		Rear End Stationary Head	
A	Channel and Removable Cover	E	One Pass Shell	L	"A" Stationary-Fixed Tube Sheet
B	Bonnet (Integral Cover)	F	Two Pass Shell with Longitudinal Baffle	M	"B" Stationary-Fixed Tube Sheet
C	Channel Integral with Tube Sheet and Removable Cover Shown: Removable Tube Bundle only	G	Split Flow	N	"C" Stationary-Fixed Tube Sheet
N	Channel Integral with Tube Sheet and Removable Cover Shown: Fixed Tube sheet only	H	Double Split Flow	P	Outside Packed Floating Head
		J	Divided Flow	S	Floating Head with Backing Device
D	Special High Pressure Closure	K	Kettle Type Reboiler	T	Pull-Through Floating Head
		X	Cross Flow	U	U Tube Bundle
				W	Externally Sealed Floating Tubesheet

Appendix A: TEMA designation system. From Standards of Tubular Exchanger Manufacturers Association, 8th Edition, 1999.

Appendix B: HTRI Bundle Specification

BUNDLE SPECIFICATION

652 TUBES 5/8" X 30 X 13/16"

BAFFLE THICKNESS 1/4 (0.250)

DS	Shell Inside Diameter	23.265	In	LBH	Baffle Cut Height to DS	5.441	In
DB	Baffle Outside Diameter	23.0469	In	BCA	Baffle Cut Out (115.6°)	2.0197	Radian
DOTL	Diameter Over Outer Tube Limit	22.8588	In	PT	Tube Pitch	0.8125	In
LTPP	Tube Partition Width	0.50	In	SMT	Minimum Space Between Tubes	0.1875	In
LTRP	Tube Row Distance Perpendicular			LB1	Baffle Spacing Entry	10.4560	In
	To Flow Direction	0.40625	In	LBCC	Baffle Spacing Central	9.8125	In
LTRF	Tube Row Distance in Flow			LB2	Baffle Spacing Exit	10.4560	In
	Direction	0.70364	In	LTI	Tube Length Between Tube Sheets	89.625	In

DATE: FEBRUARY 1964	HTRI DATA BOOK 1 SHELL AND TUBE – SEGMENTAL BAFFLES ONE SHELL PASS	UNIT CODE NO: 023 ORIGINAL REFERENCE: WESTERN SUPPLY CO BUNDLE 24 – 96 DWG. E6720-CG

154.178 mm

154.178 mm

TEMA type	AEP	
Shell diameter	591.000	mm
Outer tube limit	580.174	mm
Height under inlet nozzle	21.479	mm
Height under outlet nozzle	21.479	mm
Tube diameter	15.867	mm
Tube pitch	20.637	mm
Tube layout angle	30	
Number of tubes (calculated)	654	
Number of tie rods	6	
Number of seal strip pairs	0	
Number of passes	2	
Horizontal passlane width	15.875	mm
Vertical passlane width	15.875	mm
Baffle cut % diameter	23.4	

TUBEPASS DETAILS

Pass	Rows	Tubes
1	15	330
2	15	330

SYMBOL LEGEND

○	Tube
◎	Tie rod
⊘	Impingement rod
⊗	Dummy tube
●	Seal rod
▭	Seal strip/Skid bar

2 / 1

Appendix C: Derivation of Sensibility Analysis Equation

For a shell and tube heat exchanger with a constant tube wall temperature, the energy balance on the shell-side fluid is:

$$\dot{M}\overline{c_p}(T_{out}-T_{in})=h_{shell}A_H\frac{(T_{wall}-T_{in})-(T_{wall}-T_{out})}{\ln\left(\frac{T_{wall}-T_{in}}{T_{wall}-T_{out}}\right)} \tag{C.1}$$

Equation (C.1) can be rewritten as:

$$\frac{\rho_{in}u_{in}D_n}{\mu_{in}}\frac{\overline{\mu c_p}}{\overline{k_f}}\left(\frac{\mu_{in}}{\overline{\mu}}\right)\left(\frac{\ell_H}{D_n}\right)\left(\frac{A_{in}}{A_H}\right)\ln\left(\frac{T_{wall}-T_{in}}{T_{wall}-T_{out}}\right)=\frac{h_{shell}\ell_H}{\overline{k_f}} \tag{C.2}$$

T_{wall} is the outside tube wall temperature. If the temperature variation along the tube walls is not significant, T_{wall} can also be considered as the average tube wall temperature. The subscripts "in" and "out" refer to the values and properties at inlet and outlet, respectively. In Equations (C.1) and (C.2), ℓ_H is the heat transfer characteristic length of the heat exchanger and D_n is the inside diameter of the inlet nozzle. $\overline{c_p}$, $\overline{\mu}$ and $\overline{k_f}$ are the average values of shell-side heat capacity, dynamic viscosity and thermal conductivity, respectively, and are calculated at average bulk temperature. The dimensionless parameter γ is introduced as:

$$\gamma=\left(\frac{\mu_{in}}{\overline{\mu}}\right)\left(\frac{\ell_H}{D_n}\right)\left(\frac{A_{in}}{A_H}\right) \tag{C.3}$$

Applying Equation (C.3) in (C.2) and using the dimensionless numbers results in:

$$\gamma Re_{inlet}\overline{Pr}\ln\left(\frac{\theta-1}{\theta-\theta_o}\right)=Nu \tag{C.4}$$

In Equation (C.4), θ and θ_o are:

$$\theta=\frac{T_{wall}}{T_{in}} \quad , \quad \theta_o=\frac{T_{out}}{T_{in}} \tag{C.5}$$

The dimensionless outlet temperature θ_o results in:

$$\theta_o=\theta-(\theta-1)\exp\left(-\frac{Nu}{\gamma Re_{inlet}\overline{Pr}}\right) \tag{C.6}$$

The Nusselt number is directly proportional to the Reynolds number. At zero velocity where the forced convection Reynolds number is equal to zero, the Nusselt number has a certain value greater than zero. If Nu_0 defines the Nusselt number at zero velocity and $f(Re_{inlet}, \overline{Pr})$ represents the function defining the proportionality of the Nusselt number to the Reynolds and Prandtl numbers, one obtains:

$$\theta_o=\theta-(\theta-1)\exp\left(-\frac{Nu_0+f(Re_{inlet}, \overline{Pr})}{\gamma Re_{inlet}\overline{Pr}}\right) \tag{C.7}$$

As it is described before, any average shell-side physical property $\overline{\eta}$ is calculated as an averaging integral:

$$\overline{\eta}=\frac{1}{T_{out}-T_{in}} \int_{T_{in}}^{T_{out}} \eta dT \tag{C.8}$$

The average physical property represented in Equation (C.8) can be approximated by considering T_{out} equal to T_{wall}. This is true for heat exchangers with high specific heat transfer area such as compact heat exchangers even if the mass flow rate of the shell-side fluid is considerable. Moreover, for shell-side fluids with less dependency on temperature, this approximation is legitimate, too. The estimation of average physical properties facilitates the analysis of the sensibility of Nusselt number with outlet temperature.

When the inlet velocity goes to zero, the residence time of the shell-side fluid tends to infinity and therefore, the outlet temperature of the shell-side fluid approaches the tube wall temperature. This is mathematically understandable by applying Re_{inlet} equal to zero in Equation (C.7). It is important to define the minimum value of Nusselt number Nu_0, which occurs for Re_{inlet} equal to zero.

Alternatively, at very high Reynolds number, the shell-side fluid residence time tends to zero and hence, the outlet temperature of the shell-side fluid tends to the inlet temperature. This is helpful to determine the order of magnitude of $f(Re_{inlet}, \overline{Pr})$ with respect to Reynolds number. In summary:

$$\lim_{Re_{inlet}\to 0} \theta_o = \lim_{Re_{inlet}\to 0} \left\{ \theta-(\theta-1)\exp\left(-\frac{Nu_0+f(Re_{inlet}, \overline{Pr})}{\gamma Re_{inlet}\overline{Pr}} \right) \right\}=\theta \tag{C.9}$$

$$\lim_{Re_{inlet}\to +\infty} \theta_o = \lim_{Re_{inlet}\to +\infty} \left\{ \theta-(\theta-1)\exp\left(-\frac{Nu_0+f(Re_{inlet}, \overline{Pr})}{\gamma Re_{inlet}\overline{Pr}} \right) \right\}=1 \tag{C.10}$$

Considering the conceptual behavior described in the previous paragraphs and Equations (C.9) and (C.10), it is understandable that:

$$\lim_{Re_{inlet}\to +\infty} \left\{ \exp\left(-\frac{Nu_0+f(Re_{inlet}, \overline{Pr})}{\gamma Re_{inlet}\overline{Pr}} \right) \right\}=1 \tag{C.11}$$

This means that the order of magnitude of $f(Re_{inlet}, \overline{Pr})$ with respect to the Reynolds number has to be less than one. In addition, the value of the Nusselt number increases by increasing the forced Reynolds number, therefore:

$$\frac{dNu}{dRe_{inlet}} > 0 \tag{C.12}$$

It also means that the order of magnitude; $\overline{\overline{O}}$, of $f(Re_{inlet}, \overline{Pr})$ with respect to the Reynolds number has to be greater than zero. Finally the mathematical properties of $f(Re_{inlet}, \overline{Pr})$ are:

$$f(Re_{inlet}, \overline{Pr})\big|_{Re_{inlet}=0}=f(0, \overline{Pr})=0 \tag{C.13}$$

A6

If the order of magnitude is presented by $\bar{\bar{O}}$, it results:

$$0 < \bar{\bar{O}}\{f(\text{Re}_{\text{inlet}}, \overline{\text{Pr}}), \text{Re}_{\text{inlet}}\} < 1 \qquad (\text{C}.14)$$

The correlations reported in the Delaware method and in the VDI handbook fulfill condition (C.14). According to the VDI method, the value of Nu_0 is:

$$\text{Nu}_0 = 0.3 f_W f_A \qquad (\text{C}.15)$$

Based on the specific Reynolds number Re_φ, $f(\text{Re}_{\text{inlet}}, \overline{\text{Pr}})$ is defined as:

$$f(\text{Re}_{\text{inlet}}, \overline{\text{Pr}}) = f_W f_A \left\{ 0.4409 \text{Re}_\varphi \overline{\text{Pr}}^{2/3} + \frac{0.00137 \text{Re}_\varphi^{1.8} \overline{\text{Pr}}^2}{\left[2.443\left(\overline{\text{Pr}}^{2/3}-1\right)+\text{Re}_\varphi^{0.1}\right]^2} \right\}^{1/2} \qquad (\text{C}.16)$$

Therefore, the order of magnitude of $f(\text{Re}_{\text{inlet}}, \overline{\text{Pr}})$ with respect to the Reynolds number according to the VDI method is between 0.5 and 0.8.

An analysis based on the Delaware method shows that the order of magnitude of $f(\text{Re}_{\text{inlet}}, \overline{\text{Pr}})$ with respect to the Reynolds number lies between 0.333 and 0.612.

Therefore, it is sense full to consider the utmost order of magnitude of $f(\text{Re}_{\text{inlet}}, \overline{\text{Pr}})$ with respect to the Reynolds number equal to 0.8.

$$\text{Max}\, \bar{\bar{O}}\{f(\text{Re}_{\text{inlet}}, \overline{\text{Pr}}), \text{Re}_{\text{inlet}}\} = 0.8 \qquad (\text{C}.17)$$

Knowing the properties of the function that describes the shell-side Nusselt number, it is straightforward to evaluate the sensibility of the Nusselt number (and also the pressure drop) with the outlet temperature of the shell-side fluid.

Differentiating Equation (C.6) yields:

$$1 = (\theta-1)\frac{\dfrac{d\text{Nu}}{d\theta_o}\gamma\text{Re}_{\text{inlet}}\overline{\text{Pr}} - \text{Nu}\dfrac{d(\gamma\text{Re}_{\text{inlet}}\overline{\text{Pr}})}{d\theta_o}}{\left(\gamma\text{Re}_{\text{inlet}}\overline{\text{Pr}}\right)^2}\exp\left(-\frac{\text{Nu}}{\gamma\text{Re}_{\text{inlet}}\overline{\text{Pr}}}\right) \qquad (\text{C}.18)$$

On the other hand:

$$\frac{d(\gamma\text{Re}_{\text{inlet}}\overline{\text{Pr}})/d\theta_o}{\gamma\text{Re}_{\text{inlet}}\overline{\text{Pr}}} = \frac{d(\overline{c_p}/\overline{k_f})/d\theta_o}{\overline{c_p}/\overline{k_f}} = \frac{d\overline{c_p}/d\theta_o}{\overline{c_p}} - \frac{d\overline{k_f}/d\theta_o}{\overline{k_f}} = \frac{1}{\theta_o-1}\left(\frac{c_p}{\overline{c_p}}-\frac{k_f}{\overline{k_f}}\right) \qquad (\text{C}.19)$$

Applying Equation (C.19) into Equation (C.18) and rearranging the result yields:

$$\frac{d\text{Nu}}{\text{Nu}} = \left\{\frac{1}{\theta-1}\frac{\gamma\text{Re}_{\text{inlet}}\overline{\text{Pr}}}{\text{Nu}}\exp\left(\frac{\text{Nu}}{\gamma\text{Re}_{\text{inlet}}\overline{\text{Pr}}}\right)+\frac{1}{\theta_o-1}\left(\frac{c_p}{\overline{c_p}}-\frac{k_f}{\overline{k_f}}\right)\right\}d\theta_o \qquad (\text{C}.20)$$

At very high Reynolds number where T_{out} approaches T_{in}, the average values of c_p and k_f tend to their local values at T_{out}, too. Moreover, a comprehensive study for different shell-side

fluids over a wide range of temperatures, pressures, as well as inlet Reynolds numbers shows that the following assumption is legitimated specially when the inlet velocity is high or the heat transfer area is small.

$$\frac{1}{\theta-1}\frac{\gamma Re_{inlet}\overline{Pr}}{Nu}\exp\left(\frac{Nu}{\gamma Re_{inlet}\overline{\overline{Pr}}}\right) \gg \frac{1}{\theta_o-1}\left(\frac{c_p}{\overline{\overline{c_p}}}-\frac{k_f}{\overline{\overline{k_f}}}\right) \tag{C.21}$$

By considering the negligibility presented in Equation (C.21), a small change in θ_o, will lead a change in the Nusselt number of

$$\left|\frac{\Delta Nu}{Nu}\right| \approx \frac{\theta_o}{|\theta-1|}\frac{\gamma Re_{inlet}\overline{Pr}}{Nu_0+f\left(Re_{inlet},\overline{Pr}\right)}\exp\left(\frac{Nu_0+f\left(Re_{inlet},\overline{Pr}\right)}{\gamma Re_{inlet}\overline{Pr}}\right)\left|\frac{\Delta\theta_o}{\theta_o}\right| \tag{C.22}$$

Since $\Delta\theta_o/\theta_o$ is equal to $\Delta T_{out}/T_{out}$, the relative error of the Nusselt number, $\|\varepsilon_{Nu}\|$, can be represented as a function of the relative error of the outlet temperature, $\|\varepsilon_T\|$.

$$\|\varepsilon_{Nu}\|=\pm\frac{\theta_o}{|\theta-1|}\frac{\gamma Re_{inlet}\overline{Pr}}{Nu_0+f\left(Re_{inlet},\overline{Pr}\right)}\exp\left(\frac{Nu_0+f\left(Re_{inlet},\overline{Pr}\right)}{\gamma Re_{inlet}\overline{Pr}}\right)\|\varepsilon_T\| \tag{C.23}$$

Equation (C.23) can be presented as a function of the inlet Stanton number St_{inlet}, since $Nu=Nu_0+f\left(Re_{inlet},\overline{Pr}\right)$:

$$\|\varepsilon_{Nu}\|=\pm\frac{\theta_o}{|\theta-1|}\frac{\gamma}{St_{inlet}}\exp\left(\frac{St_{inlet}}{\gamma}\right)\|\varepsilon_T\| \tag{C.24}$$

The shell-side pressure drop is approximately proportional to the square of the Reynolds number.

$$\overline{\overline{O}}\{\Delta p, Re_{inlet}\} \cong 2 \tag{C.25}$$

Considering Equation (C.17), the shell-side pressure drop is proportional to the shell-side Nusselt number as follows:
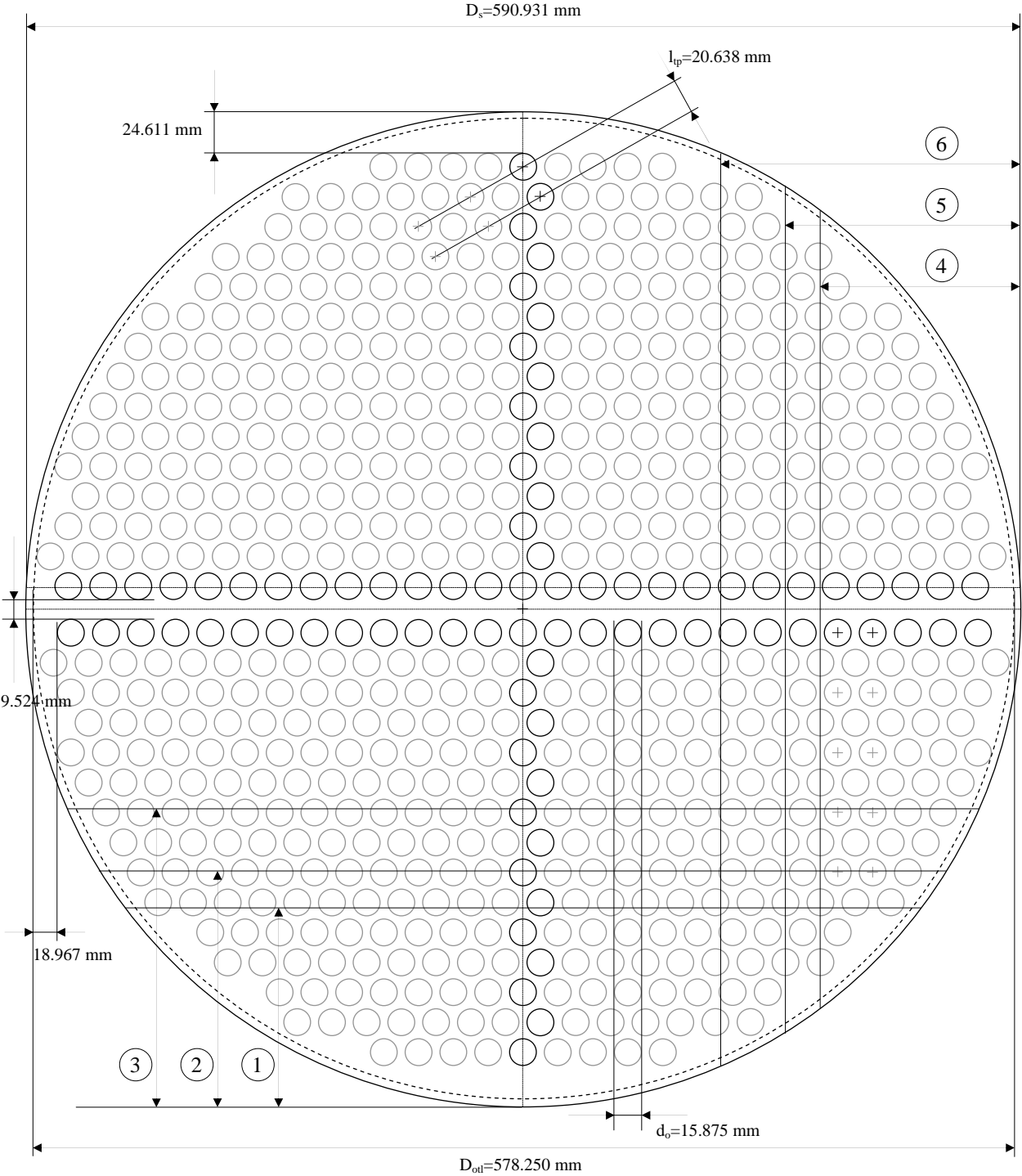
$$Min\,\overline{\overline{O}}\{\Delta p, Nu\} = 2.5 \tag{C.26}$$

Therefore,

$$\left|\frac{d\Delta p}{\Delta p}\right| \approx 2.5\left|\frac{dNu}{Nu}\right| \tag{C.27}$$

Applying Equation (C.24) into Equation (C.27), the relative error of the shell-side pressure drop, $\|\varepsilon_{\Delta p}\|$, can be represented as a function of the relative error of the outlet temperature, $\|\varepsilon_T\|$.

$$\|\varepsilon_{\Delta p}\|=\pm 2.5\frac{\theta_o}{|\theta-1|}\frac{\gamma}{St_{inlet}}\exp\left(\frac{St_{inlet}}{\gamma}\right)\|\varepsilon_T\| \tag{C.28}$$

A8

Appendix D: Tube Layout for Shell and Tube Heat Exchanger with 660 Tubes

D_s=590.931 mm

l_{tp}=20.638 mm

24.611 mm

6

5

4

9.524 mm

18.967 mm

3 2 1

d_o=15.875 mm

D_{otl}=578.250 mm

Horizontal baffle orientation:
(1) BC=20%, (2) BC=24% and (3) BC=30%
Vertical baffle orientation:
(4) BC=20%, (5) BC=24% and (6) BC=30%